“Effect of neuromodulators on second messengers and neuronal activity in the mouse retina visualized by optogenetic sensors”

Von der Fakultät für Mathematik, Informatik und Naturwissenschaften der RWTH Aachen University zur Erlangung des akademischen Grades einer Doktorin der Naturwissenschaften genehmigte Dissertation

vorgelegt von

Master of Science
Safaa Belaidi

aus Nador, Marokko

Berichter: Universitätsprofessor Dr. Frank Müller
Universitätsprofessor Dr. Marc Spehr

Tag der mündlichen Prüfung: 19.07.2018

Diese Dissertation ist auf den Internetseiten der Universitätsbibliothek online verfügbar.

1. Berichterstatter: Prof. Dr. Frank Müller
2. Berichterstatter: Prof. Dr. Marc Spehr

In loving memory of my late beloved mother

To my beloved father

With love and eternal appreciation

Table of contents

Figures and Tables I
Abbreviations III
Abstract IX
Zusammenfassung XI
1. Introduction 1
1.1. Anatomy of the retina 1
1.2. Phototransduction and signal processing 2
1.3. Light adaptation processes 5
1.4. Glutamatergic signaling in the retina 7
1.4.1. AMPA receptors 7
1.4.2. Kainate receptors 8
1.4.3. NMDA receptors 8
1.5. Neurotransmitters in the retina 9
1.5.1. Dopamine 9
1.5.2. Nitric oxide 10
1.5.3. Adenosine 11
1.5.4. Melatonin 12
1.6. Genetically encoded FRET-based sensors 12
1.6.1. Calcium sensor TN-L15 13
1.6.2. cAMP/PKA sensor AKAR4 14
1.7. Aim of the Study 15
2. Material and Methods 17
2.1. Animals 17
2.2. General buffers and solutions 17
2.3. Molecular biology 20
2.3.1. Plasmids 20
2.3.2. Kits 20
2.3.3. Transformation of competent cells 20
2.3.4. DNA isolation 21
2.3.5. Quantification of nucleic acids by spectroscopy 21
2.3.6. Restriction digestion 22
2.3.7. Agarose gel electrophoresis 22
2.4. Cell cultures 23
2.4.1. Stable cell line culture 23
2.4.1.1. Human Embryonic Kidney 293 cells 23

2.4.1.2. Preparation of coverslips ... 24
2.4.1.3. Liposome-mediated transfection ... 24
2.4.2. Primary culture of dissociated retinal neurons ... 25
2.4.2.1. Preparation of coverslips ... 25
2.4.2.2. Isolation of retinae ... 26
2.4.2.3. Dissociation of isolated retinae ... 26
2.4.2.4. Liposome-mediated transfection ... 27
2.4.2.5. Fixation of dissociated retinal neurons ... 27
2.5. Widefield-imaging ... 27
2.5.1. Imaging setup ... 27
2.5.2. Perfusion chamber ... 28
2.5.3. Calcium imaging with Fluo-4 ... 28
2.5.4. Data acquisition ... 28
2.5.5. Data evaluation ... 29
2.6. FRET-based imaging ... 30
2.6.1. FRET-based imaging in TN-L15 wholemount retina ... 30
2.6.2. FRET-based imaging in dissociated retinal neurons ... 30
2.6.3. Data acquisition ... 30
2.6.4. Data evaluation ... 31
2.7. Immunochemistry ... 31
2.7.1. Immunocytochemistry ... 32
2.7.2. Immunostaining of retinal cryosections ... 32
2.7.2.1. Isolation and fixation of retinae ... 32
2.7.2.2. Sectioning ... 33
2.7.2.3. Immunostaining of cryosections ... 33
2.7.2.4. Antibodies ... 33
2.8. Confocal Laser Scanning Microscopy ... 35
2.9. Pharmaceuticals ... 36
2.10. Software ... 37
3. Results ... 38
3.1. Impact of neuromodulators on glutamate-induced changes in $[Ca^{2+}]_i$ in GCs of the intact retina ... 38
3.1.1. Studying DA effects on iGluR-mediated responses in GCs ... 40
3.1.1.1. DA affects the AMPA-induced changes in $[Ca^{2+}]_i$ in GCs ... 42
3.1.1.1.1. AMPA induced changes in $[Ca^{2+}]_i$ in GCs ... 42
3.1.1.1.2. DA reduced the AMPA-induced changes in $[Ca^{2+}]_i$ in GCs ... 45
3.1.1.1.3. Different dopamine receptors affect AMPA-induced calcium responses ... 47

3.1.1.2. DA affects the kainate-induced changes in $[Ca^{2+}]_i$ in GCs 53
3.1.1.2.1. Kainate induced changes in $[Ca^{2+}]_i$ in GCs 53
3.1.1.2.2. DA had slight effects on the kainate-induced changes in $[Ca^{2+}]_i$ in GCs 56
3.1.1.2.3. Different dopamine receptors affect kainate-induced calcium responses 58
3.1.1.2.4. D1Rs affect the kainate-induced calcium signaling most likely via PKA 62
3.1.1.3. DA affects the NMDA-induced changes in $[Ca^{2+}]_i$ in GCs 65
3.1.1.3.1. NMDA induced changes in $[Ca^{2+}]_i$ in GCs 65
3.1.1.3.2. DA had slight effects on the NMDA-induced changes in $[Ca^{2+}]_i$ in GCs 66
3.1.1.3.3. Dopamine receptors affect NMDA-induced changes in $[Ca^{2+}]_i$ in GCs 69
3.1.2. Studying the effects of NO on iGluR-mediated responses in GCs of the TN-L15-retina 74
3.1.2.1. NO enhanced the AMPA-induced changes in $[Ca^{2+}]_i$ in GCs 75
3.1.2.2. NO had slight effects on the kainate-induced changes in $[Ca^{2+}]_i$ in GCs 77
3.1.2.3. NO enhanced the NMDA-induced changes in $[Ca^{2+}]_i$ in GCs 79
3.1.3. Studying the effects of Melatonin on the iGluR-mediated responses in GCs of the TN-L15-retina 81
3.1.4. Studying the effects of adenosine on the iGluR-induced calcium responses in GCs of the TN-L15-retina 84
3.1.5. Studying whether VGCCs are involved in the iGluR-induced calcium responses 87
3.1.6. Studying the acting site of A1Rs during modulation of iGluR-induced calcium responses 90
3.2. Immunohisto- and cytochemical studies of retinal neurons 96
3.2.1. D1Rs and D2Rs are probably expressed on GC dendrites 96
3.2.2. AKAR4-expressing retinal neurons express PKA 99
3.2.3. Immunocytochemical analysis of D1Rs in cultured retinal neurons 100
3.3. Studying the cAMP/PKA pathway in cultured retinal neurons 105
3.3.1. DA-induced changes in $[cAMP]_i$ and PKA activity 105
3.3.2. Blockade of PKA prevents phosphorylation of AKAR4 sensor 107
3.3.3. Studying the purinergic signaling in cultured retinal neurons 108
3.3.4. Impact of AD on DA-induced responses in cultured retinal neurons 110
4. Discussion 119
4.1. The iGluR induced changes in $[Ca^{2+}]_i$ in GCs of the intact retina 120
4.1.1. Using the TN-L15 sensor as indicator for changes in $[Ca^{2+}]_i$ in GCs 120
4.1.2. Morphological and functional diversity of GCs 120
4.1.3. Activation of iGluRs mediate distinct calcium responses in GCs 121
4.1.4. AMPA receptor properties established in other studies 122
4.1.5. Kainate receptor channel properties established in other studies 123

4.1.6. NMDA receptor channel properties established in other studies 124
4.1.7. Origin of calcium signal in retinal GCs 124
4.2. DA modulates the iGluR-induced calcium responses in a distinct manner 125
4.2.1. DA affected the iGluR-induced calcium responses 125
4.2.2. D1Rs and D2Rs are expressed in the inner retina 126
4.2.3. Activation of D1Rs decreased the non-NMDA-induced, but not the NMDA-induced calcium responses in GCs 127
4.2.4. D2Rs affected the iGluR-induced calcium responses in GCs 128
4.2.5. Molecular mechanisms underlying dopaminergic action 128
4.3. Various neurotransmitters affect iGluR-induced calcium responses in GCs 131
4.3.1. Nitric oxide promotes iGluR-induced calcium responses 131
4.3.2. Melatonin affected kainate- and NMDA-induced calcium responses in GCs 132
4.3.3. A1Rs affected the iGluR-induced calcium responses 134
4.4. DA and AD modulate the cAMP/PKA pathway in cultured retinal neurons 137
4.5. Outlook 141
References 143
Danksagung 161
Erklärung 163

Figures and Tables

Figures

Figure 1.1: Cellular organization of the retina. 2
Figure 1.2: Synaptic circuitry of the retina....3
Figure 1.3: The classical pathways of DRs....10
Figure 1.4: Mechanism of the FRET-based calcium sensor TN-L15. 14
Figure 1.5: PKA phosphorylates the AKAR4 sensor leading to an increase in the FRET efficiency 15
Figure 2.1: DNA bands of the different clones showed similar results....23
Figure 3.1: TN-L15 is expressed in GC-somata and processes within the IPL of the TN-L15-expressing retina. 39
Figure 3.2: AMPA induced a change in the fluorescence signal of the TN-L15 sensor in GCs....41
Figure 3.3: TN-L15-expressing GCs responded reversibly and repeatedly to AMPA. 44
Figure 3.4: DA affected the calcium signaling and AMPA receptors activity in GCs. 46
Figure 3.5: Activation of D1Rs led to a strong reduction in the AMPA-induced calcium signaling. 48
Figure 3.6: Activation of D2Rs enhanced the AMPA-induced calcium signaling in retinal GCs. 50
Figure 3.7: Activation of D1Rs and/or D2Rs had opposite effects on the AMPA-induced calcium signaling in GCs. 52
Figure 3.8: TN-L15-expressing GCs responded reversibly and repeatedly to kainate. 55
Figure 3.9: DA showed differential effects on calcium signaling and kainate-induced calcium responses in GCs. 57
Figure 3.10: DA affected the kainate-induced calcium responses in GCs. 58
Figure 3.11: Activation of different dopamine receptors affected the kainate-induced calcium responses in different ways. 59
Figure 3.12: Activation of D1Rs and/or D2Rs had opposite effects on the kainate-induced calcium responses....62
Figure 3.13: D1Rs affected the kainate-induced calcium responses most likely via cAMP/PKA cascade. 64
Figure 3.14: NMDA induced reversible and reproducible increases in YFP/CFP ratio in GCs....66
Figure 3.15: DA affected the calcium signaling and the NMDA-induced calcium responses in some GCs. 67
Figure 3.16: DA decreased the NMDA-induced calcium responses slightly in GCs. 68
Figure 3.17: Activation of D1Rs did not affect the NMDA-induced calcium responses. 69
Figure 3.18: Activation of D2Rs affected the NMDA-induced calcium responses variably. 71
Figure 3.19: Activation of D2 receptors modulates the NMDA-induced calcium responses. 73
Figure 3.20: The NO-donor SNAP increased the AMPA-induced calcium changes in GCs. 76
Figure 3.21: NO affected the kainate-induced calcium responses slightly in a small population of GCs. 78
Figure 3.22: NO increased the NMDA-induced calcium changes in the majority of GCs. 80
Figure 3.23: NO differentially affected iGluR-induced calcium responses. 81
Figure 3.24: Melatonin affected the calcium responses induced via kainate and NMDA receptors. 82
Figure 3.25: Relative frequency of the iGluR-induced calcium responses with or without MT....83

Figure 3.26: The adenosine A1R agonist GR affected the iGluR-induced calcium responses. 85
Figure 3.27: Relative frequency of the iGluR-induced calcium responses with or without the A1R agonist GR.....86
Figure 3.28: Blockade of CaChs affected the iGluR-induced calcium responses. 88
Figure 3.29: Statistical analyses of the effects of blocking L- and N-type CaChs on the iGluR calcium responses.....89
Figure 3.30: Relative frequency of the iGluR-induced calcium responses with and without CaChs blockers. 90
Figure 3.31: Statistical analyses of the effect of the A1R agonist GR 79236 on AMPA-induced calcium responses.....91
Figure 3.32: Statistical analyses of the effect of the A1R agonist GR 79236 on kainate-induced calcium responses.....93
Figure 3.33: Statistical analyses of NMDA-induced calcium responses. 94
Figure 3.34: D1Rs are expressed in the synaptic layers of the mouse retina.....97
Figure 3.35: D1Rs and D2Rs are abundantly expressed in the IPL in the TN-L15-retina. 98
Figure 3.36: AKAR4-expressing retinal neurons express PKARIIβ. 100
Figure 3.37: ACs were found positive for D1Rs in dissociated retinal neurons.....101
Figure 3.38: D1Rs are expressed in some GABAergic ACs in dissociated retinal neurons.....102
Figure 3.39: D1Rs are expressed in PKCα-positive neurons.....103
Figure 3.40: Some D1R-positive neurons express PKARIIβ.....104
Figure 3.41: DA-induced changes in cAMP/PKA activity in cultured retinal neurons visualized by the AKAR4 sensor. 106
Figure 3.42: DA activates the cAMP/PKA pathway in cultured retinal neurons. 107
Figure 3.43: AD induced changes in YFP/CFP ratio in a subset of cultured retinal neurons. 109
Figure 3.44: DA induced changes in PKA activity in all cells, while only few cells responded to AD. 111
Figure 3.45: AD may affect the DA-induced increase in PKA activity in cultured retinal neurons. 113
Figure 3.46: Activation of DRs and A1Rs simultaneously induced variable responses in cultured retinal neurons.....115
Figure 3.47: Stimulation of D1Rs and A1Rs simultaneously induced a further increase in PKA activity in some retinal neurons. 117

Tables

Table 2.1: Composition of the mixture of the restriction digestion.....22
Table 2.2: cDNA used for transient transfection of HEK293 cells or retinal primary cultures.....25
Table 2.3: List of the primary antibodies used in this project. 34
Table 2.4: List of the secondary antibodies used in this project with the appropriate dilution and sources where they were purchased.....35
Table 2.5: List of the pharmaceuticals used in this study.....36
Table 2.6: List of the software used for data acquisition, processing and evaluating. 37
Table 3.1: Summary of the results of the pharmacological studies on the iGluR-induced calcium responses. 95

Abbreviations

$[Ca^{2+}]_i$	intracellular calcium concentration
$[cAMP]_i$	intracellular cAMP concentration
$[cGMP]_i$	intracellular cGMP concentration
[DNA]	DNA concentration
°C	degree celsius
⌀	diameter
A1R	adenosine 1 receptor
A2AR	adenosine 2A receptor
A2BR	adenosine 2B receptor
A3R	adenosine 3 receptors
AA-NAT	aralkylamine N-acetyltransferase
AC	amacrine cell
ACy	adenylate cyclase
AD	adenosine
AKAR4	A kinase activity reporter 4
AM	acetoxymethyl ester
Amp	ampicillin
AMPA	α-amino-3-hydroxy-5-methyl-4-isoxazolepropionic acid
AR	adenosine receptor
ATP	adenosine triphosphate
BC	bipolar cell
BD	binding domain
bidest	double-distilled
BPF	band pass filter
Bp	base pair
Ca^{2+}	calcium
CaBP	calcium-binding protein-28 kDa

CaCh	calcium channel
cAMP	cyclic adenosine monophosphate
CBC	cone bipolar cell
cDNA	complementary DNA
CFP	cyan fluorescent protein
cGMP	cyclic guanosine monophosphate
CI-AMPA	calcium impermeable AMPA
CICR	calcium-induced calcium release
CLSM	confocal laser scanning microscopy
CMF-Hanks	calcium-magnesium-free Hanks
CMV	cytomegalovirus (promoter)
CNG	cyclic nucleotide-gated
CNQX	6-cyano-7-nitroquinoxaline-2,3-dione
CNS	central nervous system
CPA	*N*-cyclopentyladenosine
CP-AMPA	calcium permeable AMPA
Cx36	connexin 36
Cy2, Cy3, Cy5	carbocyanin-Derivate
D1R	dopamine receptor 1
D2R	dopamine receptor 2
D3R	dopamine receptor 3
D4R	dopamine receptor 4
D5R	dopamine receptor 5
DA	dopamine
DAG	diacylglycerol
DIV	days *in vitro*
DMEM	Dulbecco´s modified eagle medium
DMSO	dimethyl sulfoxide
DNA	desoxyribonucleic acid

DPCPX	1,3-dipropyl-8-cyclopentylxantine
DR	dopamine receptor
e.g.	*exempli gratia* (for example)
EDTA	ethylenediaminetetraacetic acid
EMCCD	electron multiplying charge-coupled-device
eNOS	endothelial nitric oxide
ES	extracellular solution
et al.	*et alii* (and so on)
EtOH	ethanol
FBS	fetal bovine serum
Fig.	figure
FP	fluorescent protein
FRET	Förster-resonance energy transfer
GABA	γ-Aminobutyric acid
GAD	glutamic acid decarboxylase
GC	ganglion cell
GCL	ganglion cell layer
GFP	green fluorescent protein
G_i	inhibitory G-protein
GIRKs	G-protein coupled inwardly-rectifying potassium channels
GlyT	glycine transporter
$G_o\alpha$	α-subunit of inhibitory G-protein
GPCR	G-protein coupled receptors
G_q	PLC-coupled G-protein
G_s	stimulatory G-protein
Gβγ	βγ-subunit of a G-protein
HC	horizontal cell
HEK293	human embryonic kidney cells 293
HEPES	2-[4-(2-hydroxyethyl)piperazin-1-yl]ethanesulfonic acid

hrs	hours
ICC	immunocytochemistry
i.e.	id est
iGluR	ionotropic glutamate receptor
INL	inner nuclear layer
iNOS	inducible nitric oxide synthase
IP_3	inositol trisphosphate
ipGC	intrinsically photosensitive ganglion cell
IPL	inner plexiform layer
IS	inner segments
ISBN	International Standard Book Number
K^+	potassium
KA	kainate
Kan	kanamycin
kDa	kilo Dalton
L-AP4	2-Amino-4-phosphonobutyric acid
LB	lysogeny broth
LED	light-emitting diode
MC	Müller cell
MEM	minimal essential medium
MF-CA3	mossy fiber synapses in the hippocampus
mGluR	metabotropic glutamate receptor
MIP	maximal intensity projection
MT	melatonin
MT1	melatonin receptor 1
MT2	melatonin receptor 2
MWP	multiwell plate
n	number
n.s.	not significant

NAc	*nucleus accumbens*
NADPH	Dihydronicotinamide-adenine dinucleotide phosphate
NMDA	*N*-Methyl-D-aspartate
NO	nitric oxide
norm.	normalized
nNOS	neuronal nitric oxide synthase
NOS	nitric oxide synthase
ONL	outer nuclear layer
OPL	outer plexiform layer
OS	outer segments
p.a.	*pro analysi*, for analysis
Px	postnatal day x
PA	paraformaldehyde
PB	phosphate buffer
PBS	phosphate buffered saline
PCR	polymerase chain reaction
PDE	phosphodiesterase
PDL	poly-D-lysine
PKA	protein kinase A
PKARIIβ	protein kinase A, regulatory subunit IIβ
PKC	protein kinase C
PKCα	protein kinase C, α isoform
PLC	phospholipase C
PLL	poly-L-lysine
PP2A	phosphatase 2A
PR	photoreceptor
PTX	pertussis toxin
RBC	rod bipolar cell
RNA	ribonucleic acid

ROI	region of interest
RT	room temperature
sec	second
sGC	soluble guanylyl cyclase
SNAP	S-Nitroso-N-acetyl-DL-Penicillamine
SNC	*S*-nitroso-cysteine
TAE	TRIS-Acetat-EDTA (buffer)
TE	TRIS-EDTA (buffer)
TH	tyrosine hydroxylase
TIFF	Tagged Image Format File
TnC	troponin C
TN-L15	troponin C-based biosensor
TRPM1	transient receptor potential melastatin 1
U	units (enzymatical)
UV	ultra violet
vGlut1	vesicular glutamate transporter 1
w/	with
YFP	yellow fluorescent protein

The usual abbreviations of the *International System of Units* (SI) were used. Multiples and fractions of units were specified by metric prefixes.

Abstract

The present study addresses the question, whether the retinal neuromodulators dopamine (DA), adenosine (AD), nitric oxide (NO) and melatonin (MT) may support control of light sensitivity of the retina by modulating glutamatergic transmission. The retina has the striking feature to adjust its sensitivity and so to adapt to changes in light intensities that vary over a large range of ten orders of magnitude. In the retina, glutamate is responsible for the vertical signal transmission from photoreceptors via bipolar cells to ganglion cells (GCs). A large number of neurotransmitters are released at different sites in the retina and under different light conditions. Second messengers play a major role in cellular signaling pathways and in retinal adaptation. Modulating glutamatergic signaling may be an important contribution to light adaptation. DA, AD and MT act on G-protein-coupled receptors (GPCRs), leading to changes in the concentration of cyclic adenosine monophosphate ($[cAMP]_i$), directly coupled to changes in protein kinase A (PKA) activity. In addition to the cAMP/PKA pathway, alternative pathways involving calcium (Ca^{2+}) have been suggested. NO acts on soluble guanylyl cyclase (sGC), leading to changes in the concentration of cyclic guanosine monophosphate ($[cGMP]_i$), a second messenger that plays an important role in many cell types in the retina. The present study was designed to characterize the calcium responses induced by specific agonists of ionotropic glutamate receptors (iGluRs) in GCs and investigate if and how neuromodulators influence these responses.

To monitor changes in $[Ca^{2+}]_i$ in GCs of the intact retina, I made use of a transgenic mouse line that expresses the genetically encoded Förster-Resonance-Energy-Transfer (FRET)-based calcium sensor TN-L15 in GCs. Activation of iGluRs by their specific agonists AMPA, kainate and NMDA resulted in an increase in $[Ca^{2+}]_i$ in all GCs. Simultaneous activation of dopamine 1 receptors (D1Rs) reduced the non-NMDA-induced calcium responses, while the NMDA-induced calcium responses were not affected. Activation of D2Rs induced the opposite effect; it increased AMPA and kainate induced calcium responses. The effect on NMDA-induced calcium responses was more complicated: activation of D2Rs reduced the NMDA-induced calcium responses in 33% of the cells and enhanced it in 6% of the cells. Activation of adenosine 1 receptors (A1Rs) reduced all iGluR-induced calcium responses. Activation of melatonin receptors only slightly decreased the kainate- and NMDA-induced calcium responses.

Interestingly, the NO-donor SNAP led to an increase in the sensitivity of the GCs. Pharmacological studies suggested that D1Rs most probably act via activation of PKA, as their impact was almost abolished when PKA was inhibited. Thus, these neuromodulators may play an important role in adjusting the sensitivity of the GCs in retinal adaptation processes.

In retinal primary cultures mainly composed of amacrine cells, I expressed the FRET-based PKA sensor AKAR4 to monitor changes in the cAMP/PKA pathway by retinal neuromodulators. All cells responded to stimulation with DA with an increase in PKA activity, most likely mediated via activation of D1Rs. Within the same neuron, DA and AD interacted and affected PKA activity. AD decreased the PKA activity, already increased by DA, in a subpopulation of retinal neurons. This antagonism was predicted by the classical view of A1R- and D1R-induced signaling. However, in another subpopulation simultaneous activation of A1Rs and D1Rs resulted in an additive stimulating effect on PKA activity. This observation suggests that besides the antagonistic pathways, simultaneous activation of A1Rs and D1Rs may activate alternative signaling pathways.

Zusammenfassung

Die vorliegende Arbeit befasst sich mit der Frage, ob die retinalen Neuromodulatoren Dopamin (DA), Adenosin (AD), Stickstoffmonoxid (NO) und Melatonin (MT) die Anpassung der Netzhaut an verschiedene Helligkeiten durch Modulation der glutamatergen Transmission unterstützen können. Die Retina kann ihre Empfindlichkeit regulieren und sich so an Lichtintensitäten anpassen, die über den bemerkenswert großen Bereich von mehr als zehn Größenordnungen variieren. Glutamat ist für die vertikale Signalübertragung von Photorezeptoren über Bipolarzellen zu den Ganglienzellen (GC) verantwortlich. Viele Neurotransmitter werden an verschiedenen Stellen in der Retina unter verschiedenen Lichtbedingungen freigesetzt. Sekundäre Botenstoffe spielen eine wichtige Rolle in zellulären Signalwegen und in der Lichtadaptation. Die Modulation der glutamatergen Signalübertragung könnte einen wesentlichen Beitrag zur Lichtadaptation darstellen. DA, AD und MT wirken über G-Protein-gekoppelte Rezeptoren, was zu Veränderungen in der intrazellulären Konzentration von zyklischem Adenosinmonophosphat ($[cAMP]_i$) führt, das die Aktivität der Proteinkinase A (PKA) kontrolliert. Neben dem cAMP/PKA-Signalweg sind alternative Signalwege mit Calcium (Ca^{2+}) involviert. NO wirkt auf die lösliche Guanylatzyklase, was zu Veränderungen in der Konzentration von zyklischem Guanosinmonophosphat ($[cGMP]_i$) führt, einem sekundären Botenstoff, der eine wichtige Rolle in vielen Zelltypen der Netzhaut spielt. Die vorliegende Studie wurde durchgeführt, um die Calciumantworten nach Aktivierung ionotroper Glutamatrezeptoren (iGluR) mittels spezifischer Agonisten in den GC zu charakterisieren und ihre Modulation durch die oben genannten Neuromodulatoren zu untersuchen.

Um Veränderungen in der $[Ca^{2+}]_i$ in GC der intakten Retina zu verfolgen, habe ich eine transgene Mauslinie verwendet, die den genetisch kodierten Förster-Resonanzenergietransfer (FRET)-basierten Calciumsensor TN-L15 in GC exprimiert. Aktivierung der iGluR durch die spezifischen Agonisten AMPA, Kainat und NMDA führte zu einer Erhöhung der $[Ca^{2+}]_i$ in allen GC. Die gleichzeitige Aktivierung der Dopamin-1-Rezeptoren (D1R) reduzierte die Nicht-NMDA-induzierten Calciumantworten, hatte aber keinen Einfluss auf die NMDA-induzierten Calciumantworten. Aktivierung der D2R induzierte den gegenteiligen Effekt; sie erhöhte die Nicht-NMDA-induzierten

Calciumantworten. Bei den NMDA-induzierten Calciumantworten, war die Situation komplizierter: in 33% der Fälle führte die Aktivierung der D2R zur Verringerung der Calciumantworten, in 6% zur Verstärkung. Aktivierung von Adenosin-1-Rezeptoren (A1R), führte zur Verringerung aller iGluR-induzierten Calciumantworten. Die Aktivierung von Melatoninrezeptoren verringerte die Kainat- und NMDA-induzierten Calciumantworten nur leicht. Interessanterweise führte die Verwendung des NO-Donors SNAP zu einer Erhöhung der Empfindlichkeit der GC. Pharmakologische Untersuchungen zeigten, dass D1R höchstwahrscheinlich über eine Aktivierung der PKA wirken, da ihr Einfluss bei Inhibition von PKA fast vollständig aufgehoben war. Diese Neuromodulatoren könnten bei der Anpassung der Lichtempfindlichkeit der GC in retinalen Adaptationsprozessen eine wichtige Rolle spielen.

In einer Primärkultur retinaler Neuronen, die hauptsächlich aus Amakrinzellen besteht, habe ich den FRET-basierten PKA Sensor AKAR4 exprimiert, um die Regulation des cAMP/PKA-Signalwegs durch retinale Modulatoren zu untersuchen. Alle Zellen reagierten auf die Stimulation mit DA mit einem Anstieg der PKA Aktivität, die höchstwahrscheinlich auf Aktivierung von D1R beruht. An individuellen Neuronen konnten Interaktionen zwischen DA und AD festgestellt werden, beide beeinflussten die PKA Aktivität. AD verringerte die PKA Aktivität, die bereits durch DA erhöht worden war, in einer Subpopulation retinaler Neuronen. Dieser Antagonismus wird durch die klassische Betrachtung der Signalwege von A1R und D1R vorhergesagt. In einer anderen Subpopulation dagegen führte die Aktivierung der A1R und D1R zu einer additiven Verstärkung der PKA Aktivität. Diese Verstärkung des cAMP/PKA-Signalwegs weist darauf hin, dass die Co-Aktivierung beider Rezeptoren neben den antagonistischen auch alternative Signalwege aktivieren kann.

1. Introduction

Our eyes are our most important sensory organs that enable us the visual perception of the surrounding environment. Through the eyes, we can detect possible dangers, food and sexual partners. Thus, vision is crucial for our survival. Most of the sensory information accounted from the brain originates from visual information (C. Van Essen 2004). The most vital layer of the eye that allows perception of the light is the retina with its highly complex circuitry.

1.1. Anatomy of the retina

The mammalian retina is an approximately 200 μm thick sensory tissue (Wässle 2004). The vertebrate retina is a well-organized tissue in which structure and function are highly correlated to produce a complex visual output. The Spanish neuroscientist Ramón y Cajal was a pioneer in the investigation of the microscopical structure of the retina and Nobel Prize Awardee (1906). The retina is composed of five major cell classes (Fig. 1.1): Photoreceptors (PRs) that can be categorized into rods and cones (for review see (Dowling 1987)). Rods are highly sensitive to light and are responsible for dim light vision (scotopic vision), while cones ensure high-acuity vision at daylight (photopic vision). In humans, cone density is highest in the fovea, whereas rod density is maximal in the parafoveal regions (Osterberg 1935, Curcio *et al.* 1990). The outer segments (OS) of PRs are the site of phototransduction, while the inner segments (IS) host housekeeping processes. The cell bodies of the PRs form the outer nuclear layer (ONL). PRs are glutamatergic neurons; they synapse onto second order glutamatergic bipolar cells (BCs) and horizontal cells (HCs) in the first synaptic layer, the outer plexiform layer (OPL). HCs modulate the vertical transmission between the PRs and the BCs. The inner nuclear layer (INL) contains cell bodies of HCs, BCs and amacrine cells (ACs). Müller cells (MCs) are the radial glial cells of the retina; their somata are also located in the INL (Fig. 1.1). The inner plexiform layer (IPL) is the second synaptic layer, where BCs synapse onto the output neurons: the ganglion cells (GCs) as well as on ACs. ACs are involved in the modulation of the transmission between BCs and GCs (for review see (Müller & Kaupp 1998, Wässle 2004)). Finally, GCs relay the collected information to the higher center of the central nervous system (CNS) via the optic nerve for visual

perception (Masland 2001, Wässle 2004). The retinal nerve fiber layer (NFL) is formed by the GC axons (Fig. 1.1).

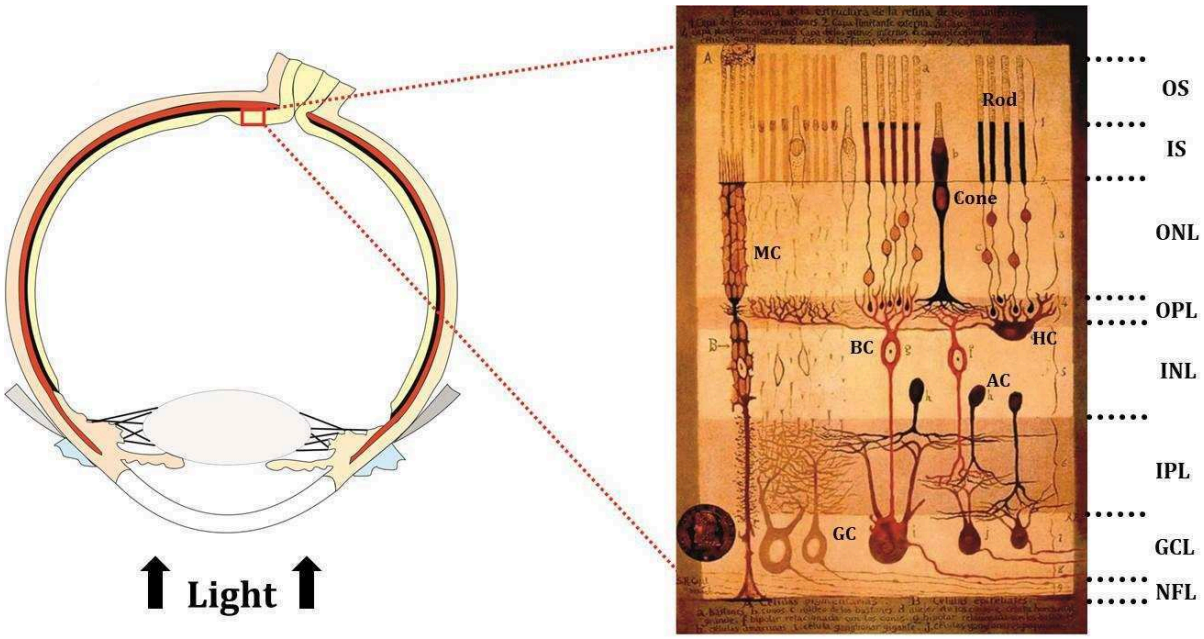


Figure 1.1: Cellular organization of the retina. Left: Section through the human eye ball (Dr. Anja Mataruga, ICS-4, FZ-Jülich). The arrows indicate the direction of the light. Light passes through the retina from the GC side. **Right:** Schematic drawing of the retina by Santiago Ramón y Cajal (ca. 1900). The retina comprises highly organized cellular and synaptic layers. OS: outer segments; IS: inner segments; ONL: outer nuclear layer; OPL: outer plexiform layer; INL: inner nuclear layer; IPL: inner plexiform layer; GCL: ganglion cell layer; NFL: nerve fiber layer.

1.2. Phototransduction and signal processing

Rods and cones are the light sensitive cells that mediate typical aspects of vision. Both are depolarized in darkness and hyperpolarize upon illumination. In the dark, a high number of voltage-gated calcium channels (VGCCs) in the synaptic terminal of PRs are open. Accordingly, the rate of transmitter release, glutamate, is high. Ion channels in the OS allow Na^+ and Ca^{2+} to flow into the cell to maintain the depolarized state of PRs. The nucleotide cyclic guanosine monophosphate (cGMP) regulates the opening and closure of these channels. In darkness, cGMP-gated ion channels (cyclic nucleotide-gated channels, CNG channels) in the OS are kept open due to high levels of cGMP. When a photon is absorbed by an opsin, the photopigment in the OS, the opsin becomes activated. The activated opsin stimulates the G-protein transducin, which in turn activates the phosphodiesterase (PDE). PDE converts cGMP to GMP and thereby lowers the cGMP concentration ($[cGMP]_i$) in the OS. As a consequence, CNG channels are closed

and the PRs hyperpolarize leading to less glutamate release (reviewed in (Müller & Kaupp 1998)). This process is referred to as phototransduction.

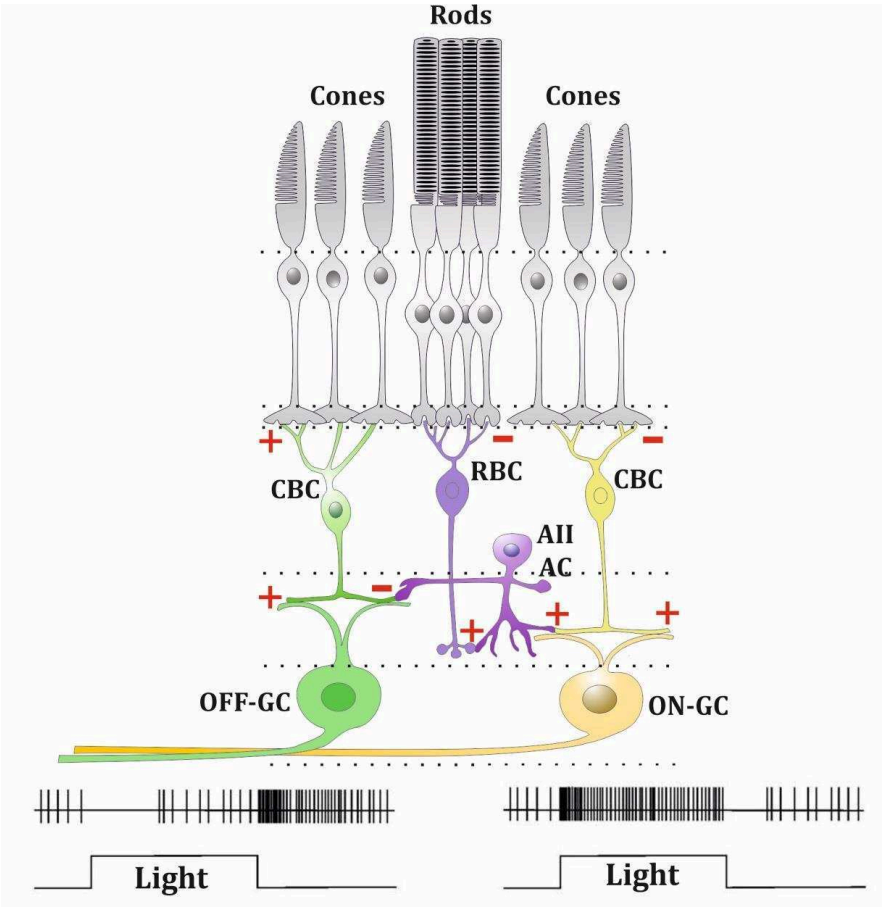


Figure 1.2: Synaptic circuitry of the retina. Signal transmission between PR terminals and dendrites of BCs is mediated by glutamate. Different BCs respond differently to glutamate based on the receptors at their dendrites: iGluRs or mGluRs (see main text). Along the OFF-pathway (green), the signal from cones to OFF-cone BCs (CBC, green) is conveyed in a sign-conserving way as they express iGluRs (indicated by the red plus sign). Since GCs also express iGluRs, GCs that receive input from the OFF-CBC are OFF-GCs (green). Thus, OFF-GCs hyperpolarize at light-onset similar to the cones (OFF-pathway, green). Along the ON-pathway (yellow), the signal to ON-cones BCs (CBC, yellow) is relayed in a sign-inverting way, as they express mGluRs (indicated by the red minus sign). Thus, ON-CBCs, and consequently ON-GCs, are depolarized at light onset (yellow). ON-GCs show bcs signalincreased action potential rate light-onset, while OFF-GCs show increased action potential rate at light-offset. Rod BCs (RBC, violet) express mGluRs at their dendrites (indicated by the red minus sign) and are ON-BCs. Thus, RBCs are depolarized at light-onset and hyperpolarized at light-offset and relay their signal in a sign-conserving way to the AII ACs. AII ACs serve to conduct rod signals to GCs. AII ACs are electrically coupled to ON-CBCs, i.e. they transfer their signal in a sign-conserving way into the ON-pathway. At the same time, AII ACs make inhibitory (glycinergic) synapses onto OFF-CBCs, and inhibit them (indicated by the red minus sign). Figure modified from (Frings S. 2014).

Two parallel pathways result from the cone circuitry: the ON- and the OFF-pathway (Fig. 1.2). In the mammalian retina, PRs provide input to 14 types of BCs (Boycott & Wässle 1991, Euler & Wässle 1995, Mataruga *et al.* 2007, Wässle *et al.* 2009, Euler *et al.* 2014, Behrens *et al.* 2016). Two major classes of BCs can be distinguished: ON-BCs and OFF-BCs. Their responses are determined by two different glutamate receptor classes at

their dendrites. ON-BCs have metabotropic glutamate receptors 6 (mGluR6) at their dendrites (Nomura *et al.* 1994, Vardi *et al.* 2000). In this way, the signal received from PRs is reversed by the ON-BCs (Fig. 1.2, negative signs in red); they are hyperpolarized in darkness when the sustained glutamate release at the OPL is high. The mGluR6 is a G-protein coupled receptor (GPCR); binding of glutamate induces a signaling cascade that leads to closure of the transient receptor potential melastatin 1 (TRPM1) channels. TRPM1 are non-selective cation channels, their closure results in a hyperpolarization of the ON-BCs membrane (Shen *et al.* 2009). Upon illumination, glutamate release from PRs is diminished and TRPM1 channels open, leading to a depolarizing ion influx (Morgans *et al.* 2009). As a result, the ON-BCs release glutamate in the IPL where they synapse onto ON-GCs leading to their depolarization (Fig. 1.2). OFF-BCs have ionotropic glutamate receptors (iGluRs) at their dendrites and follow the light response of PRs. In darkness, where glutamate release is high, iGluRs are open leading to depolarization of OFF-BCs (Fig. 1.2, CBC, green, positive sign in red). As a result, OFF-BCs release glutamate in the IPL, where in turn OFF-GCs are depolarized (Fig. 1.2, green, positive sign in red). Upon illumination, glutamate release from PRs decreases, the iGluRs are closed leading to hyperpolarized OFF-BCs and subsequently hyperpolarized OFF-GCs (Peichl 1992, Ghosh *et al.* 2004). The level of stratification of BCs is important for sublamination of the IPL. The IPL can be subdivided into two sublayers: the upper one forms the OFF-sublamina and the lower one the ON-sublamina. In the OFF-sublamina, OFF-BCs synapse onto OFF-GCs, while ON-BCs synapse onto ON-GCs in the ON-sublamina. Rod-BCs are ON-BCs, which stratify in the innermost part of the ON-sublamina. However, they do not synapse directly onto GCs, but onto ACs that relay rod signals into both ON- and OFF-channel.

The signal transmission between BCs and GCs occur in the IPL in a sign-conserving way by glutamatergic synapses. ACs modulate the excitation of GCs directly by feedforward inhibition or indirectly by feedback inhibition, where ACs synapse onto axon terminals of BCs. In the mammalian retina, approximately 30 types of ACs have been identified based on their morphology (Kolb *et al.* 1981, Vaney 1990, Boycott & Wässle 1991, MacNeil & Masland 1998, Masland 2012). The large variety of ACs reflects the wide variety of modulatory functions complied by this cell class. ACs use their dendrites pre- and postsynaptically and use different neurotransmitters. Two neurotransmitters are mainly responsible for inhibition via ACs: γ-aminobutyric acid (GABA) and glycine. In the mouse retina, glycinergic and GABAergic ACs represent more

than 80% of the AC population (Marc 1988, Nguyen-Legros *et al.* 1997, Lin & Masland 2006). There is a large diversity among ACs, three typical ACs are well described. The glycinergic AII cells are small-field cells, they are involved in funneling rod BC signals into cone pathways (Fig. 1.2, AII AC). The A17 cells are wide-field cells, they mediate feedback inhibition and gain control of rod BCs (Boycott & Wässle 1991, Bloomfield & Dacheux 2001, Schubert & Euler 2010). The dopaminergic ACs are wide-field cells, they are involved in adjusting the signal processing of retinal neurons to the ambient light level (Herrmann *et al.* 2011). GCs are the output neurons of the retina; they receive excitatory input from BCs and inhibitory input from ACs. They encode the collected information into electrical signals and relay them via the optic nerve to visual centers in the brain (Masland 2001, Wässle 2004). In the mouse retina, based on their light-evoked responses and basic anatomical criteria, at least 32 different functional GCs could be distinguished (Baden *et al.* 2016).

1.3. Light adaptation processes

The retina has the striking feature to adjust its sensitivity and so adapt to changes in light intensity from a starry night to a sunny day. To extract high level information from natural scenes, the retina has to cope with an enormous range of brightness covering more than ten orders of magnitude (Rodieck 1998). This task is managed by adaptation processes that occur in two distinct phases: a fast one and a slow one (Calvert *et al.* 2002). During light adaptation, the response of retinal cells to light stimuli of a given brightness become weaker – the retina changes its operating range. Light adaptation rests on three major columns.

1. Rods and cones are allotted to different parts of the light intensity spectrum. Based on their high sensitivity, rods are specialized for vision at night or at dusk and dawn, the so-called scotopic vision. In contrast, the less sensitive cones provide for vision at bright day light, the so-called photopic vision. Finally, mesopic vision represents a transition state, where both PRs are active.

2. Photoreceptors can adapt. Rods are very light sensitive; they are able to respond to single photons. This makes it particularly challenging for rods to respond to brighter stimuli, as their response saturates in moderately bright light. Light adaptation processes decrease rod sensitivity, thus extending their operating range (Pugh *et al.*

1999, Burns & Baylor 2001, Fain *et al.* 2001). An increase in the ambient illumination is accompanied by an increase in transducin and consequently in PDE activity. As a result, $[cGMP]_i$ is lowered and the CNG channels are closed inducing a reduction in the light response (Tamura *et al.* 1991, Müller & Kaupp 1998, Calvert *et al.* 2002). The reduction of Ca^{2+} influx triggers light adaptation in both cones and rods (for review: (Müller & Kaupp 1998, Pugh *et al.* 1999)). In particular, adaptive mechanisms control the amplification factor in the phototransduction cascade and, hence, change the input – output relation.

3. Additional adaptive processes also reside within the retinal network. For example, light responses can be attenuated by reducing synaptic efficiency at chemical or electrical synapses. At chemical synapses, transmitter release or the action of transmitters on the postsynaptic site may be modulated. At electrical synapses, conduction of gap junctional channels can be modulated. Postsynaptic HCs modulate the activity of VGCCs in the axon terminals of PRs, thus help to adjust the operating range of the PRs (Kamermans & Fahrenfort 2004). AII ACs have been found to regulate cell-to-cell coupling in a dopamine (DA)-dependent manner (Kothmann *et al.* 2009, Li & O'Brien 2012). AII ACs, which contact rod BCs, are also affected by the reduced glutamate release of the rod BCs and thus the loss of sensitivity is assignable to the whole retinal network (Dunn *et al.* 2006). Gap junctions ensure signal transduction as well as processing (Volgyi *et al.* 2013). With increased ambient light, the size of the HC network becomes reduced by closing gap junctions (Xin & Bloomfield 1999). The adaptation processes are mediated by a variety of second messengers and neurotransmitters that are released from retinal cells dependent on the ambient light level. Nitric oxide (NO) and DA are released by specific ACs, their concentration is higher during day (Djamgoz *et al.* 2000, Doyle *et al.* 2002, Witkovsky 2004). Adenosine (AD) may be released by some MCs and some GCs via nucleoside transporters (Uckermann *et al.* 2006). Moreover, Ecto-nucleotidases induce degradation of the extracellular ATP to ADP and finally to AD (Perez *et al.* 1986, Santos *et al.* 1999, Abbracchio *et al.* 2009). AD has been found to inhibit calcium channels (CaChs) in cones in tiger salamander and thus leading to reduction of glutamate release (Ribelayga & Mangel 2005, Stella *et al.* 2007). Melatonin (MT) is produced by PRs, with higher levels during the night and lower levels during day (Besharse & Iuvone 1983, Tosini & Fukuhara 2003).

The present study addresses the question, whether retinal neuromodulators like dopamine may control light sensitivity of the retina by modulating glutamatergic transmission. Chapter 1.4 deals with glutamatergic signaling in the retina, while chapter 1.5 covers retinal neuromodulators.

1.4. Glutamatergic signaling in the retina

Glutamate is the most important excitatory neurotransmitter in the CNS and, therefore, in the retina. In darkness, glutamate is released from PR synaptic terminals. Glutamate can be taken up from the synaptic cleft via glutamate transporters into PRs or MCs (Rauen & Kanner 1994, Rauen *et al.* 1998, Pow & Barnett 2000). In the OPL, glutamate acts on postsynaptic glutamate receptors on HCs and BCs. Two classes of glutamate receptors are distinguished: iGluRs and mGluRs. The mGluRs belong to the superfamily of GPCRs, ON-BCs were found to express mGluR6 (Nomura *et al.* 1994, Vardi *et al.* 2000). Thus, HCs and OFF-BCs are depolarized while ON-BCs are hyperpolarized in darkness (Vandenbranden *et al.* 1996). Three main subtypes of iGluRs are named based on their selectivity for the agonists AMPA (α-amino-3-hydroxy-5-methyl-4-isoxazolepropionic acid), kainate (KA) and NMDA (*N*-methyl-D-aspartate). AMPA and kainate receptors belong to the non-NMDA family. The non-NMDA receptors are mainly permeable for Na^+ and K^+, although some isoforms also conduct Ca^{2+}, while NMDA receptors are characterized by their strong permeability for Ca^{2+}. Activation of non-NMDA receptors induces influx of Na^+, which in turn results in a membrane depolarization. Through Ca^{2+} permeability, activation of NMDA receptors produces long-lasting changes in the postsynaptic neurons (reviewed in (Yang 2004)).

1.4.1. AMPA receptors

AMPA receptors are tetrameric ion channels, four subtypes are distinguished: GluR1-GluR4 (Nakanishi 1992, Rosenmund *et al.* 1998). In the mouse retina, the INL and GCs were found to express AMPA receptors (Zhang *et al.* 2011). By application of AMPA, Sun and colleagues showed that ACs and GCs were activated; immunohistochemical studies revealed that the IPL was intensely labeled (Sun & Kalloniatis 2006). In the mammalian retina, AMPA receptors are expressed in AII ACs (Ghosh *et al.* 2001). Differential expression of subunit results in the formation of distinct types of AMPA receptors in different retinal cell types (Grunder *et al.* 2000). Moreover, it has been

shown that AMPA receptors that differ in subunit composition also differ in their Ca^{2+} permeability. The resulting differences in Ca^{2+} permeability may affect signal transmission and propagation (Bochet *et al.* 1994, Angulo *et al.* 1997). AMPA receptors are involved in light-induced fast glutamatergic transmission in the retina in both OPL and the IPL (Massey 1990, Hartveit 1997).

1.4.2. Kainate receptors

Kainate receptors were originally described by Watkins and coworkers, five KA receptor subunits have been described (Davies *et al.* 1979, Watkins & Evans 1981, Hollmann & Heinemann 1994). Kainate receptors are non-selective cation channels; their function is also depending on the subunit composition, in some cases kainate receptors show low conductivity for Ca^{2+} (Ferrer-Montiel & Montal 1996). Kainate receptors are characterized by a fast desensitizing response to kainate and glutamate (Lerma 1997, Grunert *et al.* 2002). Two families of kainate receptors are distinguished based on their affinity to kainate (Kristensen *et al.* 2016): GluR5-GluR7 are denoted by low-affinity (Bettler *et al.* 1992, Sommer *et al.* 1992), KA1 and KA2 have high-affinity (Werner *et al.* 1991, Sakimura *et al.* 1992). In the OPL, kainate receptors ensure transmission between cones and certain OFF-BCs (reviewed in (Huettner 2003)). Using in situ hybridization, kainate receptor subunit mRNAs were found to be differentially distributed throughout the INL and ganglion cell layer (GCL). Cell types expressing kainate receptors include HCs, BCs, ACs and GCs (Brandstätter *et al.* 1998). Using immunohistochemical studies, GluR6 and GluR7 were found in HCs, ACs, GCs and most likely also in BCs of the rat retina (Peng *et al.* 1995).

1.4.3. NMDA receptors

NMDA receptors are tetrameric non selective cation channels; their opening requires binding of glutamate and the relief of a magnesium ion (Mg^{2+}) block (Dingledine *et al.* 1999, Voglis & Tavernarakis 2006). NMDA-gated currents have slower kinetics than KA- and AMPA-gated channels (Mayer & Westbrook 1987). Seven subunits of NMDA receptors have been described: NR1, NR2A-NR2D, NR3A and NR3B (Moriyoshi *et al.* 1991, Ikeda *et al.* 1992, Meguro *et al.* 1992, Ishii *et al.* 1993, Traynelis *et al.* 2010). The NR1 subunit is common to all NMDA receptors, which can co-assemble as homomeric receptor (Moriyoshi *et al.* 1991, Monyer *et al.* 1992) or together with other

subunits as heteromeric receptor (Moriyoshi *et al.* 1991, Ishii *et al.* 1993, Meguro *et al.* 1992). NMDA receptors were found in some ACs, in particular in AII ACs, as well as GCs (Massey & Miller 1990, Yang & Wu 1991, Cohen & Miller 1994). In primate GCs, blockade of NMDA receptors resulted in a more transient light response (Cohen & Miller 1994). The excitatory response of GCs mediated by NMDA receptors is increased when the cell is depolarized by input mediated by non-NMDA receptors. This suggests a strong interplay between NMDA and non-NMDA receptors in signal transmission (Diamond & Copenhagen 1993).

1.5. Neurotransmitters in the retina

Signal processing generally depends upon a complement of neurotransmitters that are released at synapses between individual neurons. While glutamate is the excitatory neurotransmitter of the vertical pathway from PRs to GCs, GABA and glycine are the major inhibitory neurotransmitters. A variety of neurotransmitters and neuromodulators has a diverse role in the function of the retina. In this chapter, I will focus on DA, NO, AD and MT, thought to play a role in light adaptation processes.

1.5.1. Dopamine

Dopaminergic retinal neurons express tyrosine 3-mono-oxygenase (tyrosine hydroxylase, TH), the rate-limiting enzyme of catecholamine biosynthesis (Nguyen-Legros 1988). With 30 cells/mm^2, the total number of dopaminergic neurons per retina is relatively low (Dkhissi *et al.* 1996). In the mouse retina, the dopaminergic cells have extensive dendritic and axonal processes that facilitate signal transmission to remote sites within the IPL (Versaux-Botteri *et al.* 1984, Witkovsky *et al.* 1993, Keeley & Reese 2010).

Dopamine receptors (D1R-D5R) are GPCRs, they differ in their affinity for DA as well as in their function. Two families have been distinguished: activation of the D1R-family (D1Rs and D5Rs) activates the adenylate cyclase (ACy) and thus increases the concentration of cyclic adenosine monophosphate ($[cAMP]_i$) (Fig. 1.3). The D2R-family (D2Rs-D4Rs) is negatively coupled to ACy, its activation results in a decrease in the $[cAMP]_i$ (Fig. 1.3). In the mammalian retina electrical coupling via gap junctions between AII ACs or between dopaminergic ACs is affected through a D1R mechanism (Hampson

et al. 1992). D1Rs have been found in HCs, BCs (type 5 and 7), ACs and GCs in the mammalian retina (Veruki & Wässle 1996, Nguyen-Legros *et al.* 1997, Hayashida *et al.* 2009, Usai 2014). The D2Rs were found on dopaminergic ACs, where they act as autoreceptor (Dubocovich & Weiner 1985). Cohen and colleagues demonstrated that rods and cones express D4Rs (Cohen *et al.* 1992). D4Rs regulate the uncoupling of PRs by dephosphorylation of connexin 36 (Cx36) (Li *et al.* 2013). D5Rs have been found in the retinal pigment epithelium (Versaux-Botteri *et al.* 1997); D3Rs are not expressed in the retina.

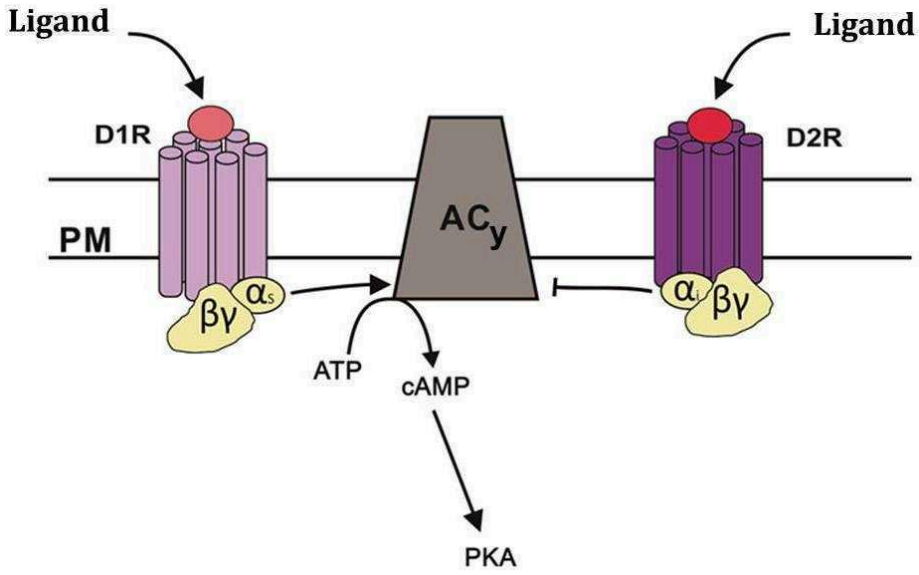


Figure 1.3: The classical pathways of DRs. DRs are GPCRs that couple to ACy. Members of the D1R family (D1Rs and D5Rs) are positively coupled to the ACy, their activation increases the $[cAMP]_i$ and PKA activity. Activation of members of the D2R family (D2Rs-D4Rs) inhibits the ACy leading to a decrease in the cAMP production and consequently in PKA activity. ATP: Adenosine triphosphate; PM: Plasma membrane; α_s: stimulating α subunit; α_i: inhibiting α subunit; βγ: βγ subunits; D1R: dopamine 1 receptor family; D2R: dopamine 2 receptor family.

1.5.2. Nitric oxide

Nitric oxide (NO) – previously known as endothelium-derived relaxing factor - has been implicated in many physiological pathways in the retina. Nitric oxide synthase (NOS) catalyzes NO via a redox pathway that converts L-arginine to L-citrulline and NO. Three main isoforms of NOS have been described: endothelial (eNOS), neuronal (nNOS) and inducible (iNOS) (Goldstein *et al.* 1996). NO stimulates the soluble guanylyl cyclase (sGC), which in turn produces cGMP (Arnold *et al.* 1977, Guimaraes *et al.* 2001). Using NADPH-diaphorase staining, nNOS expression was suggested in ACs and displaced ACs

in the GCL (Dawson *et al.* 1991, Koistinaho *et al.* 1993, Kim *et al.* 1999). NO may be involved in the control of light transmission, as it modulates voltage-gated ion channels in rods (Kurenny *et al.* 1994). Using immunostaining against cGMP and pretreatment with NO, it has been shown that NO modulates cGMP levels in ACs and BCs (Zhao 2010, Blom *et al.* 2012). Antibodies against the major target for NO, the sGC, demonstrated that many retinal neurons in the inner retina express sGC (Ding & Weinberg 2007). NO is also involved in retinal blood flow (Deussen *et al.* 1993, Wiencke *et al.* 1994).

1.5.3. Adenosine

Adenosine (AD) is an endogenous nucleoside generated by dephosphorylation of AMP by a 5'nucleotidase; it plays an important role in signal transmission, as a neuromodulator and as a neuroprotective in the retina and the brain (Kreutzberg *et al.* 1978, Blazynski & Perez 1991, Roth 2004, Zhong *et al.* 2013). AD receptors (ARs) belong to the family of GPCRs; they are subdivided into four subtypes: A1, A2A, A2B and A3 receptors (Fredholm *et al.* 2011). Activation of A1 and A3 receptors (A1Rs and A3Rs), both negatively coupled to ACy, leads to a decrease in the $[cAMP]_i$ and protein kinase A (PKA) activity. By contrast, activation of A2A and A2B receptors (A2ARs and A2BRs) stimulates the ACy. As a result, $[cAMP]_i$ and PKA activity increase. Using biochemical, pharmacological and anatomical techniques, the presence of AD and/or ARs in the retina has been demonstrated (Senba *et al.* 1986, Perez *et al.* 1988, Paes de Carvalho *et al.* 1990, Zhang *et al.* 2006). A1Rs were localized in the IPL, in the GCL and in the optic nerve, while A2AR mRNA was found in PRs, in the INL and in the GCL (Braas *et al.* 1987, Blazynski & Perez 1991, Kvanta *et al.* 1997, Li *et al.* 2013). In the rat retina, A3Rs were found in the GCL and IPL (Zhang *et al.* 2006). AD has been found to inhibit the release of many classical neurotransmitters via the A1Rs through inhibition of CaChs (Fredholm & Dunwiddie 1988, Wu & Saggau 1994, Dunwiddie & Masino 2001). AD's circadian rhythm has the opposite phase as DA, it exhibits higher levels in darkness and lower levels at daytime (Ribelayga & Mangel 2005). In the mouse retina, gap junctions in PRs facilitate the relay of input from rod signals into the cone pathway during mesopic vision. DA and AD, via A2ARs, most likely co-regulate PR coupling through phosphorylation of Cx36 in a PKA-dependent manner (Li *et al.* 2013). AD was found to modulate VGCC currents in goldfish, salamander and rat retina via A1Rs (Zhang & Schmidt 1999, Sun *et al.* 2002, Hartwick *et al.* 2004).

1.5.4. Melatonin

Melatonin (MT) is synthesized from serotonin through two enzymatic steps in PRs (Wurtman & Axelrod 1968, Cardinali 1981, Klein 2007). As a lipophilic molecule, MT diffuses passively across cell membranes and cell layers (Cardinali *et al.* 1972, Morin *et al.* 1997). MT acts on two different receptors (MTs), which belong to the superfamily of GPCRs (Fujieda *et al.* 1999, Liu *et al.* 2016). Both receptors MT1 and MT2 are negatively coupled to ACy, their activation leads to decrease in the $[cAMP]_i$ and PKA activity. MT is an important circadian signal in the retina that has reciprocal and antagonistic relationship with DA (Nguyen-Legros *et al.* 1997, Tosini & Dirden 2000). MT has been found to inhibit DA release by acting via a presynaptic melatonin heteroreceptor (Dubocovich *et al.* 1997). Based on immunohistochemical and molecular studies MT1 mRNA has been localized to PRs, ACs and GCs. MT2 immunoreactivity was found in BCs and GCs as well as in the IS of the PRs (Savaskan *et al.* 2002, Scher *et al.* 2003, Dubocovich *et al.* 2010). MT inhibits neurotransmitter release by MT2 receptors via regulation of the intracellular calcium concentration (Dubocovich 1995). In carp retina, MT was found to modulate the glutamatergic signaling between cones and HCs. MT depolarized the cell membrane of H1 cells and reduced their light responses (Huang *et al.* 2005).

1.6. Genetically encoded FRET-based sensors

Second messengers like calcium or cAMP play important roles in adaptation. This chapter introduces genetically encoded sensors used in this study for the detection of second messengers. Optogenetics refers to a technology that combines genetic tools and optical control to target isolated cells or cells in living tissue. This rapidly evolving technique has made a significant impact on neuroscience, as it enables specific modulation of complex neural tasks with high temporal and spatial resolution (Deisseroth *et al.* 2006, Scanziani & Hausser 2009, Rein & Deussing 2012). Recent advances in optogenetics have made an outstanding contribution to monitor specifically the dynamics of different intracellular signaling components. Much attention has been devoted to genetically encoded fluorescent biosensors to visualize molecular dynamics and intracellular interactions. Fluorescent biosensors make use of the Förster-resonance energy transfer (FRET) from one excited fluorophore (donor molecule) to another

fluorophore (acceptor molecule) (Clegg *et al.* 1993, Sekar & Periasamy 2003). FRET requires a sufficiently short distance between the two fluorophores (<10 nm) and the overlapping between the emission spectrum of the donor fluorophore and the excitation spectrum of the acceptor fluorophore (Sapsford *et al.* 2006, Broussard *et al.* 2013). The working principle of genetically encoded FRET-based sensors depends on the usage of auto-fluorescent proteins such as green fluorescent protein (GFP) from the jellyfish *Aequorea Victoria* (Shimomura *et al.* 1962) or spectrally different variants of fluorescent proteins (FPs). The advantages of FRET-based sensors lie in the fact that they can be expressed in single cells and intact tissue with high specificity using cell type specific promotors (Dunn *et al.* 2006, Heim *et al.* 2007). Generally, these sensors are small enough to be produced without problems by the host cell and can be easily expressed in a variety of cell types by using transfection techniques such as lipofection (Zelphati *et al.* 2001, Zhang *et al.* 2001).

1.6.1. Calcium sensor TN-L15

Genetic encoding enables cell specific and subcellular targeting. Thus, optical reporters have been constructed for vesicle release, changes in neurotransmitter concentration and intracellular calcium dynamics (Lin & Schnitzer 2016). The genetically encoded FRET-based calcium sensor TN-L15 was used to visualize cellular calcium dynamics in GCs of the transgenic mouse line TN-L15 (Heim et al. 2007). The sensor TN-L15 consists of the truncated fast chicken skeletal muscle troponin-C (csTnC) and two fluorophores: the cyan fluorescent protein (CFP) and a variant of the yellow fluorescent protein (YFP), citrine. The calcium-binding protein csTnC exhibits four binding sites for Ca^{2+}-ions. Binding of Ca^{2+} to TnC leads to a conformational change in the protein, resulting in a decrease of the distance between CFP and citrine. An increase in the FRET efficiency results in an increase of the emission signal of YFP, with a concomitant mirror-reversed decrease in the emission signal of CFP (Fig. 1.4). An increase in the FRET efficiency reflects an increase in the calcium concentration $[Ca^{2+}]_i$ (Heim & Griesbeck 2004). The calcium sensor TN-L15 was found to be expressed in approximately 80% of the GCs in the TN-L15 mouse line (Müller *et al.* 2007).

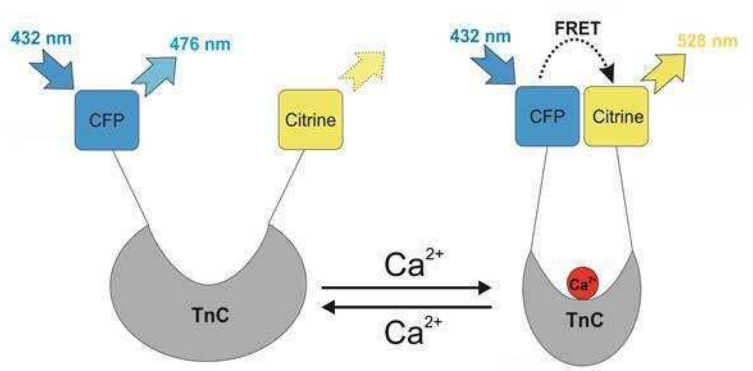


Figure 1.4: Mechanism of the FRET-based calcium sensor TN-L15. The calcium sensor is based on the truncated chicken skeletal muscle troponin C (TnC), which is sandwiched between the two fluorescent proteins CFP and the YFP variant citrine. CFP is excited at 432 nm and emission of YFP is monitored at 528 nm. Upon binding of Ca^{2+}, a conformational change in the protein takes place, thereby enhancing the FRET from CFP to citrine. The change in the ratio of YFP/CFP is used as indicator for changes in $[Ca^{2+}]_i$.

1.6.2. cAMP/PKA sensor AKAR4

Neurotransmitters and neuromodulators have profound effects on neuronal activity, leading to long-term changes mediated by second messengers (West *et al.* 2002). Activation of several receptors mentioned above, leads to changes in the $[cAMP]_i$ and consequently in the activity of the downstream signaling protein PKA (Fig. 1.5, A). A large number of genetically encoded FRET-based sensors have been used to monitor spatial and temporal compartmentalization of cAMP and its target proteins (Willoughby *et al.* 2006, Sprenger & Nikolaev 2013, Gorshkov & Zhang 2014). The A-kinase activity reporter (AKAR) consists of a phosphoamino acid-binding domain (14-3-3τ) and a PKA-specific substrate comprised between CFP and YFP (Zhang *et al.* 2004). Several variants of AKARs are available: the AKAR4 variant comprises cerulean, which is a brighter CFP variant, and Venus, an improved version of YFP (Depry *et al.* 2011). Increase in the $[cAMP]_i$ activates the PKA, which in turn phosphorylates the AKAR4 sensor resulting in a conformational change. As a result, the distance between the two fluorophores cerulean and venus decreases and the FRET efficiency increases (Fig. 1.5, B). Conversely, dephosphorylation of the AKAR4 sensor via phosphatases reverses the process and the FRET efficiency decreases (Chen *et al.* 2014).

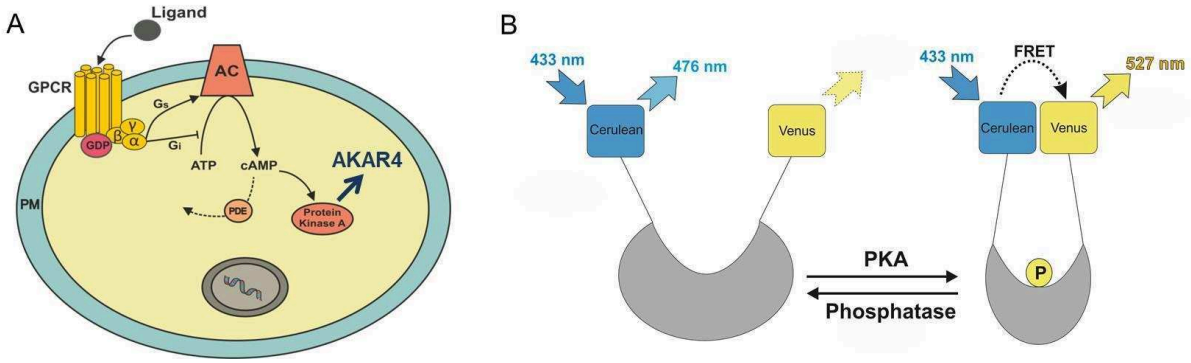


Figure 1.5: PKA phosphorylates the AKAR4 sensor leading to an increase in the FRET efficiency. (A): GPCRs couple to ACy, their activation lead to increase in the $[cAMP]_i$ and PKA activity. Activated PKA phosphorylates the AKAR4 sensor. **(B):** AKAR4 phosphorylation results in a conformational change. The decrease of the emission signal of CFP is accompanied by a mirror-reversed increase in the emission signal of YFP. These changes result in an increase in YFP/CFP ratio, which reflects an increase in PKA activity.

1.7. Aim of the Study

Light adaptation processes occur at every level of the retina. PRs register changes in the ambient light and adjust their sensitivity accordingly. In the retinal network, signal transmission and propagation is modulated by neuromodulators that are released upon light stimulation and act via second messenger cascades. In this study, I address two questions.

First, do retinal neuromodulators like dopamine or adenosine activate internal second messenger cascades? Do these neuromodulators interact within a single cell? In this context, I will study the dynamics of cAMP in primary cultured retinal neurons. This culture is mainly composed of ACs. Using the AKAR4 sensor and lipofection technique, I will investigate changes in cAMP-dependent PKA activity in response to stimulation of DA and AD receptors. The AKAR4 sensor enables monitoring changes in $[cAMP]_i$ via PKA activity with high temporal and spatial resolution.

Second, signal propagation through the retina vitally depends on glutamatergic signaling. Modulating glutamatergic transmission may be an important contribution to adaptation processes. In this part of the study, I will employ a transgenic mouse line that expresses the calcium sensor TN-L15 in GCs (Müller *et al.* 2007). In the intact retina, calcium responses will be imaged in GCs that are stimulated with the agonists at iGluRs AMPA, kainate, and NMDA. It will be tested whether these calcium responses are modulated by retinal neuromodulators like DA, AD, MT and NO.

The molecular mechanisms underlying light adaptation are still not fully understood. There seems to be a complex interaction of many neurotransmitters and the resulting signaling molecules. This study should contribute to a better understanding of adaptation-related signaling processes in the complex system of the retina.

2. Material and Methods

2.1. Animals

Neonatal C57Bl/6N mice at the age of postnatal day 1 (P1) to P5 were used for retinal dissociated cultures. Adult mice (C57Bl/6N) from 2 months and over were used for immunohistochemistry. Mice were obtained from Charles River (Sulzfeld, Germany) or from a local animal breeding facility at the Forschungszentrum Jülich. Transgenic mice expressing the genetically encoded calcium sensor TN-L15 were bred at the local animal facility at the Forschungszentrum Jülich; the mouse line was obtained as a gift from Dr. O. Griesbeck, MPI for Neurobiology, Martinsried, Germany. All experiments were approved and in compliance with the German Law for Protection of Animals, the Forschungszentrum Jülich and the Landesamt für Natur, Umwelt und Verbraucherschutz (LANUV) of North-Rhine Westphalia.

2.2. General buffers and solutions

Chemicals and reagents with purity grade pro analysi (p.a.) were purchased from AppliChem (Darmstadt, Germany), Bio-Techne (Wiesbaden, Germany), Biozym (Hessisch Oldendorf, Germany), Enzo (Lörrach, Germany), GE Healthcare (Freiburg, Germany), Invitrogen (Darmstadt, Germany), Merck (Darmstadt, Germany), MWG-Biotech (Ebersberg, Germany), Qiagen (Hilden, Germany) and Sigma Aldrich (Munich, Germany). Materials and buffers for cell culture, primary cell culture and tissue culture were obtained from Gibco (Darmstadt, Germany). All solutions were prepared with bi-distilled water unless specified otherwise, sterilized by filtration or autoclaved at 121°C for 20 min.

10% sucrose:	10% sucrose with 0.05% NaN_3 dissolved in 0.1 M PB
30% sucrose:	30% sucrose with 0.05% NaN_3 dissolved in 0.1 M PB
Ames high K^+:	20 mM potassium bicarbonate added; pH adjusted to 7.4 with 22.6 mM sodium bicarbonate while bubbling with a gas mixture of 95% O_2 and 5% CO_2

Ames medium:	pH adjusted to 7.4 with 22.6 mM sodium bicarbonate while bubbling with a gas mixture of 95% O_2 and 5% CO_2 (Sigma Aldrich, A1420)
Ampicillin (Amp):	100 mg/ml in H_2O (AppliChem, A0839)
Aqua Polymount:	Polyscience, 18606
Chemiblocker (C) 5%:	diluted 1:20 with 0.1 M PB (EMD Millipore, 2170)
CMF-Hanks':	Calcium-Magnesium-free Hanks' Balanced Salt Solution (Sigma Aldrich, H6648) buffered with 10 mM HEPES (1 M; sterile filtered; pH adjusted to 7.4 with NaOH) to pH 7.4
Competent bacteria:	TOP10F (Invitrogen)
CT:	5% C with 0.5% Triton X
CTA:	5% C with 0.5% Triton X and 0.05% NaN_3
DH10:	500 ml DMEM (GIBCO, 41090-028) supplemented with 10% FBS (GIBCO, 10270-106) and 1% Antibiotic/Antimycotic (100X; GIBCO, 15240-062)
$DMEM_{neuro}$:	DMEM (GIBCO, 61965-026) supplemented with 1% Antibiotic-Antimycotic (100x; GIBCO, 15240-062), 1% Sodium-Pyruvate (Sigma Aldrich, S8636), 25 mM HEPES (1 M; sterile filtered), 1% N2 Supplement (GIBCO, 17502-048) and 10% Fetal Bovine Serum (GIBCO, 10270-106).
DNA-Ladder:	Lambda (λ)-DNA/*Eco*RI+*Hind*III Marker (Thermo Scientific, SM0191)
ES_{neuro}:	145 mM NaCl, 5 mM KCl, 1 mM $CaCl_2*2H_2O$, 1 mM $MgCl_2*6H_2O$, 10 mM HEPES, 10 mM D-Glucose*H_2O; adjusted to pH 7.4

ES_{normal}:	120 mM NaCl, 5 mM KCl, 2 mM $CaCl_2$*$2H_2O$, 2 mM $MgCl_2$*$6H_2O$, 10 mM HEPES, 10 mM D-Glucose*H_2O; adjusted to pH 7.4
Fixative:	4% Paraformaldehyde (PA) in PB
Fluo4-AM:	Invitrogen, F14201; dissolved in dimethyl sulfoxide (DMSO) to a final concentration of 2 mM
Hank's:	136.89 mM NaCl, 5.36 mM KCl, 1.25 mM $CaCl_2$*$2H_2O$, 0.81 mM $MgCl_2$*$6H_2O$, 10 mM HEPES, 5.55 mM D-Glucose*H_2O; adjusted to pH 7.4
HEPES:	1 M in H_2O bidest adjusted to pH 7.4 with NaOH
Kanamycin:	Antibiotic derived from *Streptomyces Kanamyceticus* (Sigma Aldrich, K1377)
Laminin:	10 µg/ml in H_2O (Invitrogen, L2020)
LB agar:	5 g/l NaCl, 2 g/l $MgSO_4$*7 H_2O, 10 g/l NZ amine, 5 g/l yeast extract, 7.5 g/l Agarose
LB medium:	1% Baktotrypton, 0.5% yeast extract, 1% NaCl
Lipofectamine 2000:	Transfection reagent (Invitrogen, 11668-019)
M10:	500 ml MEM (GIBCO, 41090-028) supplemented with 1% Antibiotic/Antimycotic (100X; GIBCO, 15240-062), 10% FBS (GIBCO, 10270-106), and 1% MEM not essential amino acids (GIBCO, 11140-035)
OPTI-MEM:	Gibco, 51985-026
Papain:	dissolved in CMF-Hanks to 20 U/ml (Worthington, LK003178)
PB:	81 mM Na_2HPO_4, 19 mM NaH_2PO_4, pH 7.4
PBS:	130 mM NaCl, 7 mM Na_2HPO_4, 3 mM NaH_2PO_4, pH 7.4
PDL:	0.1 mg/ml poly-D-Lysine (Sigma, P6407) in H_2O

PLL:	0.1 mg/ml poly-L-Lysine (Sigma, P1399) in H_2O
SYBR® Safe DNA Gel Stain:	Invitrogen, S33102
TAE buffer:	40 mM Tris/Acetate pH 7.5, 1 mM EDTA
TE buffer:	10 mM Tris/HCl pH 7.5, 1 mM EDTA; pH 8.0
Trypsin-EDTA:	Gibco, 253000-054

2.3. Molecular biology

2.3.1. Plasmids

pcDNA3.1:	Invitrogen, V795-20
pCMV6:	Obtained from Hannover, Germany

2.3.2. Kits

Ligation:	Rapid DNA Ligation Kit (Thermo Fisher Scientific, K1422)
Maxiprep:	QIAGEN Plasmid Maxi Kit (Qiagen, 12165)
Miniprep:	NucleoSpin® Plasmid (Macherey & Nagel, 740588-250)
PCR clean-up:	NucleoSpin® gel and PCR clean-up (Macherey-Nagel, 740609-250)

2.3.3. Transformation of competent cells

The process of transformation consists in introducing a foreign deoxyribonucleic acid (DNA) into a cell. It enables storing and replicating plasmids. Competent bacteria (TOP10F) were transformed with plasmid DNA that carries a resistance gene to antibiotics, such as ampicillin (Amp) or Kanamycin (Kan), for use as a selectable marker in bacteria. Frozen competent TOP10F cells were gently thawed on ice. Fifty µl of competent cells were incubated with 5 µl of plasmid DNA for 10 min on ice. Cells were then incubated in a water bath at 42°C for 1 min and immediately returned to ice for additional 5 min. Then, 200 µl LB medium was added and the cells were incubated at

37°C for 20 min. In this step, the transformed cells amplify the transformed plasmid and begin to express the antibiotic resistance gene before encountering the antibiotic. After incubation, bacteria were plated onto LB agar plates with appropriate selection antibiotics using a fire polished glass pipette. Bacterial colonies grew during overnight incubation at 37°C. On the following day, grown clones were picked using an autoclaved toothpick and grown in tubes with 5 ml LB medium containing 1:1000 diluted selection antibiotics (Amp or Kan) in a roller shaker at 37°C overnight. For maxiprepping of DNA (maxi-culture), 500 ml LB medium with the appropriate antibiotic was inoculated with a mini culture and shaked at 37°C overnight. The next morning, the mini- or maxi-culture was used for DNA isolation.

2.3.4. DNA isolation

The NucleoSpin® gel and PCR clean-up kit (Macherey-Nagel) was used for DNA isolation from mini-cultures. Following the manufacturer's protocol, mini-cultures were pelleted using a standard benchtop microcentrifuge at 11000 rpm for 30 s. Sample solutions were mixed with a succession of buffers, then transferred onto a NucleoSpin® column and centrifuged at 11000 rpm for 10 min. Spin column membranes were washed with the provided buffers and air dried. For DNA elution, the membrane was incubated with 30 µl TE buffer at room temperature (RT) for 1 min. For DNA collection, the NucleoSpin® column was centrifuged at 11000 rpm for a min. For further processing the DNA was eluted in H_2O. For DNA extraction from maxi-cultures, the QIAGEN Plasmid Maxi Kit (Qiagen) was used according to the manufacturer's protocol.

2.3.5. Quantification of nucleic acids by spectroscopy

For the quantification of DNA preparations, DNA concentration [DNA] was determined using the NanoDrop 2000 spectrophotometer (Thermo Fisher Scientific). Before measuring the [DNA], the spectrophotometer had to be blanked using the solution of the eluted DNA, TE or H_2O (see DNA isolation). Nucleic acids (DNA or RNA) maximally absorb at 260 nm, whereas proteins depict a maximal absorbance at 280 nm. Thus, the ratio of nucleic acid to protein is an indicator of the purity of the DNA sample and the higher the absorbance, the higher the [DNA]. An absorption value of 1.0 amounts a [DNA] of 50 µg/ml. A good purity ranges between 1.8 and 2.0.

2.3.6. Restriction digestion

Restriction enzymes cleave double-stranded DNA at specific target sequences, called restriction sites, into fragments. Since the size of the vector backbone (pcDNA3.1 or pCMV6) and the plasmid insert are known, specific restriction enzymes are chosen in such a way that the plasmid is cut into specific sized fragments. The resulted fragments are then analyzed by gel electrophoresis.

Restriction digests were performed with FastDigestTM Restriction Endonucleases and the reaction buffers according to manufacturer's protocol (Thermo Fisher Scientific). Restriction digests were carried out at 37°C for 45-60 min using an end volume of 20 µl with enzyme units not exceeding 10% of the total sample (Table 2.1). The digested DNA was separated onto agarose gels.

	Volume
DNA	0.5 µl
Fast Digest Enzyme 1	0.2 µl
Fast Digest Enzyme 2	0.2 µl
10X FastDigest Green Buffer	1 µl
H_2O bidest	Ad to 20 µl
Total volume	20 µl

Table 2.1: Composition of the mixture of the restriction digestion

2.3.7. Agarose gel electrophoresis

Gel electrophoresis is the standard procedure for separating DNA fragments based on their size and charge for visualization and purification. DNA fragments are separated using an electrical field that move the negatively charged DNA towards a positive electrode. Shorter fragments migrate faster than longer ones through the pores of the gel, this phenomenon is called sieving. The size of the pores in the agarose gel depends on the amount of the agarose concentration used. The size of the fragments needed to be separated ranges between 1000-8000 base pairs (Bp), 1% agarose gels were used for

the separation of DNA. Agarose was heat-dissolved in TAE buffer at 60°C. Visualization of DNA bands was achieved by adding SYBR® Safe DNA Gel Stain, a highly sensitive stain, to the agarose gel cooled down to 50°C. This dye has fluorescence excitation maxima at 280 and 502 nm and an emission maximum at 530 nm. Agarose gel was poured into a gel tray harboring well combs and let to solidify at RT. Samples were mixed to the loading buffer and loaded into the sample bags of the gels, one bag was left for the DNA ladder λDNA/EcoRI+HindIII Marker (Thermo Fisher Scientific). The electrophoresis was run in TAE buffer at 90-120 V. For analyzing the size of the separated DNA fragments, the gel was excited at 280 nm and detected at 530 nm using the Biorad Gel DocTM XR+ System (Bio-Rad; Munich) and images were obtained using Image Lab software (Bio-Rad). The resulting DNA bands were compared to the bands from the DNA ladder for identification of DNA sizes (Fig. 2.1).

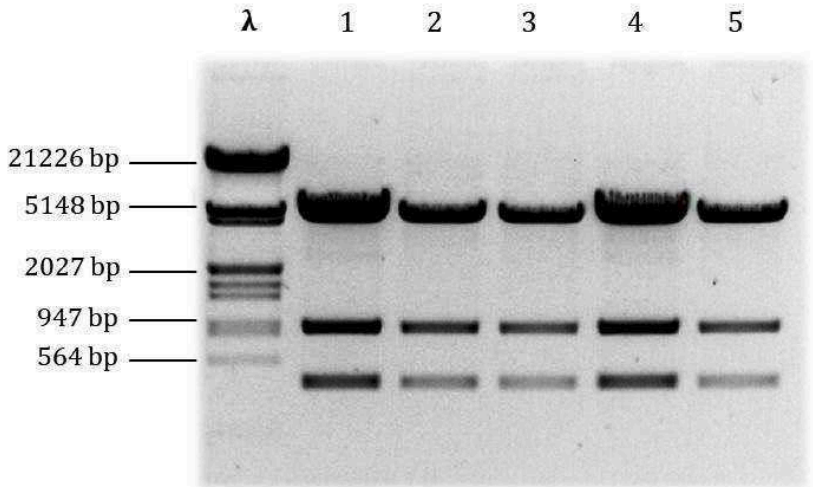


Figure 2.1: DNA bands of the different clones showed similar results. The DNA ladder λDNA/EcoRI+HindIII (λ) served as a marker to identify the size of the bands obtained from the single clones. Here exemplarily shown for the mouse clone of adenosine A2AR.

2.4. Cell cultures

2.4.1. Stable cell line culture

2.4.1.1. Human Embryonic Kidney 293 cells

Human Embryonic Kidney 293 (HEK293) is a cell line derived from human embryonic kidney cells. HEK293 cells were generated by transformation of cell cultures with adenovirus 5 DNA (Graham *et al.* 1977). They were cultured in M10 or DH10 medium at 37°C, 5% CO_2 and 95% relative humidity in 10 cm petri dishes. The generation time of HEK293 cells takes approximately 24 hours (hrs), the medium was

exchanged every second day and the cells were split twice a week at a confluency of about 90%. Cells were detached from the culture dish with 1 ml trypsin w/EDTA at 37°C. Trypsination was stopped by adding 10 ml warm medium. Cells were dissociated by pipetting the solution up and down. They were then pelleted by 5 min centrifugation at 200 g and 22°C. The cell pellet was resuspended in 10 ml medium and the cell number was determined by a Neubauer-hemocytometer (cell chamber). Cells were seeded at a density of approximately 8-10 x 10^5 cells per 10 cm dish.

After 30 passages, cells were discarded and a new aliquot of frozen cells was thawed in a 37°C water bath. To remove DMSO, cells were diluted in 10 ml medium and centrifuged at 200 g and 22°C for 5 min. The cell pellet was resuspended in 10 ml medium and transferred to 10 cm petri dishes.

2.4.1.2. Preparation of coverslips

For cultivation of cells, single glass coverslips (Ø 13 mm) were placed in each well of a 24 multiwell plate (MWP). Each coverslip was covered with 500 µl of poly-L-Lysine (PLL) solution for approximately 2 hrs at RT. The PLL stock solution (1 mg/ml) was diluted to 1:10 with sterile H_2O. After coating, the PLL solution was removed and the coverslips were washed twice with H_2O bidest and dried before cells were seeded.

2.4.1.3. Liposome-mediated transfection

Cells were transfected using Lipofectamine 2000, a cationic liposome based reagent, at a density of 4 X 10^5 cells/coverslip. The cationic liposomes, with a positively charged head group, form complexes with negatively charged nucleic acids and facilitate their condensation. The liposomes, with positive charges at their surface, mediate the interaction and the fusion with the negatively charged plasma membrane of the cells. The nucleic acids cross into the cytoplasm and reach the nucleus for gene expression. The transfection mixture was prepared by mixing 100 µl OPTI-MEM, 1 µl Lipofectamine and 0.5–1 µg DNA (depending on construct) per well (Table 2.2). The mixture was vortexed for 10 sec and 100 µl were added gently to each well containing 200 µl medium. Cells were incubated at 37°C, 5% CO_2 and 95% relative humidity for 1 hr. Afterwards, the transfection mixture was removed; the cells were shortly rinsed with warm fresh medium and then 500 µl medium per well were added. Cells were incubated

at 37°C, 5% CO_2 and 95% relative humidity until the following day, when they were used for imaging experiments.

Construct	Backbone	Coded protein	Origin
AKAR4	pcDNA3	PKA activity sensor AKAR4	Dr. S. Mehta, Johns Hopkins University
D1R-GFP	pCMV6	GFP-tagged D1R	Origene, MG226226
Adora2a (Myc-DDK-tagged)	pCMV6	Adenosine A2A receptor	Origene, MR226318
Adora2b (Myc-DDK-tagged)	pCMV6	Adenosine A2B receptor	Origene, MR227279

Table 2.2: cDNA used for transient transfection of HEK293 cells or retinal primary cultures

For immunocytochemistry (ICC) cells were fixed in paraformaldehyde (PA): for fixation, the medium was removed and 250 µl of 4% PA were added to each well. Fixation was carried out for 5 min at RT, then the fixative was removed and the cells were washed with 0.1 M PB twice for 10 min each. The cells were stored at 4°C in PB + 0.05% NaN_3.

The stable cell line HEK293 was used during the preliminary proof of principle experiments conducted to test the functionality of the AKAR4 sensor in combination with D1s or A2 receptors. Furthermore, calcium images were conducted using this cell line for a better understanding although these results were not presented in the results part of this thesis.

2.4.2. Primary culture of dissociated retinal neurons

2.4.2.1. Preparation of coverslips

The day before seeding the cells, sterile coverslips (Ø 13 mm) were coated with poly-D-Lysine (PDL). For primary culture PDL was favored over PLL since it is less prone to protease-mediated breakdown. The coverslips were placed onto a piece of parafilm (Bemis Company Inc., Oshkosh, WI) in a petri dish to avoid overflow of the PDL solution. Coverslips were coated with 180 µl of a 0.1 mg/ml PDL stock solution and incubated at RT overnight, with the UV-light turned on for 2 hrs to ensure sterility. On

the following day, the coverslips were washed twice with sterile distilled water and then incubated with 180 µl of a 10 µg/ml laminin stock solution at RT for 2-3 hrs.

2.4.2.2. Isolation of retinae

Neonatal mouse pups of the C57BL/6N strain at the age of P1 to P4 were sacrificed by decapitation for retina preparation. The preparation procedure was carried out under semi-sterile conditions: the preparation surface and all instruments were disinfected with 70% EtOH. Eyes were carefully removed using curved scissors by cutting the optic nerve and transferred to a petri dish containing sterile warm Hank's solution. The eyeball was pierced between the cornea and the sclera with a fine injection needle. Along the *ora serrata* the eyeball was cut open using a micro dissecting scissor. Following, the anterior part (lens, cornea and vitreous body) was separated from the eyecup. With a pair of forceps, the retina was isolated by removing the eyecup and cutting the optic nerve. The retinae (2-8) were then transferred into a 1.5 ml Eppendorf tube filled with 1 ml of 37°C warm Hank's solution. The following steps were performed under sterile conditions in a laminar flow hood.

2.4.2.3. Dissociation of isolated retinae

The 1 ml Hank's solution was exchanged by 1 ml warm Calcium-Magnesium-free Hank's Balanced Salt Solution (CMF-Hank's, Sigma Aldrich) and retinae were incubated for 5 min at 37°C in the water bath. Following, the CMF-Hank's solution was removed carefully and 1 ml pre-warmed papain solution (20 units of papain were dissolved in 1 ml CMF Hank's) was added and retinae were incubated for 20 min at 37°C in the water bath. Afterwards, the papain solution was removed carefully and the retinae were washed twice with pre-warmed $DMEM_{neuro}$ to inactivate the papain. Cells were gently dissociated in 1 ml of fresh $DMEM_{neuro}$ by pipetting the solution up and down several times using a 100 µl plastic tip (Nerbe-Plus, Germany). When the retinae were fully dissociated the cell number was determined in a hemocytometer. Before the cells were seeded, the laminin solution was removed from the coverslips without letting them dry completely. Then, 150 µl of adjusted cell suspension containing 300000 cells were added onto the coated surface of every coverslip and the petri dishes with the coverslips were kept at 37°C, 5% CO_2 and 95% relative humidity for 1–2 hrs to let the cells attach to the surface of the coverslips. Afterwards, the cell suspensions and the coverslips were

transferred into a 24 MWP and the total volume was adjusted to 500 µl per well. The medium was fully exchanged by fresh medium after 4 days, and then half of the medium every second day. The primary cultures were kept up to 10 days in vitro (DIV).

2.4.2.4. Liposome-mediated transfection

Transient transfection of dissociated retinal neurons was performed on 3 to 7 DIV by using Lipofectamine® 2000 transfection reagent. Similar to the transfection assay with HEK293 cells, a mixture of 100 µl OPTI-MEM, 1 µl Lipofectamine 2000 and 1 µl AKAR4-DNA (corresponding to 0.5 µg) per well to be transfected was prepared. After short vortexing of the mixture, the medium of each well was reduced to 200 µl and 100 µl of the transfection mixture were added. The cells were incubated at 37°C, 5% CO_2 and 95% relative humidity for 1 hr. After incubation, the solution was aspirated, the cells were shortly washed with pre-warmed fresh $DMEM_{neuro}$ and then 500 µl of $DMEM_{neuro}$ were added to each well. The cells were used on the following day for imaging experiments.

2.4.2.5. Fixation of dissociated retinal neurons

Dissociated retinal neurons of 4 to 8 DIV were fixed for immunocytochemistry. For fixation, the medium was removed and 250 µl of 4% PA were added to each well. Fixation was carried out for 5 min at RT, then the fixative was removed and the cells were washed with 0.1 M PB twice for 10 min each. The cells were stored at 4°C in PB + 0.05% NaN_3.

2.5. Widefield-imaging

2.5.1. Imaging setup

FRET-based imaging experiments were performed using a custom-built setup also used for calcium imaging experiments. The microscope used was an upright microscope of the Carl Zeiss microscope company (Examiner.Z1) with a 40 X/1.0 water objective. Two filter sets were used: the filter set 47 (489047-0000) and the filter set 38 (1031-346), both from Zeiss. The light-emitting diode (LED) generated excitation lights with 420 nm and 470 nm wavelengths (Zeiss). Emitted light was detected by an EMCCD camera (iXon; Model No. DV885JCV-VP; cooled EMCCD, Andor Technology).

2.5.2. Perfusion chamber

All imaging experiments were performed at RT using a home-built perfusion chamber. A coverslip with adherent cells was carefully placed into the center of the measuring chamber containing solution (ES: HEK293 cells; ES_{neuro}: dissociated retinal neurons). During measurements, the perfusion chamber was continuously perfused with solution using a gravity-driven multichannel perfusion system. Up to eight different solutions, including the washing solution, could be applied. The solutions were filled into syringes (50 ml) placed vertically above the perfusion chamber; after opening the syringes, the solution entered the measuring chamber via a plastic tube with a flow rate of 2.5-3.5 ml/min, and was aspirated from the chamber by a roller pump through a second plastic tube. This flow rate allows a rapid exchange of the solutions in the measuring range (approximately 30 sec).

2.5.3. Calcium imaging with Fluo-4

In order to monitor changes in $[Ca^{2+}]_i$, cells were loaded with the synthetic calcium indicator Fluo-4-AM (Invitrogen, Germany). The green-fluorescent indicator is able to cross the plasma membrane due to the protection of its charged groups by acetoxymethyl (AM) esters. Once inside the cell, cellular esterases cleave the AM groups and the indicator cannot leave the cytoplasm. The loading solution was composed of 1.5 µl Fluo-4-AM (2 mM in DMSO) per 500 µl ES_{neuro}. A coverslip with adherent cells was incubated for 25-30 min at RT in the dark. Afterwards, the coverslip was directly transferred to the custom-made measuring chamber and continuously perfused with ES_{neuro} via a gravity-driven perfusion system. Calcium imaging experiments on retinal cultures were performed in order to study the iGluR-induced calcium responses in cultured retinal cells, and the effects of activation of ARs. The results were not presented in this thesis.

2.5.4. Data acquisition

Fluo-4 is excited maximally at a wavelength of 494 nm; the emission maximum is at 506 nm. The fluorescence intensity increases upon Ca^{2+}-binding about 100 fold (Invitrogen). Using the setup imaging described above, cells loaded with Fluo-4-AM were excited at 470 nm and the LED intensity ranged between 2 and 4%. The excitation

light was passed through a 470/40 nm band pass filter (BPF) whereas the emission light was passed through a 525/50 nm BPF. Excitation and emission light were separated by a dichroic mirror FT 495 (Carl Zeiss, Germany). Emitted light was finally detected by an iXon cooled EMCCD (Andor Technology). During measurements, cells were continuously excited and perfused with ES_{neuro} and the desired agents. Images were captured at 0.5 Hz and stored as stacks of TIFF files.

2.5.5. Data evaluation

ImageJ software (NIH) was used for image analysis. The original data were initially processed by choosing a region of interest (ROI) in the background of the image, where there are no cells. The fluorescence intensity of this background was subtracted from the fluorescence intensity of the ROI of the cell of interest. In order to separate real changes in $[Ca^{2+}]_i$ and variations due to dye concentration, spatial variation in cell thickness and detection efficiency, the fluorescence signal was calculated as relative fluorescence change ΔF/F using the following equation:

$$\frac{\Delta F}{F} = \frac{(F - F_0)}{F_0}$$

where F_0 denotes the background-subtracted pre-stimulus fluorescence level (20 sec before stimulus) and F the background-subtracted fluorescence level after stimulus (Yuste & Konnerth 2005). After generating diagrams, statistical analysis was conducted in Excel (Microsoft 2010), Origin (OriginPro 2018G) and/or SigmaPlot (SigmaPlot 12.0). In order to compare different responses to each other, the amplitude values of the responses were defined by calculating the differences between peak maximum and the baseline shortly before stimulation. The values were normalized to that of the first response and a quantitative evaluation was performed using SigmaPlot (SigmaPlot 12.0). The response amplitudes of the fluorescence changes under experimental conditions were compared to the response amplitudes under control conditions (ctrl). The difference was considered as statistically not significant (n.s.) at $p>0.05$, as weakly significant at $p\leq0.05$ (*), as moderately significant at $p\leq0.01$ (**) and as highly significant at $p\leq0.001$ (***).

2.6. FRET-based imaging

2.6.1. FRET-based imaging in TN-L15 wholemount retina

Retinae of TN-L15 adult mice were deeply anesthesized with isoflurane (Piramal Healthcare Ltd, UK) and decapitated using scissors. Eyes were quickly enucleated and transferred into a small petri dish with oxygenated Ames solution. Under a binocular microscope, the eyeball was locally opened by a fine injection needle. The eyeball was cut open along the *ora serrata* using fine scissors. Following, the front part of the eye was discarded from the posterior part with the retina. With a pair of forceps, the retinae were isolated from the eyecup, and then each retina was cut into three pieces. One piece of the retina was used for one single imaging experiment, while the remaining pieces were kept in darkness in oxygenated Ames solution for the following experiments. Using a small spoon one piece of the retina was transferred into the measuring chamber containing Ames solution. The PR side was positioned facing the chamber bottom; and the retina was flattened and fixed by placing carefully a custom-made harp (U-shaped strand covered with nylon strings) on the GC side. During the whole measurement the retina was perfused with oxygenated Ames (Sigma Aldrich, Germany) solution with or without the tested reagents.

2.6.2. FRET-based imaging in dissociated retinal neurons

A coverslip with adherent cells, which were transiently transfected with the AKAR4 sensor 24 hrs prior to measurement (see chapter 2.4.2.4), was carefully transferred into the custom-made measuring chamber. During the whole measurement, cells were continuously perfused with ES_{neuro} with or without the tested agents.

2.6.3. Data acquisition

The excitation/emission maxima of the fluorophores CFP and YFP are 435/485 nm and 508/524 nm respectively. The AKAR4 sensor was excited at a wavelength of 420 nm with an LED intensity of 3-5%. The LED light was reflected by a dichroic mirror FT 455 (Carl Zeiss, Germany), where the excitation and emission light was separated. The emission light was then passed through an image splitter (505 nm), allowing the separation and simultaneous detection of CFP and YFP emission by the iXon camera (Andor Technology). During the whole measurement, cells were always exposed to

excitation light. Images were stored as stacks of TIFF files and the acquisition rate was set to 0.5 Hz.

2.6.4. Data evaluation

The original data were processed using a software plugin based on Matlab (MathWorks) which was programmed by Dr. Luru Dai (formerly ICS-4, FZ Jülich). Each image consisted of two partial images; the CFP and the YFP fluorescence, the correlation between both signals allows the assessment of the changes occurring in the cells. Within the program, the background-subtracted fluorescence level of a defined ROI in both CFP and YFP images was determined and a ratio was calculated as YFP/CFP. Afterwards, the ratio (YFP/CFP) was further processed using the following formula in Excel (Microsoft 2010):

$$\frac{(R_t - R_0)}{R_0}$$

where R_t denotes the ratio at time t, and R_0 the base line ratio shortly before stimulation. The ratio was plotted graphically over time using Origin (OriginPro 2018G). When using the AKAR4 sensor, a rise in the YFP/CFP ratio reflects an increase in PKA activity (see chapter 1.6.2), which depends on a rise in $[cAMP]_i$. In the case of the TN-L15 sensor, a rise in the YFP/CFP ratio reflects an increase in $[Ca^{2+}]_i$ (see chapter 1.6.1). After generating diagrams, statistical analysis was conducted in Excel (Microsoft 2010), Origin (OriginPro 2018G) and/or SigmaPlot (SigmaPlot 12.0). Further data processing was performed as described in chapter 2.5.5.

2.7. Immunochemistry

Immunostaining is a technique used to detect protein expression. Immunostaining was performed at RT by using antigen-specific primary antibodies and fluorescently conjugated secondary antibodies. Using primary antibodies directed against different antigens and raised in different species in conjunction with highly cross-adsorbed secondary antibodies labeled with different fluorophores allows simultaneous detection of several antigens.

2.7.1. Immunocytochemistry

ICC staining of cultured cells (HEK293 and dissociated retinal neurons) was performed on coverslips in a 24 MWP. Before staining, PB + 0.05% NaN_3 was removed, fixed cells were incubated with primary antibodies diluted in CTA (Table 2.3) for 1 h. After incubation, cells were washed twice with 0.1 M PB for 10 min each to remove unbound primary antibodies. Afterwards, cells were incubated with fluorescent-labeled secondary antibodies diluted in CTA (Table 2.4) for 30 min in the dark. After that, cells were again washed twice with 0.1 PB for 10 min each. Finally, coverslips were embedded in Aqua Polymount (Polysciences, Warrington, USA) so that the side with the cells faces the Superfrost plus glass slides (J1800AMNZ, Thermo Fisher Scientific). Stained cultures were stored at 4°C in the dark.

To stain nuclei, TO-PRO3 (Invitrogen, Germany) was added to the secondary antibody solution. TO-PRO3 intercalates into the DNA and thus stains the nuclei of all the cells allowing cell counting especially when determining the transfection rate of the cells (data not shown). The stained sections were stored at 4°C and examined with a confocal laser scanning microscope (CLSM).

2.7.2. Immunostaining of retinal cryosections

2.7.2.1. Isolation and fixation of retinae

Adult C57BL/6N mice were deeply anesthesized with isoflurane (Piramal Healthcare Ltd, UK) and decapitated using scissors. Eyes were quickly enucleated and transferred into a small petri dish with 4°C Hank's solution. Under a binocular microscope, the eyeball was locally opened by a fine injection needle. The eyeball was cut open along the *ora serrata* using fine scissors. Following, the front part of the eye was discarded from the posterior part with the retina. Retinae were kept in the eyecup during fixation and subsequent cryoprotection. The eyecups were fixed for 30 min in 4% PA at RT. After fixation, the eyecups were washed twice with 0.1 M PB for 10 min each and cryoprotected by infiltration in graded sucrose: 10% for 1 h and 30% overnight at 4°C, respectively.

2.7.2.2. Sectioning

Retinae were carefully isolated from the eyecups and flat mounted on a glass slide covered with a piece of parafilm. The remaining sucrose solution was removed using a filter paper and the retinae were covered with NEG50TM (Thermo Fisher Scientific, Germany), an optimal cutting temperature (OCT) compound, and immediately frozen in the cryostat at -50°C (Microm HM 560; Thermo Fisher Scientific, Germany). Frozen retinae were mounted on a specimen stage cooled down to -15°C and were vertically sectioned at 18 µm thickness with a -20°C cold blade. Cryosections were collected on Superfrost plus glass slides, and were either directly used for immunostaining or stored at -20°C for later usage.

2.7.2.3. Immunostaining of cryosections

Retinal cryosections on glass slides were encircled with a grease pen (Fettstift, Liquid Blocker; Science Services, Germany) that allows using small incubation volumes (100-150 µl). Retina sections were incubated with primary antibodies (Table 2.3) diluted in CTA overnight at RT in a humid chamber. On the following day, sections were washed twice in 0.1 M PB for 10 min each, and then incubated with secondary antibodies (Table 2.4) diluted in CTA for 1 hr in the dark at RT. After washing twice with 0.1 PB for 10 min each, sections were covered with a drop of Aqua Polymount (Polysciences, Warrington, USA) and covered with a glass coverslip (VWR, 631-0144).

2.7.2.4. Antibodies

Primary ABs	Antigen	Host	Dilution	Origin
AB5585	Recoverin	rb	1:2000	Chemicon, ab5585
CaBP	Calbindin	rb	1:2000	Abcam, ab11426
Cal	Calretinin	gt	1:3000	Chemicon, ab1550
ChaT	Cholinacetyl-transferase	ms	1:400	Millipore, MAB5270
D1mono	Dopamine receptor 1	rt	1:500	Sigma, d187

D2	Dopamine receptor 2	rb	1:100	Millipore, ab5084p
GAD65	Glutamic acid decarboxylase isoform 65	ms	1:4000	Chemicon, ab26113
GAD65/67	Glutamic acid decarboxylase isoforms 65 and 67	rb	1:1000	Chemicon, ab1511
GFP	Green fluorescent protein	ch	1:1000	Chemicon, ab16901
		rb	1:8000	Abcam, ab290
Gly	Glycine	rt	1:3000	(Pow *et al.* 1995)
GlyT1	Glycine transporter 1	gt	1:2000	Chemicon, ab1770
$G_o\alpha$	G-protein alpha o	ms	1:16000	Chemicon, mab3073
PKARIIb	Protein kinase A	rb	1:500	Chemicon, ab1614
		ms	1:2000	BD Biosciences, p54720
PKCα	Protein kinase C alpha	rb	1:2000	Santa Cruz, sc208
Syt2	Synaptic vesicle associated protein (synaptotagmin-2)	ms	1:1000	Zebrafish International Resource Center, ZDB-ATB-081002-25
TH	Tyrosine hydroxylase	ms	1:500	Sigma, t2928
		ch	1:500	Neuromics, ch23006
vGlut1	Vesicular glutamate transporter 1	gp	1:30000	Chemicon, ab5905

Table 2.3: List of the primary antibodies used in this project. Antibodies are listed including the appropriate dilution, species in which they were raised and the sources. Abbreviations: ABs: antibodies; ch: chicken; gt: goat; gp: guinea pig; ms: mouse; rb: rabbit; rt: rat.

Secondary ABs	Dilution	Origin
gt anti rt A488	1:500	Invitrogen, A11006
gt anti rb A488	1:500	Invitrogen, A11034
d anti gt Cy2	1:400	Dianova, 705-225-147
d anti gp Cy2	1:400	Dianova, 706-225-148
d anti rb Cy2	1:400	Dianova, 711-225-152

d anti ms Cy3	1:100	Dianova, 715-165-150
d anti rb Cy3	1:100	Dianova, 711-165-152
d anti rt Cy3	1:500	Dianova, 712-165-153
d anti rb Dy649	1:500	Dianova, 711-495-152
d anti rt Cy5	1:200	Dianova, 712-175-153
gt anti ch Dy549	1:800	Dianova, 103-505-155

Table 2.4: List of the secondary antibodies used in this project with the appropriate dilution and sources where they were purchased. Abbreviations: ABs: antibodies; ch: chicken; d: donkey; gt: goat; gp: guinea pig ms: mouse; rb: rabbit; rt: rat.

TO-PRO®3 staining was conducted during the incubation of the secondary antibodies in a 1:1000 dilution.

2.8. Confocal Laser Scanning Microscopy

CLSM allows scanning of optical sections with high resolution and depth selectivity. This technique scans a sample sequentially point by point at different depths; the intensity of lasers and filter settings were controlled by the Leica LAS AF software. The microscope (TCS SP5 II, Leica Microsystems, Germany) was equipped with an Argon laser, that generates the wavelengths of 458 nm (for CFP) and 488 nm (for Cy2 and GFP), and three Helium-Neon lasers which generate the wavelengths of 543 nm (for Cy3), 594 nm (for Alexa594) and 633 nm (for Cy5, Alexa647, DyLight649 and TO-PRO®3). In many cases, serial pictures of different focal planes were obtained (so-called z-stacks) and the distance between different focal planes was set at about 0.5 µm. The sequential scanning mode was used to rule out crosstalk between the fluorescence detection channels in multiple stained samples. Band pass filters of 465-490 nm for CFP, 500-540 nm for Cy2 and GFP, 555-605 nm for Cy3, 610-635 nm for Alexa594, and 650-750 nm for Cy5, Alexa647, DyLight649, TO-PRO®3 were used to allow signals between the two given wavelengths to pass. All fluorescence micrographs were artificially colored. When necessary, the recorded z-stacks were converted into 2D images using the software ImageJ (tool: “Maximum Intensity Projection”, MIP) to show the structures of the cells and their processes within one image as a projection. Optical images were acquired with 20x/0.70 oil or 63x/1.32-0.6 oil immersion objectives at a resolution of

1024x1024 pixels. For image processing the Leica LAS AF software, ImageJ and Adobe Photoshop were used (Table 2.6).

2.9. Pharmaceuticals

Pharmaceutical	Stock	Biological function	Distributor
Dopamine hydrochloride	10 mM in H_2O	Dopamine receptor agonist	Sigma Aldrich, H8502
SKF 38939	10 mM in H_2O	D1-receptor agonist	Sigma Aldrich, D047
Quinpirole	20 mM in H_2O	D2-receptor agonist	Sigma Aldrich, Q102
CPA	100 mM in DMSO	A1-receptor agonist	Tocris, 1702
DPCPX	10 mM in DMSO	A1-receptor antagonist	Tocris, 0439
GR 79236	100 mM in H_2O	A1-receptor agonist	Tocris, 1957
CGS 21680 hydrochloride	20 mM in DMSO	A2A-receptor agonist	Tocris, 1063
Adenosine	10 mM in H_2O	Adenosine receptor agonist	Sigma Aldrich, A9251
Adenosine	10 mM in H_2O	Adenosine receptor agonist	Tocris, 3624
H89	20 mM in H_2O	Protein kinase A inhibitor	Tocris, 2910
Melatonin	20 mM in DMSO	Melatonin receptor agonist	Sigma Aldrich, M5250
SNAP	100 mM in DMSO	NO donor	ENZO, BML-CN210
L-Glutamat	50 mM in H_2O	Glutamate receptor agonist	Sigma Aldrich, G1251
AMPA	5 mM in H_2O	AMPA receptor agonist	Sigma Aldrich, A0326
Kainate	20 mM in H_2O	Kainate receptor agonist	Sigma Aldrich, K0250
NMDA	100 mM in H_2O	NMDA receptor agonist	Sigma Aldrich, M3262

Table 2.5: List of the pharmaceuticals used in this study. AMPA: α-amino-3-hydroxy-5-methyl-4-isoxazolepropionic acid; CPA: *N*-Cyclopentyladenosine; DPCPX: 1,3-dipropyl-8-cyclopentylxantine; NMDA: *N*-methyl-D-aspartate; SNAP: S-Nitroso-N-acetyl-DL-penicillamine.

2.10. Software

Software	Purpose	Producer
Adobe Photoshop	Image processing	Adobe
Andor Solis X-1707	Data aquisition	Andor
Corel Draw X6	Image processing	Corel
Excel Professional Plus 2010	Data analysis	Microsoft
Image J	Data analysis, Image processing	National Institutes of Health (NIH)
LAS AF	Data acquisition, Image processing	Leica Application Suite X
Matlab	FRET data analysis	The MathWorks
OriginPro 2018G	Statistical analysis, Diagrams	OriginLab
Power Point Professional Plus 2010	Image processing	Microsoft
SigmaPlot10	Statistical analysis	Systat Software GmbH
Vector NTI	Sequence analysis Restriction analysis Plasmid construction	Life Technologies
Word Professional Plus 2010	Word processing	Microsoft

Table 2.6: List of the software used for data acquisition, processing and evaluating.

3. Results

3.1. Impact of neuromodulators on glutamate-induced changes in $[Ca^{2+}]_i$ in GCs of the intact retina

This chapter describes the action of glutamate receptor agonists on ganglion cells (GCs) of the intact retina, and how this action is modulated by the retinal neuromodulators dopamine (DA), adenosine (AD), melatonin (MT) and nitric oxide (NO). GCs are the output neurons of the retina, they collect and integrate all the information coming from the retinal network and relay it to higher visual centers in the brain via the optical nerve. At least 32 different functional types of GCs in the mouse retina have been distinguished (Kong *et al.* 2005, Farrow & Masland 2011, Baden *et al.* 2016).

Glutamate is the principal neurotransmitter of the retina and mediates the excitatory pathway. Information processing starts at the first synapse layer, where glutamate release is high in the dark due to depolarized PRs. Puller and colleagues assigned differential expression of AMPA and kainate receptors to distinct types of OFF-BCs in the mouse retina (Puller *et al.* 2013). In contrast, ON-BCs express the metabotropic glutamate receptor mGluR6. BCs provide synaptic inputs to GCs. GCs and ACs may express all ionotropic glutamate receptor (iGluR) subunits (Hamassaki-Britto *et al.* 1993, Müller *et al.* 1992, Brandstätter *et al.* 1998). Activation of iGluRs induces changes in the $[Ca^{2+}]_i$, either by calcium influx through iGluRs or by calcium influx through VGCCs that become activated upon iGluR-mediated depolarization. Glutamate is rapidly removed from the synaptic cleft by high efficient uptake by glial cells or by presynaptic re-uptake systems (Clements *et al.* 1992, Vandenbranden *et al.* 1996, Hartwick *et al.* 2004). To overcome this machinery, appropriate agonists for the different iGluRs were employed that are not removed by re-uptake systems.

In order to monitor glutamate-induced changes in $[Ca^{2+}]_i$, I made use of a transgenic mouse line (Heim *et al.* 2007) that expresses the genetically encoded calcium sensor TN-L15 in the majority of GCs (Müller *et al.* 2007). The calcium sensor TN-L15 is based on the truncated fast chicken skeletal muscle troponin C (csTnC), which is sandwiched between CFP as donor and citrine as acceptor fluorophore. The pair of fluorophores was engineered for fluorescence resonance energy transfer (FRET); binding of calcium to

TnC leads to a conformational change in the protein, thus enhancing the energy transfer between the two fluorophores (Heim *et al.* 2007). Hence, an increase in the YFP/CFP ratio results from a decrease in donor fluorescence accompanied by an increase in acceptor fluorescence and was used as an indicator for the increase in $[Ca^{2+}]_i$.

In order to test whether TN-L15 was effectively expressed in GCs of the mouse retina, I made use of appropriate immunohistochemical markers and confocal microscopy. Vertical cryosections of the TN-L15-expressing retina were double-labeled for GFP, to intensify the TN-L15-fluorescence and for calretinin, a calcium-binding protein, which labels three horizontal bands within the IPL and somata in the INL and GCL (Ghosh *et al.* 2004). Confocal images of double-labeled cryosections revealed TN-L15-expression in the somata of GCs as well as in their processes in the IPL (Fig. 3.1, A). GCs with different soma size were distinguished (Fig. 3.1, A, arrowheads). A very weak labeling was found in two somata within the INL (asterisk). Calretinin staining revealed positive neurons in the INL (Fig. 3.1 B, arrow 2) and in the GCL (Fig. 3.1, B, arrows 1 and 3). Within the IPL, three strata formed by dendritic processes were immunoreactive for calretinin (Fig. 3.1, B, 1-3); they can be used as a guide for the precise subdivision of the IPL. The superposition in Fig. 3.1 C, revealed a co-labeled soma in the GCL (arrow 3), which indicates most likely a GC. Arrow 1 shows a calretinin-positive soma without TN-L15-expression, it is most likely a displaced AC. TN-L15-positive processes of the GCs within the IPL were found in both ON- and OFF-layer suggesting that the TN-L15 sensor is expressed in both ON- and OFF-GCs (Fig. 3.1, C).

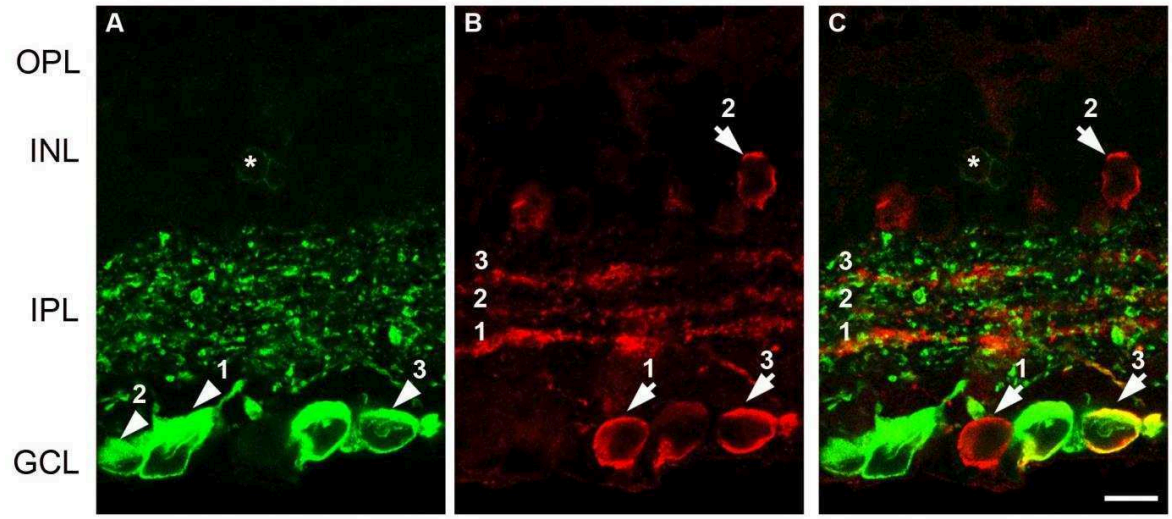


Figure 3.1: TN-L15 is expressed in GC-somata and processes within the IPL of the TN-L15-expressing retina. Vertical section of the TN-L15-expressing retina was stained with anti-GFP **(green, A)** and anti-calretinin **(red, B). (C)** The merge of both channels shows a GC, which is double-labeled for GFP and calretinin (arrow 3). Scale bar 10 µm.

3.1.1. Studying DA effects on iGluR-mediated responses in GCs

In this chapter I will investigate the action of DA on glutamate-induced calcium changes in GCs. First, AMPA, Kainate and NMDA receptors in GCs were investigated separately by applying the appropriate agonists. The calcium responses of the GCs were characterized, and then DA or the specific D1R or the D2R agonists were applied during stimulation of the single iGluRs to see whether they affect these calcium responses.

Acutely isolated TN-L15 retinae were superfused four times with the agonists AMPA (5 µM), Kainate (20 µM) or NMDA (300 µM) for 30 sec each, in between the retinae were washed with Ames solution for 10.5 min. The TN-L15-expressing GC shown in Fig. 3.2 was stimulated with AMPA four consecutive times, followed by washout phases with Ames solution. The response in cellular fluorescence occurred with a characteristic time delay, introduced by the perfusion system. Only a few seconds after the first AMPA application was stopped, the cell responded with a decrease in CFP fluorescence and a mirror-reversed increase in YFP fluorescence (Fig. 3.2, A); these changes result in an increase in the YFP/CFP ratio (Fig. 3.2, B). This increase in YFP/CFP ratio is in agreement with a rise in $[Ca^{2+}]_i$ since binding of calcium to the TN-L15 sensor enhances the FRET efficiency between CFP and YFP. The YFP/CFP ratio increased transiently to 46%, and then recovered back to baseline. The three following AMPA applications also induced mirror-reversed changes in the CFP and YFP fluorescence intensities, resulting in increases of the YFP/CFP ratio of about 95%. Interestingly, while the last three responses showed barely any variance, they were larger than the first response (Fig. 3.2, B).

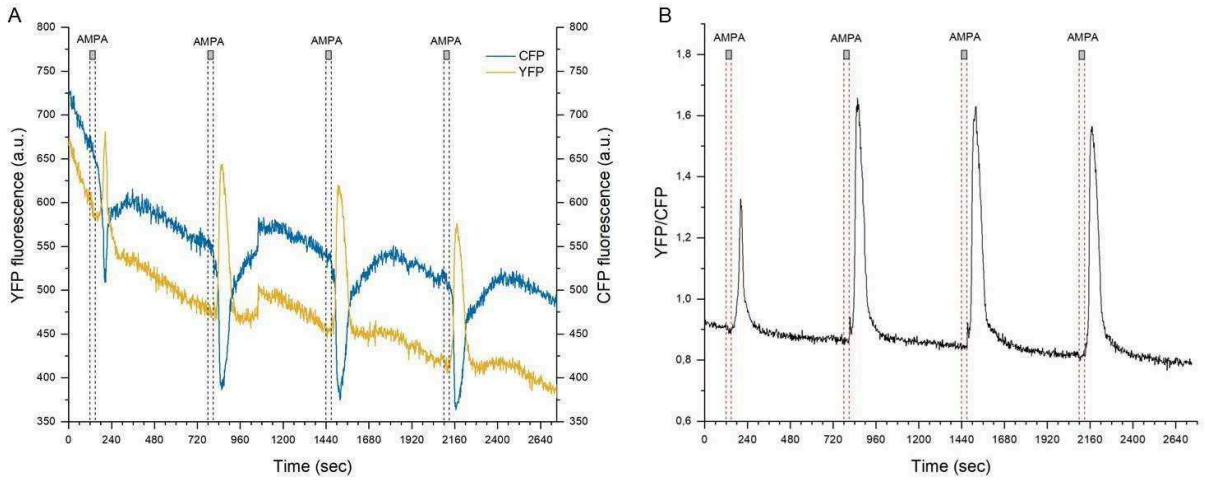


Figure 3.2: AMPA induced a change in the fluorescence signal of the TN-L15 sensor in GCs. (A): Fluorescence intensities of CFP and YFP for one GC stimulated with 5 µM AMPA were plotted in artificial units (a.u.). With a delay that was introduced by the perfusion system, each AMPA application triggered reproducible and reversible changes in CFP and YFP fluorescence. Upon each application the CFP fluorescence signal (cyan) decreased transiently while the YFP fluorescence signal (yellow) increased transiently. All treatments with AMPA induced mirror reversed changes in the CFP and YFP fluorescence signals, which recovered towards the baseline during the washout phase. Both fluorescence traces decreased over time, indicating a slight photobleaching, with YFP being bleached stronger than CFP. **(B):** Ratio of YFP/CFP for the GC shown in A. The ratio of YFP/CFP was plotted over time, it was considered as a change in the $[Ca^{2+}]_i$ only when the CFP and YFP fluorescence signals exhibited mirror reversed changes. CFP: cyan fluorescent protein; YFP: yellow fluorescent protein.

In the majority of the cells, the first response differed from the three subsequent responses in terms of shape, amplitude and/or the length of the response. Moreover, in some cells upon washout, the value of the YFP/CFP ratio did not recover towards the baseline after the first response or it was much lower than the baseline (data not shown). The reason for the difference between the first and the three other responses is unknown. In summary, AMPA lead to a reproducible and reversible increase in the YFP/CFP ratio. In all FRET-imaging experiments, only mirror-reversed changes in the fluorescence of the two fluorophores were considered as authentic responses. In the following experiments, such increases in the YFP/CFP ratio will be interpreted as rise in $[Ca^{2+}]_i$.

To investigate the effect of retinal neuromodulators on glutamate receptor induced changes in $[Ca^{2+}]_i$, the following paradigm, henceforth termed “standard paradigm”, was used. Throughout the experiment, the retina was superfused with AMES solution. The iGluR agonist was applied four times for 30 s, followed by washout periods. The first response was ignored and in the following, the second response will be referred to as the first one (Fig. 3.3, A). In cases, in which neuromodulator activity was tested, the neuromodulator was applied 2.5 min before as well as during the subsequent iGluR

agonist application. Upon washout, the iGluR agonist was applied for the fourth time (defined as third response).

3.1.1.1. DA affects the AMPA-induced changes in $[Ca^{2+}]_i$ in GCs

3.1.1.1.1. AMPA induced changes in $[Ca^{2+}]_i$ in GCs

Acutely isolated TN-L15 retinae were stimulated with AMPA according to the standard paradigm described above. Thus, 462 TN-L15-expressing GCs were stimulated with AMPA, all cells responded to AMPA. However, only responses that reflected mirror-reversed changes in CFP and YFP fluorescence signals were considered as authentic FRET-responses. Likewise, responses that exhibited considerable photobleaching or considerable noisy signals, so that the responses are badly discernible were excluded. In total, 331 TN-L15-expressing GCs from 14 retinae pieces and eight experiment days were included in the analysis and were set as 100%. The stimulations resulted in a reversible and reproducible change in the YFP/CFP ratio and, hence, $[Ca^{2+}]_i$, and within individual cells the responses were similar in terms of shape and length. Two general types of calcium responses were observed: GCs that responded to stimulation with 5 µM AMPA with a transient increase in $[Ca^{2+}]_i$ and represent with 92% the majority of the cells (Fig. 3.3, A) and GCs that responded with a more sustained increase in $[Ca^{2+}]_i$, these cells represent 8% (Fig. 3.3, B).

The cell shown in Fig. 3.3, A is the same cell shown in Fig. 3.2; the ratio trace was shortened and shows the three last responses referred to as response 1-3. Furthermore, all values were normalized to the YFP/CFP ratio during the first 20 sec before the first AMPA stimulation. In the transient response type shown in Fig. 3.3, A the YFP/CFP ratio started to increase about 10-30 sec after AMPA was applied, the peak was rapidly reached within approximately 30 sec. The ratio change was about 95%. The signal rapidly started to recover back to baseline and the total response lasted for approximately 2 min; all three responses were similar (Fig. 3.3, A). In many GCs, the increase in YFP/CFP ratio already started towards the end of the AMPA application (data not shown), the duration and the shape of the responses were similar to the illustrated response in Fig. 3.3, A. In the sustained response type, FRET ratio increased rapidly still during application of AMPA, or within the 30 sec after the application was stopped. The peak was reached within 30-60 sec, exhibited a ratio change of 53%, then the fluorescence signal started to recover gradually towards the baseline; the duration

of the sustained response was about 4-6 min. The second and third responses exhibited a ratio change of 49% and 44% respectively (Fig, 3.3, B). There was no correlation between the soma size of the GCs and the different response types observed, though this may indicate the involvement of different GC types, since at least 32 different functional GCs have been described (Baden *et al.* 2016). Another possible explanation could be the different expression level of the AMPA receptors in the GCs, and/or the expression of different AMPA subunits, where the GluA2 subunit is critical in determining AMPA receptor signaling properties (Jones *et al.* 2012).

As illustrated in Fig. 3.3, A and B, the amplitudes of the responses could decrease over time, so that the amplitude of the last response was 3-20% smaller than the first one. This behavior is called "rundown" effect; it appears in many physiological experiments and should be considered for all imaging experiments studied in this project. It can be explained by the length of the measurement (approximately 1 hour), during which response properties of the recorded cells may change slightly. Moreover, the two fluorophores, CFP and particularly YFP, showed photobleaching. This bleaching effect becomes stronger over time (see Fig. 3.2, A). Bleaching was slightly stronger for YFP than for CFP, which could cause the incomplete recovery of the ratio signal towards the baseline. In different cells, the response amplitudes (RAs) could change differently. There were cells without rundown effect or with only a slight change over time. But there were also cells, where the RAs became bigger over time (Fig. 3.3, C, blue).

In order to statistically analyze the AMPA-induced calcium responses and the possible effects of the related drugs in further experiments, the RAs were determined. For all the pharmacological studies, the amplitude of the second response, with or without the related drugs, was normalized to the amplitude of the first response and was referred to as $Response_{Max}(2)/Response_{Max}(1)$. The RAs in the presence of the related drugs were compared to the RAs of the control experiments (ctrl) and were tested for significance. Throughout this chapter, RAs were grouped into the following five ranges: 1) RAs, which exhibited less than 50% of the initial RAs (light brown), 2) RAs between 50-80% (orange), 3) RAs between 80-100% (black), 4) RAs between 100-200% (blue) and 5) RAs that were higher than the initial RAs by at least a factor of 2 (green). This depiction was used for the description of the results obtained in the pharmacological studies. The majority of the cells (57%) exhibited RAs between 80-100% (Fig. 3.3, C, black). There were cells with moderate changes, 14% of the cells

responded with RAs between 50-80% (orange), and 28% with RAs between 100-200% (blue). The cells grouped in the blue bar responded to each of the consecutive AMPA treatments with higher RAs over time, which recovered back to baseline during washout after every response. The strongest YFP/CFP ratio change was achieved in a GC, where the RA exhibited 160%, meaning an increase in the YFP/CFP ratio during the second response by a factor of 1.6 compared to the first response. In all these four types of cells, the third responses were similar to the second ones in terms of shape, amplitude and length (Fig. 3.3, C).

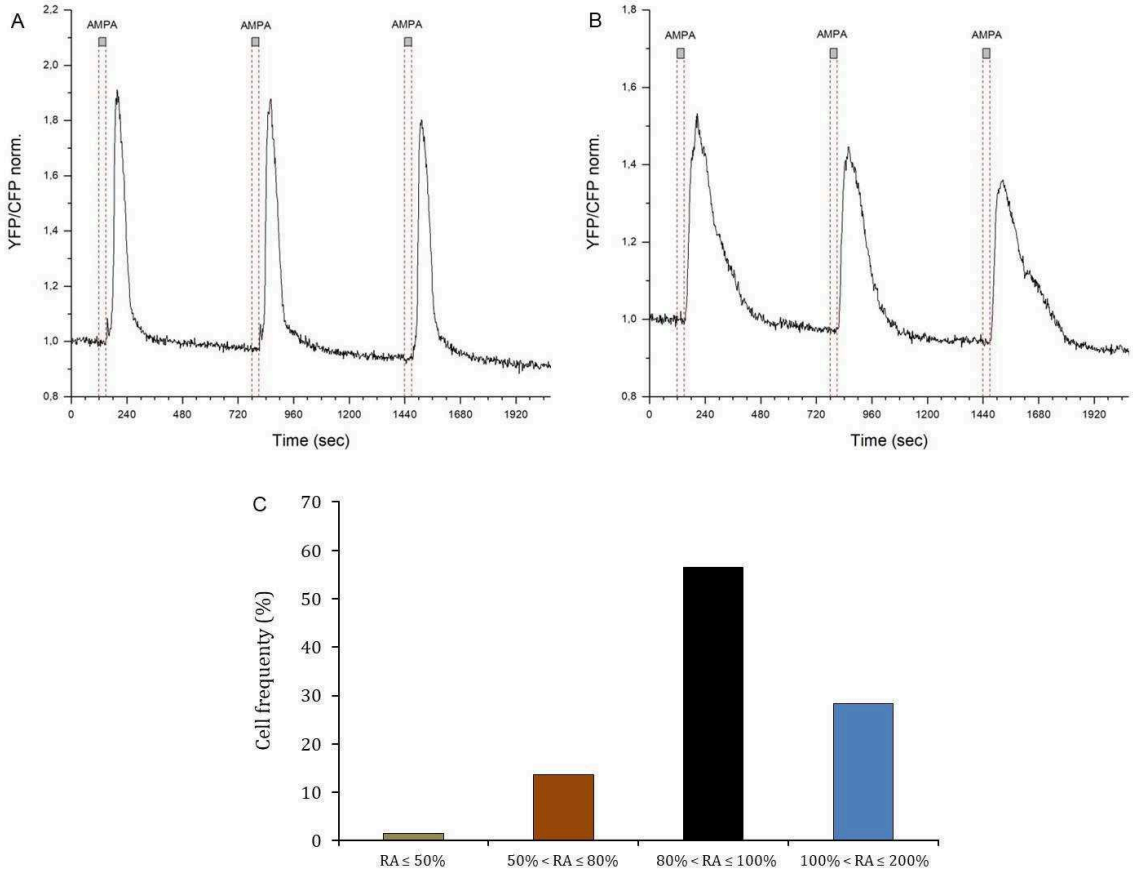


Figure 3.3: TN-L15-expressing GCs responded reversibly and repeatedly to AMPA. AMPA (5 µM) induced a significant increase in YFP/CFP ratio, interpreted as an increase in $[Ca^{2+}]_i$; the ratio was plotted over time. In 92% of the GCs, AMPA elicited a transient response similar to the GC illustrated in **(A)**. A sustained response of one GC to AMPA is shown in **(B)**; similar responses were observed in 8% of the cells. The values of the YFP/CFP ratio were normalized to the average value of 20 sec before the first stimulation. **(C):** Relative frequency of the responses to the second AMPA treatment in respect to the RAs. RAs were subdivided in four groups and cell frequency was determined and plotted in a bar graph. RAs, which exhibited less than 50% of the initial RAs (light brown), RAs between 50-80% (orange), RAs between 80-100% (black) and RAs between 100-200% (blue).

3.1.1.1.2. DA reduced the AMPA-induced changes in $[Ca^{2+}]_i$ in GCs

In order to test the effect of DA on the AMPA receptors activity, 86 TN-L15-expressing GCs from four retina pieces were treated according to the standard paradigm with the second treatment occurring in the presence of 20 µM DA (Fig. 3.4). In 80% of the cells DA alone did not affect the calcium signaling. Fig. 3.4, A shows the response of a GC, which responded to AMPA with a transient increase in the YFP/CFP ratio of 50%, the response lasted for approximately 2 min; upon washout, the cell recovered back to baseline. Application of DA did not elicit any change in the YFP/CFP ratio. During DA application the AMPA-induced calcium response was lower in amplitude with a change of 30% in YFP/CFP ratio and duration of approximately 70 sec. Upon washout, the cell recovered and responded to the last AMPA stimulation with an increase of 40% in the YFP/CFP ratio (Fig. 3.4, A).

In 20% of the GCs treated with DA, DA alone elicited a change in the $[Ca^{2+}]_i$. Such a cell is shown in Fig. 3.4, B. The cell responded to the first AMPA application with a biphasic response with a maximal increase in YFP/CFP of 36%. About 30 sec after DA was applied, the fluorescence signal started to increase, reached a peak within 60 sec with a ratio change of 17%, and then started to decrease gradually. Still in the presence of DA, upon AMPA application, the YFP/CFP ratio started to increase again by 22%, and then recovered to beneath the baseline. The third AMPA response showed a 30% change in the ratio. In the cells that responded to DA alone with an increase in YFP/CFP, it was difficult to compare the AMPA-induced changes in the presence and absence of DA. Therefore, these cells were excluded from the statistical analysis. Statistical analysis shown in Fig. 3.4, C, revealed that there was a significant difference between calcium responses to AMPA and to AMPA in the presence of DA (Mann-Whitney Rank Sum Test: $p^{***} \leq 0.001$, n=68). The distribution of the response amplitudes of the GCs treated with DA showed a slight shift distribution to lower RAs when compared to ctrl cells (n=331).

The effects of DA on the AMPA response were diverse; in some cells the amplitudes were up to 50% smaller than the initial response while they remained unchanged in other cells. Since responses to AMPA under ctrl conditions showed a certain variance in the amplitudes of the second and third responses (Fig. 3.3, C), it was important to subdivide the responses to DA and AMPA into similar ranges. The comparison of the percentages among each other should clarify whether there is an effect of DA on the

AMPA-induced calcium responses. The cell frequency in every range of RAs is plotted in a bar graph and is shown in Fig. 3.4, D. The majority of the cells (62%) responded with amplitudes between 50-80% (orange bar). The RAs were even smaller than 50% of the initial responses in 9% of the cells (light brown). In 28% of the cells (black) the RAs exhibited moderate changes with amplitudes between 80-100% (Fig. 3.4, D). The shift of the AMPA-induced calcium responses to reduced changes in $[Ca^{2+}]_i$ in the presence of DA became clearer in the bar graph depiction (Fig. 3.4, D).

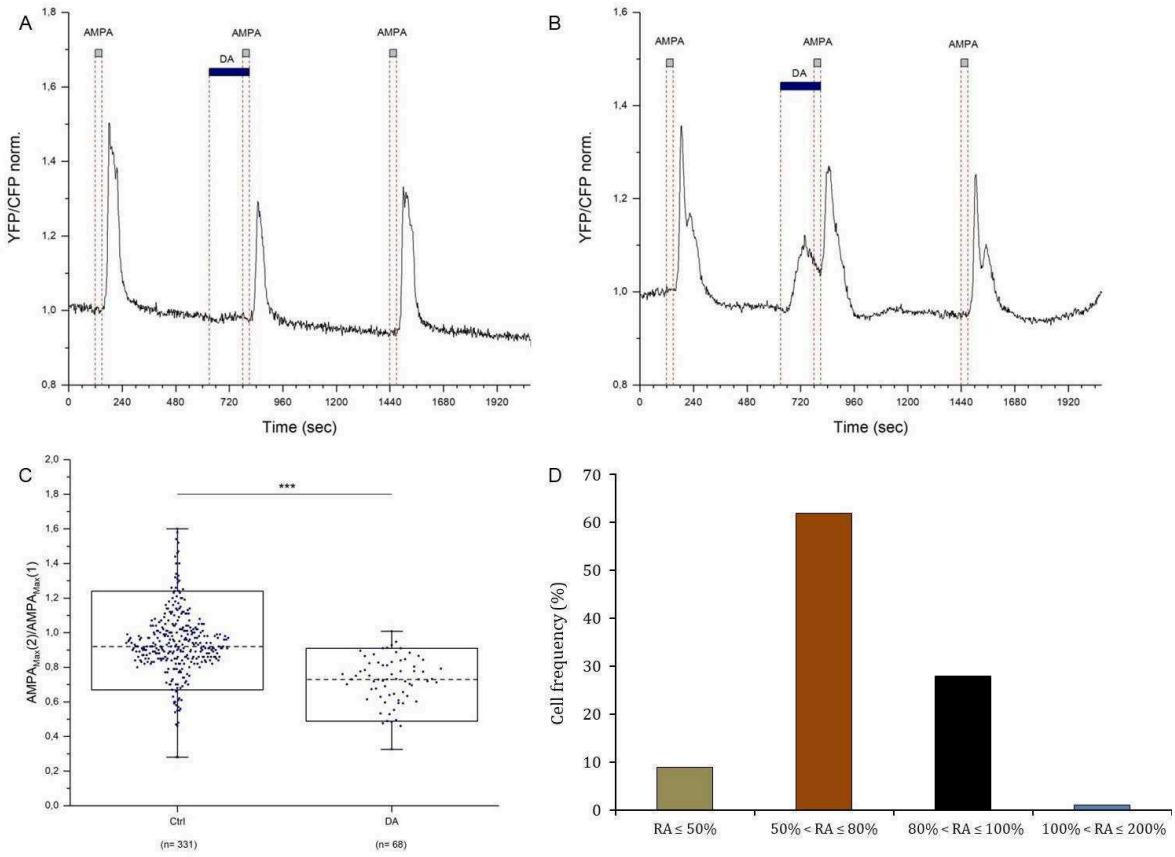


Figure 3.4: DA affected the calcium signaling and AMPA receptors activity in GCs. (A): Transient response of a GC to AMPA, DA diminished the AMPA response and the cell recovered toward the baseline. **(B):** Transient response of a GC, which responded to each of the AMPA and the DA treatments. **(C):** The second RAs to AMPA of the GCs treated with or without DA were normalized to the initial response and data of each cell were plotted as box plot. Each dot represents the response of one cell. The dashed lines indicate the mid-point of the data: the so-called median indicates that half of the cells responded with this amplitude or lower and half of the cells responded with this amplitude or higher; Ctrl: 0.92, n=331; DA: 0.73, n=68.. The whiskers above and below the box represent the 95th and the 5th percentiles, respectively, the box represents 90% of the cells. The AMPA-induced increase in $[Ca^{2+}]_i$ is significantly diminished by DA (Mann-Whitney Rank Sum Test: p***≤0.001). **(D):** Relative frequency of the responses to the second AMPA treatment in the presence of DA in respect to the RAs. RAs were subdivided in four groups and cell frequency was determined and plotted in a bar graph. RAs, which exhibited less than 50% of the initial RAs (light brown), RAs between 50-80% (orange), RAs between 80-100% (black) and RAs between 100-200% (blue). DA: dopamine, 20 µM.

3.1.1.1.3. Different dopamine receptors affect AMPA-induced calcium responses

There are five types of dopamine receptors (DRs), which could be involved in the effects observed with DA. D1Rs and D5Rs belong to the D1 like receptor family and couple positively to ACy; in contrast, D2Rs-D4Rs form the D2 like receptor family and couple negatively to ACy (Andersen *et al.* 1990, Niznik & Van Tol 1992, Sibley & Monsma 1992, Civelli *et al.* 1993, Vallone *et al.* 2000). Using the D1R agonist SKF 38939 (1 µM) or the D2R agonist quinpirole (1µM), I attempted to attribute the effects observed with DA on the AMPA-induced changes in $[Ca^{2+}]_i$.

Ninety TN-L15-expressing GCs from five retina pieces were tested for the modulatory effect of SKF 38393 on AMPA responses according to the standard paradigm. Stimulation with SKF 38393 alone did not elicit any change in the $[Ca^{2+}]_i$ of the TN-L15-expressing GCs. The GC shown in Fig. 3.5, A responded to AMPA with a transient increase in the YFP/CFP ratio of 58%. Approximately 2 min after the application of AMPA was stopped, the signal recovered towards the baseline. The stimulation of D1Rs diminished the AMPA-induced increase in $[Ca^{2+}]_i$ by about 75%. The response lasted for 1 min and the signal recovered back to baseline. The GC recovered fully and the third AMPA treatment elicited an increase in YFP/CFP ratio of 62% with a similar kinetic as the initial response. The effect of SKF 38393 was reversible; the majority of the cells (91%) showed a recovery and the third response was higher than the second one. In fact, in some cells the third AMPA-induced calcium response was even enhanced and the RA was higher than the RA of the first response (Fig. 3.5, B). The cell shown in Fig. 3.5, B responded to AMPA with an increase in YFP/CFP ratio of 26%. The response lasted for 2.5 min. Under stimulation of D1Rs, AMPA evoked an increase in the YFP/CFP ratio of 14%, meaning the amplitude was up to 46% smaller than the initial response and the duration of the response was reduced to 1.5 min. This behavior was observed in the majority of the cells. Interestingly, the third AMPA response induced a change in the ratio of 38%, which was even higher than the initial response and the response lasted for approximately 5 min.

In order to characterize the SKF 38393 effect of the AMPA-induced calcium responses, the cells were assigned to different groups according to the RA ranges of the second response, and were then compared to the ctrl cells (Fig. 3.3, C). It is obvious that

there was a shift to lower RAs. In 38% of the cells treated with SKF 38393, the RAs were smaller than 50% of the initial RAs (Fig. 3.5, C, light brown); some cells presented only 10% of the initial RA. Under ctrl conditions in Fig. 3.3, C only 1% of the cells was found in the same range. In 45% of the cells treated with SKF 38393, the RAs ranged between 50-80% (Fig. 3.5. C, orange), where the majority of the cells in this group exhibited RAs set below 70% of the initial RAs. In the ctrl cells, only 14% were lying in this range (Fig. 3.3, C, orange). The cells that responded to co-stimulation of AMPA and D1 receptors with RAs between 80-100% represented 10% of the cells (Fig. 3.5, C, black), while only 7% of the cells responded with a stronger RA than the initial response (Fig. 3.5, C, blue).

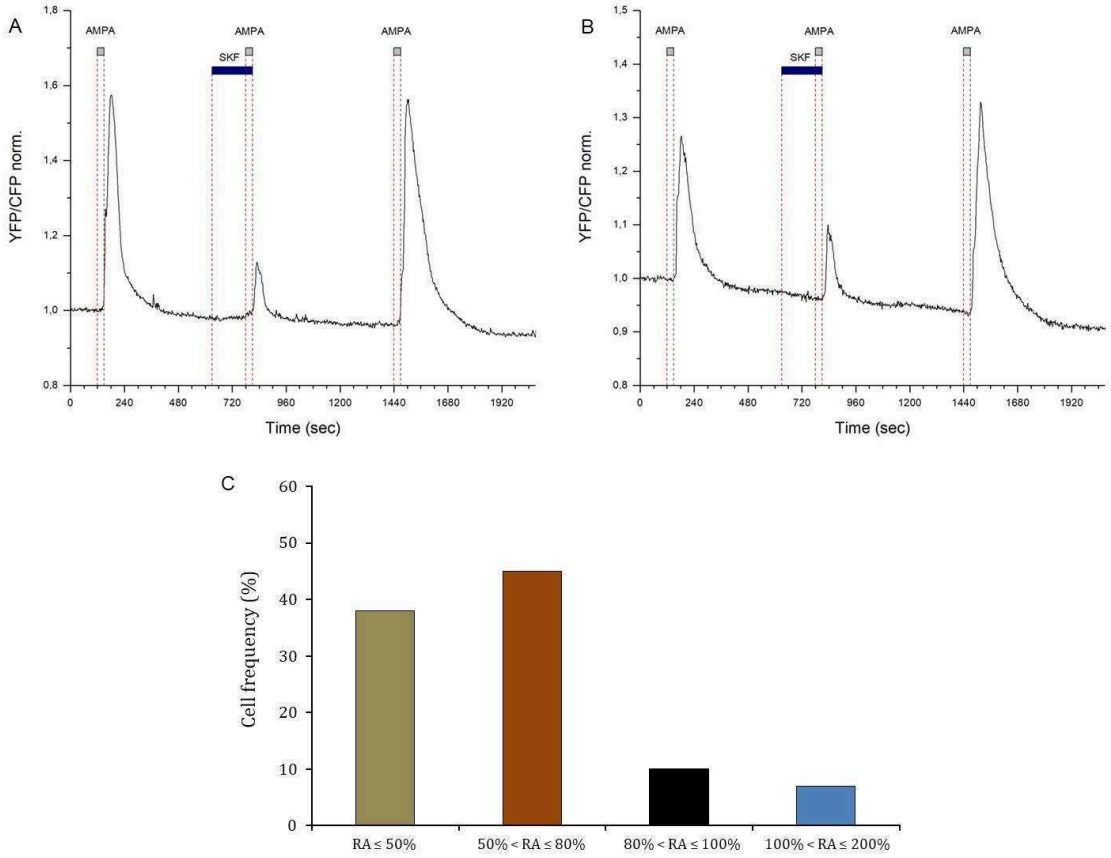


Figure 3.5: Activation of D1Rs led to a strong reduction in the AMPA-induced calcium signaling. (A): Activation of D1Rs reduced the response to AMPA in terms of amplitude and duration in the majority of the cells. **(B):** Co-activation of D1Rs affected the AMPA-induced calcium response. The third AMPA response was enhanced and lasted longer than the initial response. This behavior was observed in ca. 9% of the cells. **(C):** Relative frequency of the AMPA response amplitudes (RAs) under SKF 38393 influence. The co-activation of D1Rs and AMPA receptors affected the calcium signaling and showed a broad variance. The cells were assigned to four different groups in respect to the RAs to the second AMPA treatment in the presence of SKF 38393 (SKF). The RA of the AMPA-induced calcium increase was diminished by SKF 38393 to 50% or less in 38% of the cells (light brown), to a range between 50-80% in 45% of the cells (orange) and to a range between 80-100% in 10% of the cells (black). Only 7% of the cells responded to co-activated D1Rs and AMPA receptors with a stronger increase in YFP/CFP ratio than the initial response by a factor up to 2 (blue).

Activation of D1Rs had a stronger impact on the AMPA-induced calcium responses than application of DA (Fig. 3.4). One possible interpretation is that during DA application, not only D1Rs but also D2Rs were activated, that might have antagonized D1R action. It could, therefore, be hypothesized that D2R agonists have the opposite effect on AMPA-induced calcium signals than D1R agonists. In order to find out whether D2Rs may also modulate the AMPA-induced calcium responses, 68 TN-L15-expressing GCs from three retina pieces were tested for the modulatory effect of quinpirole on AMPA responses according to the standard paradigm. Fig. 3.6 A shows the response of one GC, which responded to the first AMPA treatment with a transient increase in the YFP/CFP ratio of 52%, thus an increase in $[Ca^{2+}]_i$. The signal started to increase towards the end of the AMPA application, reached a peak within 40 sec and started to recover back to baseline within approximately 2 min. Stimulation of D2Rs and AMPA receptors simultaneously elicited a strong change in the YFP/CFP ratio of 116%, indicating an enhanced calcium response compared to the responses induced by AMPA alone. The signal peaked within approximately 40 sec and then recovered back towards the baseline 4 min later; the fluorescence baseline kept decreasing during the washing phase. The third AMPA treatment elicited an increase in YFP/CFP ratio of 35%. Similar to the first response, the peak was reached within 40 sec after what the signal recovered back and underneath the baseline after approximately 2.5 min (Fig. 3.6, A). Stimulation with quinpirole alone did not elicit any changes in YFP/CFP ratio in none of the GCs. The changes in the second RAs exhibited a large variance and ranged from 82% of the first RA to 566%. The relative frequency of cells treated with quinpirole in respect to the RAs determined by calculating the $AMPA_{Max}(2)/AMPA_{Max}(1)$ is shown in Fig. 3.6, B. Clearly, as hypothesized above, there was a shift towards higher RAs. Only 9% of the cells responded to co-stimulation with quinpirole and AMPA with a RA between 80-100% (black), while the majority of the GCs in the ctrl (57%, Fig. 3.3, C) were counted among this group. The response to AMPA in the presence of quinpirole exhibited RAs between 100-200% in 50% of the cells; in this group many GCs responded with an enhanced calcium response by a factor of 2 (Fig. 3.6, B, blue). Under ctrl conditions, 28% of the cells were counted to this range, the strongest response measured exhibited a RA that was higher than the initial RA by a factor of 1.6 (Fig. 3.3, C, blue). In fact, 41% of the cells responded with a much stronger RA than the initial one, by a factor of 2-5.66 (Fig. 3.6, B, green); in all these cells, YFP/CFP ratio recovered towards the baseline and the response

lasted longer than the initial one. These cells responded to the third AMPA treatment similar to first application, meaning that the quinpirole action was reversible.

From the previous experiments, it is most likely that the impact observed with DA alone is evoked via activation of diverse DRs; activation of D1Rs led to a strong decrease of the AMPA-induced calcium changes in the majority of the cells. Activation of D2Rs was shown to have opposite effects: it increased the AMPA induced calcium changes in the majority of the cells to a very high level. In order to confirm, whether the simultaneous activation of D1Rs and D2Rs operate antagonistically and possibly resemble the impact induced via stimulation with DA (Fig. 3.4), 50 TN-L15-expressing GCs were stimulated with 1 µM SKF 38393 and 1 µM quinpirole simultaneously following the protocol used in the previous experiments.

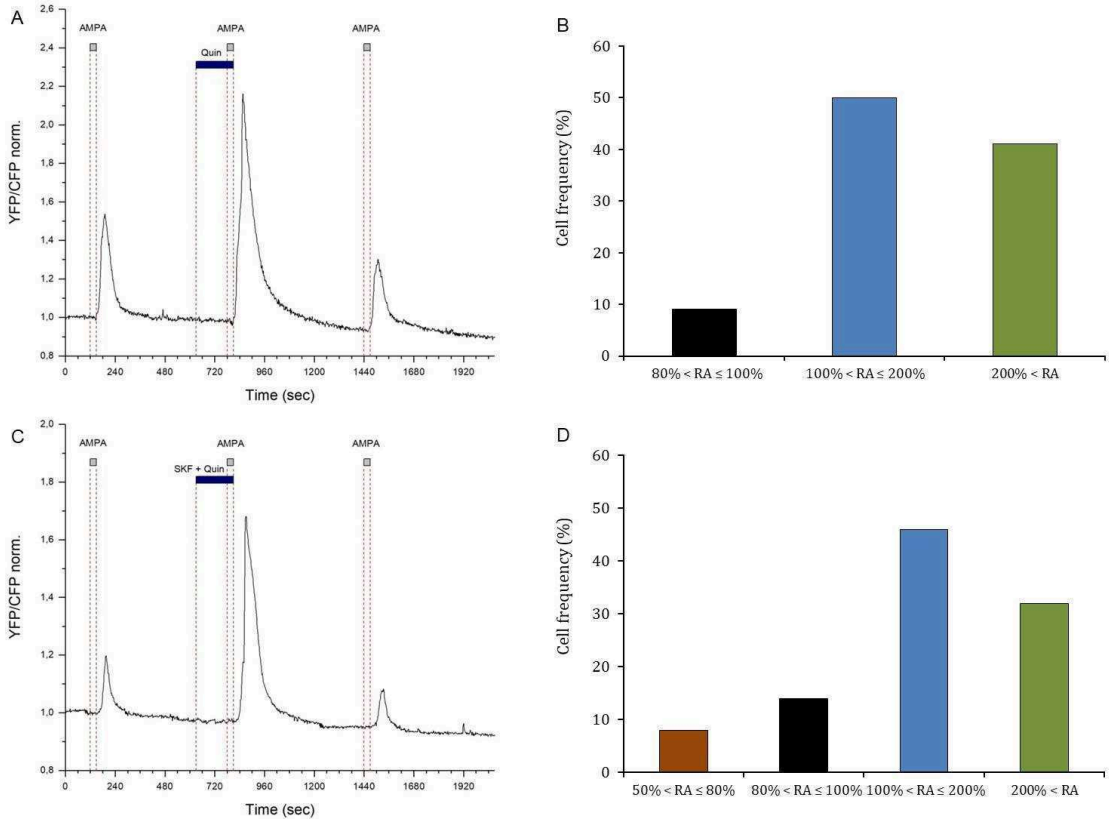


Figure 3.6: Activation of D2Rs enhanced the AMPA-induced calcium signaling in retinal GCs. (A): Activation of D2Rs raised the response to AMPA in terms of amplitude and duration in the majority of the cells. **(B):** Relative frequency of the AMPA RAs under quinpirole (Quin) influence. The co-activation of D2Rs and AMPA receptors enhanced the calcium responses. The cells were assigned to three different groups in respect to the RAs in the presence of quinpirole. Quinpirole raised the AMPA-induced calcium increase in more than 90% of the GCs: 50% of the cells (blue), exhibited RAs in a range between 100-200%, while 41% of the cells showed RAs enhanced by a factor of up to 5.6 (green). Only 9% of the cells responded to AMPA with RAs that ranged between 80-100% (black). **(C):** Co-activation of D1Rs and D2Rs enhanced the AMPA-induced calcium responses. **(D):** Relative frequency of the AMPA RAs under stimulation with SKF 383939 (SKF) and quinpirole (Quin). In respect to the AMPA RAs, four groups of cells were identified. In 8% of the cells, the RAs ranged between 50-80% (orange) and 14% responded with RAs between 80-100% (black). The RAs ranged between 100-200% in 46% of the cells (blue). In 32% of the cells, the RAs were raised by a factor of up to 5.5 (green).

Fig. 3.6, C shows the response of one GC to stimulation with AMPA with a transient increase in YFP/CFP ratio of 20%. The fluorescence signal started to increase after the application was stopped, peaked within 60 sec, and then recovered towards the baseline; all in all the response lasted for 2.5 min. Stimulation with SKF 38393 and quinpirole did not elicit any change in the $[Ca^{2+}]_i$, however it enhanced the AMPA-induced calcium response. Within 60 sec after the stimulation was stopped, the YFP/CFP ratio increased to 77% then started to recover back to baseline; the response lasted for approximately 5 min. After washout, the GC reacted to AMPA stimulation with an increase in the YFP/CFP ratio of 16%, after 2.5 min the fluorescence signal recovered back to baseline (Fig. 3.6, C). The relative frequency of the GC responses in respect to the RAs variance is shown in Fig. 3.6, D. The smallest group with 8% of the cells exhibited RAs between 50-80% (orange), the smallest second RA was measured in a GC with 72%, and the third RA represented only 33% of the initial RA. In all these cells the third response was smaller than the second one (data not shown). In contrast, the GCs stimulated with DA or SKF 38393 showed a clear recovery. Thus, these cells may depict a peculiar rundown behavior not observed under ctrl conditions or, a prolonged action of this combination of neuromodulators. The GCs with RAs ranging between 80-100% constituted 14% of the cells (black), similarly these cells responded to the AMPA treatments in a reversible and reproducible way with a slight rundown effect (Fig. 3.6, D). The RAs to AMPA in the presence of quinpirole and SKF 38393 was increased in 46% of the cells to values between 100-200% (blue; Fig. 3.6, D); similar to the results observed in the presence of quinpirole with 50% (black; Fig. 3.6, B). Up to 32% of the cells responded to AMPA with an enhanced calcium response by a factor of 2-5.5 when D1Rs and D2Rs were co-activated (Fig. 3.6, D, green).

Statistical analyses shown in Fig. 3.7, A summarize the AMPA-induced changes in $[Ca^{2+}]_i$ in the ctrl cells (ctrl, n=331), in cells treated with 1 µM SKF 38393 (SKF, n=90), in cells treated with 1 µM quinpirole (Quin, n=68) and in cells treated simultaneously with 1 µM SKF 38393 and 1 µM quinpirole (Quin + SKF, n=50). The second RAs, with or without the related drugs, were normalized to the initial RAs, and data of each pharmacological study were plotted as box plots. Each dot represents the response of one GC. Considering the totality of the GCs stimulated with SKF 38393, the AMPA-induced calcium response was strongly and significantly diminished (Mann-Whitney Rank Sum Test: $p^{***} \leq 0.001$, n=90, median=0.58). In the presence of quinpirole the

AMPA-induced calcium response was significantly enhanced (Mann-Whitney Rank Sum Test: p***≤0.001, n=68, median=1.83). There is a significant difference between ctrl cells and cells stimulated with SKF 38393 and quinpirole simultaneously; the AMPA-induced calcium response was here again enhanced and there was a significant difference to the ctrl cells (Mann-Whitney Rank Sum Test: p***≤0.001, n=50, median=1.29). This impact is most likely induced via activation of D2Rs, since there is no significant difference between the impact induced via activated D2Rs alone and the impact of co-activated D1Rs and D2Rs (Mann-Whitney Rank Sum Test: p=0.06; Fig. 3.7, A).

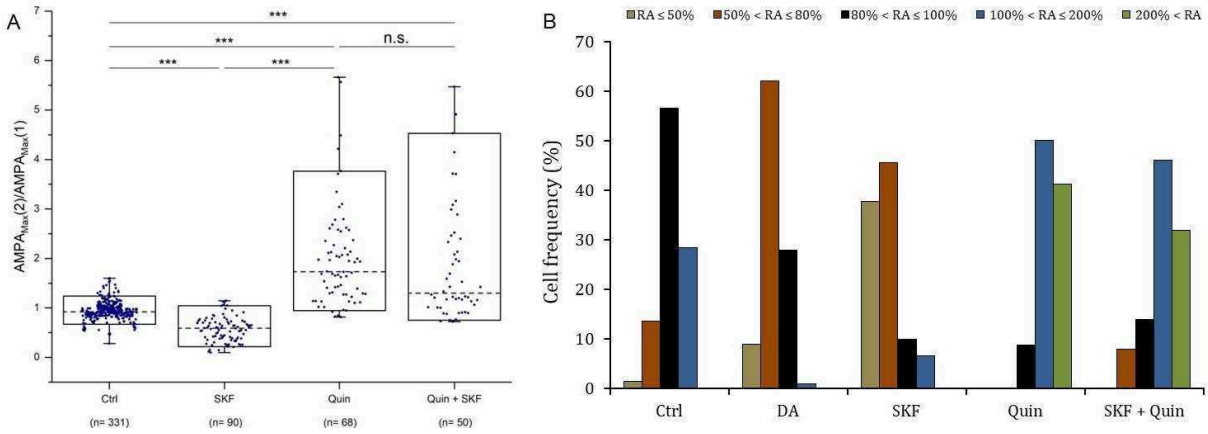


Figure 3.7: Activation of D1Rs and/or D2Rs had opposite effects on the AMPA-induced calcium signaling in GCs. (A): The RAs with or without the related drugs were normalized to the respective initial RAs and data were plotted as box plots. Each dot represents the $AMPA_{Max}(2)/AMPA_{Max}(1)$ of one cell. The dotted lines show the medians (Ctrl: 0.92, n=331; SKF 38393 (SKF): 0.58, n=90; Quinpirole (Quin): 1.83, n=68; Quin+SKF: 1.29, n=50). In each box plot, the median divides the box into two parts: the upper part is greater, the lower part is less than the median. The whiskers above and below the box represent the 95th and the 5th percentiles, respectively. The AMPA-induced increase in $[Ca^{2+}]_i$ is significantly diminished by SKF, significantly enhanced by Quin, and Quin+SKF (Mann-Whitney Rank Sum Test: p***≤0.001, respectively). There is no significant difference between the impact induced by activation of D2Rs or activation of D1Rs and D2Rs simultaneously (Mann-Whitney Rank Sum Test: p=0.06). **(B):** Summary of the Relative frequencies of the AMPA RAs under ctrl conditions and in the presence of the related drugs. RAs were assigned to different groups in respect to the RAs. RAs were subdivided in five groups: RAs, which exhibited less than 50% of the initial RAs (light brown), RAs between 50-80% (orange), RAs between 80-100% (black), RAs between 100-200% (blue) and RAs that were higher by at least a factor of 2 (green). DA: dopamine, 20 µM; SKF: SKF 38393 (1 µM); Quin: Quinpirole, (1 µM).

The summary of the relative frequencies of cells under ctrl conditions and in the presence of the related drugs is shown in Fig. 3.7, B and should illustrates the impacts induced of the AMPA-induced calcium responses. For the majority of the ctrl cells (57%), RAs for the second AMPA treatment represented 80-100% of the initial RAs. The remaining cells showed moderate changes, thus there were assigned to two groups: cells with RAs between 50-80% (14%) and cells with RAs between 100-200% (28%). In the presence of DA there was an inclination towards reduced responses. The majority of the cells (62%) responded with amplitudes between 50-80% and to a greater degree, 9% of

the cells responded with amplitudes that were smaller than 50%. These effects were much more pronounced under specific activation of D1Rs (with 1 µM SKF 38393). In total, cells that responded with amplitudes smaller than 50 % (38%) and cells that responded with amplitudes between 50-80% (45) represented together 83% of the cells. While under ctrl conditions these two groups represented 15% of the cells. With activation of D2Rs or both D1Rs and D2Rs, none of the cells responded to AMPA with such depressed calcium responses. On the contrary, there was a clear drift to right, meaning to stronger responses, hence to higher changes in $[Ca^{2+}]_i$ in response to AMPA. Under activation of D2Rs 41% of the cells, under co-activation of D1Rs 32% of the cells responded with RAs that were higher by at least a factor of 2 (Fig. 3.7, green). This kind of responses was never found under ctrl conditions or under DA or SKF 38393 impact.

In summary, activation of D1Rs reduced while activation of D2Rs increased the AMPA-induced calcium signals in GCs. The results indicate that AMPA-induced signaling can be modulated by at least these two dopamine receptor types. When agonists for D1R and D2R were co-applied, the impact of D2R seemed to override the D1R effect. The co-application of D1R and D2R agonists did not mimic the action of DA that is expected to activate both receptor types. First, DA reduced AMPA-induced signaling, albeit to a lesser extent than the D1R agonist. Second, DA alone changed $[Ca^{2+}]_i$ in X% of GCs, while this effect was never observed with specific agonists at D1R or D2R alone or in combination. Such differences may be attributed to different concentrations of ligands employed or, alternatively, by activation of additional dopamine receptors by DA, that are not activated by SKF 38393 and quinpirole. However, it is also conceivable that with DA more DR subtypes than only D1R and D2R are simultaneously stimulated, which may have antagonistic effects and may further modulate calcium signaling in retinal GCs; these receptors may be expressed on the GCs themselves or in the network on presynaptic cells.

3.1.1.2. DA affects the kainate-induced changes in $[Ca^{2+}]_i$ in GCs

3.1.1.2.1. Kainate induced changes in $[Ca^{2+}]_i$ in GCs

Kainate-induced calcium responses were studied using the same paradigm as for AMPA-induced responses. In total, 444 TN-L15-expressing GCs were stimulated with kainate using the standard paradigm. All cells responded to kainate application. By reason of photobleaching, noisy signals or unauthentic changes in CFP and YFP

fluorescence signals, many cells were excluded. Thus, 290 TN-L15-expressing GCs from 16 retina pieces and nine experiment days were analyzed. Kainate stimulations resulted in a reversible and reproducible change in the YFP/CFP ratio and thus in $[Ca^{2+}]_i$. Two general types of kainate-induced calcium responses were observed: GCs that responded to stimulation with 20 µM kainate with a transient increase in $[Ca^{2+}]_i$ and represent with 74% the majority of the cells (Fig. 3.8, A and B) and GCs that responded with a more sustained increase in $[Ca^{2+}]_i$, these cells represent 26% (Fig. 3.8, C and D).

The cell shown in Fig. 3.8, A responded with a transient increase in YFP/CFP ratio and thus in $[Ca^{2+}]_i$. The fluorescence signal started to increase towards the end of the kainate stimulation, peaked within 30 sec and exhibited a ratio change of 61%. The signal started to recover back to baseline approximately 1.5 min later, where it remained during the whole washing phase. Similar to the first kainate treatment, the cell responded to the second and third treatments with ratio changes of 57% and 52% respectively; all responses exhibited a similar kinetic in terms of shape, amplitude and length. This group of cells could be further subdivided: 10% of the GCs of the transient increase type were found to exhibit a second peak within the same response (Fig. 3.8, B). After the fluorescence signal peaked with a ratio change of 51% in response to stimulation with kainate, the cell started to recover and immediately peaked again within less than 30 sec. The second peak was slightly weaker; following the fluorescence signal recovered towards the baseline within 2.5 min. In response to the second kainate treatment, the fluorescence signal started to increase immediately when the application was stopped, peaked within 15-20 sec with a change of 43%, then decreased fast to two-thirds of the amplitude before peaking again for the second time. The fluorescence signal started to recover back to baseline and the response lasted for approximately 2.5 min. During the third response, in a similar way, the cell responded with two peaks, hereby the first peak dropped up to 50% of its amplitude corresponding to 41% ratio change, before the fluorescence signal peaked a second time. The response lasted for 2.5 min before the fluorescence signal recovered back to baseline (Fig. 3.8, B). In other cells, where the responses exhibited two peaks, all three responses showed a similar kinetic. Indeed two peaks could be distinguished; however, there were no such discrepancy between the responses as shown for the cell in Fig. 3.8, B.

The cell shown in Fig. 3.8, C responded to kainate with a fast and long-lasting increase in $[Ca^{2+}]_i$. Immediately after the kainate application was stopped, the

fluorescence signal started to increase and peaked within approximately 45 sec with a ratio change of 61%. Then, the fluorescence signal recovered slowly back to baseline after 6.5 min. Similarly, the second and third treatments elicited a fast and long-lasting increase in YFP/CFP ratio with changes of 57% and 48% respectively; the second and third responses lasted for 7.5 and 8 min respectively. Interestingly, 22% of the GCs with the sustained response type exhibited two peaks similar to the population observed in the GCs with the transient type (Fig. 3.8, B). The GC shown in Fig. 3.8, D responded to kainate with a fast increase in $[Ca^{2+}]_i$, the signal peaked within 10 sec with a change of 46%, dropped up to one third of its amplitude, then increased again to reach 80% of the initial peak. The response lasted for approximately 5 min. The second and third responses lasted for 6 min each; hereby the second peaks were slightly higher than the first peaks and occurred after the first peaks dropped up to 50% of their amplitudes.

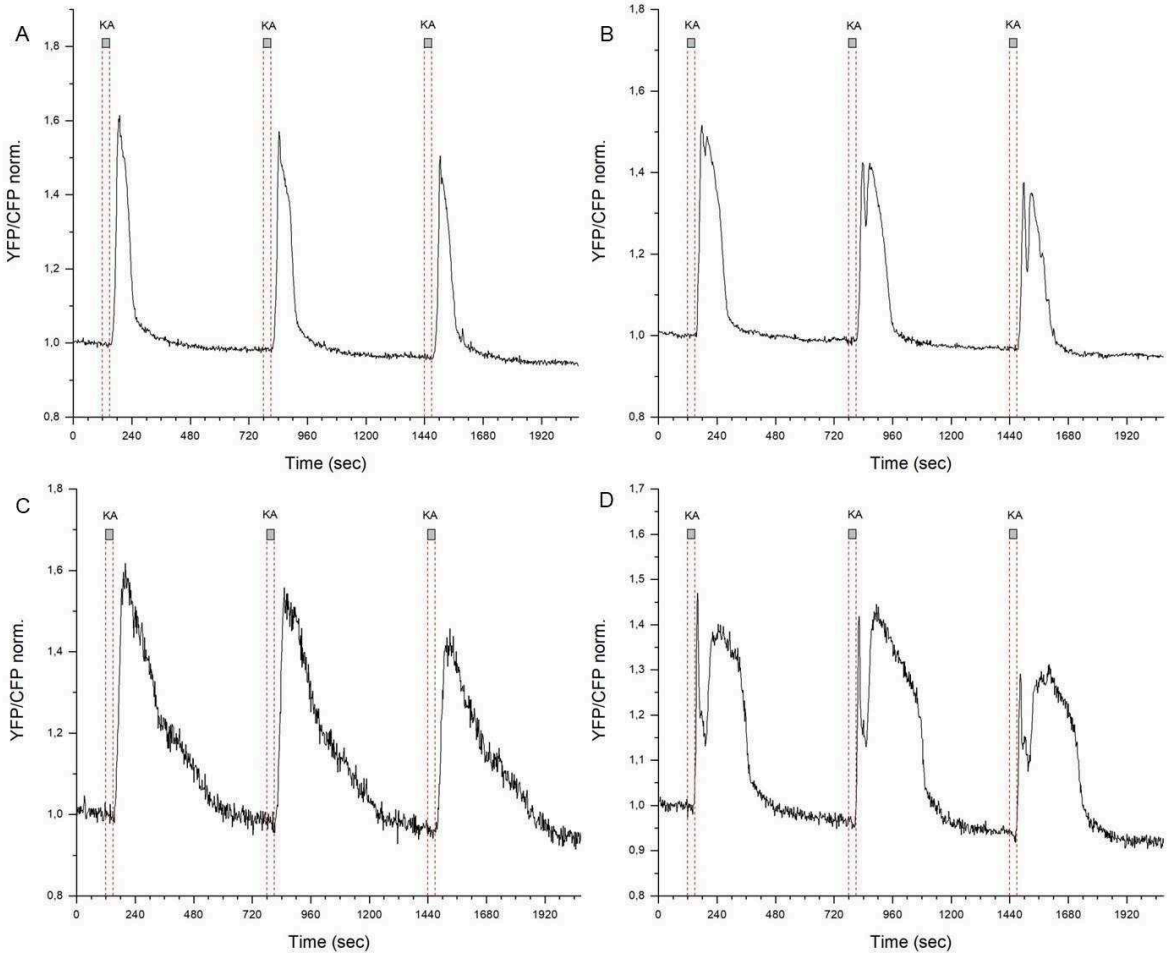


Figure 3.8: TN-L15-expressing GCs responded reversibly and repeatedly to kainate. (A): Kainate (20 µM) induced a transient increase in YFP/CFP ratio three consecutive times. The responses lasted on average for 2 min each. **(B):** The transient responses to three kainate exposures display the presence of two peaks occurring successively, or just after the first peak dropped up to the half of its amplitude. These responses lasted for approximately 2.5 min. **(C):** Sustained increases in YFP/CFP ratio in a GC in response to kainate. The responses lasted for approximately 6.5 min. **(D):** In this GC, the increases in YFP/CFP ratio display two peaks; the first ones were transient whereas the second ones were stronger and lasted over minutes.

The most likely explanation is that the different calcium responses are exhibited by different GC populations, which may differ in the expression level of kainate receptors and/or the expression of different kainate subunits. Kainate receptors properties are defined by the diverse expression pattern of subunits (GluK 1-5) and auxiliary subunits (Neto1 and Neto2), which may determine the temporal kinetics, even though the mechanisms behind are still incompletely understood (Lindstrom *et al.* 2014).

3.1.1.2.2. DA had slight effects on the kainate-induced changes in $[Ca^{2+}]_i$ in GCs

To test the effect of DA, 67 TN-L15-expressing GCs of the intact retina were recorded according to the standard paradigm. The cell shown in Fig. 3.9, A responded to kainate with a fast and transient increase in YFP/CFP ratio of 53%, the signal recovered back to baseline and the whole response lasted for 2.5 min. In this cell, the stimulation with DA did not elicit any change in the fluorescence signal. During stimulation with DA and kainate, the fluorescence signal increased fast and transiently, peaked within 30 sec with 36% ratio change and started to recover back to baseline; the response duration was shortened to less than 2 min. The third stimulation with kainate induced an enhanced increase in YFP/CFP ratio of 62% and the response lasted for 2.5 min similar to the first response (Fig. 3.9, A). In 12% of the GCs treated with DA, stimulation of DRs alone induced an increase in YFP/CFP ratio. The cell shown in Fig. 3.9, B responded to kainate with a fast and transient increase in YFP/CFP ratio; the fluorescence signal dropped to approximately one third of its amplitude where it stayed during the washout phase. About 30 sec after stimulation with DA had started, the YFP/CFP ratio increased again, peaked within 1 min and started to recover slowly. Still during application of DA, kainate increased the fluorescence signal again. The response to kainate in the presence of DA was transient; the fluorescence signal recovered back to baseline gradually over 8 min. This cell responded to the third kainate exposure with a fast and transient increase in YFP/CFP ratio (Fig. 3.9, B). In these cells (n=8), the real amplitude of the second kainate-induced response could not be determined precisely, since the response was superimposed on the response to DA. Thus, these cells were not taken into consideration, when RAs of the ctrl and DA experiment were statistically analyzed. All the cells treated with DA belong to the transient type, and there was no discernible difference between responses with one or two peaks.

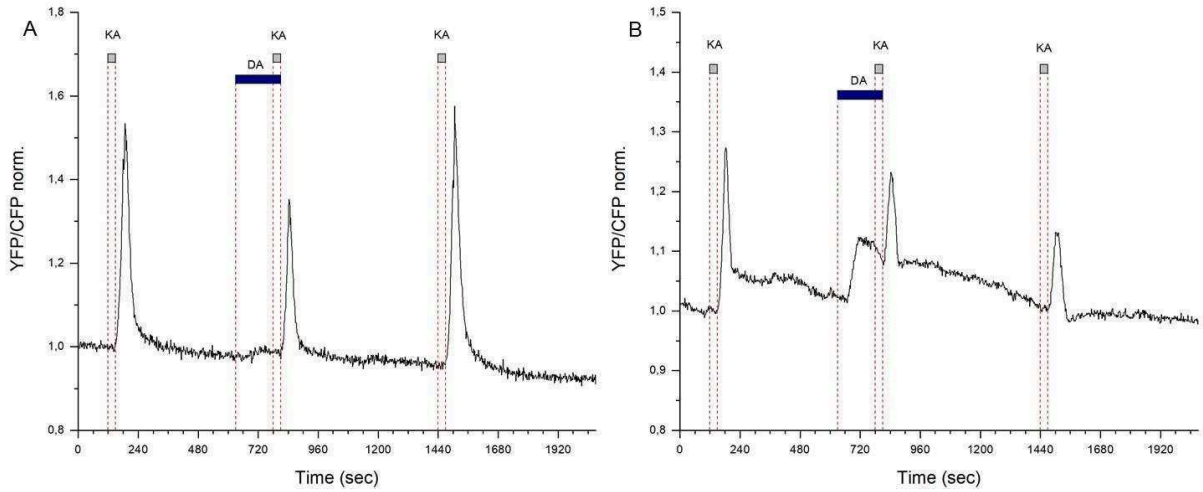


Figure 3.9: DA showed differential effects on calcium signaling and kainate-induced calcium responses in GCs. (A): Transient response of a GC to kainate (20 µM), in the presence of DA the kainate-induced changes in $[Ca^{2+}]_i$ was diminished. The YFP/CFP ratio recovered back to baseline and the cell responded to the third kainate exposure with an enhanced and transient increase in the YFP/CFP ratio. **(B):** DA induced a sustained increase in YFP/CFP ratio, the cell responded to all three kainate treatments with a transient increase in YFP/CFP ratio.

Statistical analysis of the effects of DA on the kainate-induced changes in $[Ca^{2+}]_i$ revealed that there was a significant difference between GCs treated with DA and the ctrl cells (Mann-Whitney Rank Sum Test: p***≤0.001, n=59; Fig. 3.10, A). The distribution of the RAs of the GCs treated with DA showed a slight shift distribution to lower amplitudes when compared to ctrl cells (n=290).

In order to better clarify the effects of DA, the RAs were assorted in groups similar to the classification of AMPA RAs (Fig. 3.3, C) and then compared to each other (Fig. 3.10, B). Under control conditions (ctrl), the majority of the cells responded with amplitudes between 80-100% (46%, black) and 100-200% (47%, blue). Only 7% of the cells responded between 50-80% (orange). With DA, there was an inclination to reduced RAs. Thus, in addition to cells that responded in a similar way as the ctrl cells (34%, black and 24%, blue), the group of cells with RAs between 50-80% was formed by 29% of the cells (orange). Moreover, 13% of the cells responded with amplitudes that were smaller than 50% of the initial responses (Fig. 3.10, B, light brown).

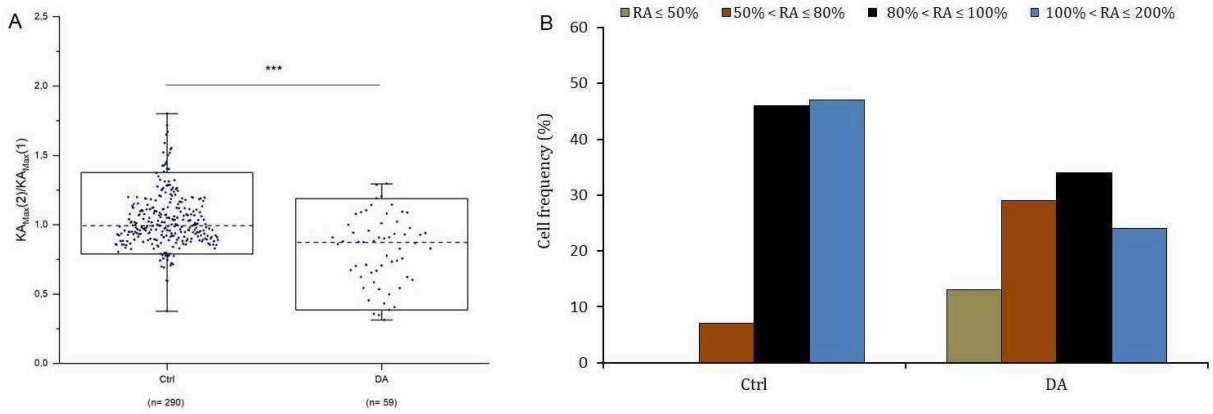


Figure 3.10: DA affected the kainate-induced calcium responses in GCs. (A): Statistical analysis of the RAs to kainate (20 µM) with or without DA (20 µM). The RAs were normalized to the respective initial RAs and data were plotted as box plots. Each dot represents the $KA_{Max}(2)/KA_{Max}(1)$ of one cell (KA=kainate). The dotted lines show the medians (Ctrl: 0.99, n=290; Dopamine (DA): 0.87, n=59). In each box plot, the median divides the box into two parts: the upper part is greater, the lower part is less than the median; the whiskers above and below the box represent the 95th and the 5th percentiles, respectively. The kainate-induced increase in $[Ca^{2+}]_i$ is significantly diminished by DA (Mann-Whitney Rank Sum Test: p***≤0.001). **(B):** Relative frequency of the cells in respect to the RAs with or without DA. The cells were assigned to four different groups: RAs that displayed less than 50% of the initial RAs (light brown), between 50-80% (orange), between 80-100% (black) and RAs that were greater up to a factor of 2 (blue).

3.1.1.2.3. Different dopamine receptors affect kainate-induced calcium responses

In order to find out which DRs are involved in the impact of DA on the kainate-induced calcium responses, TN-L15-expressing GCs of the intact retina were exposed to kainate, with the second treatment occurring with the D1R agonist SKF 38393, the D2R agonist quinpirole, or both D1R and D2R agonists simultaneously. The kainate-induced responses in the presence of the related agonists were then compared to the responses of the ctrl experiment.

Sixty-one TN-L15-expressing GCs from three retina pieces were exposed to three consecutive kainate treatments (20 µM) according to the standard paradigm. Stimulation with SKF 38393 alone did not elicit any change in the YFP/CFP ratio. The GC showed in Fig. 3.11, A responded to kainate with a transient increase in the YFP/CFP ratio of 81%. Approximately 3 min after the application was stopped, the signal recovered towards the baseline. The stimulation of D1Rs did not elicit any change in the YFP/CFP ratio, but diminished the kainate response strongly in this cell by 90%. The response to kainate was brief, the cell recovered back to baseline within 90 sec. The GC recovered fully from SKF 38393 treatment and the third kainate treatment elicited an increase in YFP/CFP ratio of 85%; the fluorescence signal started to recover in a much

decelerated way to reach the baseline after 7 min (Fig. 3.11, A). The majority of the cells that reacted to kainate in the presence of SKF 38393 with impairment in calcium responses, showed full recovery of RA and reacted to the third kainate exposure with a prolonged response. The recovery of the responses to kainate indicates that the impairment of the second kainate response was reversible and was indeed due to activation of D1Rs with SKF 38393 and not to a rundown effect. In most cells, the second response was depressed and shortened, when compared to the initial response In many other cells, the second response was depressed but prolonged so that it lasted twice as long as the initial response (data not shown).

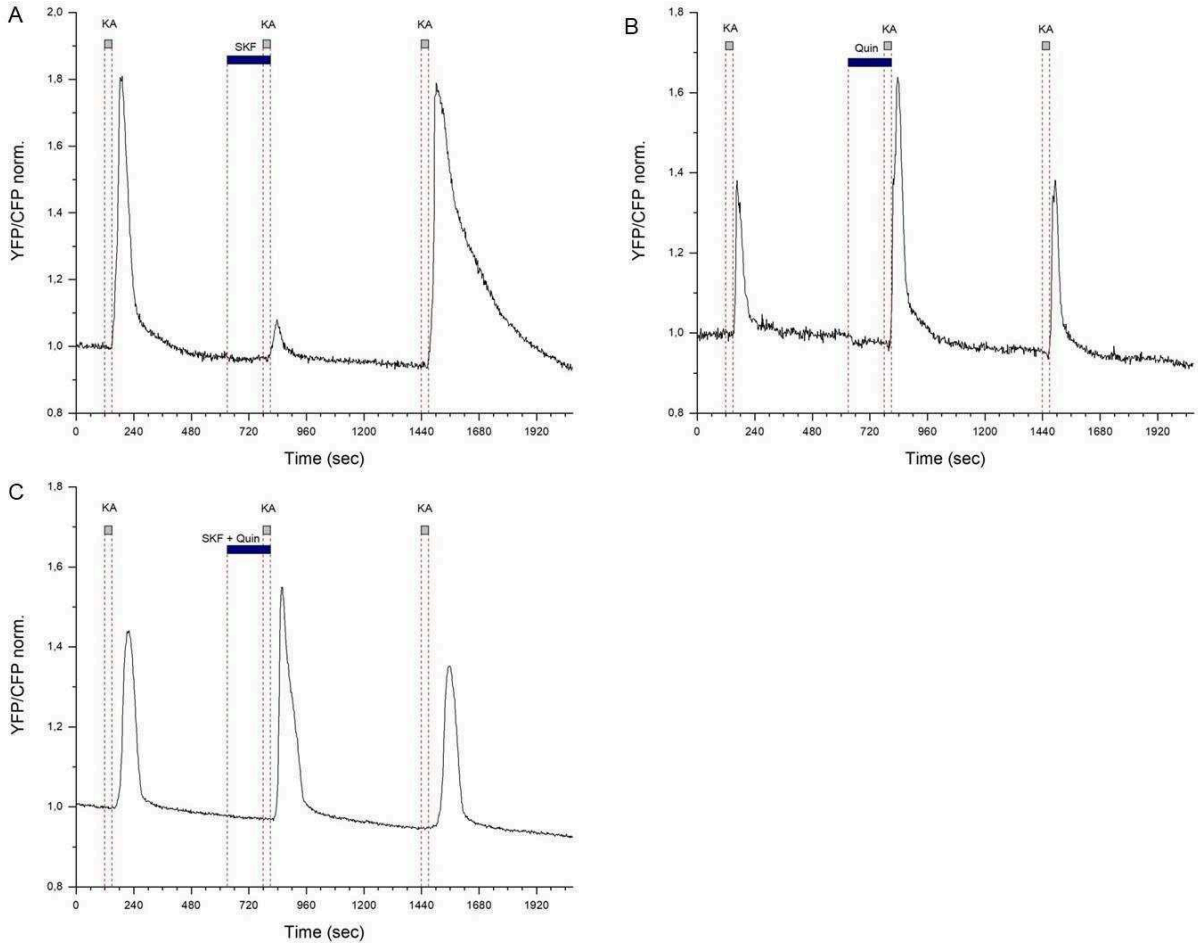


Figure 3.11: Activation of different dopamine receptors affected the kainate-induced calcium responses in different ways. (A): Activation of D1Rs led to a strong reduction in the kainate-induced calcium response, the RA was up to 90% smaller than the initial RA. After recovery, the cell responded to kainate with a strong and long-lasting increase in YFP/CFP ratio. **(B):** Activation of D2Rs led to an enhanced kainate-induced calcium response. The kainate treatments elicited fast and transient increases in YFP/CFP ratios. **(C):** Co-activation of D1Rs and D2Rs enhanced the kainate-induced calcium response.

In order to determine whether stimulation with the D2R agonist quinpirole (1 µM) affects the kainate-induced calcium responses, 55 TN-L15-expressing GCs from three retina pieces were used according to the standard paradigm. In none of the GCs, there was a change in YFP/CFP ratio in response to quinpirole alone. The GC shown in Fig. 3.11, B responded to kainate with a fast and transient increase in YFP/CFP ratio of 38% and the fluorescence signal recovered back to baseline. Activation of kainate receptors in the presence of quinpirole led to an enhanced increase in the YFP/CFP ratio. Just before the stimulus of D2Rs and kainate receptors was stopped, the fluorescence signal increased by 66% and peaked within 40 sec; the whole response lasted approximately 3 min. This cell responded to the first and third kainate exposures with a fast and transient increase in the YFP/CFP ratio, whereby the third response was slightly stronger (Fig. 3.11, B). In other cells, the kainate-induced calcium response was increased by a factor up to 5 when compared to the initial response.

To determine whether stimulation of D1Rs and D2Rs affect the kainate-induced calcium responses in a similar way as stimulation with DA, additional experiments were performed by applying D1R and D2R agonists simultaneously (Fig. 3.11, C). Thus, 28 TN-L15-expressing GCs were stimulated with kainate three consecutive times with the second occurring in the presence of 1 µM SKF 38393 and 1 µM quinpirole. The results were quite different from those obtained in the DA experiment (Fig. 3.9, A and B). In the majority of the cells, the second RA was at least as high as the initial response or rather higher up to a factor of 3. Fig. 3.11, D illustrates the YFP/CFP changes of one GC in response to the distinct stimuli. Stimulation of kainate receptors in the presence of SKF 38393 and quinpirole resulted in an enhanced calcium response when compared to the initial response (Fig. 3.11, C). This effect was similar to the effect of quinpirole alone on kainate-induced calcium responses (Fig. 3.11, B), albeit weaker. The responses to the third kainate treatments showed full recovery, the amplitudes were comparable to the ctrl conditions, indicating that the effect was reversible and was due to the related agonists.

Statistical analyses shown in Fig. 3.12, A summarize the kainate-induced changes in $[Ca^{2+}]_i$ in GCs under ctrl conditions (n=290), treated with 1 µM SKF 38393 (n=61), with 1 µM quinpirole (n=55) and in GCs treated with both 1 µM SKF 38393 and 1 µM quinpirole simultaneously (n=28). The second RAs, with or without the related drugs, were normalized to the initial RAs set as 100%, and data of each cell were plotted as box

plots; each dot represents the response of one GC. The representation revealed that there was a significant difference between the ctrl cells and cells treated with SKF 38393 (Mann-Whitney Rank Sum Test: p***≤0.001). Considering the total of the GCs, activation of D1Rs (with 1 µM SKF 38393) reduced the kainate-induced calcium signaling and there was a shift to smaller calcium responses. Stimulation of D2Rs enhanced the kainate-induced calcium responses, there was a statistically significant difference to the ctrl cells (Mann-Whitney Rank Sum Test: p=0.03). The distribution of the RAs exhibited a strikingly broad distribution (Fig. 3.12, A). There was a significant difference between the cells treated with SKF 38393 and the cells treated with quinpirole (Mann-Whitney Rank Sum Test: p***≤0.001). Activation of D1Rs and D2Rs simultaneously affected barely the kainate-induced calcium signaling and there was no significant difference to the ctrl cells nor to the cells treated with quinpirole alone (Mann-Whitney Rank Sum Test: p=0.37 and p=0.45 respectively; Fig. 3.12, A).

The relative frequencies of cells in respect to the second RAs under ctrl conditions and in the presence of the related drugs are summarized in Fig. 3.12, B. For the majority of the ctrl cells, RAs for the second kainate application were between 80-120% of the first response and, therefore, fell into the RA classes with amplitudes between 80-100% (46%) or 100-200% (47%). With DA there was an inclination towards reduced responses. The RAs were between 50-80% in 29% of the cells (orange); they were found to be smaller than 50% of the initial RAs in 14% (light brown) of the cells. Under ctrl conditions such massive reductions were not found. These effects were much more pronounced under specific activation of D1Rs (with 1 µM SKF 38393). The drift to left, meaning to reduced RAs was more prominent; more than 90% of the cells responded with reduced amplitudes. When D2Rs or both D1Rs and D2Rs were activated, none of the cells responded to kainate with such depressed calcium response as observed under activation of D1Rs. Under activation of D2Rs, 42% of the cells responded with amplitudes between 100-200% (blue) and 16% of the cells with amplitudes higher by at least a factor of 2 (green). Under stimulation of D1Rs and D2Rs, similar, albeit weaker, effects were observed. Under DA influence or activation of D1Rs alone, none of the cells responded with such intensified calcium responses. Thus, activation of D2Rs induced opposite effects as D1Rs and showed an inclination to the right, meaning to enhanced calcium responses.

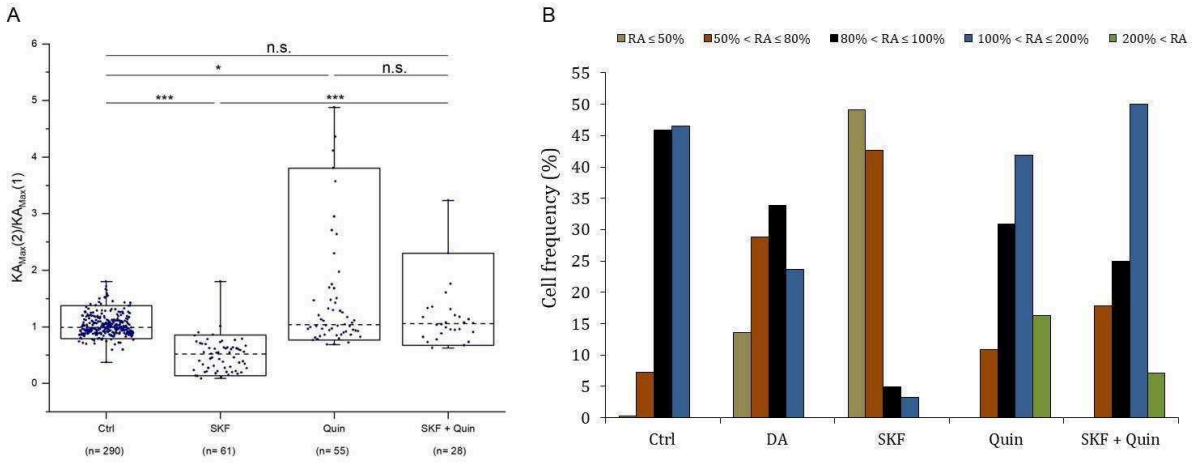


Figure 3.12: Activation of D1Rs and/or D2Rs had opposite effects on the kainate-induced calcium responses. (A): Statistical analysis of the RAs in response to kainate with or without the related drugs. The RAs were normalized to the respective initial RAs and data were plotted as box plots. Each dot represents the $KA_{Max}(2)/KA_{Max}(1)$ of one cell (KA=Kainate). The dotted lines show the medians (Ctrl: 0.99, n=290; SKF 38393 (SKF): 0.52, n=61; Quinpirole (Quin): 1.04, n=55; SKF+Quin: 1.05, n=28). In each box plot, the median divides the box into two parts: the upper part is greater, the lower part is less than the median; the whiskers above and below the box represent the 95th and the 5th percentiles, respectively. The kainate-induced increase in $[Ca^{2+}]_i$ was significantly diminished by SKF 38393 (Mann-Whitney Rank Sum Test: p***≤0.001), significantly enhanced by quinpirole (Mann-Whitney Rank Sum Test: p*≤0.05), and statistically not different when D1Rs and D2Rs were simultaneously activated (Mann-Whitney Rank Sum Test: p=0.37). **(B):** Relative frequency of the kainate RAs with or without the relative drugs were subdivided in five groups and plotted in a bar graph. RAs, which exhibited less than 50% of the initial RAs (light brown), RAs between 50-80% (orange), RAs between 80-100% (black), RAs between 100-200% (blue) and RAs that were higher than the initial RAs by at least a factor of 2 (green). Ctrl=control; DA=dopamine; SKF=SKF 38393; Quin=quinpirole.

In summary, it becomes evident that activated D1Rs affected the kainate-induced calcium responses negatively, leading to a reduction of the changes in $[Ca^{2+}]_i$, while activation of D2Rs rather evoked an enhancement of the kainate-induced calcium responses. The moderate changes observed under stimulation with DA or with SKF 38393 and quinpirole simultaneously might be the result of additional opposite effects, suggesting concomitant antagonistic impacts of the DRs.

3.1.1.2.4. D1Rs affect the kainate-induced calcium signaling most likely via PKA

In the previous chapter (3.1.1.2.3) activation of D1Rs reduced the calcium signaling in response to kainate dramatically (Fig. 3.11, A); a similar pattern could be observed in the AMPA experiments (Fig. 3.5, A). The D1Rs are generally coupled to $G\alpha_s$ that activates the ACy and cause the conversion of ATP to cAMP and consequently an increase in the activity of PKA. To investigate whether the impairment in calcium signaling provoked by activation of D1Rs is indeed mediated by the PKA, I made use of the PKA specific inhibitor H89 (Varella *et al.* 1997), which should block the PKA and abolish partially or

fully the effects observed. Forty-one TN-L15-expressing GCs were exposed to 20 µM kainate for 30 sec followed by a washout phase of 6 min. Afterwards, cells were perfused with 100 µM H89 for 2 min and then simultaneously with 1 µM SKF 38393 for another 2.5 min. Kainate was applied for 30 sec during stimulation of D1Rs and concurrent blockade of PKA. Following, cells were washed out with Ames for 10.5 min before a third kainate application and a washout phase succeeded, respectively.

In 73% of the cells, the stimulation of D1Rs under blockade of PKA did not elicit any change in YFP/CFP ratio. In many cells the blockade of PKA seemed to slightly decrease or increase the YFP/CFP ratio respectively, however, when taking a closer look at the original signaling traces, it becomes clear that these changes in the ratio rather resulted from interferences in CFP or YFP fluorescence signal or in both. The GC shown in Fig. 3.13, A responded to kainate with a sustained increase in the YFP/CFP ratio of 41%, the response lasted for approximately 4.5 min. During blockade of PKA and stimulation of D1Rs, there was a slight disturbance in the response signal, which might not originate from physiological effects. Stimulation of kainate receptors resulted in an increase of 47% in the YFP/CFP ratio, the response reflected two peaks, the first one occurring very fast and transiently, the second peak appeared after the first one dropped to half of its amplitude and lasted for further 4.5 min. The third kainate treatment evoked a weak calcium response with a change in YFP/CFP ratio of 10% and a length of 3.5 min (Fig. 3.13, A). Interestingly, in this experiment none of the cells showed full recovery in terms of the third response, in almost all cells the amplitude of the third response did not reach 50% of the initial response. In 27% of the cells, kainate evoked an increase in YFP/CFP ratio, the fluorescence signal recovered back to baseline and did not exhibit any change in YFP/CFP ratio during application of H89. However, activation of D1Rs under blockade of PKA increased weakly the YFP/CFP ratio (data not shown). In the absence of the PKA specific inhibitor H89, activation of D1Rs did not elicit any change in YFP/CFP ratio as previously shown in Fig. 3.11, A. The responses to kainate under blockade of PKA and activation of D1Rs were not affected. Nevertheless, these cells were not taken into consideration in the statistical analysis, since shortly before the kainate response emerged, the ratio was affected.

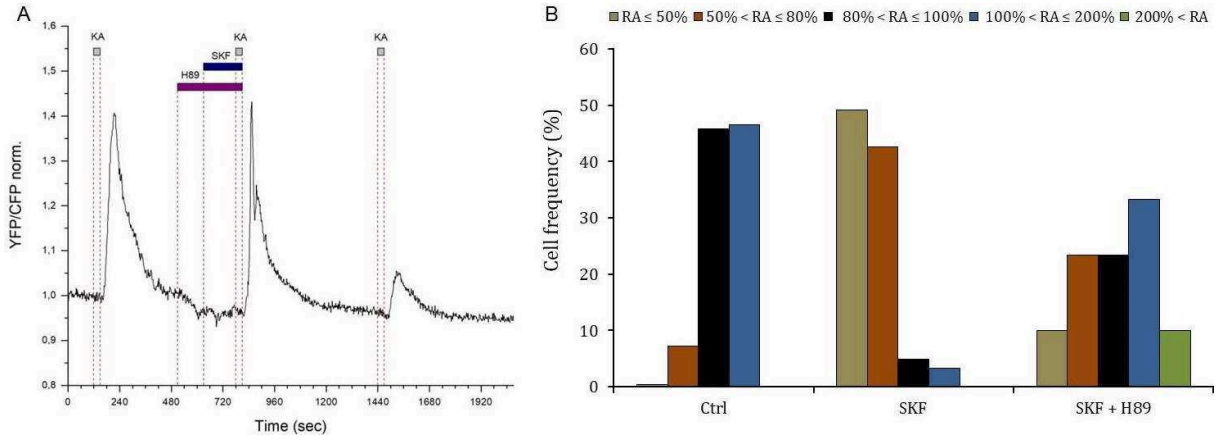


Figure 3.13: D1Rs affected the kainate-induced calcium responses most likely via cAMP/PKA cascade. (A): Kainate induced sustained increases in YFP/CFP ratio; stimulation of D1Rs during blockade of PKA did not affect the kainate-induced calcium responses. The third kainate-induced calcium response was very weak. **(B):** Activation of D1Rs by SKF 38393 reduced the kainate-induced calcium responses clearly. Blockade of PKA by H89 attenuated the impact of D1Rs on the kainate-induced calcium responses. RAs were subdivided in five groups: RAs, which exhibited less than 50% of the initial RAs (light brown), RAs between 50-80% (orange), RAs between 80-100% (black), RAs between 100-200% (blue) and RAs that were higher than the initial RAs by at least a factor of 2 (green). Ctrl=control; SKF=SKF 38393 (1 µM); H89=*N*-[2-[[3-(4-Bromophenyl)-2-propenyl]amino]ethyl]-5-isoquinolinesulfonamide dihydrochloride (100 µM).

The relative frequency of the cells in respect to the RAs was determined (Fig. 3.13, B). The GCs treated with SKF 38393 showed a clear shift to reduced calcium responses when compared to the ctrl cells (light brown and orange). During blockade of PKA and concomitant stimulation of D1Rs, the responses were diverse. There were cells that responded similar to ctrl cells showing no specific effect of activated D1Rs (black and blue). Other cells responded with reduced RAs (light brown and orange). In these cells, the impact of SKF 38393 was not impaired by blockade of PKA. Up to 33% of the cells responded to kainate and SKF 38393 under blockade of PKA with amplitudes between 100-200% (blue), while only 3% of the cells were found in this range when PKA was not blocked. Moreover, a population of GCs was found to respond with enhanced calcium responses to kainate and SKF 38393 (Fig. 3.13, B, green). Such effects were never seen under ctrl conditions or activation of D1Rs alone (Fig. 3.13, B).

Statistical analyses (data not shown) revealed that there was a significant difference between the ctrl cells and cells treated with SKF 38393 and H89 (Mann-Whitney Rank Sum Test: p***=0.001; ctrl: n=290; SKF+H89: n=38). Similarly, the effects induced via stimulation of D1Rs were significantly different under blockade of PKA (Mann-Whitney Rank Sum Test: p***≤0.001; SKF: n=61; SKF+H89: n=38).

The kainate-induced calcium response was dramatically affected by activation of D1Rs in the majority of the GCs; this inhibitory effect was partially prevented by blockade of PKA in the majority of the GCs, demonstrating the involvement of the cAMP/PKA cascade. The fact that the kainate-induced calcium response was still impaired in some cells could be explained by high D1Rs expression level. In these GCs, activation of D1Rs could induce a high cAMP production so that not all activated PKA could be inhibited with 100 µM of H89. In some GCs, the kainate-induced calcium response was even enhanced under these experimental conditions; indicating that another mechanism may be involved such as calcium-induced calcium release from internal calcium stores (CICR).

3.1.1.3. DA affects the NMDA-induced changes in $[Ca^{2+}]_i$ in GCs

3.1.1.3.1. NMDA induced changes in $[Ca^{2+}]_i$ in GCs

In the vertebrate retina, *N*-METHYL-D-ASPARTATE (NMDA) receptors are found in horizontal cells (HCs) (Shen *et al.* 2006), on a subset of amacrine cells (ACs) and on GCs (Slaughter & Miller 1983, Massey & Miller 1990, Mittman *et al.* 1990, Dixon & Copenhagen 1992). In the inner retina, NMDA receptors are involved in mediating signal transmission from bipolar cells (BCs) to ACs and GCs, moreover they could be involved in modulating the inhibitory feedback from ACs to BCs (Shen *et al.* 2006).

In order to investigate the NMDA-induced calcium response and their susceptibility to dopaminergic modulation, 426 TN-L15-expressing GCs were stimulated with NMDA using the standard paradigm. Similar to the analysis of cells treated with AMPA or kainate, only responses without massive photobleaching or noisy signals and with authentic changes in CFP and YFP fluorescence signals were taken into consideration. In total, 297 TN-L15-expressing GCs of the intact retina were stimulated with the specific agonist NMDA (300 µM) according to the standard paradigm. All cells responded to NMDA application. As NMDA receptors are blocked by Mg^{2+}-ions at very negative membrane potential, this result may indicate that GCs are not strongly hyperpolarized at resting conditions. Similar to AMPA- and kainate-induced calcium responses, two general types of responses were observed: transient and sustained responses. GCs that responded to stimulation with NMDA with a transient increase in YFP/CFP ratio and thus in $[Ca^{2+}]_i$ represented with 79% the majority of the cells (Fig. 3.14, A). A sustained increase in $[Ca^{2+}]_i$ was found in the remaining 21% of the cells (Fig. 3.14, B). The cell

shown in Fig. 3.14, A responded with a transient increase in YFP/CFP ratio of 88%, the signal fluorescence peaked within 30 sec. The fluorescence signal recovered rapidly back to baseline and the length of the response was about 2.5 min. The response was reversible and reproducible; the second and third responses were similar in terms of shape and length. They showed a slight rundown effect with a change in YFP/CFP ratio of 83% and 73% respectively (Fig. 3.14, A). On the other hand, the GC shown in B responded promptly with a strong increase in YFP/CFP ratio of 97%, the signal fluorescence decreased in a two stage way: rapidly up to two-thirds of the amplitude and then slower over a shoulder. The fluorescence signal recovered back to baseline after a total length of 4.5 min. The second and third responses exhibited a similar shape and lasted for 5 and 5.5 min with a change in YFP/CFP ratio of 85% and 73% respectively (Fig. 3.14, B).

The RAs triggered by NMDA treatments were calculated; following the RAs were normalized to the initial ones by calculating the ratio $NMDA_{Max}(2)/NMDA_{Max}(1)$. Later on, the ratios in the presence of the related drugs were compared to the ctrl, and data were subdivided in ranges depending on the variance of the changes.

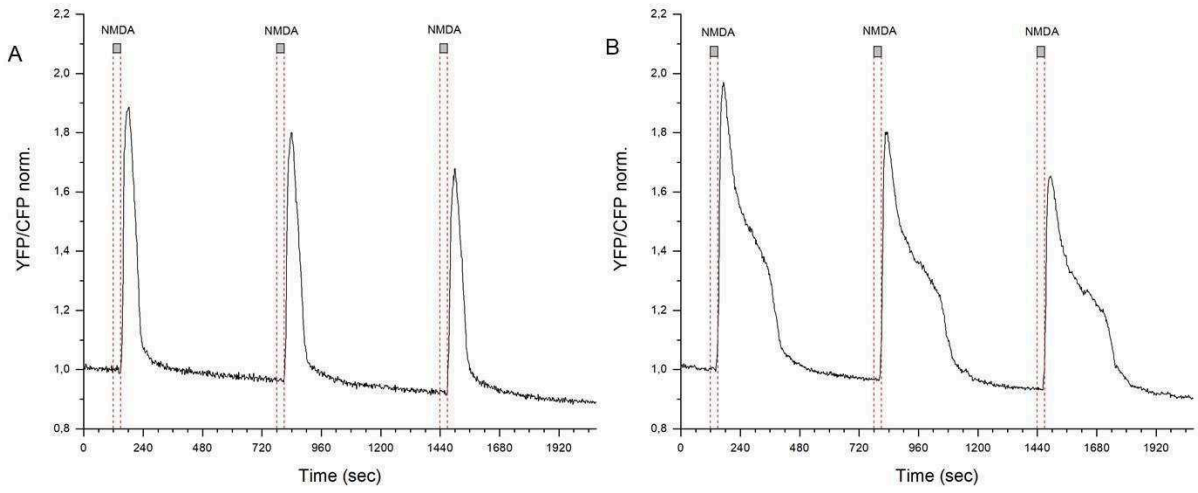


Figure 3.14: NMDA induced reversible and reproducible increases in YFP/CFP ratio in GCs. (A): NMDA (300 µM) induced strong and transient increases in YFP/CFP ratio, thus in $[Ca^{2+}]_i$. The responses showed a slight rundown effect. **(B):** NMDA induced strong and long-lasting increases in YFP/CFP ratio. The responses lasted between 4.5 and 5.5 min.

3.1.1.3.2. DA had slight effects on the NMDA-induced changes in $[Ca^{2+}]_i$ in GCs

To test the effect of DA (20 µM) on the NMDA-induced changes in $[Ca^{2+}]_i$, 95 TN-L15-expressing GCs of the intact retina were exposed to NMDA according to the standard

paradigm. The cell shown in Fig. 3.15, A responded to NMDA with a fast and transient increase in YFP/CFP ratio of 88%, the signal recovered back to baseline and the whole response lasted for 2.5 min. Stimulation with NMDA in the presence of DA induced a fast and transient increase in YFP/CFP ratio of 64%; the fluorescence signal peaked within 30 sec and the response length was shortened to less than 2 min. The third stimulation with NMDA induced an enhanced increase in YFP/CFP ratio of 74% and the response lasted for 2.5 min similar to the first one (Fig. 3.15, A). The stimulation with DA did not elicit any change in YFP/CFP ratio in 79% of the cells as shown exemplarily for this cell (Fig. 3.15, A). In 21% of the GCs treated with DA, there was an increase in YFP/CFP ratio in response to DA as shown in Fig. 3.15, B. The cell responded to the first NMDA treatment with a fast and transient increase in YFP/CFP ratio of 35%. About 30 sec after stimulation with DA started, the fluorescence signal increased and peaked within 1 min with a change of 21% then started to recover slowly. The fluorescence signal dropped to approximately one third of its amplitude and kept decreasing very slowly. Stimulation with NMDA in the presence of DA induced an increase in YFP/CFP ratio of 29%, still before the cell recovered fully from the response to DA. This response was short and transient; the cell recovered back to baseline and responded to the third NMDA treatment with a fast but prolonged increase in YFP/CFP ratio of 31% (Fig. 3.15, B). Not all cells that responded to DA alone exhibited such a strong response. In the majority of the GCs the DA-induced increase in YFP/CFP ratio was slow and weak (data not shown).

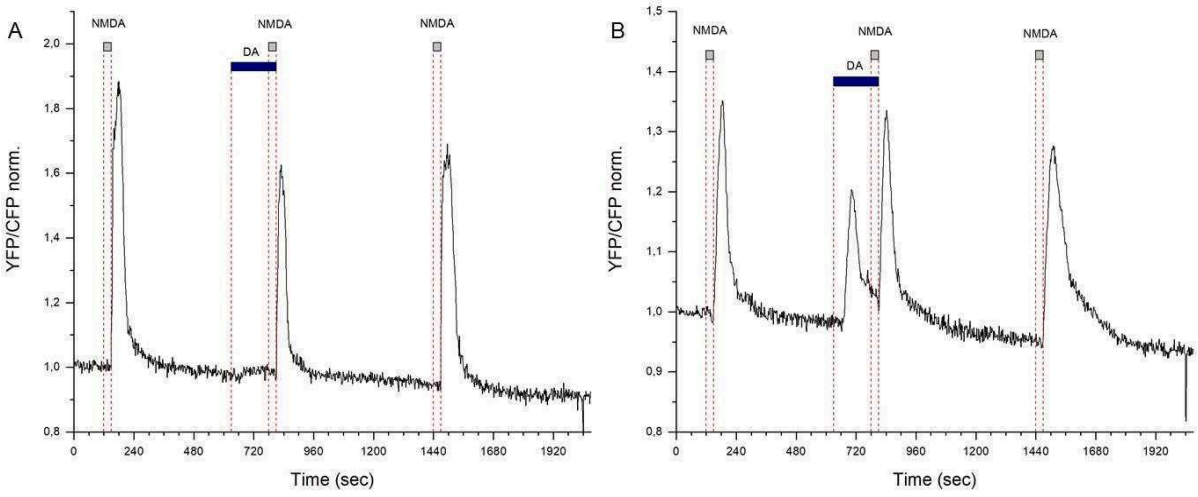


Figure 3.15: DA affected the calcium signaling and the NMDA-induced calcium responses in some GCs. (A): NMDA (300 µM) induced transient increases in YFP/CFP ratio, thus in $[Ca^{2+}]_i$. In the presence of DA (20 µM) the NMDA-induced calcium response was slightly reduced. **(B):** NMDA and DA induced transient increases in YFP/CFP ratio, the last response was prolonged.

The GCs, whose NMDA-induced response overlapped with the DA-induced response were excluded from the statistical analysis. Statistical analysis shown in Fig. 3.16, A reveals that the NMDA-induced changes in $[Ca^{2+}]_i$ in GCs were reduced in the presence of DA (20 µM). Indeed, there was a significant difference between ctrl cells and cells treated with DA (Mann-Whitney Rank Sum Test: p***≤0.001). In order to better clarify the wide distribution of the RAs, the cells were assigned to different groups according to the RA ranges of the second responses (Fig. 3.16, B). Under ctrl conditions, the majority of the cells (71%) responded with amplitudes between 80-100% (Fig. 3.16, B, black). There were cells that responded with amplitudes with moderate changes (orange and blue). In the presence of DA, the RAs to NMDA showed an inclination to reduced RAs. The largest group was constituted of 41% of the cells with RAs between 50-80% (Fig. 3.16, B, orange). Moreover, a further range of RAs emerged; 11% of the cells responded with amplitudes smaller than 50% (Fig. 3.16, B, light brown).

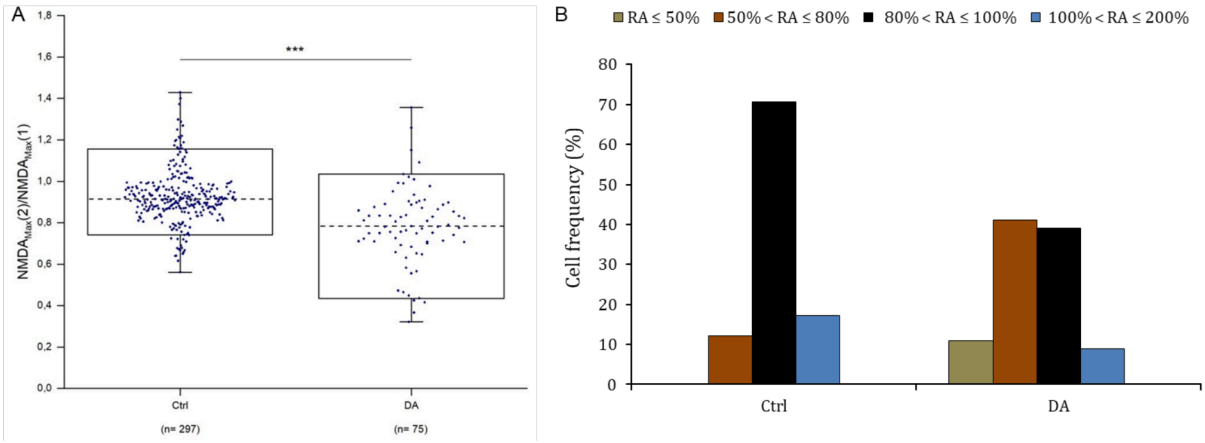


Figure 3.16: DA decreased the NMDA-induced calcium responses slightly in GCs. (A): Statistical analysis of the RAs in response to NMDA (300 µM) with and without DA (20 µM). The RAs were normalized to the respective initial RAs and data were plotted as box plots. Each dot represents the $NMDA_{Max}(2)/NMDA_{Max}(1)$ of one cell. The dotted lines show the medians (Ctrl: 0.97, n=297; Dopamine (DA): 0.78, n=75). In each box plot, the median divides the box into two parts: the upper part is greater, the lower part is less than the median; the whiskers above and below the box represent the 95th and the 5th percentiles, respectively. The NMDA-induced increase in YFP/CFP ratio and thus in $[Ca^{2+}]_i$ is significantly diminished by DA (Mann-Whitney Rank Sum Test: p***≤0.001). **(B):** Relative frequency of the RAs to NMDA with and without 20 µM DA. Different groups of RAs could be distinguished: RAs that were smaller than 50% (light brown), RAs between 50-80% (orange), RAs between 80-100% (black) and RAs between 100-200% (blue).

The statistical analysis and the distribution of the RAs with or without DA shown in Fig. 3.16 indicate that DA tends to reduce the NMDA-induced calcium responses in GCs slightly, but significantly.

3.1.1.3.3. Dopamine receptors affect NMDA-induced changes in $[Ca^{2+}]_i$ in GCs

As shown so far, application of DA induced a slight decrease in the calcium responses induced by both non-NMDA and by NMDA receptors. In the case of AMPA and kainate receptors this decrease was mediated by activation of D1Rs as it was mimicked by application of 1 µM SKF 38393. In order to find out whether activation of D1Rs modulates the NMDA calcium responses in a similar way, 105 TN-L15-expressing GCs of the intact retina were exposed to NMDA and 1 µM SKF 38393 according to the standard paradigm. The GC shown in Fig. 3.17, A responded to NMDA treatment with an increase in YFP/CFP ratio of 61% for the first and second stimulations and 52% for the third one. Stimulation of D1Rs did not affect the NMDA-induced calcium responses (Fig. 3.17, A).

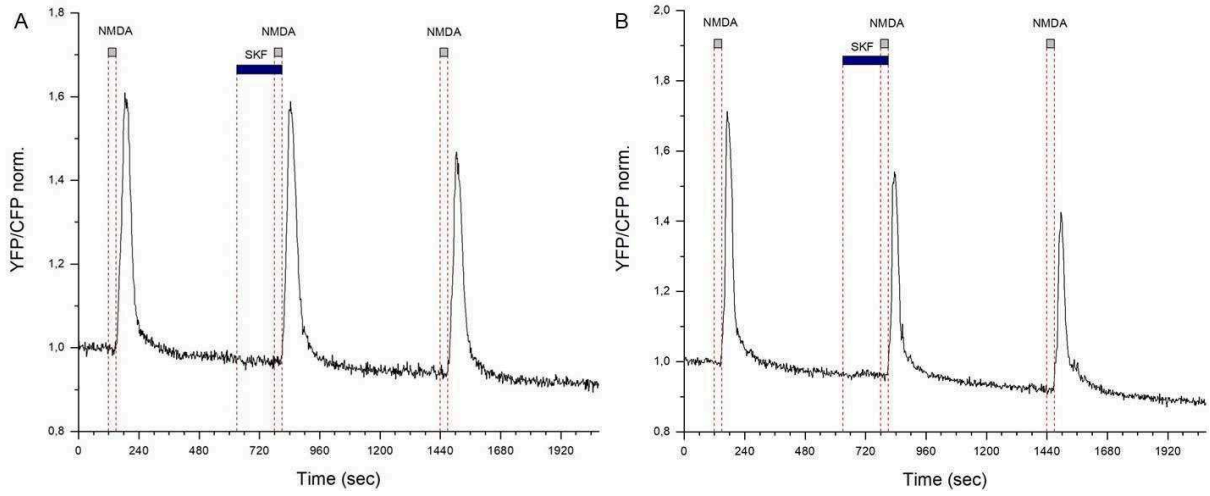


Figure 3.17: Activation of D1Rs did not affect the NMDA-induced calcium responses. (A): Application of NMDA induced an increase in the YFP/CFP ratio, the cell responded in a reversible and reproducible way. Stimulation of D1Rs did not affect the NMDA-induced calcium response. **(B):** NMDA induced an increase in YFP/CFP ratio; stimulation of D1Rs induced a weak increase in the YFP/CFP ratio, which lasted approximately 2 min.

There were cells that responded weaker in the presence of SKF 38393; however, this seems to be related to a rundown effect (Fig. 3.17,B). The GC shown in Fig. 3.17, B responded to the first NMDA application with a transient and fast increase in YFP/CFP ratio of 71%. The fluorescence signal recovered fully towards the baseline within 2.5 min. Activation of D1Rs did not elicit any change in YFP/CFP ratio. The NMDA application in the presence of SKF 38393 induced a similar increase in the fluorescence signal in terms of shape and duration. The increase in YFP/CFP ratio was about 57%. After recovery, the cell responded to NMDA with an increase in YFP/CFP ratio of 49% (Fig. 3.17, B). Thus, the reduction in the responses over time seems to be related to a rundown effect, rather to activation of D1Rs.

In the presence of DA (Figs. 3.15 and 3.16), the NMDA-induced calcium response was significantly diminished; however, no clear-cut effects were observed upon activation of D1Rs (Fig. 3.17). It was, therefore, tested whether the DA-induced effects were mediated by activation of D2Rs. Thus, 82 TN-L15-expressing GCs were treated with NMDA (300 µM) and quinpirole (1 µM) according to the standard paradigm.

In 98% of the GCs, activation of D2Rs alone did not elicit any change in the $[Ca^{2+}]_i$, however the NMDA-induced calcium responses were variably affected. Only two cells (2%) responded to quinpirole with an increase in YFP/CFP ratio (data not shown). However, the fluorescence signal in these cells was more noisy than usual or it did not recover from the changes in the YFP/CFP ratio. Thus, these effects were not clear enough and were not taken into consideration (data not shown). The GC shown in Fig. 3.18, A responded to the first and third NMDA treatments with transient increases in the YFP/CFP ratio of 62% and 53% respectively; responses lasted approximately 3 min. During application of quinpirole, NMDA changed the YFP/CFP ratio only by 17%, the response was shortened to 90 sec (Fig. 3.18, A). In contrast, in the GC shown in Fig. 3.18, B the activation of D2Rs enhanced the NMDA-induced calcium response. The first and last NMDA treatments elicited increases in YFP/CFP ratio of 37% and 44% and a duration of 5 and 6 min respectively. In the presence of quinpirole, NMDA induced an increase in YFP/CFP ratio of 57%; the whole response lasted for 7 min (Fig. 3.18, B).

Since activation of D1Rs did not affect NMDA-induced calcium responses, a simultaneous activation of D1Rs and D2Rs should not strongly differ from the effects seen with quinpirole alone. Forty-nine TN-L15-expressing GCs were tested for the effect of 1 µM SKF 38393 and 1 µM quinpirole using the standard paradigm (Fig. 3.18, C and D). Compared to the effects seen with quinpirole alone (Fig. 3.18, A and B), the effects of the agonists mixture on the NMDA-induced calcium responses were less variable as the extreme RA ranges were not observed. None of the cells responded with amplitudes smaller than 50% of the initial responses or higher by at least a factor of 2 as shown under quinpirole impact. The cell shown in Fig. 3.18, C responded to NMDA with a transient increase in YFP/CFP ratio of 48%, the fluorescence signal recovered towards the baseline after approximately 2.5 min. Application of NMDA in the presence of SKF 38393 and quinpirole induced a transient increase in YFP/CFP ratio of 33% that lasted approximately 90 sec. In the absence of NMDA, there was no change in the $[Ca^{2+}]_i$. Following, the cell recovered fully and responded to the third NMDA application with a

transient increase in YFP/CFP ratio of 44%. The last response lasted approximately 3 min before the fluorescence signal recovered to baseline (Fig. 3.18, C). The GC shown in Fig. 3.18, D responded to the first and third NMDA applications with changes in YFP/CFP ratio of 33% and 39%, respectively. During activation of D1Rs and D2Rs simultaneously, NMDA induced an enhanced change in YFP/CFP ratio of 50% (Fig. 3.18, D).

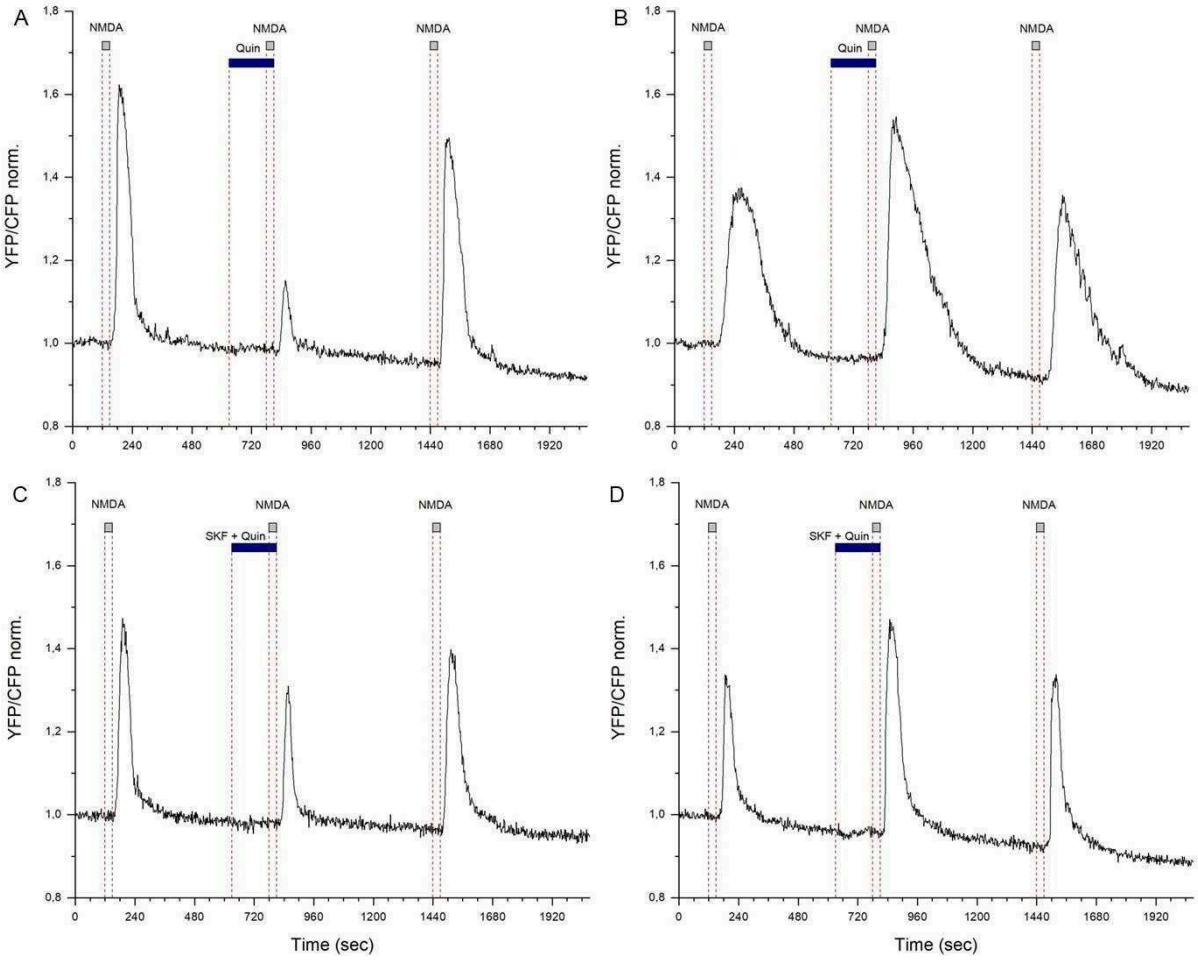


Figure 3.18: Activation of D2Rs affected the NMDA-induced calcium responses variably. (A): Application of 1 µM quinpirole clearly decreased the NMDA-induced calcium response in this GC; the cell recovered fully from this reduction and responded to the last NMDA treatment normally. **(B):** Activation of D2Rs enhanced the NMDA-induced calcium response in this GC; the cell recovered and responded to the last NMDA treatment with a smaller increase in YFP/CFP ratio. **(C):** Activation of D1Rs and D2Rs decreased the NMDA-induced calcium responses in this GC. The fluorescence signal recovered fully and responded to the third NMDA treatment with a higher change in YFP/CFP ratio. **(D):** Activation of D1Rs and D2Rs enhanced the NMDA-induced calcium response in this GC, similar to the cell shown in B.

The statistical analyses of the RAs of the NMDA-induced changes in $[Ca^{2+}]_i$ in GCs are shown in Fig. 3.19, A. GCs under ctrl conditions (n=297), treated with 1 µM SKF 38393 (n=105), with 1 µM quinpirole (n=80) and GCs treated with both 1 µM SKF 38393 and 1 µM quinpirole simultaneously (n=49) were compared to each other. The second RAs, with or without the related drugs, were normalized to the initial ones, and data were

plotted as box plots; each dot represents one GC. The activation of D1Rs did not affect the NMDA-induced calcium responses and there was no significant difference to the ctrl cells (Mann-Whitney Rank Sum Test: p=0.60). Stimulation of D2Rs resulted in a large variance; there were GCs with reduced RAs and GCs with enhanced RAs. This most probably reflects differences between different GC subtypes. In total, the responses of the cells treated with quinpirole were significantly different from the ctrl cells (Mann-Whitney Rank Sum Test: p***≤0.001). Simultaneous activation of D1Rs and D2Rs resulted in responses that did not significantly differ from the responses of ctrl cells (Mann-Whitney Rank Sum Test: p=0.08) nor from cells treated with SKF 38393 (Mann-Whitney Rank Sum Test: p=0.11). These cells differ significantly from the cells treated with quinpirole (Mann-Whitney Rank Sum Test: p=0.004; Fig. 3.19, A).

The relative frequencies of cells in respect to the second RAs in response to NMDA with or without the related drugs are summarized in Fig. 3.19, B. Under ctrl conditions, the majority of the cells (71%) responded with amplitudes between 80-100% (black). In the presence of DA (20 µM), 41% of the cells responded with reduced RAs (50-80%, orange). Moreover, here emerged for the first time RAs that were smaller than 50% (light brown). Activation of D1Rs did not affect the NMDA-induced calcium responses. The majority of the cells (71%) responded with amplitudes between 80-100% (black). Interestingly, activation of D2Rs induced various effects. There were GCs (33%) that responded with amplitudes smaller than 50% of the initial responses (light brown). There were cells that responded with amplitudes exhibiting moderate changes; these were also seen under ctrl condition. The responses were enhanced up to a factor of 2 in 26% and by at least a factor of 2 in 6% of the cells (blue and green respectively). The simultaneous activation of D1Rs and D2Rs did not affect the NMDA-induced calcium responses (Fig. 3.19, B).

In short, activation of DRs with DA showed an inclination to the left meaning to reduced calcium responses. Activation of D2Rs resulted in various effects, leading either to reduced or enhanced calcium responses, probably reflecting different GC subtypes. Activation of D1Rs or simultaneous activation of D1Rs and D2Rs did not affect the calcium responses.

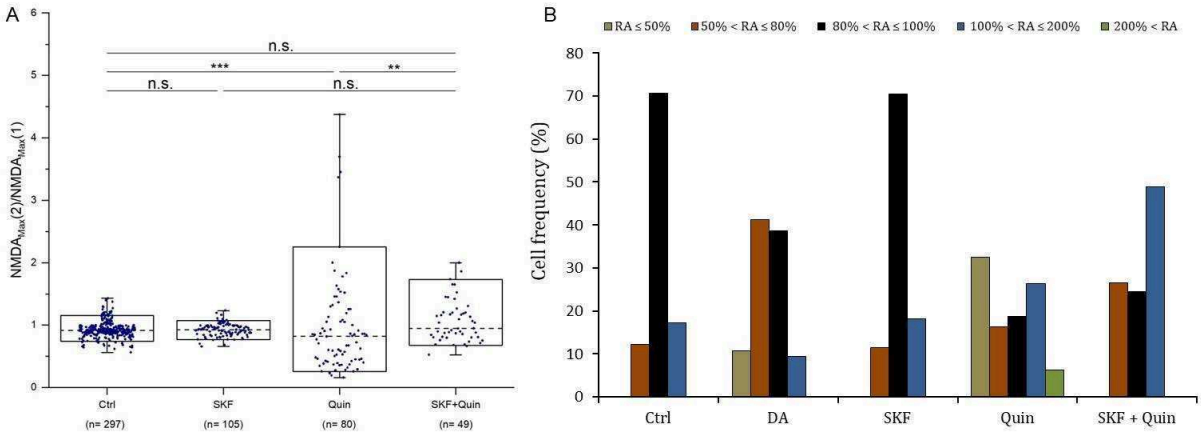


Figure 3.19: Activation of D2 receptors modulates the NMDA-induced calcium responses. (A): Statistical analysis of the RAs in response to NMDA with or without the related drugs. The RAs were normalized to the respective initial RAs and data were plotted as box plots. Each dot represents the $NMDA_{Max}(2)/NMDA_{Max}(1)$ of one cell. The dotted lines show the medians (Ctrl: 0.91 n=297; SKF 38393 (SKF): 0.92, n=105; Quinpirole (Quin): 0.82, n=80; SKF+Quin: 0.94, n=49). In each box plot, the median divides the box into two parts: the upper part is greater, the lower part is less than the median; the whiskers above and below the box represent the 95th and the 5th percentiles, respectively. The NMDA-induced change in $[Ca^{2+}]_i$ is significantly diminished by quinpirole (Mann-Whitney Rank Sum Test: p***≤0.001), statistically not different by SKF 38393 (Mann-Whitney Rank Sum Test: p=0.6), and statistically not different when D1Rs and D2Rs were simultaneously activated (Mann-Whitney Rank Sum Test: p=0.08). **(B):** Relative frequencies of cells in response to NMDA with or without the relative drugs. RAs were subdivided in five groups: RAs, which exhibited less than 50% of the initial RAs (light brown), RAs between 50-80% (orange), RAs between 80-100% (black), RAs between 100-200% (blue) and RAs that were higher by at least a factor of 2 (green). Ctrl=control; DA=dopamine (20 µM); SKF=SKF 38393 (1 µM); Quin=quinpirole (1 µM).

In summary, the calcium responses induced via activation of non-NMDA receptors were moderately reduced in the presence of dopamine, and strikingly reduced by activation of D1Rs. The moderate effect observed with dopamine lead to the assumption that several dopamine receptors with antagonizing effects might be activated. These other receptor types would suppress the strong effect seen with activation of D1Rs alone. D2Rs counteract D1Rs; indeed, their activation induced opposing effects and enhanced the non-NMDA-induced calcium responses, in particular in the case of AMPA receptors. This corroborates the assumption that in the presence of DA both dopamine receptor families are stimulated and the opposing intracellular signaling pathways counteract each other. Simultaneous activation of D1Rs and D2Rs had similar effects as activation of D2Rs alone on non-NMDA-induced calcium responses. The effects were significantly different from the effects induced via activation of D1Rs. This indicates that D1Rs did not override the impact induced via D2Rs; rather, D2R-mediated inhibition of the ACy was so strong, that the effect of D1Rs was suppressed. The effects induced via DA were slight, it is most likely that the concentration of DA used to stimulate DRs (20 µM) did not correlate with the agonist concentrations used to stimulate D1Rs and D2Rs separately with 1 µM SKF 38393 and 1 µM quinpirole, respectively. Under blockade of

PKA, there were cells that responded to kainate and SKF 38393 with reduced calcium responses. In these cells, the PKA activity was probably higher than could be blocked by the concentration used for the specific inhibitor H89, or it is also possible that these cells expressed a high level of D1Rs, so not all the PKA activated could be inhibited. Still, the effects induced via D1Rs were strongly impaired. This indicates that D1Rs affect the non-NMDA-induced calcium responses most likely via activation of PKA.

The results obtained with NMDA receptors were quite different; activation of D1Rs did not affect NMDA-induced calcium responses. In the presence of DA, there was a slight reduction in the calcium responses, which was most probably induced via activation of D2Rs. Activation of D2Rs induced diverse and opposite effects on the NMDA-induced calcium responses. This may indicate that in different GC types, D2Rs induce at least two different cellular signaling pathways, which lead to different effects.

In summary, it appears evident that activation of DRs modulates the calcium responses induced via the activation of ionotropic glutamate receptors in very distinct ways. The effects on non-NMDA- were at least partially different from the effects on NMDA-induced calcium responses suggesting most likely a direct modulation of the iGluRs. Activation of DRs induces different and distinct signaling pathways that have different and in great part counteracting effects.

3.1.2. Studying the effects of NO on iGluR-mediated responses in GCs of the TN-L15-retina

Nitric oxide (NO) is a short-lived gas produced on demand by nitric oxide synthases (NOS) from the amino acid L-arginine. NO has been implicated in many physiological and pathological processes within the retina (Guimaraes *et al.* 2001); NO increases cyclic guanosine monophosphate (cGMP) – and, hence, activity of protein kinase G - via activation of sGC. Therefore, NO might modulate activity of signaling proteins by PKG-mediated phosphorylation. Neuronal NOS was localized in ACs and displaced ACs by using NADPH-diaphorase (Dawson *et al.* 1991, Koistinaho *et al.* 1993, Kim *et al.* 1999). NO may be involved in the modulation of synaptic transmission from PRs: the NO-releasing compound SNC increased the CaCh currents in isolated salamander PRs (Kurenny *et al.* 1994). In GCs, NO donors or NOS inhibitors altered cGMP-gated synaptic

conductance (Ahmad *et al.* 1994). In this chapter, I will investigate whether NO modulates the iGluR-induced calcium responses in the GCs of the TN-L15-retina.

3.1.2.1. NO enhanced the AMPA-induced changes in $[Ca^{2+}]_i$ in GCs

In order to test the effect of the NO-donor S-Nitroso-N-acetyl-DL-penicillamine (SNAP) on the AMPA-induced calcium changes in GCs, 58 TN-L15-expressing GCs from three retina pieces were exposed to AMPA (5 µM) and the NO-donor (300 µM) according to the standard paradigm. Two different types of responses were observed. The cell shown in Fig. 3.20, A responded to AMPA with an increase in YFP/CFP ratio of 33%. The fluorescence signal started to increase approximately 60 sec after the AMPA application was stopped, and the response lasted for 3 min, then decreased to beneath the baseline. During stimulation with SNAP the fluorescence signal increased slightly, however, when looking at the original recording no clear-cut mirror reversed changes in the CFP and YFP signals typical for FRET responses could be observed (data not shown). Therefore, these slight changes have to be interpreted with caution. In the presence of SNAP, the cell responded to AMPA with an increase in YFP/CFP ratio of 16%. The fluorescence signal started to increase approximately 60 sec after the application was stopped, and recovered to beneath the baseline after 2.5 min. The third AMPA stimulation induced an increase in YFP/CFP ratio of 31% and the response lasted for 3 min (Fig. 3.20, A). The GC shown in Fig. 3.20, B responded to the first and third AMPA treatments with an increase in YFP/CFP ratio of 16% and duration of 2.5 min each. Approximately 30 sec after the second AMPA application was stopped, the fluorescence signal started to increase slowly then faster to peak with a change of 90% in YFP/CFP ratio. The fluorescence signal recovered towards the baseline after approximately 4 min and the effect of SNAP was fully reversible. The cell responded to the last AMPA application with an increase in YFP/CFP ratio of 16% (Fig. 3.20, B).

The second RAs in the presence of SNAP were normalized to the respective initial RAs, and were then compared to the ctrl cells, which were explicitly described in chapter 3.1.1.1.1 (Fig. 3.3, C). Statistical analysis shown in Fig. 3.20, C revealed that there was a significant difference between cells treated with SNAP and the ctrl cells (Mann-Whitney Rank Sum Test: p***≤0.001, n=58).

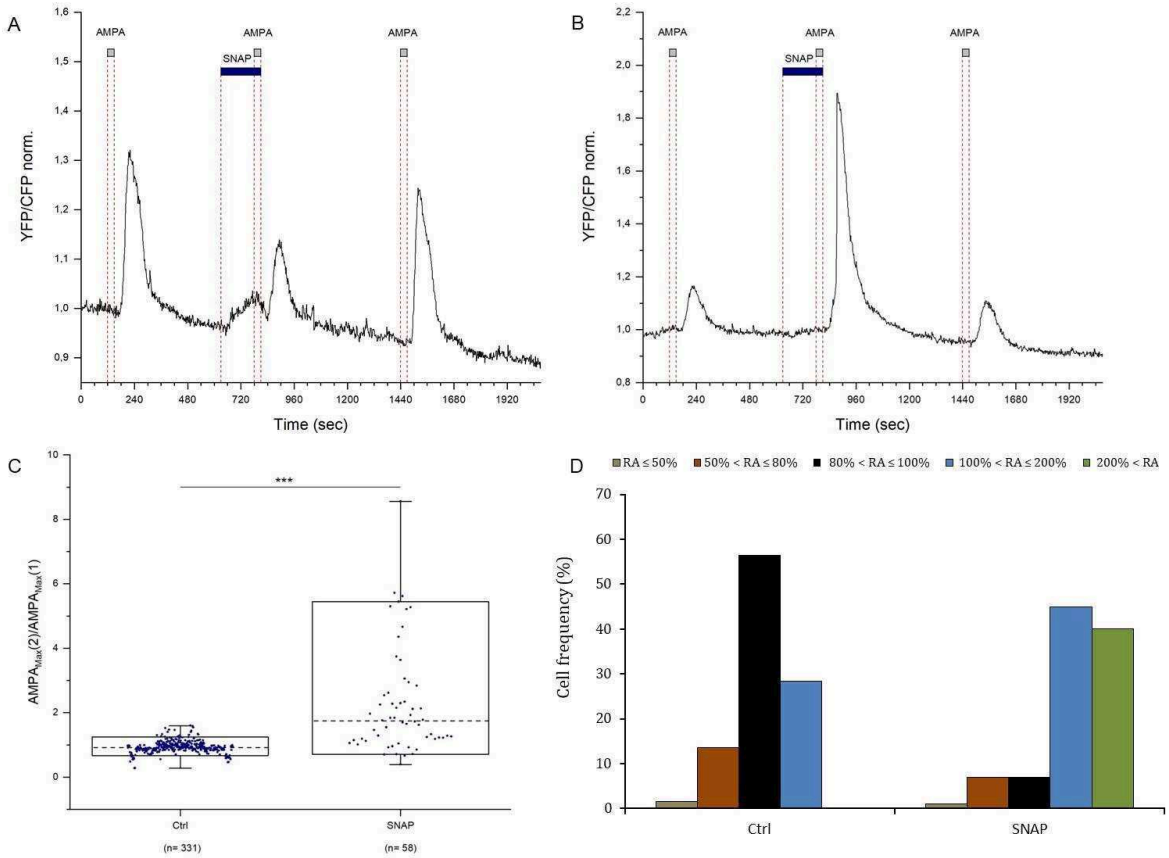


Figure 3.20: The NO-donor SNAP increased the AMPA-induced calcium changes in GCs. (A): The response of one GC to three AMPA applications. In the presence of SNAP (300 µM) the AMPA-induced calcium response was reduced. **(B):** The AMPA-induced calcium response was enhanced by a factor of 5 in the presence of SNAP when compared to the initial response; the GC recovered fully and responded to the third AMPA application similar to the first one. **(C):** Statistical analysis of the RAs in response to AMPA with or without SNAP. The RAs were normalized to the respective initial RAs and data were plotted as box plots. Each dot represents the $AMPA_{Max}(2)/AMPA_{Max}(1)$ of one cell. The dotted lines show the medians (Ctrl: 0.92, n=331; SNAP: 1.74, n=58). In each box plot, the median divides the box into two parts: the upper part is greater, the lower part is less than the median; the whiskers above and below the box represent the 95th and the 5th percentiles, respectively. The AMPA-induced increase in $[Ca^{2+}]_i$ was significantly increased by SNAP (Mann-Whitney Rank Sum Test: p***≤0.001). **(D):** Relative frequency of the cells in response to AMPA with or without SNAP. RAs were subdivided in five groups: RAs, which exhibited less than 50% of the initial RAs (light brown), RAs between 50-80% (orange), RAs between 80-100% (black), RAs between 100-200% (blue) and RAs that were higher than the initial RAs by at least a factor of 2 (green). Ctrl=control, AMPA (5 µM); SNAP=S-Nitroso-N-acetyl-DL-penicillamine (300 µM).

The NO-donor SNAP increased the AMPA-induced calcium responses in the majority of the cells (Fig. 3.20, D). The distribution of the RAs of the GCs treated with SNAP is wide when compared to the RAs of the ctrl cells. In order to better clarify the effects seen, the RAs were assorted in groups and the relative cell frequency was determined (Fig. 3.20, D). Only one cell (1%) responded with a RA that was smaller than 50% (light brown), which is shown in Fig. 3.20, A. The RAs ranging between 50-80% (orange) and between 80-100% (black) were found in 7% each. The RAs were higher up to a factor of 2 in 45% of the cells (blue). In almost all the cells of this latter group, the third RAs were smaller than the initial ones. In 40% of the cells, the RAs were higher by at least a factor

of 2 (Fig. 3.20, D, green). The strongest effect was found in a GC, which responded with a factor of 8.56 and the cell recovered fully.

In summary, these results indicate that SNAP (NO) is involved in modulation of AMPA receptors excitability. NO induced an enhancement of the AMPA-induced calcium changes in the majority of the GCs (85%). The starting $[Ca^{2+}]_i$ did not correlate with the differences observed in the responses, since it was similar in almost all the cells.

3.1.2.2. NO had slight effects on the kainate-induced changes in $[Ca^{2+}]_i$ in GCs

In the previous chapter (3.1.2.1), SNAP (NO) enhanced the AMPA-induced calcium responses in the majority of the GCs. In order to find out whether NO modulates the kainate-induced calcium responses, 68 TN-L15-expressing GCs from four retina pieces were stimulated with kainate and SNAP (300 µM) according to the standard paradigm. In the presence of SNAP, stimulation of kainate receptors induced different calcium responses. The cell shown in Fig. 3.21, A responded to the first and third kainate treatments with increases in YFP/CFP ratio of 52% and 42% respectively. In the presence of SNAP, application of kainate induced an increase in the YFP/CFP ratio of 35%. Thus, SNAP reduced the kainate-induced calcium response slightly and the cell recovered from the SNAP effect (Fig. 3.21, A). The cell shown in Fig. 3.21, B responded to kainate in the presence of SNAP with an increase in the YFP/CFP ratio of 89%. The first and third kainate applications induced increases of about 70% each. Both GCs shown in Fig. 3.21, A and B were from the transient type, nevertheless similar effects were also observed in the sustained type found in 10 % (n=7) of the cells (data not shown).

The impact of SNAP (NO) on the kainate-induced calcium responses was not obvious. The statistical analysis of the normalized RAs shown in Fig. 3.21, C indicates that there was no significant difference between the cells treated with SNAP and the ctrl cells (Mann-Whitney Rank Sum Test: p=0.091). The majority of the cells with or without SNAP responded with amplitudes in the same range (Fig. 3.21, C); the moderate variations observed under SNAP impact may go down in the statistical analysis. Thus, the RAs were subdivided in five groups and the cell frequency was determined (Fig. 3.21, D). Under SNAP impact, half of the cells responded with amplitudes between 100-200% (blue) and 28% of the cells with amplitudes between 80-100% (black). NO induced enhanced RAs in 7% of the cells by at least a factor of 2 (Fig. 3.21, D, green). The highest

RA was found in a GC with a factor of 3. Under ctrl conditions none of the cells responded in this range. The RAs of the remaining cells showed moderate variations also observed under ctrl conditions (Fig. 3.21, D).

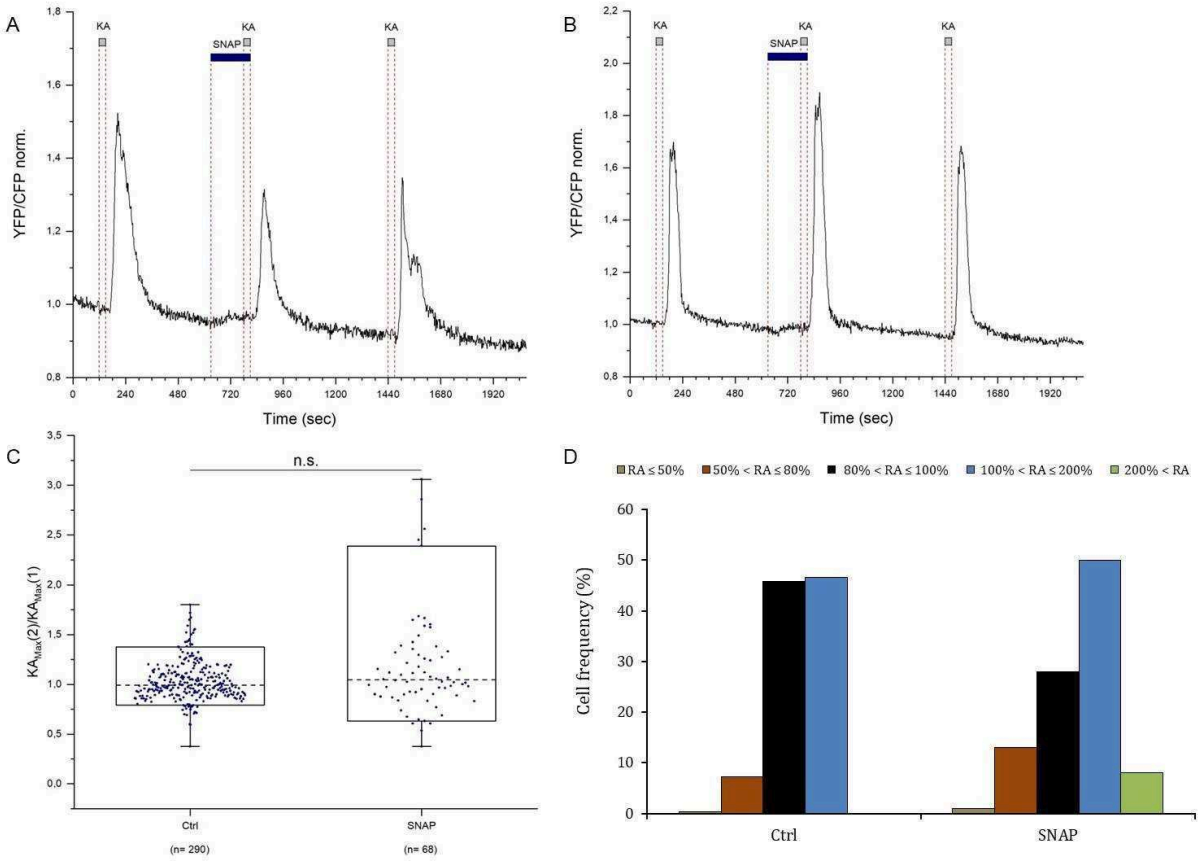


Figure 3.21: NO affected the kainate-induced calcium responses slightly in a small population of GCs. (A): The GC was stimulated with kainate (KA, 20 µM) two times in the absence of the NO-donor: SNAP (300 µM), and once in the presence of SNAP. NO reduced the kainate-induced calcium response. **(B):** The kainate-induced calcium response was increased; the GC recovered and responded to kainate similar to the first kainate treatment. **(C):** The second response amplitudes were normalized to the initial ones and data were plotted as box plot. Each dot represents the $KA_{Max}(2)/KA_{Max}(1)$ of one GC. The dotted lines show the medians (Ctrl: 0.99, n=290; SNAP: 1.04, n=68). In each box plot, the median divides the box into two parts: the upper part is greater, the lower part is less than the median; the whiskers above and below the box represent the 95th and the 5th percentiles, respectively. There was no significant difference between cells treated with SNAP and the ctrl cells (Mann-Whitney Rank Sum Test: p=0.091). **(D):** Relative frequency of cells in response to kainate with or without SNAP. RAs were subdivided in five groups: RAs, which exhibited less than 50% of the initial RAs (light brown), RAs between 50-80% (orange), RAs between 80-100% (black), RAs between 100-200% (blue) and RAs that were higher than the initial RAs by at least a factor of 2 (green). Ctrl=control, kainate (20 µM); n.s.= not significant; SNAP=S-Nitroso-N-acetyl-DL-penicillamine (300 µM).

In summary, NO did not affect the kainate-induced calcium responses in a similar way as it did with AMPA receptors. In only a small population of GCs, RAs were stronger enhanced, than would be expected by chance.

3.1.2.3. NO enhanced the NMDA-induced changes in $[Ca^{2+}]_i$ in GCs

NO enhanced the AMPA- and in a less marked way the kainate-induced calcium responses. In order to investigate whether NO affects the NMDA-induced calcium responses, 84 TN-L15-expressing GCs from four retina pieces were stimulated following the standard paradigm. The GC shown in Fig. 3.22, A responded to the three NMDA treatments with fast and transient increases in the YFP/CFP ratio of 91%, 87% and 75% respectively. The responses lasted for 60-90 sec and showed a slight rundown effect. Application of SNAP did not induce any change in $[Ca^{2+}]_i$ nor affected the NMDA-induced calcium response (Fig. 3.22, A). The GC shown in Fig. 3.22, B responded to the first NMDA treatment with an increase in the YFP/CFP ratio of 105%. In the presence of SNAP, activation of NMDA receptors induced an increase in the YFP/CFP ratio of 245%. NO enhanced the NMDA-induced calcium response by a factor of 2.3. The GC recovered towards the baseline and the enhancement induced via NO (SNAP) was reversible. The cell responded to the last NMDA treatment with an increase in the YFP/CFP ratio of 82% (Fig. 3.22, B).

The statistical analysis shown in Fig. 3.22, C revealed that there was a significant difference between the cells treated with SNAP and the ctrl cells (Mann-Whitney Rank Sum Test: $p^{***} \leq 0.001$, n=84). The NO-donor SNAP increased the NMDA-induced calcium responses in the majority of the cells (Fig. 3.22, C). In order to better clarify the wide distribution of the RAs in the presence of SNAP, RAs were assorted in groups and the relative cell frequency was determined (Fig. 3.22, D). Only 13% of the GCs responded with amplitudes between 50-80% (orange). All these cells responded to the third NMDA application with RAs that were higher than or at least as high as the second responses. However the differences were very small. In 31% of the cells the RAs were between 80-100% (black). The largest group (40%) was constituted of GCs with RAs enhanced by up to a factor of 2 (blue). The remaining GCs responded with amplitudes that were higher by at least a factor of 2 (Fig. 3.22, D, green). The highest effect was found in a GC with a RA that was higher by a factor of 5.5. These results indicate that NO is involved in the modulation of NMDA receptors in the majority of the GCs.

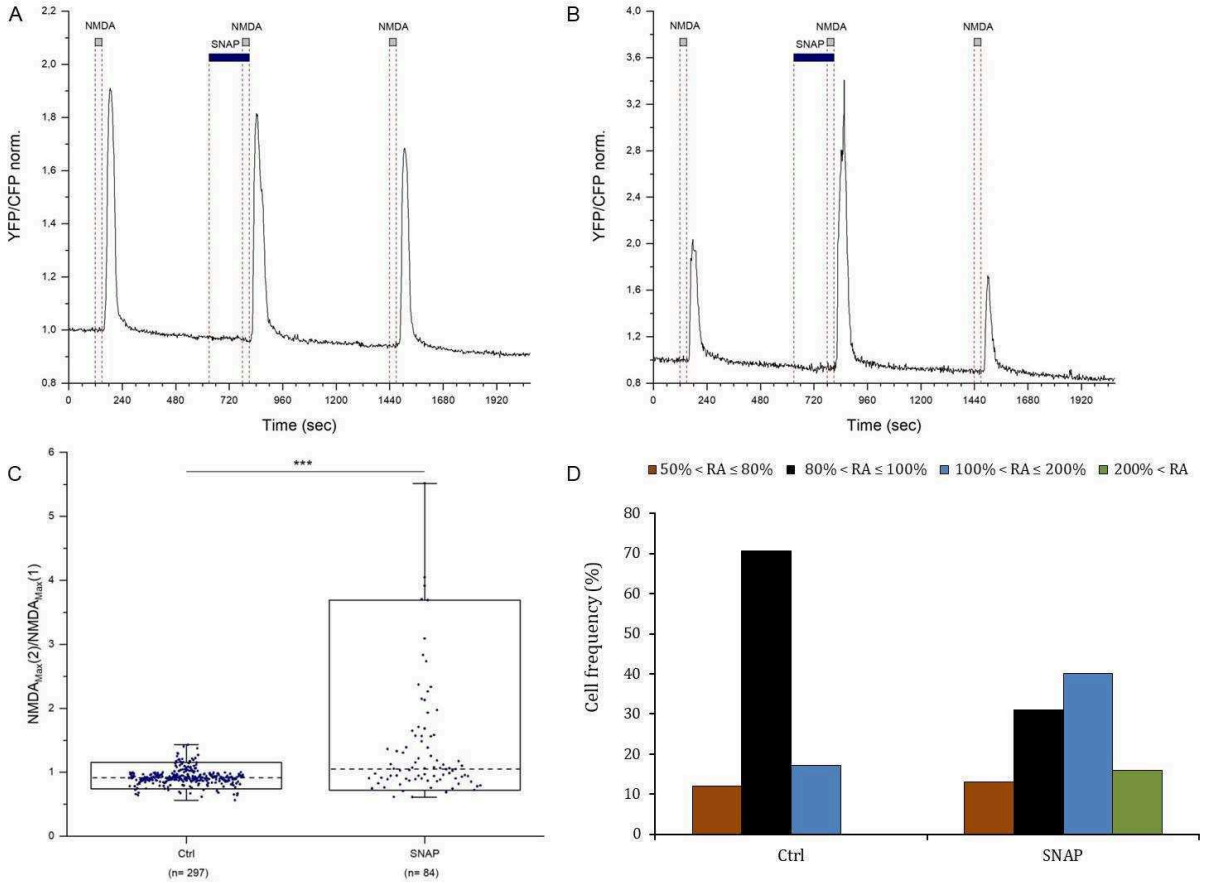


Figure 3.22: NO increased the NMDA-induced calcium changes in the majority of GCs. (A): The response of one GC to three NMDA (300 µM) applications, SNAP (300 µM) did not affect the NMDA-induced calcium response. **(B):** The NMDA-induced calcium response was enhanced by a factor of 2.3 in the presence of SNAP; the GC recovered fully and responded to the third NMDA application similar to the first one. **(C):** Statistical analysis of the RAs in response to NMDA with or without SNAP. The RAs were normalized to the respective initial RAs and data were plotted as box plots. Each dot represents the $NMDA_{Max}(2)/NMDA_{Max}(1)$ of one cell. The dotted lines show the medians (Ctrl: 0.91, n=297; SNAP: 1.05, n=84). In each box plot, the median divides the box into two parts: the upper part is greater, the lower part is less than the median; the whiskers above and below the box represent the 95th and the 5th percentiles, respectively. The NMDA-induced increase in $[Ca^{2+}]_i$ was significantly increased by SNAP (Mann-Whitney Rank Sum Test: p***≤0.001). **(D):** Relative frequency of the cells in response to NMDA with or without SNAP. RAs were subdivided in five groups: RAs, which exhibited less than 50% of the initial RAs (light brown), RAs between 50-80% (orange), RAs between 80-100% (black), RAs between 100-200% (blue) and RAs that were higher than the initial RAs by at least a factor of 2 (green). Ctrl=control, NMDA (300 µM); SNAP=S-Nitroso-N-acetyl-DL-penicillamine (300 µM).

In summary, the results shown indicate that the NO-donor SNAP modulates the iGluR-induced calcium responses. Most likely, NO released by SNAP, activates the NO/sGC pathway. Activation of PKG and subsequent protein phosphorylation might shift the calcium responses of the iGluRs to the right, that is to enhanced changes in the $[Ca^{2+}]_i$. Calcium responses induced via AMPA or NMDA receptors were stronger effected than kainate-induced calcium responses. Fig. 3.23 summarizes the effects of SNAP by reference to the cell frequency in different RA ranges. The majority of the cells responded to AMPA with RAs with moderate changes (black), the addition of SNAP enhanced the calcium responses clearly. Similar effects of SNAP, although less marked,

were observed on NMDA-induced calcium responses. In the presence of SNAP, only a small population GCs responded to kainate with enhanced calcium responses. In fact, 50% of the GCs responded with amplitudes between 100-200% (blue), however under ctrl conditions this group was also constituted from 46% of the GCs (Fig. 3.23). Indeed, under control conditions activation of kainate receptors revealed a higher change in the $[Ca^{2+}]_i$ during the second treatment in comparison to the AMPA and NMDA receptors. The distinct effects suggest that the interaction between the iGluRs and the NO/sGC pathway may differ in different GC subtypes.

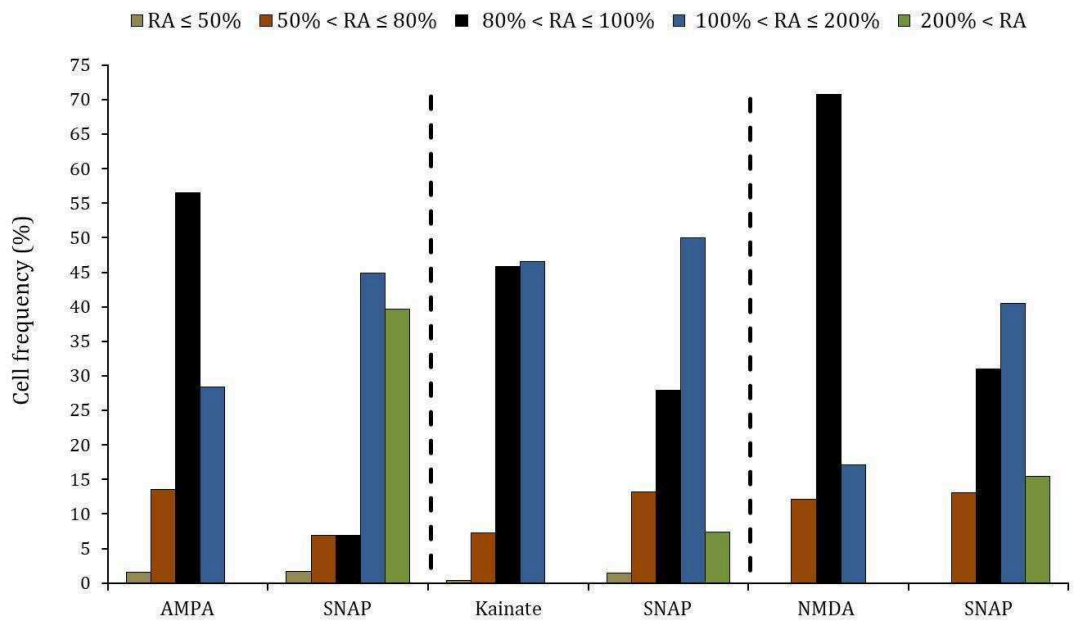


Figure 3.23: NO differentially affected iGluR-induced calcium responses. The relative frequency of the GCs in function of the second RAs. The cells were exposed to AMPA (5 µM), kainate (20 µM) or NMDA (300 µM) with and without SNAP (300 µM). The RAs were subdivided in five groups: RAs that exhibited less than 50% of the initial RAs (light brown), RAs between 50-80% (orange), RAs between 80-100% (black), RAs higher up to a factor of 2 (light blue) and RAs that were higher than the initial RAs by at least a factor of 2 (green). SNAP=S-Nitroso-N-acetyl-DL-penicillamine (300 µM).

3.1.3. Studying the effects of Melatonin on the iGluR-mediated responses in GCs of the TN-L15-retina

Melatonin (MT), an indolamine derived from tryptophan, is known as a neuroendocrine hormone, which is mainly produced by the pineal gland. MT regulates the circadian rhythm of some brain neurotransmitters and their receptors such as dopamine and glutamate (Acuna Castroviejo *et al.* 1986, Marquez de Prado *et al.* 2000). In the retina, MT is synthesized by photoreceptors in a circadian manner, with MT levels

being high at night and low during the day (Cahill & Besharse 1993, Tosini & Menaker 1998). It exerts its function on two distinct receptors, MT1 and MT2. Both receptors are G-protein coupled; they inhibit the ACy and may affect intracellular messengers. MT receptors have been demonstrated in retinal GCs (Baba *et al.* 2009).

In this chapter, I will investigate whether MT affects the iGluR-induced calcium responses in GCs of the intact retina. Thus, acutely isolated TN-L15-retinae were stimulated with AMPA (5 µM), kainate (20 µM) or NMDA (300 µM) and MT (500 nM) according to the standard paradigm. The RAs of cells treated with MT were compared to the RAs of ctrl cells (Fig. 3.24).

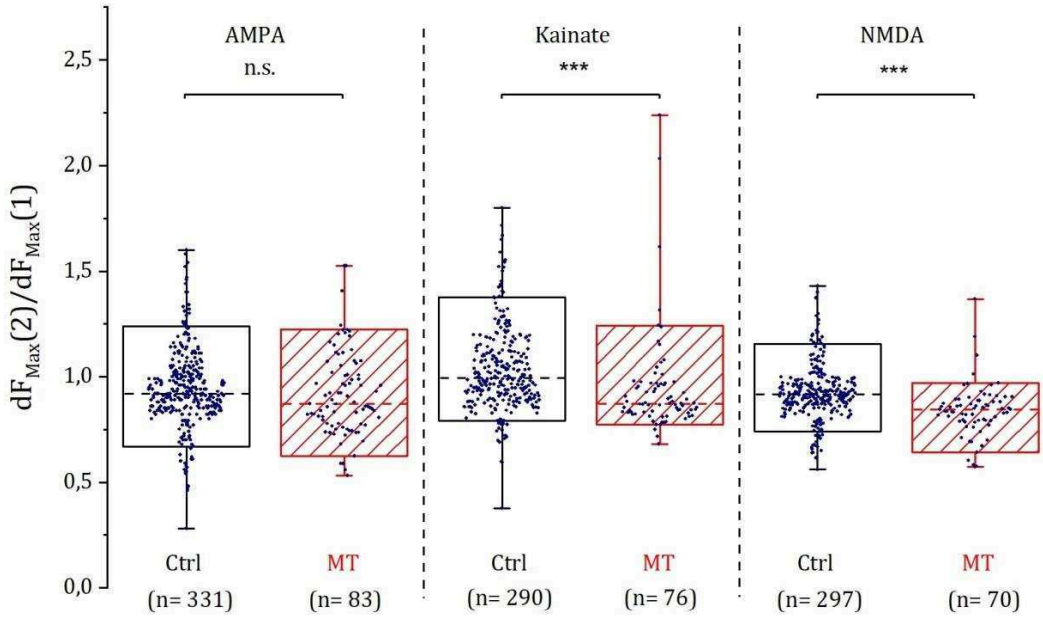


Figure 3.24: Melatonin affected the calcium responses induced via kainate and NMDA receptors. The RAs of the iGluR-induced calcium responses with and without MT (500 nM) were compared to each other. The second RAs were normalized to the initial ones and data were plotted as box plot. Each dot represents one GC; box plots represent the ctrl cells (black) and the respective cells treated with MT (red). The dashed lines indicate the medians. AMPA (5 µM): ctrl: 0.92, n=331, MT: 0.87, n=83; Kainate (20 µM): ctrl: 0.99, n=290, MT: 0.87, n=76; NMDA (300 µM): ctrl: 0.91, n=297, MT: 0.84, n=70. Activation of MT receptors did not affect the AMPA-induced calcium responses (Mann-Whitney Rank Sum Test: p=0.085). MT diminished the kainate-induced calcium responses and there was a significant difference between the ctrl cells and cells treated with MT (Mann-Whitney Rank Sum Test: p***≤0.001). MT diminished the NMDA-induced calcium responses and there was a statistically significant difference to the ctrl cells (Mann-Whitney Rank Sum Test: p***≤0.001).

Statistical analyses shown in Fig. 3.24 for the AMPA-induced calcium responses revealed no statistically significant difference between the RAs of the AMPA ctrl cells and the cells treated with MT (Mann-Whitney Rank Sum Test: p=0.085). The RAs are found in the same range as the ctrl cells and exhibit moderate changes (Fig. 3.24, left). In the presence of MT, the kainate-induced calcium responses were reduced in the majority

of the cells (Fig. 3.24, middle). Considering the totality of the cells, the median was clearly diminished and there was a statistically significant difference between the RAs to kainate alone and to kainate in the presence of MT (Mann-Whitney Rank Sum Test: p***≤0.001). Similar effects, though less marked, were observed with the NMDA-induced calcium responses (Fig. 3.24, right). There was a significant difference between the NMDA ctrl cells and cells treated with MT (Mann-Whitney Rank Sum Test: p***≤0.001).

In order to clarify the effects observed with MT, the cells were assigned to groups in respect to the RAs to the second treatments with or without MT. The relative frequency of the cells is shown in Fig 3.25.

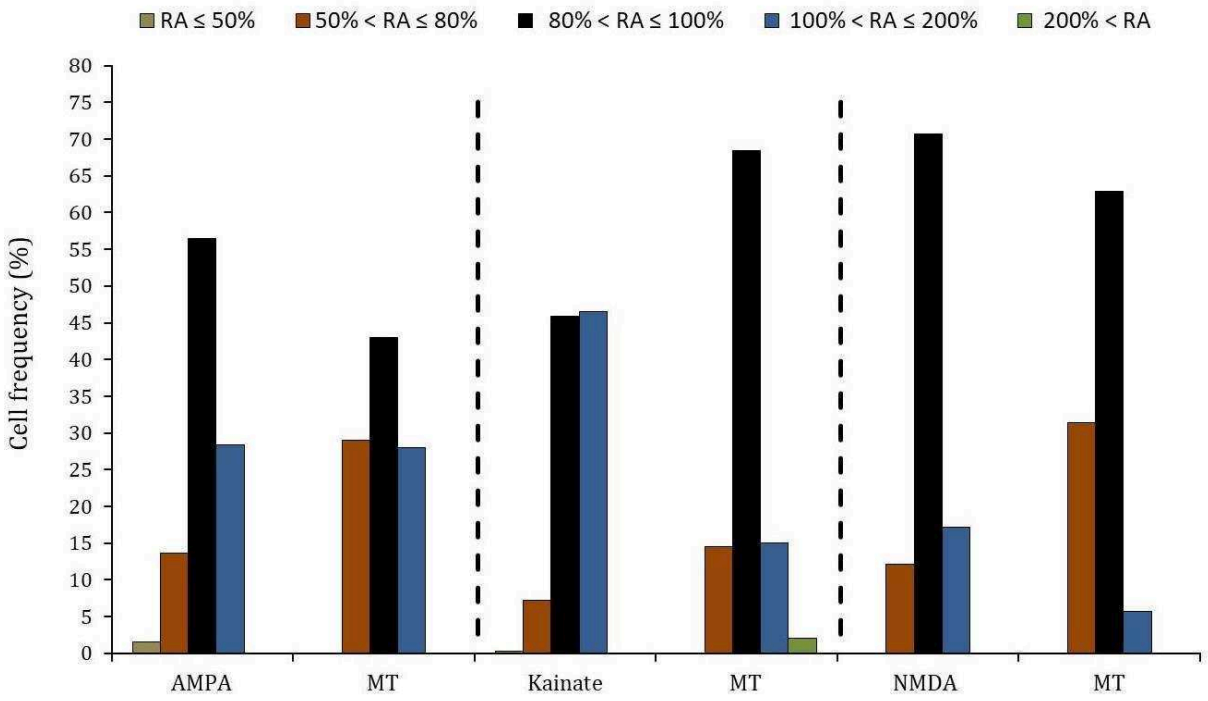


Figure 3.25: Relative frequency of the iGluR-induced calcium responses with or without MT. The normalized RAs were subdivided in five groups, and the cell frequency was determined. RAs, which exhibited less than 50% of the initial RAs (light brown), RAs between 50-80% (orange), RAs between 80-100% (black), RAs between 100-200% (blue) and RAs that were higher than the initial RAs by at least a factor of 2 (green).

The majority of the cells treated with AMPA responded with RAs between 80-100% (black), the remaining cells responded with moderate changes. In the presence of MT, the majority of the cells (42%) responded to AMPA in a similar way, meaning with amplitudes between 80-100% (black). The remaining cells responded with amplitudes that were higher up to a factor of 1.5 (blue) or 50% smaller than the initial ones (Fig. 3.25, left, orange). The RAs of cells treated with kainate ranged between 80-100% (black) and 100-200% (blue) in 46% and 47% respectively (Fig. 3.25, middle). The

majority of the cells treated with MT (68%) responded with amplitudes between 80-100%. The group of cells with RAs between 100-200% (blue) was constituted of 15% of the cells (Fig. 3.25). The RAs were higher by a factor up to 2.2 in only 2% of the cells (green). The effects of MT on the kainate-induced calcium responses are detectable only in the distribution. The group of cells with higher RAs became smaller and the group with reduced RAs larger than under ctrl conditions (Fig. 3.25, middle). Similar effects were observed concerning the NMDA-induced calcium responses (Fig. 3.25, right).

In summary, MT did not affect the AMPA-induced calcium responses. The kainate- and the NMDA-induced calcium responses were slightly though significantly affected. The groups of GCs that responded to kainate or NMDA with amplitudes between 100-200% were smaller in the presence of MT. This may indicate that MT receptors are particularly expressed in this population of GCs.

3.1.4. Studying the effects of adenosine on the iGluR-induced calcium responses in GCs of the TN-L15-retina

The nucleoside adenosine (AD) has established as neuromodulator in the central nervous system (CNS), including the retina. Four adenosine receptors (ARs) have been identified: A1, A2A, A2B und A3; all AR subtypes are G-protein-coupled receptors (GPCRs), the A1 and A3 receptors inhibit the ACy, while the A2Rs stimulate it. In the rat retina, A1Rs have been found in the inner plexiform (IPL) and GCL (Braas *et al.* 1987, Kvanta *et al.* 1997). In order to examine what role A1Rs may play in the modulation of iGluR-mediated calcium responses, acutely isolated TN-L15-retinae were stimulated according to the standard paradigm. Thus, TN-L15-expressing GCs were stimulated with AMPA, kainate or NMDA three consecutive times. During and 2.5 min before the second application, the A1R agonist GR 79236 (GR, 300 µM) was superfused.

The second RAs were normalized to the initial ones and were referred to as $RA_{Max}(2)/RA_{Max}(1)$. The box plots in Fig. 3.26 summarize the results of the statistical analyses of the ctrl cells and the cells treated with GR. Sixty-three TN-L15-expressing GCs were treated with GR during the second AMPA application. Considering the totality of the cells, activation of A1Rs decreased the AMPA-induced calcium responses. There was a statistically significant difference between the AMPA ctrl cells and cells treated with GR (Mann-Whitney Rank Sum Test: p***≤0.001). The majority of the cells

responded to AMPA in the presence of GR with smaller amplitudes; they are found in the lower part of the box (Fig. 3.26, left). Even more pronounced effects were observed on the kainate-induced calcium responses in the presence of GR (Fig. 3.26, middle, n=68). There was a statistically significant difference between the kainate ctrl cells and the cells treated with GR (Mann-Whitney Rank Sum Test: p***≤0.001). The majority of the cells responded with reduced amplitudes. The NMDA-induced calcium responses were also affected upon activation of A1Rs (Fig. 3.26, right, n=54). There was a statistically significant difference when compared to the ctrl cells (Mann-Whitney Rank Sum Test: p***≤0.001). The upper part of the red box represents cells that were located in the same range as the ctrl cells. The lower part was constituted of cells that responded with amplitudes that were much smaller. The effects on the non-NMDA-induced calcium responses were found to be significantly stronger than the effects on the NMDA-induced calcium responses (Fig. 3.26).

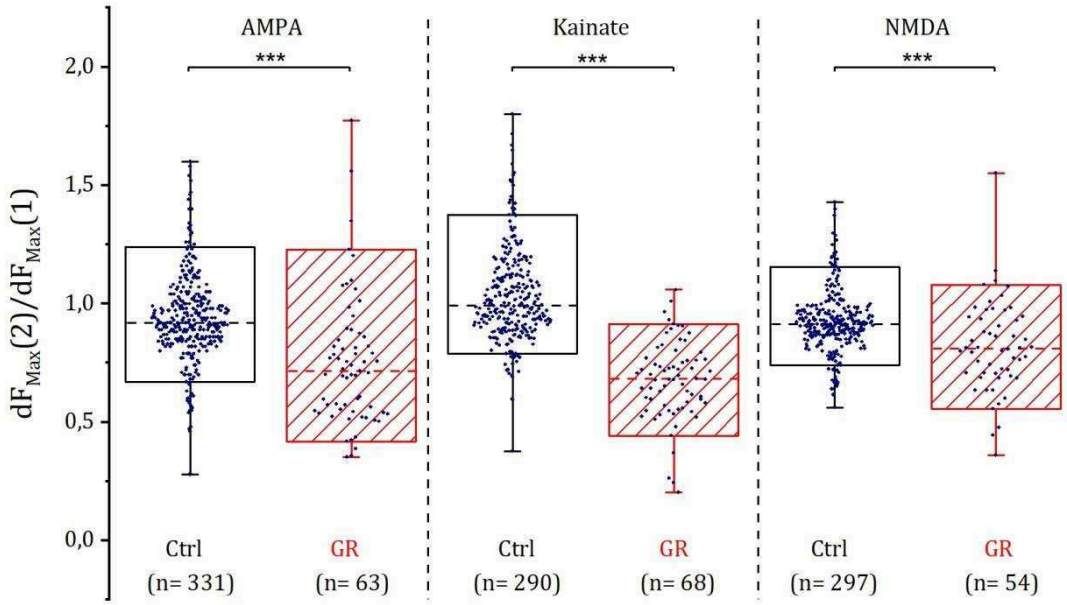


Figure 3.26: The adenosine A1R agonist GR affected the iGluR-induced calcium responses. The amplitudes of the iGluR-induced calcium responses with and without GR 79236 (GR, 300 µM) were compared to each other. The second RAs were normalized to the initial ones and data were plotted as box plot. Each dot represents one GC; box plots represent the ctrl cells (black) and the respective cells treated with GR (red). The dashed lines indicate the medians. AMPA (5 µM): ctrl: 0.92, n=331, GR: 0.71, n=63; Kainate (20 µM): ctrl: 0.99, n=290, GR: 0.68, n=68; NMDA (300 µM): ctrl: 0.91, n=297, GR: 0.81, n=54. Activation of A1Rs diminished the AMPA-, kainate- and NMDA-induced calcium responses in a statistically significant way (Mann-Whitney Rank Sum Test: p***≤0.001 each).

Cells were assigned to different groups in reference to the RAs. The cell frequencies of the ctrl cells and cells treated with GR in every range are summarized in Fig. 3.27. In the presence of the A1R agonist, the AMPA-induced calcium responses were strikingly reduced (Fig. 3.27, left). Thus, the majority of the cells (56%) responded with

amplitudes between 50-80% (orange), while this group constituted only 14% under ctrl conditions. Moreover, 11% of the cells responded with amplitudes smaller than 50% (light brown). The kainate-induced calcium responses were markedly reduced in the presence of GR; 70% of the GCs responded with amplitudes between 50-80% (orange), while only 7% of the cells under ctrl conditions responded in this range (Fig. 3.27, middle). Furthermore, 9% of the cells responded to kainate under concomitant activation of A1Rs with amplitudes smaller than 50% (light brown). These greatly reduced responses were never seen under ctrl conditions. The NMDA-induced calcium responses exhibited amplitudes between 80-100% (black) in the majority of the cells (71%) and amplitudes between 50-80% (orange) in 12% of the cells (Fig. 3.27, right). In the presence of GR, the calcium responses were shifted to the left. Thus, 43% of the cells responded with amplitudes between 50-80% (orange) and 5% with amplitudes smaller than 50% (light brown).

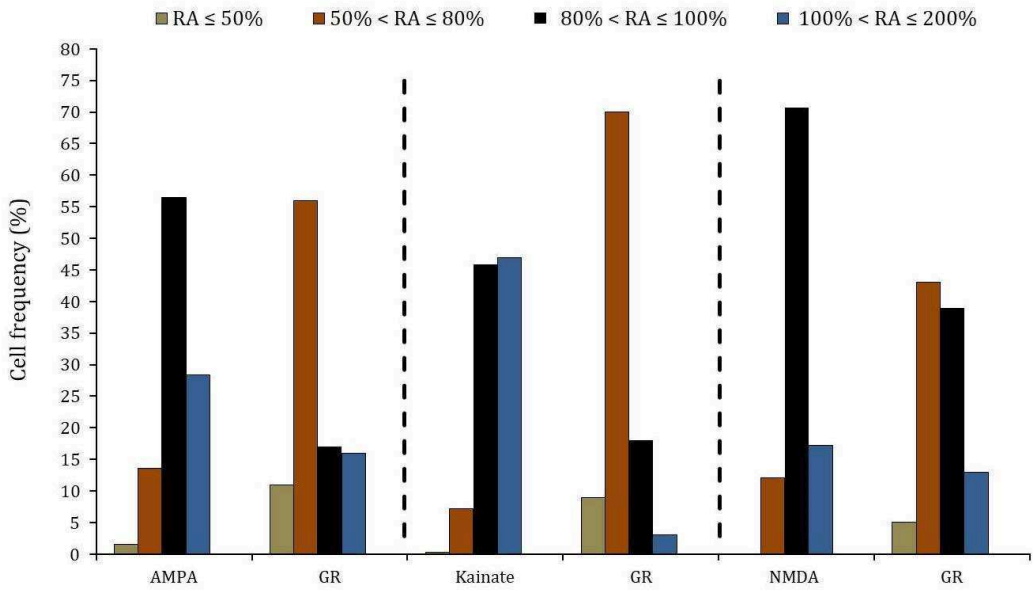


Figure 3.27: Relative frequency of the iGluR-induced calcium responses with or without the A1R agonist GR. The normalized RAs were subdivided into four groups, and the cell frequency was determined. RAs, which exhibited less than 50% of the initial RAs (light brown), RAs between 50-80% (orange), RAs between 80-100% (black) and RAs between 100-200% (blue).

In summary, these results indicate that activation of A1Rs shifted the iGluR-induced calcium responses to the left, meaning to reduced changes in the $[Ca^{2+}]_i$ in the GCs. The effects were strongest for kainate receptors, medium for AMPA receptors, and weakest for NMDA receptors. These results support a role for adenosine in the modulation of retinal GCs.

3.1.5. Studying whether VGCCs are involved in the iGluR-induced calcium responses

In the previous experiments, AMPA, kainate, and NMDA induced an increase in $[Ca^{2+}]_i$. This increase could be due to calcium influx through iGluRs. NMDA receptors are approximately three to four times more permeable to Ca^{2+} than the non-NMDA receptors, whereas AMPA receptors show a slightly greater Ca^{2+} permeability than kainate receptors. Alternatively, depolarization induced by activation of iGluRs could activate calcium influx through VGCCs that have been demonstrated to play an important role in neuronal function and physiological processing of sensory information through the retina (Winslow 1989, Sullivan & Lasater 1992, Schmitz & Witkovsky 1997). In order to test how the blockade of the VGCCs may affect the iGluR-induced calcium responses, I made use of the specific CaChs antagonists following the previous protocol. Thus, AMPA, kainate or NMDA receptors were stimulated with the specific agonists three consecutive times. A CaCh-blocker cocktail composed of the L-type specific blocker nimodipine (50 µM; (Habermann *et al.* 2003, Chen *et al.* 2014)) and the N-type specific blocker ω-conotoxin GVIA (250 µM; (Tsien *et al.* 1991)) was applied 2.5 min before and during the second application.

In total, 62 TN-L15-expressing GCs were exposed to AMPA and the blocker-cocktail. The cell shown in Fig. 3.28, A responded to AMPA application with an increase in the YFP/CFP ratio of 74%. The response lasted for 2.5 min. Following, the fluorescence signal recovered towards the baseline. Blocking the L- and N-types of CaChs did not affect the basal $[Ca^{2+}]_i$, however, the AMPA-induced response was reduced to 15%. The fluorescence signal recovered towards the baseline after approximately 90 sec. Interestingly, the third application of AMPA induced an increase of only 22%, indicating that the effect induced via blockade of CaChs was not fully reversible (Fig. 3.28, A). These two effects were observed in 61% of the cells.

The blockade of the L- and N-types of the CaChs affected the kainate- and NMDA-induced calcium responses differently. In total, 52 and 78 TN-L15-expressing GCs were tested for the role of the L- and N-types CaChs on kainate and NMDA receptors, respectively. As an example, a GC is shown in Fig. 3.28, B that was stimulated with kainate. Under blockade of the CaChs, the response to kainate was enhanced by a factor of 2.4 when compared to the initial response. The fluorescence signal recovered and the

cell responded to the third kainate treatment with an increase in the YFP/CFP ratio that was slightly smaller than the initial response (Fig. 3.28, B). This behavior was observed in 35% of the cells treated with kainate. Similar responses were also observed in response to NMDA treatments; during blockade of the CaChs the NMDA-induced calcium responses were enhanced in 29% and the third NMDA responses were stronger than the first responses (data not shown).

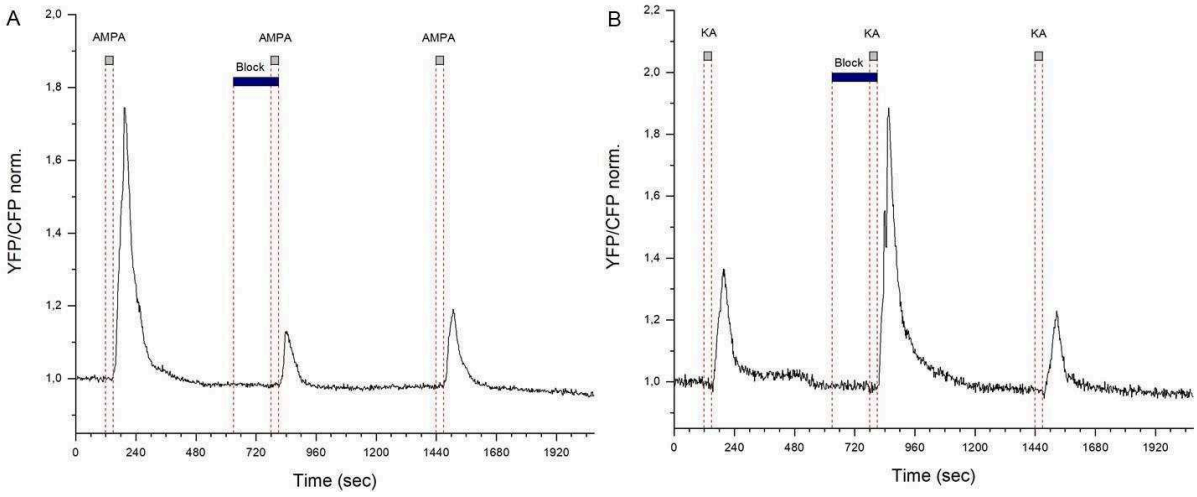


Figure 3.28: Blockade of CaChs affected the iGluR-induced calcium responses. (A): The AMPA-induced calcium response was dramatically reduced in the presence of the blocker cocktail. The third response was very small indicating that the impact was not fully reversible. **(B):** A GC that responded to kainate under blockade of CaChs with an enhanced calcium response exemplifying the effects seen on kainate and NMDA receptors. AMPA (5 µM); Kainate (20 µM); NMDA (300 µM); Block=CaChs-blocker cocktail: L-type antagonist nimodipine (50 µM) + N-type antagonist ω-conotoxin GVIA (250 µM).

The majority of the cells responded similar to the cells depicted in Fig 3.28. The statistical analyses are summarized in Fig. 3.29. The normalized RAs of cells treated with the CaChs-blocker cocktail were compared to the RAs of ctrl cells. There was a statistically significant difference between the RAs of cells under blockade of the L- and N-types CaChs and the respective controls (Mann-Whitney Rank Sum Test: p***≤0.001 each). While the AMPA-induced calcium responses were dramatically reduced in the majority of the cells, the kainate-induced calcium responses were clearly enhanced (Fig. 3.29, middle). Similar effects were observed on the NMDA-induced calcium responses although less marked (Fig. 3.29, right).

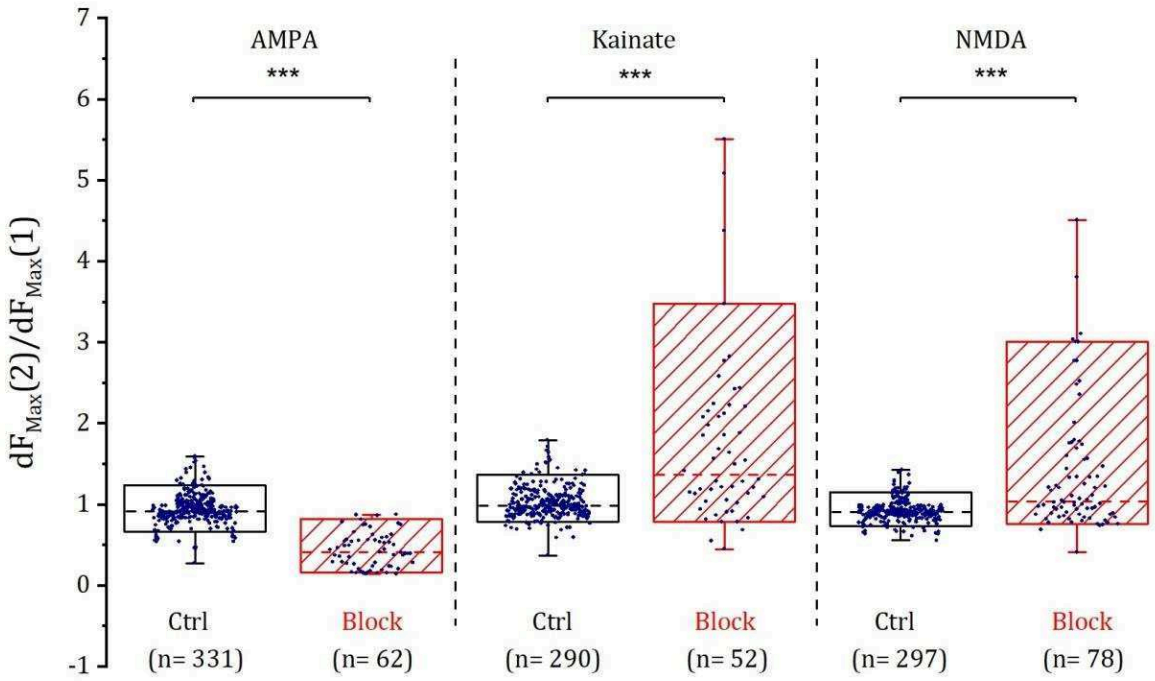


Figure 3.29: Statistical analyses of the effects of blocking L- and N-type CaChs on the iGluR calcium responses. The response amplitudes of the iGluR-induced calcium responses with and without the CaChs-blocker cocktail (Block) were compared to each other. The second RAs were normalized to the initial ones and data were plotted as box plot. Each dot represents one GC; box plots represent the ctrl cells (black) and the respective cells treated with the block (red). The dashed lines indicate the medians. AMPA (5 µM): ctrl: 0.92, n=331, Block: 0.41, n=62; Kainate (20 µM): ctrl: 0.99, n=290, Block: 1.36, n=52; NMDA (300 µM): ctrl: 0.91, n=297, Block: 1.04, n=78.

The RAs were subdivided in groups and the cell frequency was determined (Fig. 3.30). Under blockade of CaChs, the AMPA-induced calcium responses were strikingly reduced (Fig. 3.30, left). The majority of the cells (61%) responded with amplitudes smaller than 50% (light brown), and 32% responded with amplitudes between 50-80% (orange). Under ctrl conditions the majority of the cells responded with amplitudes between 80-100% (black). Blockade of L- and N-types CaChs clearly shifted the AMPA-induced calcium responses to the left meaning to reduced changes in $[Ca^{2+}]_i$. The kainate-induced calcium responses were enhanced in 31% of the cells under blockade of CaChs, by at least a factor of 2 (green). None of the cells responded to kainate with such enhanced responses under ctrl conditions (Fig. 3.30, middle).

Under ctrl conditions, the majority of the cells (71%) responded to NMDA with amplitudes between 80-100% (black). Under blockade of L- and N-types CaChs, RAs were enhanced up to a factor of 2 in 41% (blue) or by at least a factor of 2 in 15% of the cells (green). The NMDA- and the kainate-induced calcium responses were shifted to the right, meaning to higher changes in the $[Ca^{2+}]_i$.

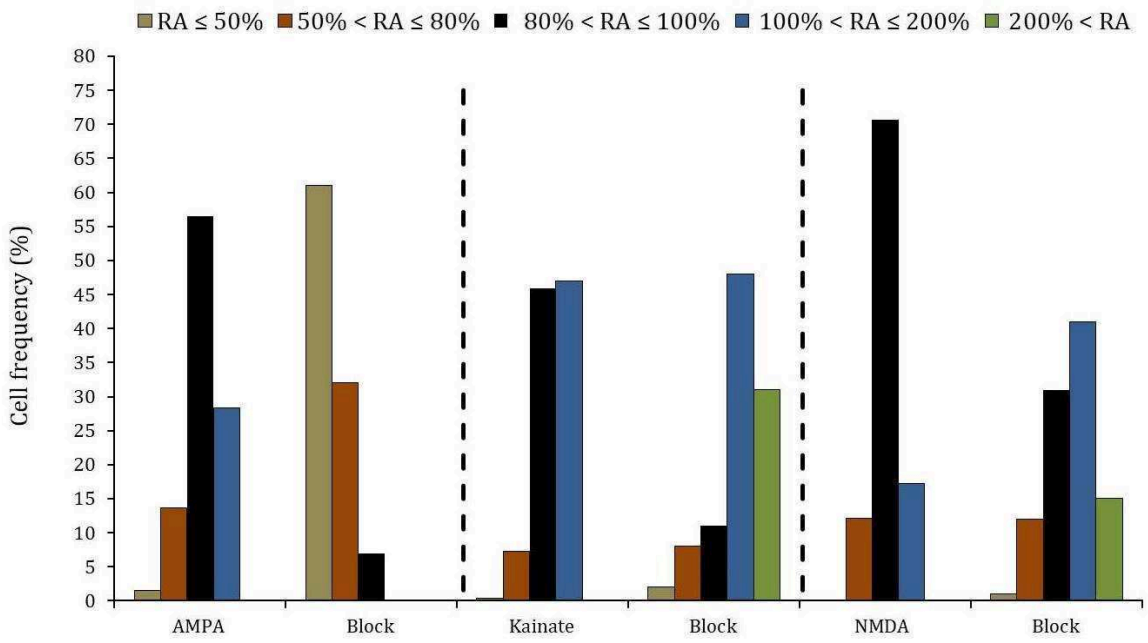


Figure 3.30: Relative frequency of the iGluR-induced calcium responses with and without CaChs blockers. The normalized RAs were subdivided in five groups, and the cell frequency was determined. RAs, which exhibited less than 50% of the initial RAs (light brown), RAs between 50-80% (orange), RAs between 80-100% (black), RAs between 100-200% (blue) and RAs that were enhanced by at least a factor of 2 (green).

In summary, these results suggest that the increase in $[Ca^{2+}]_i$ in response to AMPA, kainate or NMDA treatment can be caused by different mechanisms: calcium influx through the ligand-gated channels or through the voltage-gated calcium channels or a combination of both. The calcium responses in response to AMPA application were strongly reduced during blockade of the L- and N-types CaChs, suggesting an important calcium influx through the VGCCs. In spite of blocking the CaChs, the kainate- and the NMDA-induced calcium responses were strikingly enhanced in 35% and 29% of of cells, respectively. This suggests that calcium is released from intracellular stores (Linn & Gafka 2001) or alternatively, the calcium that diffused via kainate and NMDA channels most likely triggers calcium-induced calcium release (CICR) from internal stores.

3.1.6. Studying the acting site of A1Rs during modulation of iGluR-induced calcium responses

The results presented in the previous chapters show that DRs, A1Rs and MT receptors modulate the non-NMDA- or/and the NMDA-induced calcium responses in distinct ways. As discussed above, modulation of the iGluR-induced calcium responses can depend on modulation of iGluRs or of VGCCs. In chapter 3.1.5, the effect of the cocktail of VGCC blockers was puzzling. AMPA-induced calcium signals were reduced in

the presence of the blockers, arguing for a contribution of VGCCs in the calcium response. In contrast, responses induced by kainate and NMDA were increased in the presence of the blockers. As these results are difficult to interpret, only one set of experiments was performed with the A1R ligand GR 79236 (GR) in the presence of VGCC blockers (for responses in the absence of the blockers, see Figs. 3.26 and 3.27). The statistical analyses of the results of AMPA RAs under different conditions are shown in Fig. 3.31.

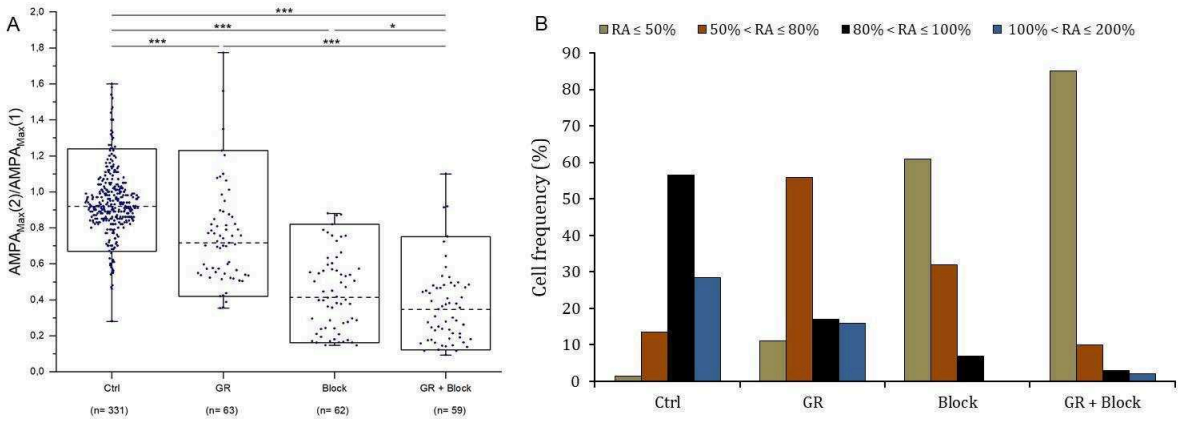


Figure 3.31: Statistical analyses of the effect of the A1R agonist GR 79236 on AMPA-induced calcium responses. (A): The normalized RAs of the AMPA-induced calcium responses (Ctrl: AMPA, 5 µM) were compared to the RAs under concomitant activation of A1Rs (GR: GR 79236, 300 µM) and/or blockade of VGCCs, Block: CaChs-blocker cocktail, L-type antagonist nimodipine (50 µM) + N-type antagonist ω-conotoxin GVIA (250 µM). Each dot represents one GC; the dashed lines indicate the medians: AMPA: ctrl: 0.92, n=331; GR: 0.71, n=84; Block: 0.41, n=62; GR + Block: 0.34, n=59. Activation of A1Rs, and/or blockade of L- and N-types VGCCs diminished the AMPA-induced calcium responses in a statistically significant way (Mann-Whitney Rank Sum Test: p***≤0.001 each). RAs to AMPA in the presence of the blocker cocktail and GR were significantly different from RAs under the impact of the blocker cocktail alone (Mann-Whitney Rank Sum Test: p*=0.019). **(B):** The normalized RAs were subdivided in four groups, and the cell frequency was determined. RAs, which exhibited less than 50% of the initial RAs (light brown), RAs between 50-80% (orange), RAs between 80-100% (black) and RAs between 100-200% (blue).

As already shown in the previous chapters, activation of A1Rs and more clearly blockade of L- and N-types CaChs diminished the AMPA-induced calcium responses in a statistically significant way (Fig. 3.31, A). Under blockade of the VGCCs and concomitant activation of A1Rs the AMPA-induced calcium responses were further reduced. There was a significant difference between the ctrl cells and cells treated with the different drugs (Mann-Whitney Rank Sum Test: p***≤0.001 each; Fig. 3.31, A). Cell frequencies in reference to the RAs under the different conditions were determined (Fig. 3.31, B). Under ctrl conditions, the majority of the cells (57%) responded with amplitudes between 80-100% (black). Just as many cells (56%) responded with amplitudes between 50-80% (orange) under activation of A1Rs. The RAs were strikingly small in 61% of the cells (light brown) under blockade of the L- and N-types CaChs, indicating

that an important fraction of the calcium influx occurs through the VGCCs. Activation of A1Rs in the presence of VGCC blockers resulted in a further reduction of the RAs, 85% of the cells responded with amplitudes that were smaller than 50% of the initial responses (light brown). Thus, there is a clear shifting of the responses to the left meaning to reduced changes in the $[Ca^{2+}]_i$ in response to AMPA under the different conditions. This shifting becomes more obvious following the four different conditions in Fig. 3.31, B from the left to the right. It is very likely that the increase in the $[Ca^{2+}]_i$ in response to AMPA is at least partially due to a calcium influx via VGCCs. Despite of the blockade of the VGCCs, activation of A1Rs continued to reduce the AMPA-induced calcium responses, suggesting that activated A1Rs may act, at least partially, directly on the AMPA receptors.

Similar experiments and accordingly analyses were performed for kainate-induced calcium signals. Statistical analyses of the results are summarized in Fig. 3.32, A. Activation of A1Rs reduced the kainate-induced calcium responses clearly, however, different from AMPA receptors the blockade of the VGCCs increased the kainate-induced calcium responses. GR in the presence of the CaChs blocker cocktail led to a huge reduction in the kainate-induced calcium responses. There was a significant difference between the ctrl cells and cells treated with the related drugs (Mann-Whitney Rank Sum Test: $p^{***} \leq 0.001$ each; Fig. 3.32, A). Cell frequencies in respect to the RAs under the different conditions were determined and are summarized in Fig. 3.32, B. Through activation of A1Rs, the RAs were shifted to the left, meaning to strongly reduced RAs (orange and light brown). Under blockade of the VGCCs, the RAs were rather shifted to the right meaning to enhanced calcium responses (green). The concomitant stimulation of A1Rs during blockade of the L- and N-types CaChs dramatically reduced the kainate-induced calcium responses. Thus, 100% of the cells responded with amplitudes that were smaller than 50% of the initial ones (light brown). In almost all these cells, the third responses showed full recovery, i.e. the RAs ranged between 43-132%, indicating that the effects seen were reversible (data not shown).

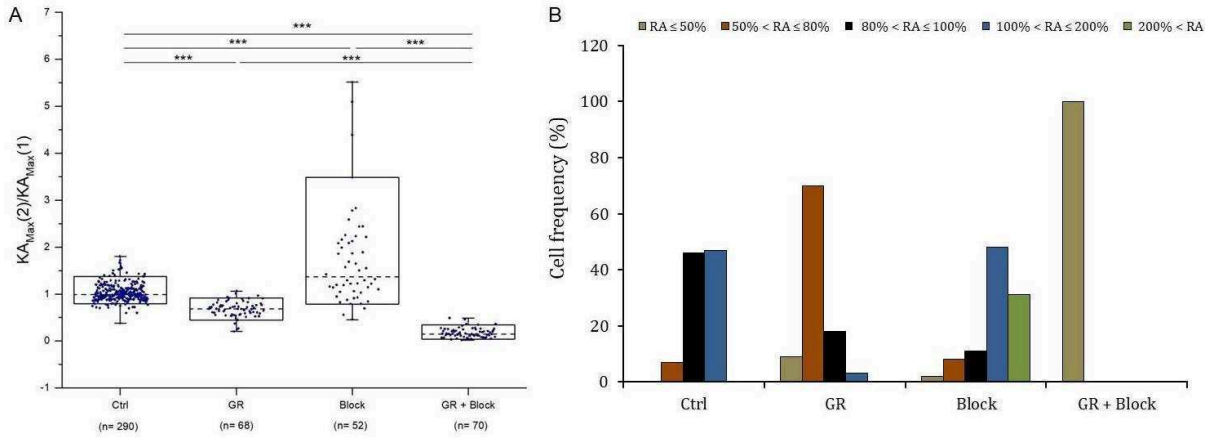


Figure 3.32: Statistical analyses of the effect of the A1R agonist GR 79236 on kainate-induced calcium responses. (A): The normalized RAs of the kainate-induced calcium responses (Ctrl: kainate, 20 µM) were compared to the RAs under concomitant activation of A1Rs (GR: GR 79236, 300 µM) and/or blockade of VGCCs, Block: CaChs-blocker cocktail, L-type antagonist nimodipine (50 µM) + N-type antagonist ω-conotoxin GVIA (250 µM). Each dot represents one GC; the dashed lines indicate the medians: Kainate: ctrl: 0.99, n=290; GR: 0.68, n=68; Block: 1.36, n=52; GR + Block: 0.15, n=70. Activation of A1Rs diminished, whereas blockade of L- and N-types VGCCs enhanced the kainate-induced calcium responses. Concomitant application of the CaChs blocker cocktail and the A1Rs-agonist dramatically decreased the kainate-induced calcium responses. There was a statistically significant difference between the ctrl cells and the cells under the different conditions (Mann-Whitney Rank Sum Test: p***≤0.001 each). **(B):** The normalized RAs were subdivided in five groups, and the cell frequency was determined. RAs, which exhibited less than 50% of the initial RAs (light brown), RAs between 50-80% (orange), RAs between 80-100% (black), RAs between 100-200% (blue) and RAs that were higher by at least a factor of 2 (green).

These results suggest that activated A1Rs may act directly on the kainate receptors to reduce the calcium influx through the kainate-gated channels, since despite blocking the VGCCs the activated A1Rs further act to reduce the changes in $[Ca^{2+}]_i$.

Fig. 3.33 summarizes the results for NMDA-induced calcium responses. Concomitant application of the CaChs blocker cocktail and GR decreased the NMDA-induced calcium responses in a statistically significant way when compared to the NMDA ctrl cells (Mann-Whitney Rank Sum Test: p***≤0.001 each). Likewise, there was a significant difference to the responses of cells in the presence of the A1R agonist GR and under blockade of VGCCs (Fig. 3.33, A). Determining the cell frequency in respect to the RAs should clarify the effects observed, the results are summarized in Fig. 3.33, B. Under GR impact, the RAs were shifted to the left meaning to reduced changes in $[Ca^{2+}]_i$ (orange and light brown). Again, similar to the effects induced on kainate receptors, blockade of the L- and N-types CaChs clearly shifted the RAs to the right meaning to higher changes in $[Ca^{2+}]_i$ (blue and green). In the presence of the VGCC blocker cocktail, activation of A1Rs shifted the NMDA-induced calcium responses to the left, meaning to reduced changes in $[Ca^{2+}]_i$ (orange and light brown). The effects were significantly different from the impact induced via activation of A1Rs alone (Fig. 3.33, B).

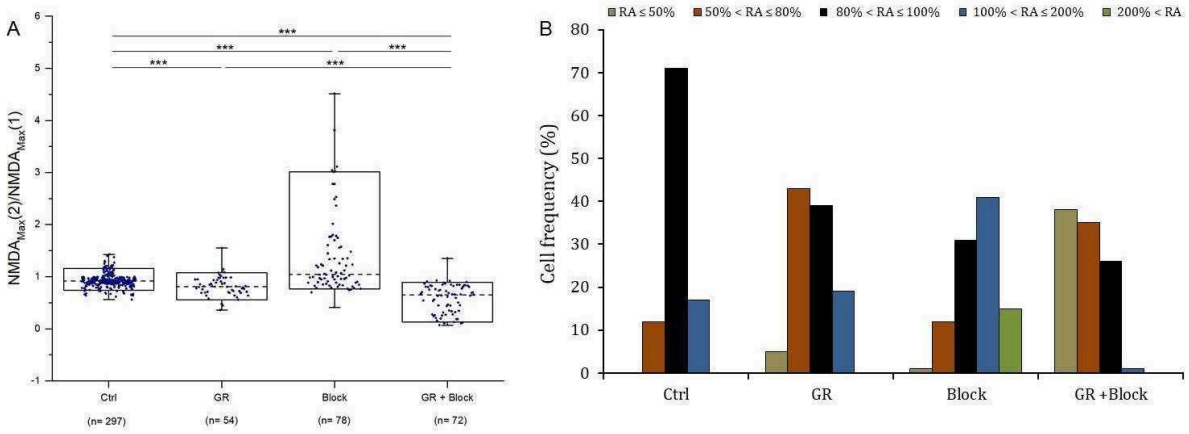


Figure 3.33: Statistical analyses of NMDA-induced calcium responses. (A): The normalized RAs of the NMDA-induced calcium responses (Ctrl: NMDA, 300 µM) were compared to the RAs under concomitant activation of A1Rs (GR: GR 79236, 300 µM) and/or blockade of VGCCs, Block: CaChs-blocker cocktail, L-type antagonist nimodipine (50 µM) + N-type antagonist ω-conotoxin GVIA (250 µM). Each dot represents one GC; the dashed lines indicate the medians: NMDA: ctrl: 0.91, n=297; GR: 0.81, n=54; Block: 1.04, n=78; GR + Block: 0.65, n=72. There was a statistically significant difference between the ctrl cells and the cells under the different conditions (Mann-Whitney Rank Sum Test: p***≤0.001 each). **(B):** The normalized RAs were subdivided in five groups, and the cell frequency was determined. RAs, which exhibited less than 50% of the initial RAs (light brown), RAs between 50-80% (orange), RAs between 80-100% (black), RAs between 100-200% (blue) and RAs that were higher by at least a factor of 2 (green).

Taken together, these results show that activation of A1Rs decreased the non-NMDA- and the NMDA-induced calcium responses significantly. The blockade of L- and N-types CaChs led to different results: while the AMPA-induced calcium responses were significantly reduced, the kainate- and the NMDA-induced calcium responses were clearly enhanced. This suggests that at least an important fraction of the AMPA-induced change in the $[Ca^{2+}]_i$ may arise from the VGCCs. The activation of kainate or NMDA receptors under blockade of VGCCs induced a further increase in the changes in the $[Ca^{2+}]_i$, possibly the influx through the ligand-gated channels became stronger and/or the receptors may trigger other cellular signaling cascades that further enhance the calcium responses. Interestingly, irrespective of whether the VGCC blocker cocktail enhanced or decreased the iGluR-induced change, in the presence of the cocktail the A1R agonist GR 79236 always lead to a decrease in the iGluR-induced change. In summary, the activation of the iGluRs led to an increase in the $[Ca^{2+}]_i$ in the GCs of the TN-L15-expressing retinae. The pharmacological approach clearly showed that the neurotransmitters DA, AD, MT, and NO differentially modulated iGluR-mediated signals in the retina. The results are summarized in Table 3.1.

	AMPA	Kainate	NMDA
DA	↓	↓	↓
D1Rs	↓	↓	—
D2Rs	↑	↑	↓↑
D1Rs + D2Rs	↑	↑	—
NO	↑	—	↑
MT	—	↓	↓
A1Rs	↓	↓	↓
CaChs blocker	↓	↑	↑
A1Rs + CaChs blocker	↓	↓	↓

Table 3.1: Summary of the results of the pharmacological studies on the iGluR-induced calcium responses. The arrows indicate how the calcium response upon stimulation of the AMPA, kainate or NMDA receptors is modulated by the pharmacological processes indicated in the left column. DA: Dopamine 20 µM; D1Rs: SKF 38393 1 µM; D2Rs: Quinpirole 1 µM; NO: SNAP S-Nitroso-N-acetyl-DL-penicillamine 300 µM; MT: Melatonin 500 nM; A1Rs: GR 79236 300 µM; CaChs blocker: L-type antagonist nimodipine (50 µM) + N-type antagonist ω-conotoxin GVIA (250 µM).

Activation of D1Rs and/or D2Rs had the same effects on the non-NMDA receptors, while the effects on the NMDA-receptors were quite different. Application of DA elicited similar effects on the non-NMDA and the NMDA receptors. NO enhanced the AMPA- and the NMDA-induced calcium responses while it had no significant or slight effects on the kainate receptors. The stimulation of MT receptors did not affect the AMPA-induced calcium responses but decreased the kainate- and the NMDA-induced calcium responses. Activation of A1Rs with or without blockade of the L- and N-types CaChs reduced the non-NMDA- and the NMDA-induced calcium responses. The blockade of the CaChs decreased the AMPA- and enhanced the kainate- and the NMDA-induced calcium responses. It becomes clearly evident that the modulation of the iGluRs occurs in a very

distinct way by the different neurotransmitters. This may be determined by a different expression level of the iGluRs and/or the receptors of the neurotransmitters.

3.2. Immunohisto- and cytochemical studies of retinal neurons

3.2.1. D1Rs and D2Rs are probably expressed on GC dendrites

In the GCs of the TN-L15-retina, activation of D1Rs and/or D2Rs affected the iGluR-induced calcium responses (see chapter 3.1.1). In order to localize the D1Rs and D2Rs, immunohistochemical studies were performed on cryosections of adult retina from C57Bl/6N or TN-L15 mice.

First, stainings against D1Rs were combined with markers for bipolar cells. The antibody against the α-isoform of the calcium-dependent protein kinase C (PKCα) is a well-suited marker for rod BCs in the mammalian retina (Negishi *et al.* 1988, Greferath *et al.* 1990). Vesicular glutamate transporters (vGluTs) play an essential role in loading glutamate into synaptic vesicles (Bellocchio *et al.* 2000). PRs and BCs, which are glutamatergic neurons, exhibit a high immunoreactivity for vGluT1 at their synaptic terminals. Vertical sections of adult mice retina were stained with antibodies against D1Rs, vGluT1 and PKCα (Fig. 3.34). Fig. 3.34, green shows that D1Rs are expressed in the synaptic layers: in the OPL (green, large arrow) and more abundantly in the IPL (green, arrows and arrowheads). Both synaptic layers were immunoreactive for vGluT1: OPL (red, large arrow, photoreceptor axon terminals) and IPL (red, arrows and arrowheads, bipolar cell axon terminals). The PKCα immunoreactivity (Fig. 3.34, blue) shows that rod BCs were completely stained: the dendritic tree (large arrow), the soma, the axon and the terminal system (arrows 1 and 2). The overlay indicates that D1Rs are co-expressed with vGluT1 in sublamina 3 (arrowheads 1 and 2). The double-labeling appears yellow (magnification, overlay). By means of the stratification pattern in the IPL, different types of BCs were identified (Ghosh *et al.* 2004). Immunohistochemical studies of the dopaminergic system in the mouse retina revealed that D1Rs are expressed in the axon terminal systems of cone BCs type 5 and 7 (Usai 2014). Arrowhead 3 indicates a co-labeling for D1Rs and vGluT1 localized in sublamina 4. This was most likely a terminal system of type 8 cone BCs, since it was PKCα-negative, however vGluT1-positive (overlay, arrowhead 3). Arrows 1 and 2 in the overviews and magnifications show terminal systems of rod BCs (PKCα-positive). These terminal systems were D1R-positive (D1Rs/PKCα) and vGluT1-positive (vGluT1/PKCα). The

D1Rs labeling was mostly membrane-bound, while the vGluT1 labeling filled the axon terminal. The large arrows shown in the magnifications indicate D1R-positive structures that were vGluT1- and PKCα-negative localized in sublamina 3/4. These are most likely dendrites of ACs or GCs that make contacts to terminal systems of the BCs (Fig. 3.34, magnifications, large arrows).

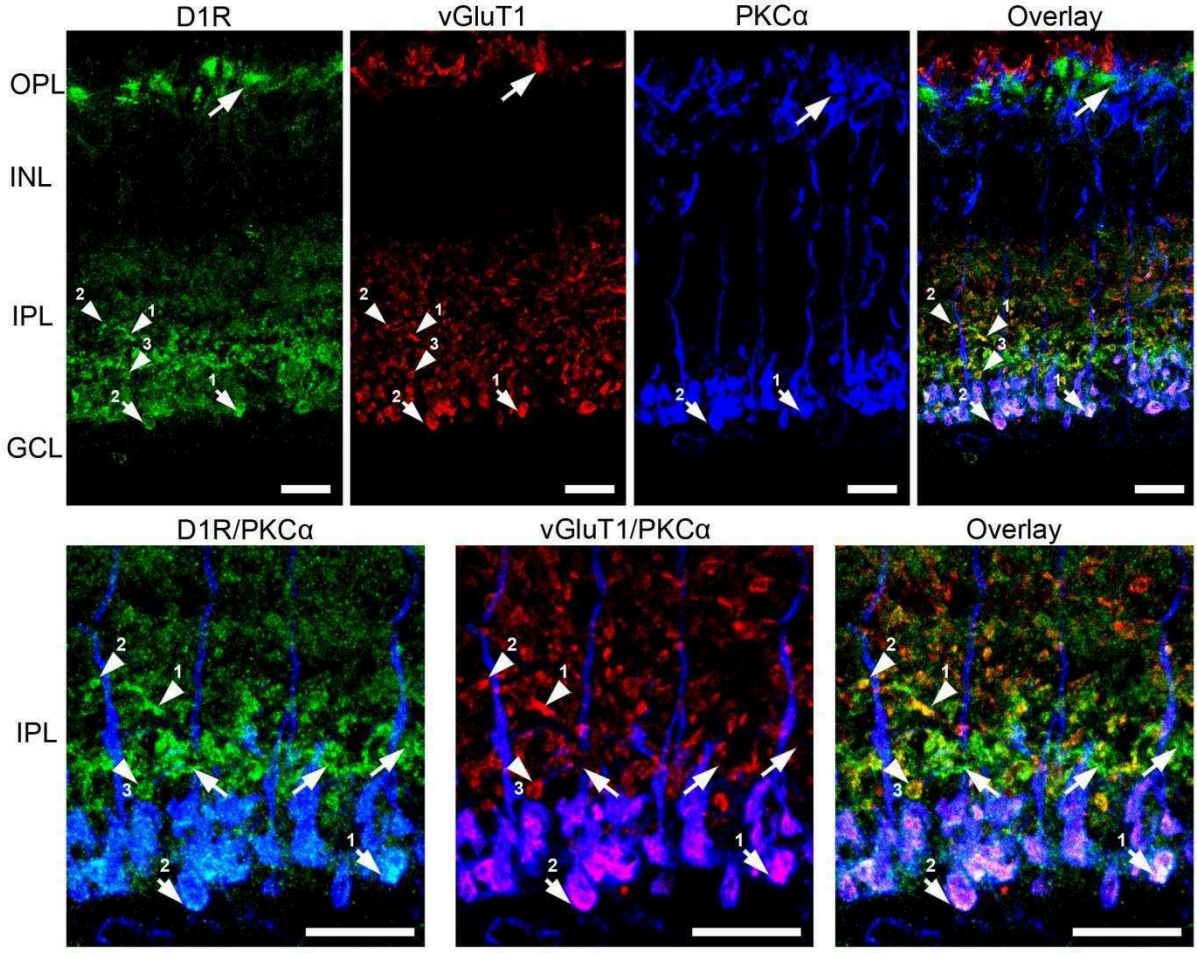


Figure 3.34: D1Rs are expressed in the synaptic layers of the mouse retina. Vertical cryosections of the mouse retina were stained with antibodies against D1Rs (green), vGluT1 (red) and PKCα (blue). D1Rs are expressed in the synaptic layers OPL (large arrow) and IPL (arrows and arrowheads). Immunoreactivity for vGluT1 was detected in the OPL (large arrow) and IPL (arrows and arrowheads). Rod BCs are completely stained with anti-PKCα: dendritic tree (large arrow), soma, axon and terminal system (arrows 1 and 2). The overlay shows that D1Rs are expressed post-synaptically to the PRs terminal system within the dendritic tree of the rod BCs (large arrows). In the IPL some terminal systems were D1R- and vGluT1-positive but not immunoreactive for PKCα (arrowheads 1-3), some terminal systems were D1R-positive but not vGluT1-positive or PKCα-positive (large arrows). Rod BCs were D1R- and vGluT1-positive (arrows 1 and 2). GCL: ganglion cell layer; INL: inner nuclear layer; IPL: inner plexiform layer; OPL: outer plexiform layer. Scale bar 10 µm.

With this finding, and by using the transgenic mouse line TN-L15, I investigated whether D1Rs and/or D2Rs may be expressed on GC dendrites. The calcium-binding protein (CaBP) is a suited marker for HCs, ACs as well as displaced ACs. Moreover, it labels three horizontal bands within the IPL (Rohrenbeck *et al.* 1987, Haverkamp & Wässle 2000).

Cryosections of the TN-L15-retina were stained with antibodies against GFP to intensify the endogenous fluorescence signal of the TN-L15 sensor (green). Furthermore, antibodies against D2Rs (red), CaBP (magenta) and D1Rs (blue) were used (Fig 3.35). In the OPL, HCs were strongly immunoreactive; the large cell body and the dendritic processes were CaBP-positive. The D1Rs immunoreactivity shows no overlapping with the CaBP immunoreactivity (data not shown). Confocal images of the overview show the staining in the inner retina (Fig. 3.35).

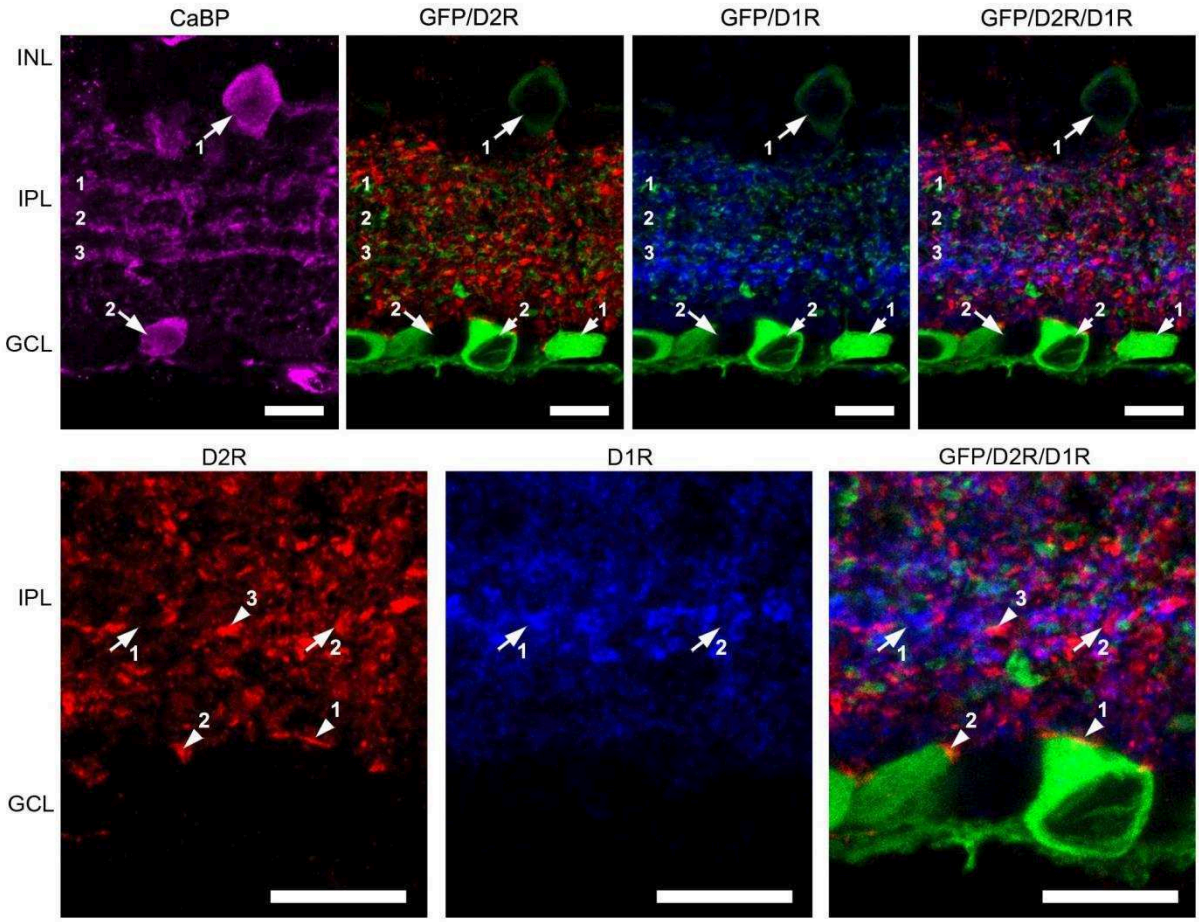


Figure 3.35: D1Rs and D2Rs are abundantly expressed in the IPL in the TN-L15-retina. Vertical cryosections of the TN-L15-retina were stained with antibodies against GFP (green), CaBP (magenta), D2Rs (red) and D1Rs (blue). The CaBP labeling was used as an orientation to better classify the structures in the IPL. Three bands could be distinguished (1-3, CaBP, magenta), ACs and displaced ACs were found CaBP-positive (large arrows 1 and 2, respectively). The arrows 1 and 2 show two TN-L15-positive GCs (green). D2R-positive structures were found in the IPL (red, arrowheads 1-3, large arrow 2). Large arrow 1 shows D1R-positive structure in the sublamina 4 (blue). The GFP/D2R/D1R overlay indicates overlapping between D2Rs labeling and GCs-soma (arrowheads 1 and 2) and dendrites (arrowhead 3). There were no co-expressed D1Rs and D2Rs (magnifications, large arrows 1 and 2). GCL: ganglion cell layer; INL: inner nuclear layer; IPL: inner plexiform layer. Scale bar 10 µm.

Fig. 3.35 shows the large cell body of a CaBP-positive AC in the inner part of the INL (CaBP, magenta, large arrow 1). Large arrow 2 shows the cell body of a CaBP-positive AC, which is localized in the GCL, and is referred to as a displaced AC. Three CaBP-

positive bands are detectable (CaBP, 1-3). Bands 1 and 3 are formed by terminal systems of ON- and OFF-cholinergic ACs, respectively. Band 2 is formed by NOS-positive ACs (Haverkamp & Wässle 2000, Ghosh *et al.* 2004). In the GFP/D2R overlay, TN-L15-positive GCs are shown (green, arrows 1 and 2). The AC in the INL shows a dim staining (large arrow 1); the cell indicated by the large arrow 2 shows no GFP labeling. In the IPL, small D2R- (red) and GFP-positive (green) structures appeared alternately covering the whole IPL up to sublamina 5. The GFP/D1R overlay indicates a strong D1R labeling in the IPL in sublamina 4. Along the IPL, D1Rs staining appeared dot-like and was less clear than the labeling shown in Fig. 3.34. This may be related to the choice of the secondary antibody, since due to the expression of TN-L15 sensor the goat anti-rat Alexa Fluor 488 could not be used. The overlay GFP/D2R/D1R shows alternating labeled structures for GFP (green), D2Rs (red) and D1Rs (blue). The magnifications should better clarify whether there are co-labeled GCs dendrites and D1Rs or D2Rs. The magnification of the IPL (red) shows D2R-positive structures (arrowheads 1-3). The large arrow 1 shows an empty spot between two D2R-positive structures; large arrow 2 shows a strongly D2R-positive structure (Fig. 3.35, red). The D1R labeling shown in the magnification (blue) revealed a D1R-positive structure (large arrow 1), which corresponds to the empty spot shown in the D2R labeling (red, large arrow 1). By contrast, large arrow 2 shows an empty spot (D1R, blue), which showed a D2R-positive structure (red, large arrow 2). The GFP/D2R/D1R overlay indicates that the previously marked D2R-positive structures are partially overlapping with the GCs membranes (arrowheads 1 and 2) or dendritic processes (arrowhead 3). However, it cannot be ruled out that ACs processes pass through in close proximity to the GCs membranes. Large arrows 1 and 2 show no co-labeling between D1R- or D2R-positive structures and GC dendritic processes.

These results indicate that both D1Rs and D2Rs are abundantly expressed in the IPL. There is evidence that GCs express D2Rs along the membrane and dendritic processes, however this was rarely observed.

3.2.2. AKAR4-expressing retinal neurons express PKA

The cDNA encoding the FRET-based biosensor AKAR4 was transiently transfected into cultured retinal neurons (4-8 DIV) by means of Lipofectamine 2000. On the following day, the expression was complete. Then, the cells were fixed and analyzed by immunocytochemistry. To amplify the endogenous fluorescent signal of AKAR4, an

antibody against GFP was used. Since transfected neurons will be used to study the cAMP/PKA signaling, it was important to determine whether PKA-expressing neurons are targets for the AKAR4 transfection. Thus, retinal neurons transfected with AKAR4 were stained with PKARIIβ, an antibody that recognizes the regulatory subunit RIIβ of PKA. Fig. 3.36 displays two AKAR4-positive neurons (AKAR4, arrows 1 and 2). The expression covers the cell bodies as well as their neurites. Immunoreactivity for PKARIIβ was found in the AKAR4-expressing neurons (PKARIIβ, arrows 1 and 2) as well as in many other retinal neurons. The overlay shows the overlapping of AKAR4 and PKARIIβ expression (overlay, arrowheads 1 and 2). Thus, transfected cells express PKARIIβ and can be used to monitor the dopaminergic and purinergic signaling using AKAR4.

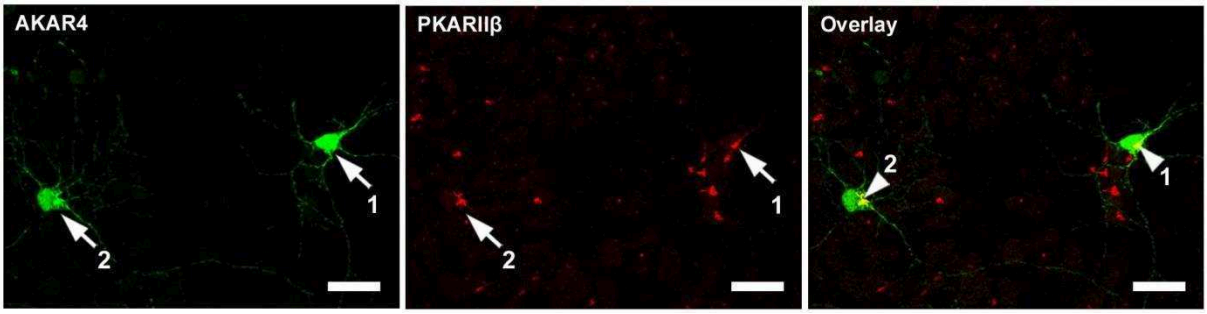


Figure 3.36: AKAR4-expressing retinal neurons express PKARIIβ. Retinal neurons dissociated from P1 mice were transfected with the cDNA encoding the AKAR4 sensor at DIV6 and stained with anti-GFP (green) and anti-PKARIIβ (red). There was a co-localization between all AKAR4-positive neurons and PKARIIβ (arrowheads 1 and 2). A large number of neurons were positive to PKARIIβ however not to AKAR4. Scale bar 20 μm.

3.2.3. Immunocytochemical analysis of D1Rs in cultured retinal neurons

In order to test whether the retinal neurons in our culture system express D1Rs, fixed cells were stained with anti-D1R antibodies. Further markers were chosen to identify specific cell types. Fig. 3.37 shows the double-staining with anti-D1R and anti-calretinin. The antibody against calretinin, a calcium-binding protein, labels ACs (see chapter 3.1, Fig. 3.1, B).

Confocal images of retinal neurons double-stained with anti-calretinin and anti-D1R antibodies revealed that a large number of cells express D1R (Fig. 3.37, arrows 1 and 2). Both cells in Fig. 3.37 have triangularly-shaped somata with multiple primary processes that give rise to secondary processes. The plasma membrane and the processes were found D1R-positive (Fig. 3.37, D1R, green). Many other cells with an oval-shaped soma were found D1R-positive (data not shown). One of the two D1R-positive cells was found

positive for calretinin (Fig. 3.37, Calretinin, red, arrow). The soma, the primary and secondary processes were immunoreactive for calretinin. The overlay shows the overlapping between calretinin and D1R immunoreactivity (arrowhead 2) and the D1R-immunoreactive/calretinin-negative retinal neuron (arrowhead 1).

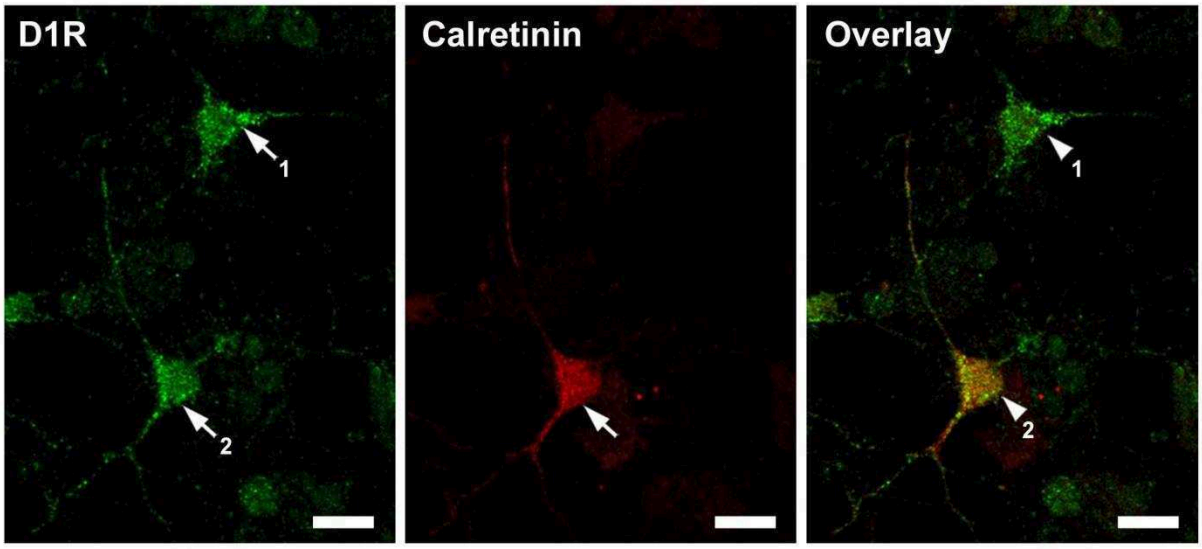


Figure 3.37: ACs were found positive for D1Rs in dissociated retinal neurons. Retinal neurons dissociated from P2 mice were double-labeled with anti-D1R (green) and anti-calretinin (red) at DIV6. The retinal neurons express the D1Rs at the level of the membrane and the dendrites (green). A calretinin-positive neuron shows a labeled cell body as well as processes (red). The overlay shows that the AC marked by anti-calretinin expresses D1Rs (arrowhead 2). Scale bar 10 µm.

ACs can be immunohistochemically distinguished by using antibodies directed against their neurotransmitters or components of the molecular machinery required for the production of these neurotransmitters. Glutamic acid carboxylase (GAD) is the enzyme that catalyzes the decarboxylation of glutamate to GABA (γ-aminobutyric acid). Thus, an antibody against the isoforms 65 and 67 (GAD65/67) was used as a marker for GABAergic ACs parallel to the anti-D1Rs (Fig. 3.38). Fig. 3.38 shows D1R immunoreactivity along the primary processes of two cells (D1R, green, arrows 1 and 2). The immunoreactivity covered a large part of the soma (arrow 1). A large number of cells were found GAD65/67-positive (GAD65/67, red, arrows 1-3). The soma size ranged between 8 and 12 µm, and the somas as well as the processes were immunoreactive for GAD65/67. Double-labeling for anti-D1Rs and anti-GAD65/67 was found in two cells (arrowheads 1 and 2). Thus, these results indicate on the one hand that GABAergic ACs form a large fraction of cells in the culture system and, on the other hand, that many GABAergic ACs express D1Rs.

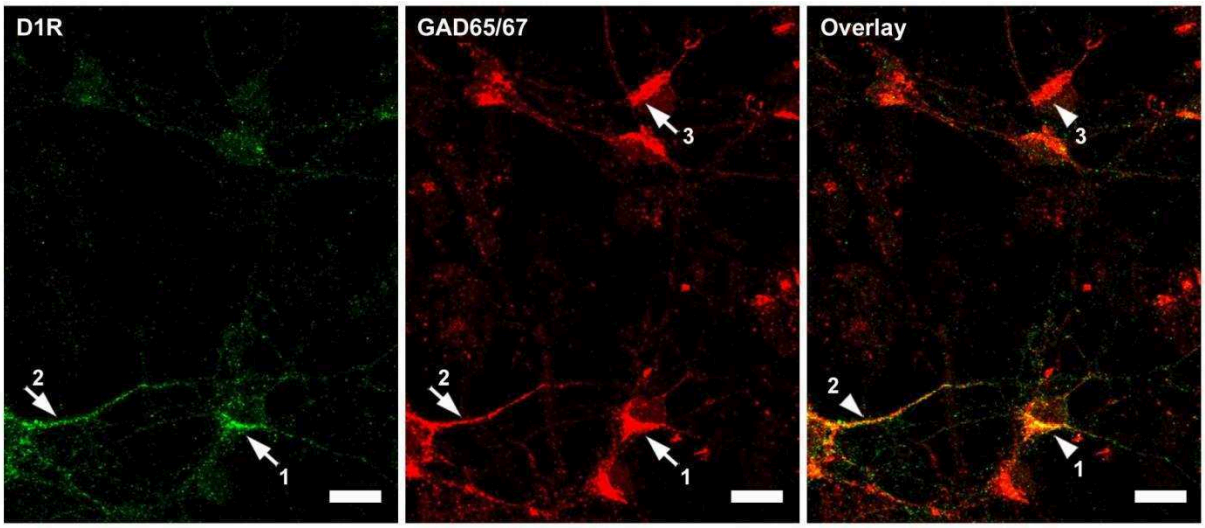


Figure 3.38: D1Rs are expressed in some GABAergic ACs in dissociated retinal neurons. Retinal neurons dissociated from P2 mice were fixed after 6DIV and stained with antibodies against D1Rs (green) and GAD65/67 (red). D1R-immunoreactivity was found in cells along the membrane and the processes (green, arrows 1 and 2). A large number of cells were found GAD65/67-immunoreactive (red, arrows 1-3). The overlay shows that some GABAergic ACs (GAD65/67-positive) express D1Rs (arrowheads 1 and 2). Scale bar 10 µm.

In order to further characterize the cell types found in our culture system and test whether they express D1Rs, dissociated retinal neurons were stained with antibodies against D1Rs, vGluT1 and PKCα (Fig. 3.39). Confocal images show several D1R-positive neurons in the culture (green, arrows 1-3). Both plasma membrane and the processes were D1R-positive, although the expression along the soma was stronger (arrow 3). The processes of one single cell were found vGluT1-positive (red, asterisk 1-2). No soma could be identified; the terminal system was also vGluT1-positive (asterisk 2). These might be processes of PRs or cone BCs. A range of cells were found PKCα-positive (blue, arrows 1-3). In other confocal images, vGluT1 immunoreactivity appeared punctiform, in agreement with localization at glutamatergic synapses (data not shown). Membrane and less strongly processes were immunoreactive for PKCα. The overlay shows that some neurons were PKCα-and D1R-positive (arrowheads 1 and 2). The PKCα-positive neuron designated by arrowhead 3, showed no D1R immunoreactivity. On the other hand, many D1R-positive neurons were not PKCα-positive. The vGluT1-positive process showed no overlapping with D1R or PKCα immunoreactivity (asterisk). Since the PKCα-positive neurons showed no vGluT1 immunoreactivity, and the environment of the dissociated cells in culture may strongly differ from the native conditions, it cannot be ruled out that these cells are ACs. Negishi and colleagues found PKC immunoreactivity in some ACs (Negishi *et al.* 1988).

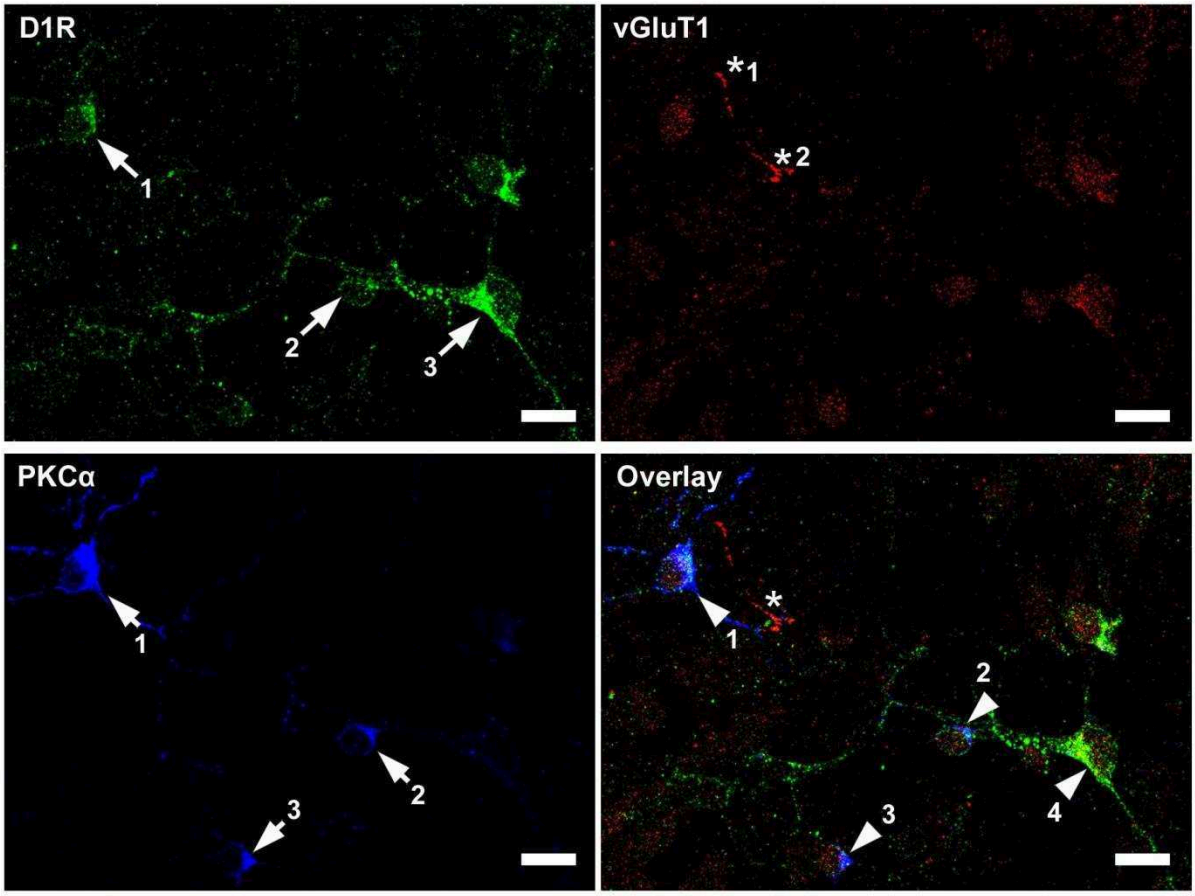


Figure 3.39: D1Rs are expressed in PKCα-positive neurons. Dissociated retinal neurons (P2) were fixed at 6DIV and stained with antibodies against D1Rs (green), vGluT1 (red) and PKCα (blue). A large number of cells were found D1R-positive along plasma membrane and processes (green, arrows 1-3). Immunoreactivity for vGluT1 was found in the terminal system of one cell (red, asterisk 1 and 2). PKCα immunoreactivity was found in several retinal neurons along the plasma membrane and processes (blue, arrows 1-3). The overlay shows that some cells were double-labeled for D1Rs and PKCα (arrowheads 1 and 2). One PKCα-positive neuron did not express D1Rs (arrowhead 3) and a D1R-positive cell did not express PKACα (arrowhead 4). There was no overlapping between the vGluT1-positive process and D1R or PKCα immunoreactivity (asterisk). Scale bar 10 µm.

According to the classical understanding of DRs, activation of D1Rs should increase the cAMP production via activation of the ACy and subsequently the PKA activity (for review see (Beaulieu & Gainetdinov 2011)). As previously shown, dissociated retinal neurons transfected with the cDNA encoding for AKAR4 were found PKARIIβ-positive (Fig. 3.36). Moreover, different cell types successfully cultured in our culture system express the D1Rs. Thus, in order to test whether D1R-positive cells express PKA, retinal neurons were double-stained with antibodies against D1Rs (Fig. 3.40, green), and against the regulatory subunit IIβ of PKA (Fig. 3.40, red). Analysis of confocal images revealed that the majority of the cultured retinal neurons were D1R-positive (green, arrows 1-4). The arrows 1 and 2 indicate the staining along the plasma membrane of two somata, the arrows 3 and 4 the stronger staining of the processes. A large number of cells were PKARIIβ-positive (red, arrows 1-4). The soma of one D1R-positive cell shows

a dim staining for PKARIIβ (arrow 1); in the second cell PKARIIβ immunoreactivity is barely visible (arrow 2). The processes were strongly stained (arrows 3 and 4). The overlay indicates that the majority of the D1R-positive cells are also PKARIIβ-positive (arrowhead 1). The processes of cell 2 were strongly stained and appear yellow (arrowhead3); the staining along the soma was very dim (arrowhead 2). Arrowhead 4 shows the overlapping of D1Rs and PKARIIβ immunoreactivity along the processes; the soma was not PKARIIβ-positive (Fig. 3.40, overlay). Further analysis indicates that some D1R-positive neurons did not express PKARIIβ (data not shown).

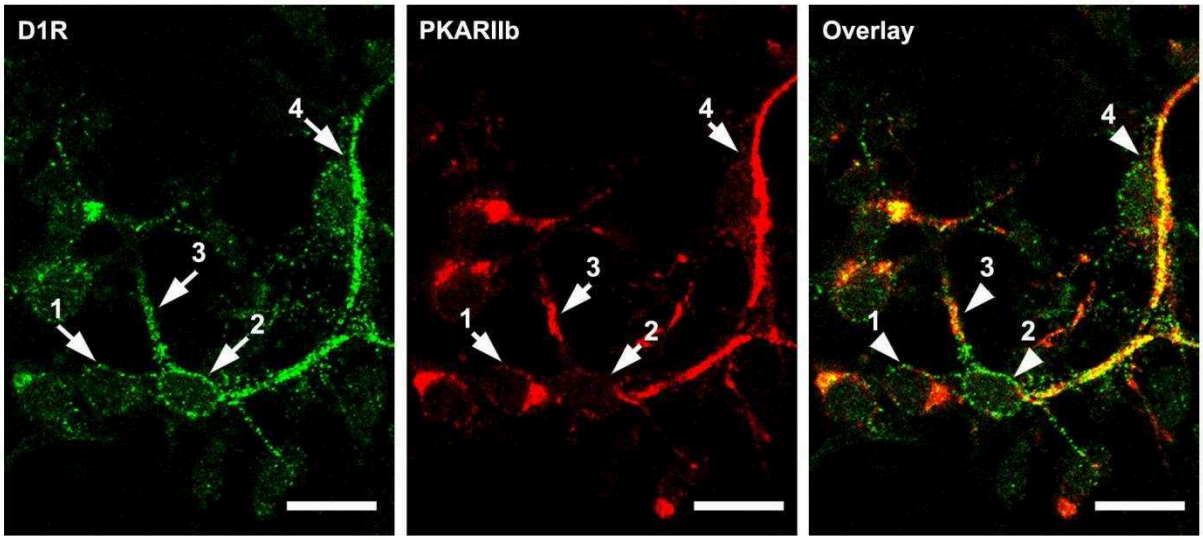


Figure 3.40: Some D1R-positive neurons express PKARIIβ. Cultured retinal neurons from P2 young mice were fixed at 6DIV and stained with anti-D1Rs (green) and anti-PKARIIβ (red). Many D1R-positive neurons were distinguished with expression along plasma membrane and processes (green, arrows 1-4). Clearly stained soma and processes of PKARIIβ-positive cells could be distinguished (red, arrows 1-4). The overlay shows that the majority of the D1R-positive cells also express PKARIIβ (arrows 1 and 3). Some D1R-positive soma did not show PKARIIβ immunoreactivity. Scale bar 10 µm.

In summary, the immunocytochemical results demonstrate that the majority of the cultured retinal cells express D1Rs. In the majority of the D1R-positive cells I also found PKARIIβ immunoreactivity. Cultured retinal neurons transfected with the cDNA encoding the AKAR4 biosensor were found to also express PKARIIβ. PKCα and D1Rs double-labeled cells were abundantly found in the cell culture, suggesting that ACs, and probably BCs do express D1Rs. The majority of the ACs labeled by anti-calretinin was found to express D1Rs. Similarly, almost all GABAergic ACs (GAD65/67) were also D1R-positive. Further cell types could be found in our culture system by using reliable cell type markers (data not shown). The G-protein $G_o\alpha$ has been found in ON-cone and rod BCs (Vardi *et al.* 1993, Vardi 1998, Haverkamp & Wässle 2000). Similar results could be found in our culture system as well as on cryosections (data not shown). Recoverin is a

calcium-binding protein and is a suitable marker for PRs and type 2 BCs in the mouse retina (Haverkamp & Wässle 2000). Neither PRs nor type 2 BCs were found D1R-positive in retinal sections or in the cell culture (data not shown).

As a summary, the culture of dissociated retinal neurons was established successfully. PRs, ACs (glycinergic and GABAergic), BCs and rarely HCs were cultured. The number of cultured cells decreased with the duration of the cultivation. The transfection process of the AKAR4 sensor by the transfection reagent Lipofectamine 2000 can also initiate cell death and thus be a limiting factor. Nevertheless, it turned out that our culture system is suitable for studying the cAMP/PKA pathway induced via activation of GPCRs, in particular DRs and ARs by using the genetically encoded FRET-based AKAR4 sensor.

3.3. Studying the cAMP/PKA pathway in cultured retinal neurons

Dopamine (DA) is released from dopaminergic ACs; it acts on a variety of retinal neurons as a neurotransmitter and a neuromodulator (Weiler *et al.* 1988, Dearry & Burnside 1989). D1 receptor family includes the D1Rs and D5Rs, which are positively coupled to the ACy and the D2 receptor family includes the D2Rs-D4Rs, which induce inhibition of the ACy (for review see (Beaulieu & Gainetdinov 2011)). Activation of D1Rs stimulates cAMP production by ACy. Elevation of $[cAMP]_i$ increases the activity of the cAMP-dependent PKA. The genetically encoded FRET-based biosensor AKAR4 *(Depry et al.* 2011) was used as a reporter for the PKA activity. This sensor was used to visualize the dopaminergic and the purinergic signaling in cultured retinal neurons.

3.3.1. DA-induced changes in $[cAMP]_i$ and PKA activity

To investigate the effects of DA on cAMP/PKA pathway in cultured retinal neurons, the following paradigm, referred to as “standard protocoll”, was used. Retinal neurons (DIV 4-8) were transiently transfected with the cDNA encoding AKAR4 by means of Lipofectamine 2000. On the following day, cells were used for imaging. Throughout the experiment, cells were perfused with ES_{neuro} solution. The agonist of interest was applied for an indicated time, followed by washout periods. The AKAR4-expressing cell (6 DIV) shown in Fig. 3.41 was stimulated with 5 µM DA for 3 min, followed by washout of 9 min. Approximately 40 sec after the stimulus had started, the cell responded to DA with a decrease in CFP fluorescence and a mirror reversed increase in YFP fluorescence (Fig.

3.41, A). The delay of 40 sec is due to the lag in the perfusion system. The changes in the YFP and CFP fluorescence signals were to be expected, since DA-induced increase in cAMP production activates PKA, which in turn phosphorylates the PKA consensus site of AKAR4. Phosphorylation of the AKAR4 sensor results in a conformational change, and consequently an increase of FRET efficiency between the two fluorophores CFP and YFP. The YFP/CFP ratio was determined by dividing the YFP fluorescence intensity by the CFP fluorescence. Following, all values were normalized to the values during the 20 sec of the recording before stimulation with DA had started (Fig. 3.41, B). In the following experiments, an increase in the YFP/CFP ratio was used as an indicator for the increase in PKA activity induced by an increase in $[cAMP]_i$.

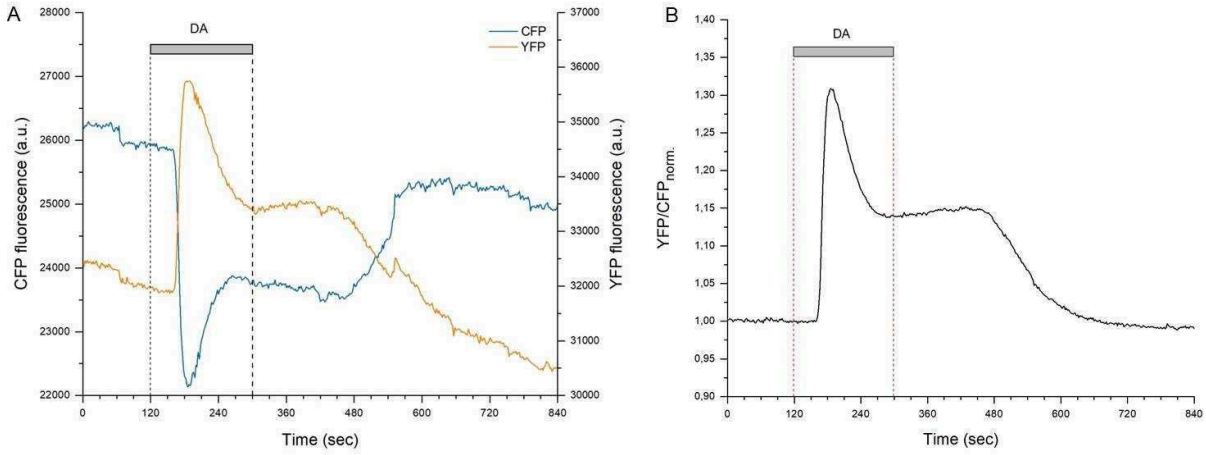


Figure 3.41: DA-induced changes in cAMP/PKA activity in cultured retinal neurons visualized by the AKAR4 sensor. Cultured retinal neurons (4-8 DIV) were transiently transfected with cDNA coding for the AKAR4 sensor. On the following day, imaging experiments were performed. **(A):** Fluorescence intensities of CFP and YFP for an AKAR4-expressing retinal neuron in response to 5 µM DA, were plotted in artificial units (a.u.) over time (sec). The response occurred with a delay of 40 sec induced by the perfusion system. The decrease in CFP fluorescence signal (cyan) was accompanied by a mirror reversed increase in YFP fluorescence signal (yellow). The changes lasted for several minutes, afterwards the signals recovered back to baseline. Both fluorescence traces decreased over time, indicating a slight photobleaching, with YFP being bleached stronger than CFP. **(B):** Ratio of YFP/CFP of the retinal neuron shown in A was plotted over time. All values were normalized to the averaged values during the 20 sec of the recording before stimulation with DA had started. AKAR4: A-kinase activity reporter 4; CFP: cyan fluorescent protein; DA: dopamine, 5 µM; YFP: yellow fluorescent protein.

The YFP/CFP ratio peaked within 30 sec with a change of 31%, started to decrease until a plateau was reached after 90 sec. The plateau lasted for 3 min, following the fluorescence signal decreased and recovered back to baseline after approximately 2.5 min (Fig. 3.41, B).

3.3.2. Blockade of PKA prevents phosphorylation of AKAR4 sensor

The phosphorylation of the AKAR4 sensor is mediated by active PKA. The PKA specific inhibitor H89 should diminish or abolish the activity of PKA and, hence, block the AKAR4 responses. In order to test this hypothesis, nine AKAR4-expressing retinal neurons (from 2 cultures) were stimulated with 5 µM DA twice for 2 min and served as ctrl (Fig. 3.42, A). Forty sec after the stimulus had started, the fluorescence signal increased and the amplitude was reached within 40 sec. The YFP/CFP ratio showed a change of 8% and the response lasted for approximately 6 min before the baseline was fully reached. The second response was quite similar to the first one in term of shape, length and amplitude (Fig. 3.42, A). In some cells the second responses were smaller, this was particularly observed in cells, were the first response lasted very long and the recovery phase became short (data not shown). Twenty-one AKAR4-expressing retinal neurons (from 5 cultures) were stimulated with 5 µM DA (2 min), all responded with an increase in YFP/CFP ratio. Following a washout phase of 10 min, cells were perfused with 25 µM H89 for 2-12 min. Still during blockade of PKA, cells were stimulated with 5 µM DA a second time. Following, the cells were perfused with ES_{neuro} solution for 10 min. The cell shown in Fig. 3.42, B responded to DA with an increase in YFP/CFP ratio of 19%. The fluorescence signal recovered fully after 4 min. During blockade of PKA (4 min), stimulation with DA did not elicit a change in YFP/CFP ratio (Fig. 3.42, B). These results are in agreement with DA activating the cAMP/PKA pathway in cultured retinal neurons.

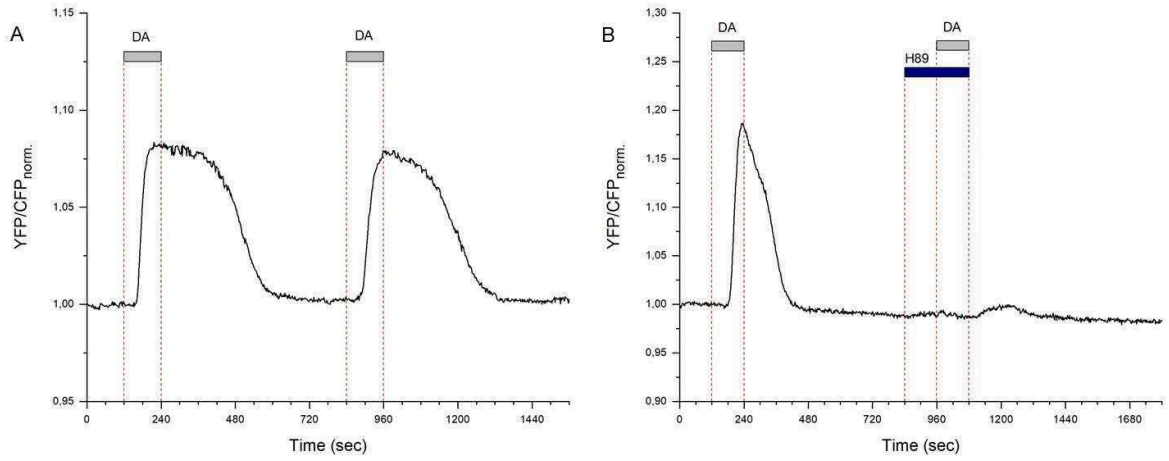


Figure 3.42: DA activates the cAMP/PKA pathway in cultured retinal neurons. (A): Stimulation of AKAR4-expressing retinal neurons with 5 µM DA (2 min) resulted in a reversible and reproducible increase in YFP/CFP ratio as shown exemplarily for this cell. **(B):** Stimulation with DA increased the YFP/CFP ratio. During blockade of PKA, stimulation with DA did not elicit any change in YFP/CFP ratio.

3.3.3. Studying the purinergic signaling in cultured retinal neurons

In the following study, I examined whether adenosine (AD) may play a role as a neurotransmitter or neuromodulator in cultured retinal neurons using the AKAR4 sensor. In total, 19 AKAR4-expressing retinal neurons (from 3 cultures) were stimulated with 5-20 µM AD for 2-6 min, followed by a washout phase of 8 min. During the whole experiment, cells were perfused with ES_{neuro} solution. Only seven cells responded to AD with an increase in YFP/CFP ratio. The cell shown in Fig. 3.43, A responded to 20 µM AD (2 min) with an increase in YFP/CFP ratio of 8%. The response occurred 30 sec after the stimulus had started and lasted for approximately 3 min. This type of responses was found in three further cells with a length of 2-3 min, albeit the amplitudes were quite smaller (data not shown). The cell shown in Fig. 3.43, B responded to AD (6 min) with an increase in YFP/CFP ratio of about 15%, which emerged approximately 30 sec after the stimulus had started. The fluorescence signal reached a plateau within 90 sec where it stayed for 4 min. Then, the fluorescence signal started to decrease and recovered back to baseline after 2 min (Fig. 3.43, B). Such sustained responses were found in two further cells that were stimulated for 2 or 4 min. In total, 37% of the cells responded to AD, while all cells responded to DA with an increase in YFP/CFP ratio (Fig. 3.42). Morphologically, there was no difference between cells responding to AD and cells that did not respond to AD. Thus, in order to test the cells for their vitality and to verify whether the same neuron expresses both DA and AD receptors, 32 AKAR4-expressing retinal neurons (from four cultures) were stimulated first with AD (3 min) and after washout with DA (2 min). Only one single cell responded neither to AD nor to DA. In 88% of the cells (n=28) AD did not elicit any change in YFP/CFP ratio, while DA induced an increase in the YFP/CFP ratio (Fig. 3.43, C).

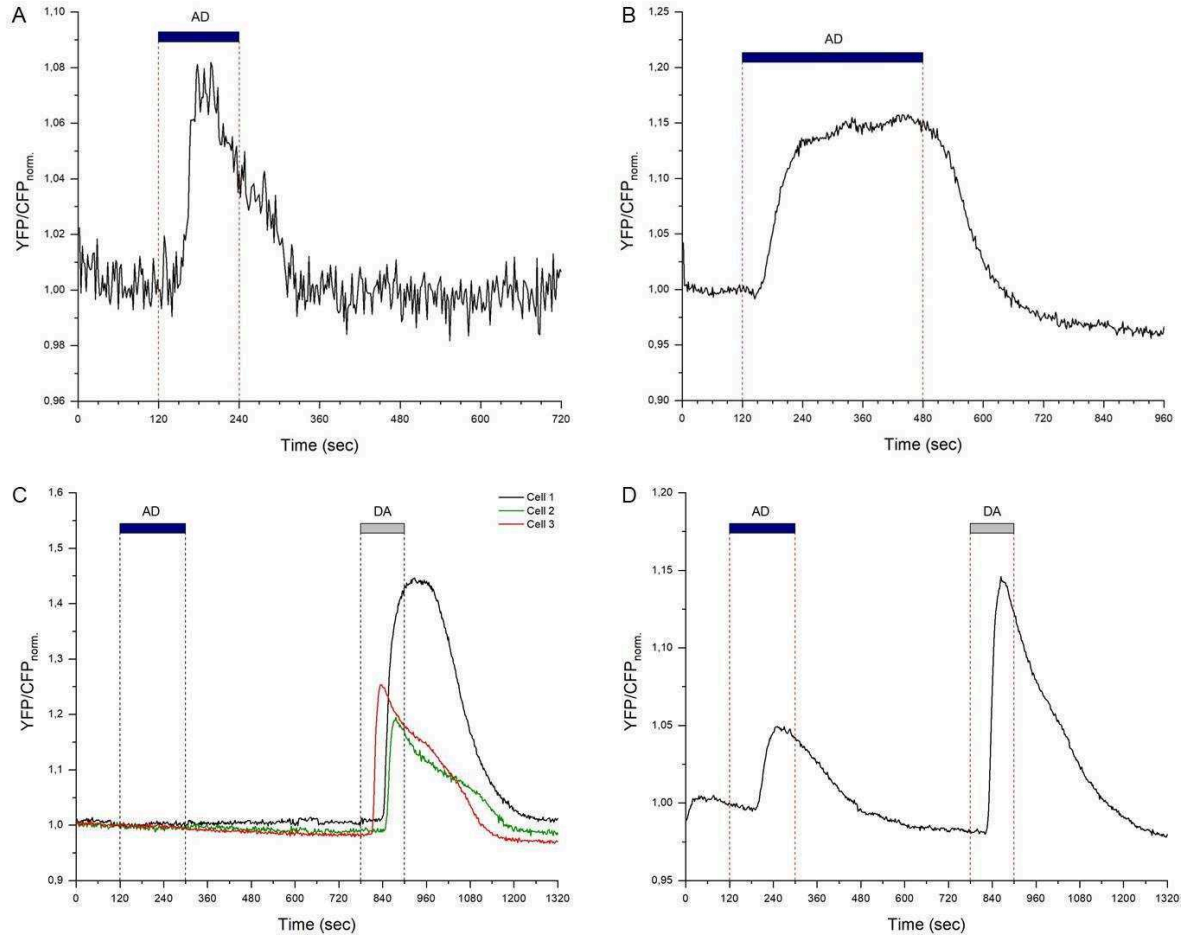


Figure 3.43: AD induced changes in YFP/CFP ratio in a subset of cultured retinal neurons. (A): Stimulation with 20 µM induced a transient increase in YFP/CFP ratio of 8%, the fluorescence signal recovered back to baseline. **(B):** Stimulation with AD induced a sustained increase in YFP/CFP ratio of 15%. The whole response lasted for approximately 10 min. **(C):** Responses of three cells to DA, AD did not induce any response in these cells. The responses differed from each other in terms of shape and amplitude, the duration was about 6 min. **(D):** The response of one cell to AD and DA with increases in YFP/CFP ratio. The DA-induced response was stronger than the AD-induced response.

Fig. 3.34, C shows the responses of three cells (1-3) to AD and DA. While AD induced no changes in the fluorescence signals, DA induced increases in YFP/CFP ratio of 44%, 20% and 26%, respectively. The three DA responses varied in terms of shape, amplitude and length of time (5-6 min). In 9% of the cells (n=3), both AD and DA elicited an increase in YFP/CFP ratio. The cell shown in Fig. 3.34, D shows exemplarily the response of one cultured retinal neuron. Approximately 60 sec after the AD stimulus had started, the YFP/CFP ratio started to increase and peaked within 60 sec with a change of 6%. The fluorescence signal started to decrease and reached the baseline within 4 min. Approximately 60 sec after the DA stimulus had started, the fluorescence signal increased transiently and peaked within 30 sec with a change of 17%. Following, the fluorescence signal started to decrease in a steady way and the baseline was reached after approximately 7 min (Fig. 3.43, D). The DA-induced response was higher by a

factor of approximately 3. In the two remaining cells, the DA-induced changes were stronger than the AD-induced responses.

In summary, I found that 20% of cultured retinal neurons express ARs, when considering cells treated with AD alone and cells treated with both AD and later on DA. AD activated the cAMP/PKA pathway detected as increase in the YFP/CFP ratio. Finally, there is good evidence for the co-expression of both ARs and DRs on the same cultured retinal neuron (9%) suggesting that both receptors may co-regulate the cellular signaling in the same retinal neuron.

3.3.4. Impact of AD on DA-induced responses in cultured retinal neurons

In order to investigate whether there is a crosstalk between ARs and DRs in cultured retinal neurons, 29 AKAR4-expressing retinal neurons were stimulated with DA (2 min) twice and in between with AD (3 min). The washout phase between two applications was kept to 8 min. Cells that were stimulated with DA twice without AD stimulation in between served as control (ctrl). Fig. 3.44, A shows the response of one AKAR4-expressing retinal neuron to two DA treatments. The cell responded to both DA applications with increases in YFP/CFP ratio of 50% and 45%, respectively. Both responses emerged roughly, peaked within few seconds and lasted for approximately 4.5 min (Fig. 3.44, A). All cells (n=8 from one culture) responded reversibly and reproducibly to DA, and the two responses of a given cell were similar (data not shown). Twenty-nine AKAR4-expressing retinal neurons (from 3 cultures) were stimulated with DA twice and in between with AD. About 86% of the cells (n=25) responded to DA twice, while AD did not elicit any change in YFP/CFP ratio as shown exemplarily for one cell in Fig. 3.44, B. This cell responded to the first DA application with an increase of 22% and to the last one with 20%. The responses were similar in terms of shape and length of time. This behavior was seen in the majority of the cells. Only one cell responded to the first DA application with an increase in YFP/CFP ratio of 22% and a duration of 5.5 min without responding to AD and second DA application (data not shown).

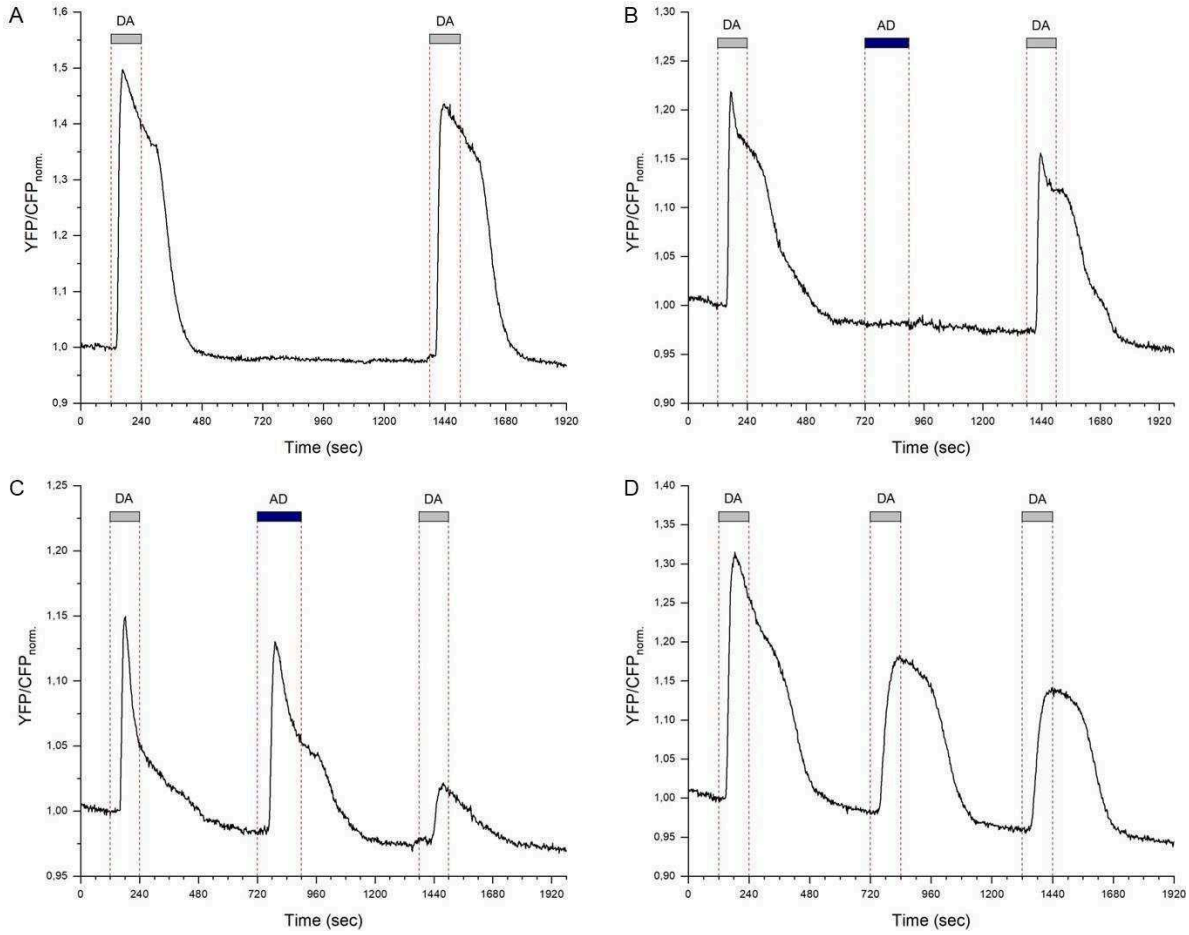


Figure 3.44: DA induced changes in PKA activity in all cells, while only few cells responded to AD. (A): The neuron displayed similar responses to both DA treatments. **(B):** The cell responded with a transient increase in YFP/CFP ratio to both DA applications; AD did not elicit any response. **(C):** This cell responded to the first DA and the AD application with a transient increase in YFP/CFP ratio of 15%. The cell recovered and responded to the last DA treatment with a change in YFP/CFP ratio of only 5%. **(D):** The neuron responded to three consecutive DA treatments with increases in YFP/CFP ratio. In 88% of the cells, the DA responses were reversible and reproducible.

In 14% of the cells (n=4), AD induced an increase in YFP/CFP ratio. The cell shown in Fig. 3.44, C responded to DA with a transient increase in YFP/CFP ratio of 15%. The fluorescence signal peaked within few seconds and started to recover back to baseline in two steps, fast and then slowly. The whole response lasted for approximately 5 min. Approximately 30 sec after the AD application had started the fluorescence signal increased, peaked with 15% change and then decreased gradually. The AD response lasted for approximately 5 min and the fluorescence signal recovered back to baseline. The last DA application induced a weak increase in YFP/CFP ratio of 5% (Fig. 3.44, C). This weak response to the last DA application was observed in all cells that responded to AD. One cell responded strongly to AD, similar to the cell shown in Fig. 3.44, C (data not shown). In the remaining two cells, the AD-induced response was much weaker than the first DA response (data not shown). The response to the final DA application was only

reduced in cells, that had previously responded to stimulation with AD (Fig. 3.44, C), but not in cells that did not respond to AD (Fig. 3.44, B) or that were stimulated only with DA two (Fig. 3.44, A) or three times (Fig. 3.44, D). These results argue against a rundown of the cAMP/PKA pathway due to repetitive stimulation. Rather, they suggest a crosstalk between the two receptor systems. Activation of AD receptors might reduce the efficiency of dopaminergic signaling in the cell.

The previous results support the assumption that ARs are expressed in cultured retinal neurons and are co-expressed with DRs in some neurons. Cells that responded to AD reflected a weaker response to DA afterwards, suggesting an impact of ARs on the DR-induced responses. In order to test this hypothesis, AKAR4-expressing retinal neurons were stimulated with 5 µM DA for 6 min, 20 µM AD were added after 2 min of DA application. Cells that were only treated with a prolonged stimulation of 5 µM DA served as control (ctrl). Ctrl cells were stimulated with 5 µM DA for 3 min (n=21 from 2 cultures) or 6 min (n=20 from four cultures). Taken together, a prolonged stimulation with DA resulted in a long-lasting increase in YFP/CFP ratio in the majority of the cells (88%). This long-lasting response type revealed two kinds of patterns: plateau-like or sustained responses (59%) and responses that formed a shoulder still during application of DA (29%). The response was transient in the remaining 12% of the cells (n=5). Fig. 3.45, A shows the responses of three AKAR4-expressing retinal neurons that were stimulated with 5 µM DA for 6 min. All responded with an increase in YFP/CFP ratio, that emerged approximately 30 sec after the stimulus was started. The fluorescence signal in cell 1 (black) peaked fast with a change of 37% and started to decrease slightly to 70% of the initial amplitude within 6 min. The fluorescence signal kept decreasing faster and recovered back to baseline after 3 min. Cell 2 (red) responded with a transient increase in YFP/CFP ratio of 21% then recovered back to baseline; the whole response lasted for 2.5 min. Cell 3 (green) responded with an increase in YFP/CFP ratio of 30%, the fluorescence signal decreased fast so that one-third of the amplitude was lost within 2 min. The fluorescence signal was relatively stable during the following 4 min bevor it fully recovered back to baseline. This type of responses was referred to as response with shoulder (Fig. 3.45, A).

In 50 AKAR4-expressing retinal neurons, two minutes after the DA stimulus was started, 20 µM AD was added (2 min). Different response patterns were observed. Fig. 3.45, B shows the responses of three cells that responded to DA with sustained increases in YFP/CFP ratio: plateau-like (cell 3, green), sustained (cell 2, red) or with shoulder (cell 1, black). In these cells AD did not alter the YFP/CFP ratio. In total, in 64% of the cells DA but not AD induced changes in YFP/CFP ratio: plateau-like or sustained responses were found in 36% of the cells (n=18), responses with shoulder in 22% of the cells (n=11) and transient responses in 6% (n=3). In the remaining 36% of the cells, AD induced two different effects: a decrease (Fig. 3.45, C, 16%) or an increase (20%) in YFP/CFP ratio (Fig. 3.45, D).

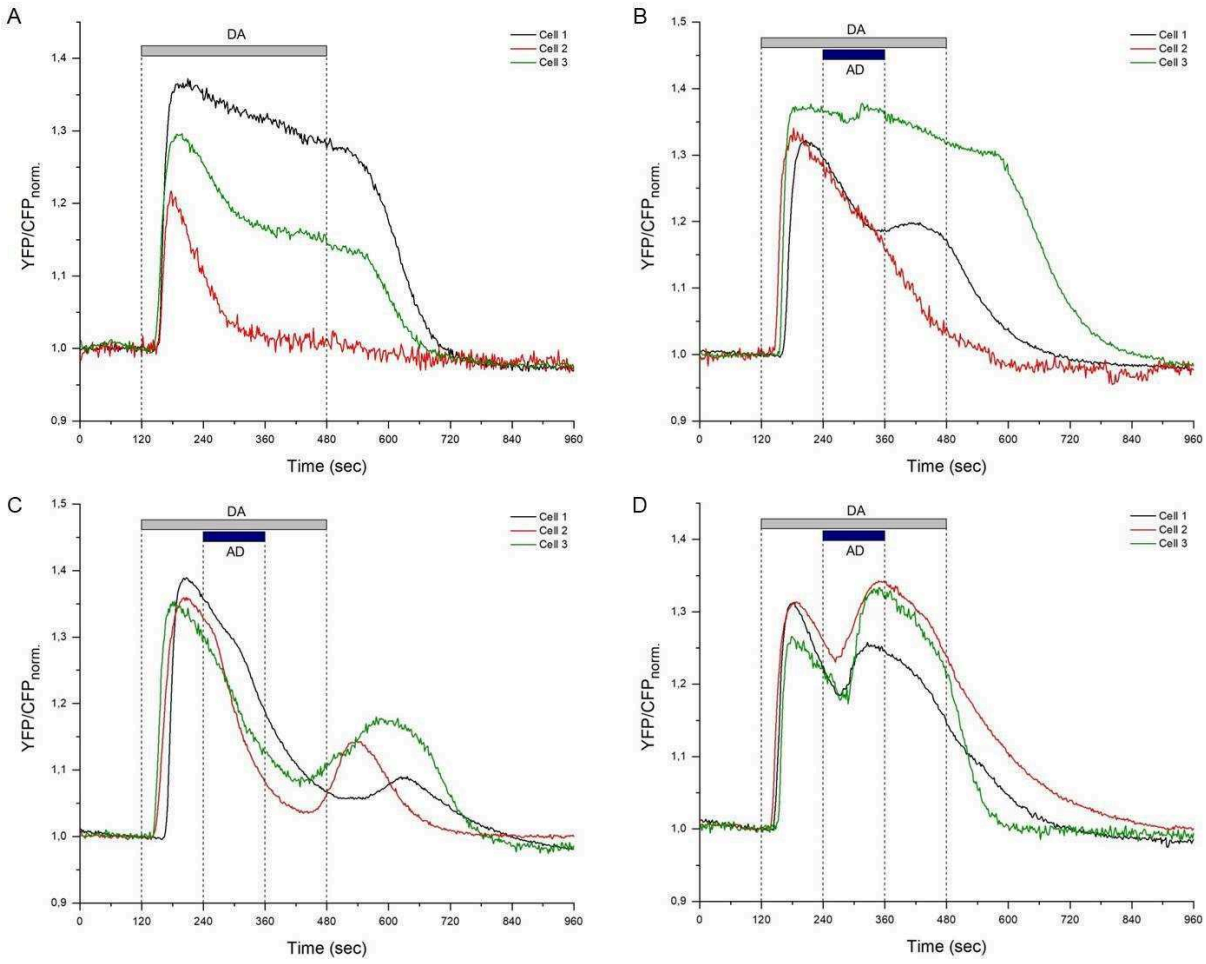


Figure 3.45: AD may affect the DA-induced increase in PKA activity in cultured retinal neurons. (A): Prolonged stimulation with DA induced increases in YFP/CFP ratio. Two responses of the sustained type are shown: a plateau-like response (Cell 1, black), and a response with a shoulder (Cell 3, green). Cell 2 responded with a transient increase. **(B):** Stimulation of ARs during prolonged application of DA did not affect the DA-induced responses. The responses of three cells are shown. **(C):** The response pattern of three cells stimulated with AD during DA application. The DA-induced increase in YFP/CFP ratio was decreased upon application of AD. **(D):** The DA-induced increase in YFP/CFP ratio was enhanced in the presence of AD. DA: dopamine (20 µM); AD: adenosine (20 µM).

In Fig. 3.45, C are shown the responses of three cells of the decrease type, the response of cell 2 will be described exemplarily. Approximately 20 sec after the DA stimulus was started, the fluorescence signal increased and the peak was reached within 50 sec before it started to decrease slowly. Approximately 30 sec after AD was added, the fluorescence signal decreased roughly, the baseline was almost reached after 2.5 min. Towards the end of the DA stimulus, the fluorescence signal increased again and lasted for 3 min (Fig. 3.45, C). Such response pattern was never observed under DA impact alone and is most likely due to activation of A1Rs that usually inhibit ACy leading to a decrease in PKA activity. The responses of three cells of the increase type are shown in Fig. 3.45, D; cell 3 (green) will be described exemplarily. The fluorescence signal started to increase 20 sec after the DA stimulus was started, exhibited a change of 27% then started to decrease slowly still during DA stimulus. The fluorescence signal exhibited only 70% of the initial amplitude 2 min later. During AD application, the fluorescence signal started to increase again and exhibited a peak that was higher than the first DA-induced change. Towards the end of the AD stimulus, the fluorescence signal started to decrease slowly and recovered back to baseline within 3 min (Fig. 3.45, D, green). This kind of responses was never seen under DA impact alone. This suggests the expression of A2Rs in these cells, which are positively coupled to ACy and their activation should increase the PKA activity.

According to the classical understanding of ARs-signaling, it was suggested that the decrease in the PKA activity may rest on the activation of A1Rs by AD (Fig. 3.45, C). Activation of A1Rs with the specific A1R agonist *N*-Cyclopentyladenosine (CPA, 10 µM) for 2 min did not elicit any changes in PKA activity (n=5, data not shown). In order to test whether activation of A1Rs reduces the PKA activity previously increased by stimulation with DA, 18 AKAR4-expressing retinal neurons were stimulated with DA for 6 min, CPA (10 µM) was added 2 min after the DA stimulus was started (Fig. 3.46).

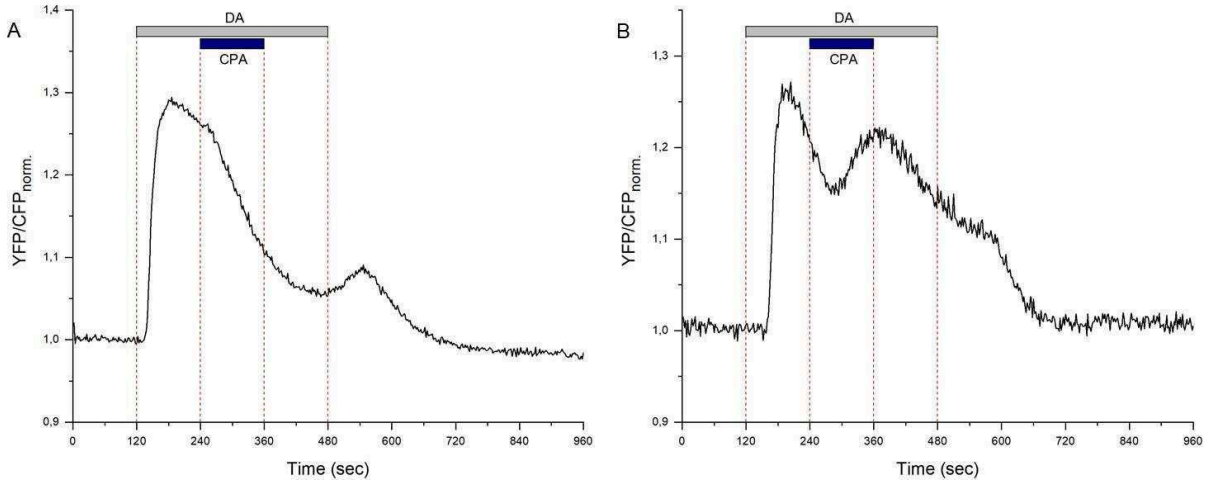


Figure 3.46: Activation of DRs and A1Rs simultaneously induced variable responses in cultured retinal neurons. (A): Activation of DRs induced an increase in PKA activity (YFP/CFP ratio). The fluorescence signal started to decrease progressively still during DA application. Activation of A1Rs decreased the fluorescence signal clearly faster. **(B):** Simultaneous activation of DRs and A1Rs led to a further increase in the YFP/CFP ratio, previously induced by activation of DRs alone. CPA: *N*-Cyclopentyladenosine (10 µM); DA: dopamine (5 µM).

In total, 56% of the cells showed no effect of activation of A1Rs, and the responses were similar to responses to DA alone (Fig. 3.45, A). Thus, 39% of the cells responded to DA with a plateau-like or sustained increase in YFP/CFP ratio and 17% showed a shoulder still during DA application (data not shown). These cells most likely do not express A1Rs. The cell shown in Fig. 3.46, A responded to DA with an increase in YFP/CFP ratio approximately 30 sec after the stimulus was started. The fluorescence signal peaked within 40 sec, and then started to decrease slowly. Additional stimulation of A1Rs induced a further, henceforth faster decrease in YFP/CFP ratio. This behavior conforms to the classical view in which A1Rs induce a decrease in ACy activity, thereby counteracting the DR-induced increase in PKA activity and was seen in 11% of the cells. The remaining 33% of the cells responded to CPA in a surprising manner: they displayed a further increase in YFP/CFP ratio. The cell in Fig. 3.46, B responded to DA with an increase in YFP/CFP ratio and the fluorescence signal started to decrease again still during DA application. This decrease went on until the fluorescence signal reached 60% of its initial amplitude approximately 1.5 min later. The fluorescence signal started to rise again 40 sec after the CPA application was started, peaked towards the end of CPA application and then started to decrease progressively. The fluorescence signal recovered fully back to baseline 2.5 min after the DA stimulus was stopped (Fig. 3.46, B). These results were surprising and cannot be explained by the opposing effects of DR and A1R activation.

In order to find out, how activation of A1Rs may affect the D1R-induced response, 27 AKAR4-expressing retinal neurons were stimulated with CPA still during the stimulation with SKF 38393. Seventeen AKAR4-expressing retinal neurons were stimulated with the specific D1R agonist SKF 38393 (100 nM) for 6 min and served as control. Fig. 3.47, A shows the responses of four cells. Stimulation with SKF 38393 led to a long-lasting increase in YFP/CFP ratio: cells 1 and 2 (black and red) showed a shoulder-like response and cells 3 and 4 (green and blue) responded with plateau-like responses (Fig. 3.47, A). All responses lasted approximately 8 min. In total, 71% of the cells responded with a plateau-like and 23% with a shoulder-like response. Only one cell (6%) responded with a transient increase in YFP/CFP ratio, however the signal was very noisy (data not shown). Application of CPA in the presence of SKF 38393 did not induce any change in YFP/CFP ratio in 56% of the cells as exemplarily shown in Fig. 3.47, B. Almost all the responses (48%) were of the plateau-like type (Fig. 3.47, B, cell 1). Cell 2 responded with a shoulder-like increase in the YFP/CFP ratio (Fig. 3.47, B). The decrease that follows switching to CPA and SKF 38393 application is most likely due to a pure SKF 38393 effect. The time delay, introduced by the perfusion system, shows that the increase in YFP/CFP ratio takes place approximately 30 sec after the SKF application was started (Fig. 3.47, B, cell 2). In 44% of the cells (n=12), the YFP/CFP ratio increased in response to SKF 38393, and then the fluorescence signal started to decrease still during D1Rs activation. Approximately 40 sec after the CPA stimulus was started, the YFP/CFP ratio increased and peaked within 2 min to a higher amplitude than induced by SKF 38393 alone (Fig. 4.47, C, cell 1 and 2). The majority of the cells that responded to CPA with a further increase in YFP/CFP ratio started to recover upon the washout of CPA and ended in a short plateau before they fully recovered (cell 1). The remaining cells responded similar to cell 2, the fluorescence signal recovered progressively following the increase induced via CPA application and reached the baseline after the stimulus was stopped. Surprisingly, none of the cells responded to CPA application with a decrease in YFP/CFP ratio (as shown in Figs. 3.45, C and 3.46, A). In order to test whether the effects seen with CPA are indeed induced via activation of A1Rs, the selective A1Rs antagonist 1,3-dipropyl-8-cyclopentylxantine (DPCPX, 10 μM) was added during SKF 38393 and CPA application (Fig. 3.47, D). Thus, during blockade of A1Rs, application of CPA should not induce the effects seen in Fig. 3.47, C. In total, 11 AKAR4-expressing retinal neurons were stimulated with SKF38393 and DPCPX for 6 min, still during this application CPA was applied for 2 min. All the cells responded similar to the

cell shown in Fig. 3.47, D. Approximately 30 sec after the stimulation was started, the fluorescence signal increased rapidly and showed a change in YFP/CFP ratio of 45%. The fluorescence signal exhibited a plateau that lasted for 6 min and then started to decrease to reach the baseline within 2.5 min (Fig. 3.47, D). The effects induced via CPA were completely abolished during blockade of A1Rs.

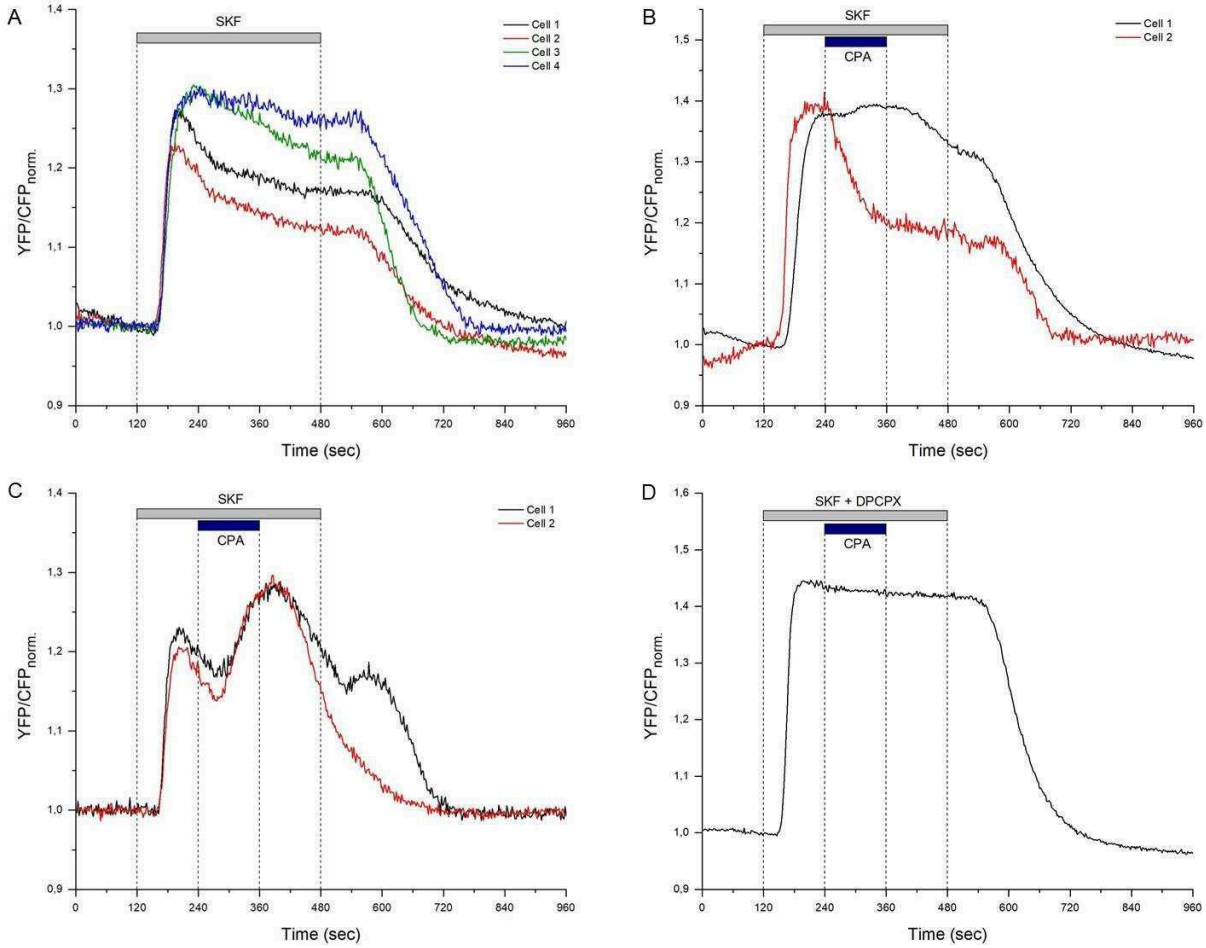


Figure 3.47: Stimulation of D1Rs and A1Rs simultaneously induced a further increase in PKA activity in some retinal neurons. (A): Prolonged stimulation (6 min) of AKAR4-expressing retinal neurons with the specific D1R agonist SKF 38393 led to a permanent increase in YFP/CFP ratio. Cells 1 and 2 showed shoulder-like, and cells 3 and 4 plateau-like responses. **(B):** The stimulation of A1Rs did not affect the SKF 38393-induced increase in YFP/CFP ratio. **(C):** Two cells responded to simultaneous stimulation of D1Rs and A1Rs with a further increase in YFP/CFP ratio, after the fluorescence signal started to recover from the response to SKF 38393 alone. **(D):** Blockade of A1Rs by the specific A1Rs antagonist DPCPX during stimulation of D1Rs completely abolished the CPA-induced increase in YFP/CFP ratio. CPA: *N*-Cyclopentyladenosine (10 µM); DPCPX: 1,3-dipropyl-8-cyclopentylxantine (10 µM); SKF: SKF38393 (100 nM).

In order to confirm the results achieved with CPA, yet another A1Rs-agonist was tested. Thus, 40 AKAR4-expressing retinal neurons were stimulated with 15-30 µM *N*-[(1*S*,2*S*)-2-Hydroxycyclopentyl]adenosine (GR 79236) using the same protocol as in Fig. 3.47, B and C. Similar results, though less marked, were found with GR 79236 in 23% of

the cells. Stimulation of A1Rs in the presence of SKF led to a slight increase in YFP/CFP ratio previously induced via activation of D1Rs alone (data not shown).

In summary, the experiments with the AKAR4 sensor show that all neurons in the retinal culture respond to DA with an increase in YFP/CFP ratio, thus in PKA activity. This effect was mimicked by SKF 38393 and is, therefore, most likely due to activation of D1Rs. In contrast, AD elicited responses only in a subset of neurons. Moreover, there is good evidence for the co-expression of both DRs and ARs and their interaction in this subset of neurons. Activation of ARs with AD in the presence of DA led in some cells to a decrease (44%), in other cells rather to a further increase in PKA activity previously raised by DA application (56%). The concomitant stimulation of A1Rs and DRs showed similar results as achieved with AD. Activation of A1Rs during application of DA decreased the DA-induced increase in PKA activity in 25% of the cells and enhanced it in 75% of the cells. Here, the total of the cells that responded to AD or CPA was considered as 100% (n=18 and n=8, respectively). Surprisingly, targeted stimulation of D1Rs with SKF 38393 and later on of A1Rs with CPA simultaneously, induced an increase in the PKA activity, but never a decrease, in 44% of the cells. This cannot be explained by the classical understanding of the D1Rs and A1Rs downstream mechanism, as D1Rs are positively coupled to ACy and A1Rs are negatively coupled to ACy. This interaction suggests a more complex association of these receptors, such as heteromer complexes.

4. Discussion

The retina must signal under a wide variety of light conditions to extract visual information from the environment. To this end, the retina adjusts its signaling mechanisms to the ambient light level. When adapting to increasing illumination, it is most important to reduce the amplitude of light responses in order to avoid saturation. Both rods and cones respond to light with a hyperpolarization, while they are depolarized in darkness. Along both ON- and OFF-pathway, signal transmission is mediated by glutamate. However, little is known about how glutamate receptors mediate the responses of retinal ganglion cells (GCs) in the mouse retina and whether these responses are modulated during adaptation. In the present study, I made use of the transgenic mouse line TN-L15 (Heim *et al.* 2007), in which this FRET-based calcium sensor is expressed in GCs. I measured changes in the internal calcium concentration ($[Ca^{2+}]_i$) in GCs in response to stimulation of the ionotropic glutamate receptors (iGluRs) by using the appropriate agonists. Furthermore, I applied specific agonists for the receptors for dopamine (DA), nitric oxide (NO), melatonin (MT) and adenosine (AD), in order to test whether they affect iGluR-induced calcium responses. I could show that the neurotransmitters affect the iGluR-induced calcium responses in distinct ways, depending on the type of iGluR and/or the neurotransmitter receptors stimulated (3.1). In addition to Ca^{2+}, cAMP is an important second messenger involved in a network of biochemical events and many of the above-mentioned transmitters were reported to couple to the cAMP/PKA pathway. In order to investigate modulation of the cAMP/PKA pathway, I made use of the retinal culture from young mice. Immunocytochemical results revealed that dissociated retinal neurons are well suited for the investigation of the purinergic and dopaminergic signaling closely linked to the cAMP/PKA pathway (3.2). Using the transfection technique, I made use of the FRET-based biosensor AKAR4 to investigate DA and AD responses as well as potential interactions between D1Rs and A1Rs in the same neuron (3.3).

4.1. The iGluR induced changes in $[Ca^{2+}]_i$ in GCs of the intact retina

4.1.1. Using the TN-L15 sensor as indicator for changes in $[Ca^{2+}]_i$ in GCs

The genetically encoded FRET-based calcium biosensor TN-L15 was used to study changes in $[Ca^{2+}]_i$ in retinal GCs. An increase in YFP/CFP ratio indicates a relative increase in $[Ca^{2+}]_i$. Three things are important to note: a) all responses were measured in the soma; b) the changes do not reveal the total $[Ca^{2+}]_i$ in the GCs, but rather the free Ca^{2+} able to bind to the sensor; c) I did not determine the absolute calcium concentration, but only changes relative to the base line. The TN-L15 sensor has a dissociation constant K_d of 1.2 µM (Heim & Griesbeck 2004), it is therefore reasonable to assume that the observed changes in $[Ca^{2+}]_i$ are in this range. The TN-L15 sensor is expressed in about 80% of the GCs of the TN-L15 transgenic mouse line (Müller *et al.* 2007) encompassing both ON- and OFF-GCs (Fig. 3.1).

4.1.2. Morphological and functional diversity of GCs

Anatomical classification of the GCs according to the morphology of their dendritic processes suggested 15-20 types (Kong *et al.* 2005, Coombs *et al.* 2006, Volgyi *et al.* 2009, Sumbul *et al.* 2014). In classical work on the domestic cat retina, three main ganglion cell types were morphologically described based on the diameter of their dendritic field: α (180-1000 µm), β (25 to 300 µm) and γ (180-800 µm) (Boycott & Wässle 1974). Peichl described another class of GCs called delta (δ) by intracellular staining with Lucifer Yellow and by reduced silver staining (Peichl 1989). The δ-GCs are characterized by dendritic ramification at the margins of the IPL. In mouse retina, Sun and colleagues classified GCs into cells with large soma and large dendritic field (RG_A), with small to medium-sized soma and small to medium-sized dendritic field (RG_B), cells with small to medium-sized soma and medium-sized to large dendritic field (RG_C). RG_{A-C} are monostratified cells, RG_D cells bistratified cells (Sun *et al.* 2002). The TN-L15-expressing GCs in the mouse retina could be grouped into three types based on their soma sizes: small, medium and large. In my results, I could not establish a correlation between soma size and the different pharmacological profile, in particular the calcium response observed upon stimulation of the iGluRs. Transient and sustained calcium responses were found in GCs of all soma sizes. According to their functionality, GCs are subdivided in: ON-GCs, which receive visual input from ON-cone BCs, OFF-GCs that

receive visual input from OFF-cone BCs, and ON-OFF-GCs, which receive visual input from both ON- and OFF-cone BCs. Using the two-photon Ca^{2+} imaging to record light-evoked activity in all cells within a patch of the GCL, Baden and colleagues described a minimum of 32 different types of GCs in the mouse retina (Baden *et al.* 2016).

4.1.3. Activation of iGluRs mediate distinct calcium responses in GCs

GCs express AMPA (Grunert *et al.* 2002, Pickard *et al.* 2002), kainate (Peng *et al.* 1995, Zhang *et al.* 1996, Pickard *et al.* 2002) and NMDA (Hartveit *et al.* 1994, Vandenbranden *et al.* 2000) receptors but, to my knowledge, not mGluRs (Liets & Chalupa 1996). In this study, I could show that activation of AMPA, kainate or NMDA receptors mediates changes in $[Ca^{2+}]_i$ in GCs, detected as changes in the YFP/CFP ratio. Every TN-L15 labeled GC responded to each of the three agonists. There was a certain variation in the ratio of the amplitude of the second response to the first response RA2/RA1 (AMPA: Fig. 3.3, C; kainate: Fig. 3.10, B; NMDA: Fig. 3.16, B). Values of 80-120% for this ratio were often observed in the absence of any neuromodulator and were considered as a normal variation. Significant deviations from this range were interpreted as effect of the applied neuromodulator. In general, the GCs responded in a reversible and reproducible way to repetitive application of a given iGluR agonist, often with a slight rundown. This indicates that under my experimental conditions, stimulation of iGluRs did not induce major changes in the surface expression or sensitivity of iGluRs that would affect subsequent responses. In chapter 3.1.1.1.1 I could distinguish two distinct temporal calcium responses in response to AMPA: a transient and a sustained increase in $[Ca^{2+}]_i$. The majority of the cells (92%) was of the transient type, while the sustained type represented only 8% of the cells. Activation of kainate receptors resulted likewise in an increase in $[Ca^{2+}]_i$, here again two types of temporal calcium responses could be distinguished (3.1.1.2.1.). The transient response was encountered in 74% of the cells, while the sustained response was found in the remaining 26%. A particularity of the kainate-induced calcium responses was the appearance of a second peak during the transient (10%) and sustained (22%) responses (Fig. 3.8, B and D, respectively). Finally, also activation of NMDA receptors resulted in an increase in $[Ca^{2+}]_i$ in the GCs. While the majority of the cells displayed a transient response (79%), sustained responses were found in 21% of the GCs (3.1.1.3.1). AMPA receptors have been found to mediate fast/transient transmission and to desensitize

quickly, up to tenfold faster than kainate receptors (Dingledine *et al.* 1999, DeVries 2000). Kainate receptors mediate slow/sustained transmission (DeVries 2000, Lindstrom *et al.* 2014).

4.1.4. AMPA receptor properties established in other studies

The iGluR-induced responses are related to the specific channel properties, which in turn are dependent on the subunit composition rather than the number of the receptors expressed as shown in several studies (Bochet *et al.* 1994, Grunder *et al.* 2000). AMPA receptors are heteromeric tetramers made up of at least two different subunits. The GluA2 subunit is critical in determining the channel signaling properties. AMPA receptors lacking GluA2 subunits are permeable to Ca^{2+} and exhibit a high single channel conductance (Washburn *et al.* 1997, Jones *et al.* 2012). Several studies showed that excitatory synapses on all functional GCs classes use both GluA2-lacking, thus Ca^{2+} permeable AMPA receptors (CP-AMPA receptors), and GluA2-containing, thus Ca^{2+} impermeable AMPA receptors (CI-AMPA receptors) (Diamond & Copenhagen 1993, Lukasiewicz *et al.* 1997, Xia *et al.* 2007). Synaptic receptor heterogeneity is a key factor underlying changes in neural activity, which in turn changes in function of the dynamically changing light environment. Xia and colleagues showed that AMPA receptors on ON-GCs undergo activity-dependent regulation. Eight hours of light deprivation generated a switch in surface AMPA receptor composition from primarily CI- to CP-AMPA receptors (Xia *et al.* 2006, Xia *et al.* 2007). Furthermore, it has been shown that the switch from predominantly CI- to CP-AMPA receptors develops within minutes after a brief light stimulus (Jones *et al.* 2012). The switch has been found to be NMDA receptor-dependent and specific to excitatory synapses in the ON-pathway. The NMDA-induced rise in $[Ca^{2+}]_i$ leads to a dynamin-dependent endocytosis of CI-AMPA receptors (Jones *et al.* 2012). This shows that the subunit composition of the receptors determines the channel properties and underscores the importance of AMPA receptors in mediating light-induced synaptic transmission. These studies suggest that the dynamic plasticity of AMPA receptors may serve as a platform for adaptation on GCs.

4.1.5. Kainate receptor channel properties established in other studies

Kainate receptors are permeable to sodium and potassium and display a low conductivity for Ca^{2+}. They are known for strong desensitization to glutamate, and may help to maintain the sensitivity to changing ambient light conditions. Kainate receptor properties and the temporal kinetic of the receptors differ depending on subunit composition and the presence of the auxiliary subunits Neto1 and Neto2 (Lindstrom *et al.* 2014). It has been proposed that differential expression of AMPA and kainate receptors is responsible for fast/transient and slow/sustained pathways in distinct OFF-cone BCs, respectively. Borghuis and colleagues measured glutamate release from BCs by using two-photon imaging of a glutamate sensor expressed on postsynaptic ACs and GCs (Borghuis *et al.* 2014). Cone driven glutamate release from BCs in both transient and sustained OFF-layers was blocked by antagonists to kainate receptors but not AMPA receptors. This underscores the essential role of kainate receptors for signaling in both transient and sustained OFF-pathways, which was confirmed by electrophysiological recordings from BCs and GCs (Borghuis *et al.* 2014). Kainate receptors on OFF-BCs support responses to high frequency light-evoked synaptic stimulation in the physiological range up to 20 Hz (Borghuis *et al.* 2014). Thus, kainate receptor signaling in OFF-BCs is not limited to slow synaptic integration. The mechanism underlying the distinct temporal kinetics in parallel pathways - fast/transient versus slow/sustained - remain incompletely understood. Both transient and sustained OFF-BC pathways, converge onto OFF-α- and OFF-δ-GCs. Many excitatory amino acids, including AMPA and kainate, were found to be not entirely selective for only one receptor class. In that regard it must be pointed out that AMPA can activate some types of kainate receptors (Herb *et al.* 1992); similarly kainate can activate AMPA receptors in a nondesensitizing manner to produce large sustained currents (Kiskin *et al.* 1986, Patneau & Mayer 1991). Kainate receptors are unusual for iGluRs, since they can also signal through GPCRs and second messengers in the CNS (Frerking *et al.* 2001, Rodrigues & Lerma 2012, Bhangoo & Swanson 2013). How the receptors couple to the metabotropic pathways remains unclear, still the dual signaling capacity of these receptors emphasizes the essential role of kainate receptors in mediating synaptic transmission and modulating network activity.

4.1.6. NMDA receptor channel properties established in other studies

NMDA receptors are tetramers that always consist of at least one NR1 subunit and the other subunits NR2A-NR2D, NR3A and/or NR3B. The subunit composition determines the pharmacological and biophysical properties of the receptor channel. Two features are particularly important: the high calcium permeability and the blockade of NMDA receptors at negative membrane potentials by Mg^{2+}. This block is relieved only when the membrane potential is sufficiently depolarized, e.g. by excitatory input mediated by non-NMDA receptors or by repetitive stimulation. NMDA receptors are activated upon high frequency synaptic transmission and play an important role in the induction of synaptic plasticity (Dingledine *et al.* 1999, Jones *et al.* 2012). Previous studies have shown that the NMDA receptor-induced long-term synaptic plasticity occurs through postsynaptic changes in the number of AMPA receptors or changes in their phosphorylation state; these changes serve to strengthen or weaken the synapse by altering the amplitude of the synaptic current (Barry & Ziff 2002, Malinow & Malenka 2002, Song & Huganir 2002). More evidence is now accumulating that NMDA and non-NMDA receptors interact with each other on GCs. NMDA receptors contribute to the excitatory response of GCs, and this task is increased when the cell is depolarized by input mediated by non-NMDA receptors (Diamond & Copenhagen 1993). An important aspect of glutamatergic signaling is excitotoxicity. Glutamate-induced death of GCs plays an important role in glaucoma and under ischemia-related conditions, e.g. vessel occlusion and diabetic retinopathy (Casson 2006, Hernandez & Simo 2012). Due to their high permeability to Ca^{2+}, it is assumed that glutamate excitotoxicity is predominantly mediated by the overstimulation of NMDA receptors (Ferreira *et al.* 1996). Bai and colleagues reported that NR2B and NR2D deficiency may protect against NMDA-induced excitotoxic retinal cell death (Bai *et al.* 2013).

4.1.7. Origin of calcium signal in retinal GCs

Upon application of iGluR agonists, I observed calcium responses in all GCs. There are several ways how stimulation of iGluRs can lead to an increase in $[Ca^{2+}]_i$. Calcium could enter through iGluRs directly (reviewed in (Pankratov & Lalo 2014)). Once stimulated, iGluRs depolarize the GCs, consequently, the VGCCs expressed on the GCs open and further Ca^{2+} can enter through these channels. Indeed, the AMPA-induced calcium response was smaller in the presence of VGCC blockers (Fig. 3.28, A). As the

experiments were performed in the intact retina, the applied iGluR agonists also worked on presynaptic cells. AMPA and kainate could depolarize OFF-cone BCs that would in turn release glutamate onto OFF-GCs. Activation of ACs would mostly lead to release of GABA and glycine and would, therefore, inhibit GCs. Presynaptically, kainate receptors modulate neurotransmitter release at glutamatergic synapses (Frerking *et al.* 2001). For example, activation of functional kainate receptors activates VGCCs in a G-protein and PKC-dependent manner in dorsal root ganglion cells (Rozas *et al.* 2003). In summary, the iGluR-induced calcium responses may reflect both activation of receptors on GCs and network responses Transient and sustained calcium responses could depend on differences in the subunit composition of iGluRs, different Ca^{2+} permeability, differences in the number of receptors expressed or different calcium clearance mechanisms.

4.2. DA modulates the iGluR-induced calcium responses in a distinct manner

Dopamine (DA) is known to play an important role in light adaptation processes in the retina; however, not all mechanisms are fully understood. The vertical signal pathway from PRs via BCs to GCs is mediated by glutamate and could be a target for dopaminergic modulation. Thus, I used DA, the D1R agonist SKF 38393 and the D2R agonist quinpirole to test whether and how they may influence iGluR-induced calcium responses.

4.2.1. DA affected the iGluR-induced calcium responses

The calcium response amplitudes (RAs) to the distinct iGluR agonists were determined. The second RAs were normalized to the first RAs and the ratio was set as control (ctrl). I could observe a certain variability in RA2/RA1 that was analyzed statistically. The RA2/RA1 ratio in the presence of DA was compared to the ctrl and was found to differ in a statistically relevant way. DA reduced the calcium responses to AMPA, kainate, and NMDA (Figs. 3.7, 3.12 and 3.19, respectively).

In my experiments, DA was only applied in between iGluR agonist stimulation. DA induced an increase in $[Ca^{2+}]_i$ in 20% of the GCs, that had previously been stimulated with AMPA, in 12% of the cells that had previously responded to kainate and in 21% of the cells that had previously been stimulated with NMDA. In a study using the same

mouse model, Sieben described a DA-induced increase in $[Ca^{2+}]_i$ in 33% of the GCs and a decrease in $[Ca^{2+}]_i$ in ca. 7 % of the GCs (Sieben 2016). Based upon experiments with L-AP4, a selective group III mGluR agonist, which blocks the ON-pathway in the retina (Shiells *et al.* 1981, Slaughter & Miller 1981, Schiller 1982, Nakajima *et al.* 1993), Sieben suggested that some cells of the increase type were OFF-GCs (Sieben 2016). Moreover, blockade of the glutamatergic input abolished the DA-induced calcium response in some GCs, indicating that DA had not affected the GC directly, but via regulation of the glutamate release from BCs. The cells of the increase type described by Sieben had the smallest soma radius among all the TN-L15-expressing GCs. In my study, I could not find this correlation. None of the cells I tested in my study responded to DA with a decrease in $[Ca^{2+}]_i$.

4.2.2. D1Rs and D2Rs are expressed in the inner retina

Since I tended to investigate the role of D1Rs in modulating iGluR-induced calcium responses, I performed immunohistochemical stainings to verify the expression of D1Rs in the mouse retina. D1Rs are expressed in both synaptic layers: IPL and OPL. In a triple staining with PKCα, a marker for rod BCs, and vGluT1, a well-suited marker for BC terminals, I could find BC terminals co-labeled with vGluT1 and D1Rs localized in sublamina 3 and 4. This finding indicates that D1Rs are most likely expressed in type 5, 7, and 8 cone BCs (Fig. 3.34). Moreover, D1Rs were found in rod BCs, the vGluT1-positive terminal systems were D1R-positive (Fig. 3.34). D1R-positive structures in sublamina 3/4 that were negative for vGluT1 and PKCα most likely represent dendrites of ACs or GCs (Fig. 3.34). Usai found that D1Rs are expressed in the soma and the axon terminal systems of cone BCs type 5 and 7 (Usai 2014). By using the exclusion principle, Usai concluded that D1Rs are most likely also expressed on GC dendrites (Usai 2014). Making use of the TN-L15 transgenic mouse line, I counterstained TN-L15-positive GC dendrites with antibodies against D1Rs and D2Rs. D1R and D2R dot-like immunoreactivity covered the whole IPL; however, no clear-cut double labeling with TN-L15 was observed (Fig. 3.35). In close proximity to GC membranes, I found D2R-positive structures, which may suggest that at least some GCs could express D2Rs along their membrane (Fig. 3.35). However, it is also plausible that these processes originate from ACs. Using a marker against HCs (CaBP), in the OPL no co-localization was found between the strongly immunoreactive dendritic processes of the HCs and D1Rs.

4.2.3. Activation of D1Rs decreased the non-NMDA-induced, but not the NMDA-induced calcium responses in GCs

The D1R agonist SKF 38393 reduced non-NMDA-induced calcium responses even stronger than DA (Figs. 3.5 and 3.11, A). As the light response is relayed to GCs via iGluRs, DA released during light adaptation and acting at D1Rs would reduce GC light responses. These results agree well with findings described by Usai (Usai 2014). Using the patch clamp technique, in absolute darkness Usai measured light responses of individual GCs from dark-adapted mouse retina. The RAs were normalized and plotted versus the light intensity. As expected, the RAs increased as a function of light intensity. Interestingly, activation of D1Rs led to a decrease of the RAs and to a shift of the stimulus-response curve to higher light intensities. This mimics the effect of light adaptation since the same stimulus induces a smaller response in a light-adapted retina than in dark-adapted retina. The finding, that activation of D1Rs modulates iGluR-mediated calcium responses suggests that dopaminergic modulation of iGluRs might contribute to light adaptation in the mammalian retina.

Stimulation of D1Rs usually leads to activation of the cAMP/PKA pathway. In agreement with this, the effect of the D1R agonist on kainate-induced calcium responses was strongly reduced in the presence of the PKA blocker H89 (Fig. 3.13). In a few cells, the effect of the D1R agonist was not fully blocked, probably, because PKA activity was particularly high in these cells. A possible explanation is that these cells express a high level of D1Rs, so not all the PKA activated could be inhibited. However, PKA-independent signaling pathways cannot be ruled out completely. Interestingly, activation of D1Rs did not affect the NMDA-induced calcium responses; there was no difference between RAs of cells treated with D1R agonist and ctrl cells (Fig. 3.17). This was surprising, since application of DA elicited a slight shift to reduced NMDA-induced calcium responses. Interactions between NMDA and D1Rs have already been shown in medium spiny neurons of the *nucleus accumbens* (NAc); activation of D1Rs increases the phosphorylation of a subunit of NMDA receptors, the NR1 subunit (Snyder *et al.* 1998). Since NR1 is common to all NMDA receptors, it is unlikely that activation of D1Rs did not affect NMDA receptors in GCs. It is plausible to hypothesize that the phosphorylation/dephosphorylation of NMDA receptors may depend on the subunit composition of the channel.

4.2.4. D2Rs affected the iGluR-induced calcium responses in GCs

The D1R agonist SKF 38393 reduced AMPA- and kainate-induced calcium responses much stronger than DA. One possible explanation is that DA not only activates D1Rs but also D2Rs that counteract the action of D1Rs. Indeed, selective activation of D2Rs strikingly enhanced AMPA-induced and kainate-induced calcium responses (Figs. 3.6, A and 3.11, B), i.e. induced opposite effects than D1Rs.

Selective activation of D2Rs decreased NMDA-induced calcium responses in a subpopulation of GCs (33%). This D2R-effect was never observed with the D1R agonist or under ctrl conditions, nor during activation of non-NMDA receptors. In a small subpopulation of GCs (6%), activation of D2Rs enhanced the NMDA-induced calcium responses. This variability in the effect of D2Rs was only observed for NMDA-induced calcium responses and raises questions. Future studies have to decipher, whether different GC types underlie the different response types.

In my experiments, activation of D2Rs typically induced opposite effects than activation of D1Rs. Stimulation of D2Rs reduces activity in the cAMP/PKA pathway. As shown by Sieben (Sieben 2016); in many cells, activation of D2Rs only leads to a drop in $[cAMP]_i$ if $[cAMP]_i$ had been raised before by other receptor types, like D1Rs (Sieben 2016). In the imaging experiments, the retina was exposed to blue excitation light. DA is released upon illumination of the retina (Witkovsky 2004). Hence, it is very likely that under my experimental conditions, DA was constantly released and D1Rs were tonically activated with the consequence of increased PKA activity. D2Rs would counteract the D1R-mediated effect, which would explain the opposite effect of D1R and D2R agonists.

4.2.5. Molecular mechanisms underlying dopaminergic action

How could dopaminergic ligands modulate iGluR-induced calcium responses in GCs? As dicussed in chapter 4.1.7, the increase in $[Ca^{2+}]_i$ could arise from calcium entering through iGluRs directly (reviewed in (Pankratov & Lalo 2014)) or through VGCCs. As dopamine receptors couple to the cAMP/PKA pathway, most likely the effects of dopaminergic ligands rely on phosphorylation or dephosphorylation of iGluRs or VGCCs. Phosphorylation could either regulate open probability of the channels or internalization, both of which would affect calcium currents. Beyond these mechanisms,

Gβγ subunits of the D2Rs directly reduce the level of activity of the L-type VGCCs (Hernandez-Lopez *et al.* 2000). Moreover, there is increasing evidence that in addition to coupling to the cAMP/PKA signaling pathway, DRs may also regulate phospholipase C (PLC) by coupling to $G\alpha_q$. Activation of PLC results in the production of inositol trisphosphate (IP_3) and diacylglycerol (DAG). This leads to activation of PKC by DAG and increase in $[Ca^{2+}]_i$ released from internal stores (Lee *et al.* 2004, Sahu *et al.* 2009). Previous studies reported that D2-class receptors modulate $[Ca^{2+}]_i$ by acting on ion channels or by triggering the release of intracellular calcium stores (Nishi *et al.* 1997, Missale *et al.* 1998). Gβγ subunits of the D2Rs have been found to activate PLC and to increase $[Ca^{2+}]_i$ in medium spiny neurons. Whether such mechanisms exist in retinal GCs is unclear, but it should be pointed out that quinpirole on its own did not elicit changes in $[Ca^{2+}]_i$ in GCs.

D2Rs may also bind to the autoreceptors expressed on dopaminergic ACs (Dubocovich & Weiner 1985). This would inhibit DA release. As discussed above, it is likey that in my experiments the excitation light triggered a continuous DA release resulting in moderate activation of D1Rs and slight decrease of iGluR-induced calcium signals. Activation of D2Rs would reduce DA release and, consequently, the cells would recover from the D1R effect. In the subpopulation of GCs, in which D2Rs reduced the NMDA-induced calcium responses, many signal pathways may be involved. As previously mentioned, the Gβγ subunits of the D2Rs may activate the PLC, leading finally to activation of PKC. It is plausible to hypothesize that some subunits of the NMDA receptors possess a phosphorylation site for PKC that was activated by DAG, resulting in less Ca^{2+} influx. Bu and colleagues revealed that PKC plays an important role in the phosphorylation of NMDA receptors in the accurate nucleus of the hypothalamus (Bu *et al.* 2015). The Gβγ subunits of the D2Rs are also involved in the regulation of N-type VGCCs in striatal interneurons (Yan *et al.* 1997). Gβγ subunits play an important role in the regulation/association of D2Rs and G-protein coupled inwardly-rectifying potassium GIRKs (Kuzhikandathil *et al.* 1998, Lavine *et al.* 2002). The D2R-induced activation of GIRKs affects the excitability of neurons and may potentially mediate several functions of DA. Whether this also happens in retinal GCs has to be further investigated.

DA is a neuromodulator that is released within a thin stratum in the IPL but can reach and affect neuronal processes far away, e.g. in the OPL (Veruki & Wässle 1996). Hence, DA concentration may be quite different at different sites in the retina. Therefore,

exogenously applied dopaminergic ligands can only partially mimic the effect of endogenously released DA. The effects induced via the specific agonists were much stronger than the effects induced via application of DA. This may be attributed to the differences in the agonist concentrations used or to the simultaneous activation of antagonistic processes mediated by D1Rs and D2Rs discussed above. Furthermore, it cannot be ruled out that besides D1Rs and D2Rs studied here, DA activated additional receptors. In another experiment (Fig. 3.6), simultaneous application of both agonists yielded similar effects, though less pronounced, as stimulation with D2R agonists. This indicates that D1Rs did not override the impact of D2Rs; rather the effects induced via D1Rs were almost completely abolished in the presence of the D2R agonist.

Taken together, these findings indicate that dopamine affects glutamatergic signaling via D1Rs and/or D2Rs. Since the two receptor families counteract each other, the expression of distinct DRs on GCs, ACs and/or BCs may be determinant for the regulation of glutamatergic signaling. But there are additional ways how DA may mediate or modulate light adaptation in the retina. DA was found to cause uncoupling of PRs via D4Rs, which are negatively coupled to ACy (Li *et al.* 2013). D1Rs modulate gap junctions between AII ACs (Hampson *et al.* 1992). In the rabbit retina, DA regulates gap junctions between AII ACs, but also between AII ACs and ON-BCs via D1Rs (Xia & Mills 2004). This reduction in the coupling between ON-BCs and AII ACs would diminish the input of rod signals into the ON-pathway and promote the transition from rod to cone vision. It has been suggested that this regulation occurs via the cAMP/PKA pathway (Kothmann *et al.* 2009). Kothmann and colleagues suggested that through activation of D1Rs PKA activity increases, which in turn phosphorylates the protein phosphatase PPA2. As a consequence, gap junctions between AII ACs become dephosphorylated, leading to a decrease in the conductance (Kothmann *et al.* 2009). During increased ambient light, the conductance through gap junctions must be minimized in order to avoid saturation of the inner retina by large rod signals.

4.3. Various neurotransmitters affect iGluR-induced calcium responses in GCs

4.3.1. Nitric oxide promotes iGluR-induced calcium responses

Nitric oxide (NO) is involved in retinal signal processing. An established source of NO in the retina is a group of nNOS-expressing ACs, which signal onto other ACs, BCs and GCs in the IPL (Kim *et al.* 1999, Pang *et al.* 2010). The enzyme soluble guanylate cyclase (sGC) is the NO receptor, its activation results in an increase in the $[cGMP]_i$ (Garthwaite 2005). Possible targets for cGMP are CNG channels depolarizing the cells by ion influx or PKG, the cGMP-dependent protein kinase (Kaupp & Seifert 2002, Hofmann *et al.* 2006). Apart from the IS and OS of the PRs (Matthews & Watanabe 1988), CNG channels were suggested to exist in BCs, HCs and in GCs (DeVries & Schwartz 1989, Shiells & Falk 1992, Miyachi *et al.* 1991, Nawy & Jahr 1990, Ahmad *et al.* 1994), but these results are discussed controversially. The role of NO in these cells and its effects on retinal signal processing are only partially understood. Several studies attempted to characterize the NO-cGMP-PKG signaling pathway for a better understanding of the role of NO in the retina. Using in situ hybridization, cGK I isoform was found in PRs along the IS and abundantly in the IPL with significant amounts in GCs of the mouse retina (Gamm *et al.* 2000). The cGK II mRNA expression pattern was similar, though not identical to that of cGK I. The presence of distinct cGK isoforms throughout the retina suggests multiple roles for the NO-cGMP-PKG signaling pathway in physiological and pathological visual processes, as NO has been implicated in the regulation of retinal neurotransmission (Ferrendelli & De Vries 1983, McMahon & Ponomareva 1996, Wexler *et al.* 1998), glaucoma (Nathanson & McKee 1995, Behar-Cohen *et al.* 1996) or diabetic retinopathy (Schmetterer *et al.* 1997). G substrate, a specific downstream component of the NO-cGMP-PKG signaling pathway originally described in the cerebellum, was localized to a subpopulation of ACs and C38-positive GCs but not to α-GCs (Nakazawa *et al.* 2005).

In my results, application of the NO-donor SNAP resulted in the enhancement of the AMPA- and NMDA-induced calcium responses, while SNAP alone did not induce any changes in $[Ca^{2+}]_i$ (see chapter 3.1.2). This contradicts a hypothesis, how NO may act in GCs proposed by Ahmad (Ahmad *et al.* 1994). According to this idea, in GCs, NO would activate sGC leading to an increase in $[cGMP]_i$. Activation of CNG channels would alter GC membrane potential and intracellular ion concentrations (Ahmad *et al.* 1994). In my

experiments, I did not notice a change in $[Ca^{2+}]_i$ upon application of SNAP. An enhancement in the kainate-induced calcium responses was found in a small subpopulation of GCs (7%); however, there was no statistically significant difference to the ctrl cells (Fig. 3.21, C and D). Similarly as discussed above for the dopaminergic activation of the cAMP/PKA pathway (chapter 4.2.5), the activation of the NO-cGMP-PKG pathway could affect the activity of iGluRs and/or VGCCs, leading to Ca^{2+} and Na^{+} inward currents, depolarization and further increase in $[Ca^{2+}]_i$ as seen in my results.

At least a part of the NO-mediated effect could reside in GCs, as SNAP increased $[cGMP]_i$ in GCs of the mouse retina (Zhao 2015). However, it is also plausible that NO may act in the retinal network. NO-donors increase $[cGMP]_i$ in subpopulations of ON-cone BCs (Koistinaho *et al.* 1993, Gotzes *et al.* 1998, Zhao 2015). Furthermore, NO was found to decrease DA release in the retina (Bugnon *et al.* 1994), to decrease electrical coupling of HCs (DeVries & Schwartz 1989) and to decrease inter BC junctions (reviewed in (Goldstein *et al.* 1996)). This would affect the receptive field size of neurons and, hence, the light responses in the retina. In type 4 cone BCs, NO accelerated the glutamate responses in a cGMP-PKG-dependent way (Vielma *et al.* 2014). These responses consist of a fast, kainate receptor-dependent phasic current and a slow, AMPA receptor mediated current. More precisely, NO affected the temporal kinetic of the type 4 cone BCs by shortening the AMPA receptor mediated component, while the kainate receptor mediated component remained unchanged (Vielma *et al.* 2014). In a subpopulation of striatal neurons, the NMDA-induced increase in $[Ca^{2+}]_i$ was greatly prolonged by co-application of NO and reduced by NOS inhibitors (Horn *et al.* 2002). The source of NO-induced calcium responses persisted in the absence of extracellular Ca^{2+}, was independent of IP_3-activated Ca^{2+} stores or cGMP production and might rather reflect a release from the mitochondrial pool (Horn *et al.* 2002).

4.3.2. Melatonin affected kainate- and NMDA-induced calcium responses in GCs

In the retina, melatonin (MT) is produced by PRs at night and has been found to play an important role in a variety of physiological processes. Various actions of MT have been attributed to distinct intracellular pathways via activation of different subtypes of MT receptors. In the dark, PRs are depolarized leading to Ca^{2+} influx. A cascade of reactions follows leading to activation of PKA, which in turn phosphorylates the N-

acetyltransferase (AA-NAT). AA-NAT is the enzyme that catalyzes the conversion of serotonin to N-acetylserotonin, the precursor of MT (Huang *et al.* 2013). Light-induced hyperpolarization reduces MT synthesis through an opposite process (Huang *et al.* 2013). There is growing evidence that MT modulates glutamatergic synaptic transmission, as has been shown in carp cone-driven HCs, where light responses are smaller and slower upon application of MT during the late day mimicking the night responses (Huang *et al.* 2005). The mechanism underlying this regulation of cone-driven HCs is thought to be mediated by modulating DA release (Ribelayga & Mangel 2005). In rat retina, MT potentiates light-evoked glycinergic signals from glycinergic ACs to GCs (Huang *et al.* 2013). MT1 receptors are GPCRs, they couple negatively to ACy, leading to a decrease in $[cAMP]_i$ and PKA activity (Reppert *et al.* 1994, Reppert *et al.* 1995). They couple to both pertussis toxin (PTX)-sensitive and PTX-insensitive G proteins (Brydon *et al.* 1999, Roka *et al.* 1999). Baba and coworkers showed that MT affects the early PR component of the electroretinogram (ERG) of the dark-adapted mouse, i.e. the a-wave. He provided evidence for the formation of MT1/MT2 heteromers in PRs (Baba *et al.* 2013). Alternative pathways other than the cAMP/PKA pathway have been suggested, which were more assigned to MT2 receptors. Thus, activation of MT2 receptors can lead to inhibition of cGMP formation (Petit *et al.* 1999), or increase PKC activity in the CNS (Hunt *et al.* 2001). McArthur and colleagues suggested an interaction of the MT2 receptors with the PLC-IP_3/DAG signaling pathway (McArthur *et al.* 1997). MT inhibited the calcium-dependent DA release in the rabbit retina (Dubocovich 1988). This effect was antagonized by the competitive non-selective MT receptor antagonist, luzindole, a finding that was confirmed by an MT2 receptor antagonist in a later study (Dubocovich *et al.* 1997). In my results, the statistical analysis revealed that MT significantly affected kainate- and NMDA-induced calcium responses but AMPA responses were not affected (see chapter 3.1.3.). Kainate and NMDA responses were affected in so far, as the relative frequency of the RAs was changed, however no clear shifting to decreased or enhanced calcium responses was established. The changes were particularly observed in a subpopulation of GCs that responded to kainate or NMDA with RAs between 50-80%. The fraction of cells in this RA range became more prominent in the presence of MT, indicating that MT tends to diminish the calcium responses in some GCs. However, these results have to be interpreted with caution as the effects were not clear and the subpopulation of GCs affected by MT was small. It must be noted that the TN-L15 transgenic mouse line was created on a C57BL/6N background, a mouse strain found to

be incapable to produce MT (Tosini & Menaker 1998, Doyle *et al.* 2002). Thus, this strain is not well suited to clarify the role of MT in modulating the glutamatergic signaling pathway.

4.3.3. A1Rs affected the iGluR-induced calcium responses

Over the past decades, many studies have shown that adenosine (AD) plays an important role in many physiological and pathological functions in the CNS and in the retina. In the retina, AD production is tightly regulated by light and dark conditions and a circadian clock, making AD levels higher in darkness (Blazynski & Perez 1991, Paes-De-Carvalho 2002, Ribelayga & Mangel 2005). AD is involved in the regulation of visual processing at the first synapse, where it can inhibit CaChs and glutamate release from rods and cones of the salamander retina (Stella *et al.* 2002, Stella *et al.* 2003, Stella *et al.* 2007). Inhibition of glutamate release from rods was linked to adenosine A2A receptors (A2ARs) via the cAMP/PKA pathway (Stella *et al.* 2002). The A2A-selective antagonist, ZM-241385, enhanced transmitter release from dark-adapted retina, suggesting that endogenous AD is present at night (Stella *et al.* 2003). The finding that AD alters visual processing at the first synaptic layer in the retina was not entirely related to inhibition of Ca^{2+} influx. DA was found to cause uncoupling of PRs via D4Rs, which are negatively coupled to ACy (Li *et al.* 2013). Pharmacological activation of A2ARs in light-adapted retina increased PR coupling, the same results were established by inhibiting D4Rs (Li *et al.* 2013). According to the classical understanding of the A2A and D4 receptors, the mechanism underlying regulation of PR coupling may rest on the competition between G_s and G_i, respectively to regulate PKA activity and thus the degree of target phosphorylation. Gap junctions between rods and cones facilitate input of rod signals into the cone pathway during mesopic vision (DeVries & Baylor 1995) and enhance the signal/noise ratio (Lamb & Simon 1976). As AD accumulates in darkness, it may act as a dark signal by increasing cell-cell coupling via A2ARs (Li *et al.* 2013). In rat inner retina, AD was found to alter glutamate-induced and voltage-dependent Ca^{2+} influx into GCs via activation of A1Rs (Hartwick *et al.* 2004). Using purified GC cultures and intact adult rat retina, Hartwick and colleagues reported that AD significantly reduced the glutamate-induced increase in $[Ca^{2+}]_i$ and inhibited calcium channel currents by 43%. These effects were blocked by an A1R antagonist but were not affected by the A2R antagonist, suggesting that AD acts most likely via activation of A1Rs (Hartwick *et al.* 2004).

Similarly, AD significantly reduced $[Ca^{2+}]_i$ in GCs of the intact retina during exposure to NMDA (Hartwick *et al.* 2004). In my study, using the A1R agonist GR 79236 I found similar results in the TN-L15-expressing mouse retina (3.1.4.). Activation of A1Rs reduced the NMDA-induced calcium responses. Moreover, I could show that A1Rs act similarly on AMPA and kainate receptors; in the latter case, the effect was more prominent. A1Rs couple negatively to ACy, leading to decrease in $[cAMP]_i$ and PKA activity and are expressed in the NFL, in the IPL and in GCs (Braas *et al.* 1987, Blazynski & Perez 1991). A further role for A1Rs in modulating GCs was provided in a study, where A1R activation induced an outward K^+ current in rat GCs via GIRKs (Newman 2003). Consequently, GCs were hyperpolarized and their excitability was reduced. My results support the role of A1Rs in modulating the excitability of GCs; however the question whether A1Rs act on the iGluRs directly or on VGCCs remained unsolved. Therefore, the action of A1Rs on VGCCs was investigated using a pharmacological approach (3.1.5). Depolarization of GCs induced via iGluRs results in opening of VGCCs and further Ca^{2+} influx. Stimulation of iGluRs under blockade of VGCCs should diminish the calcium responses. The AMPA-induced calcium responses were dramatically reduced during blockade of L- and N-types CaChs, suggesting an important calcium influx through the VGCCs. Activation of A1Rs under these conditions resulted in a further shifting to reduced calcium responses. Indeed, 85% of the GCs displayed RAs that were smaller than 50% of the initial RAs (Fig. 3.31). As VGCCs were blocked, it is assumed that the effect of A1Rs was directly at AMPA receptors. Blocking L- and N-types VGCCs clearly increased kainate- and NMDA-induced calcium responses. This was surprising, since a major potential source of Ca^{2+} entrance was eliminated. It is questionable whether these elevated changes in $[Ca^{2+}]_i$ are fully due to kainate and NMDA receptors, since such high RAs were never observed under ctrl conditions. Indeed, RAs to kainate and NMDA under blockade of L- and N-types VGCCs were enhanced up to a factor of 5.5 and 4.5, respectively. A plausible explanation for this phenomenon might be a signaling pathway that is independent of the ionotropic activity. As already suggested (4.1.5.), kainate receptors are capable of dual signaling inducing both ionotropic and metabotropic responses (Rodrigues & Lerma 2012). Ca^{2+} mobilization from intracellular stores has been suggested to contribute to the kainate-induced calcium responses (Rodrigues & Lerma 2012). In mossy fiber synapses in the hippocampus (MF-CA3), activation of kainate receptors activated the cAMP/PKA signaling pathway, which was argued to be the consequence of the rise in Ca^{2+}, activating

the Ca^{2+}/calmodulin-sensitive AC isoforms (Kwon & Castillo 2008, Rodriguez-Moreno & Sihra 2013). Activation of the GluR5-containing kainate receptors in developing CA1 neurons have been implicated in inhibiting glutamate release through presynaptic activation of G_i/G_o-protein and PKC (Sallert *et al.* 2007). To my knowledge, in the retina dual signaling of kainate receptors, inducing both ionotropic and metabotropic responses, has not been confirmed. If this is also applicable to the mouse retina, this would mean that under blockade of L- and N-types CaChs, other signaling pathways are evoked to ensure elevated $[Ca^{2+}]_i$. Another possible explanation for the unexpected increase in $[Ca^{2+}]_i$ may be related to an action of the CaChs blocker upstream, meaning in the network. In salamander retina, L- and N-types CaChs regulate the release of glycine from ACs (Bieda & Copenhagen 2004); blocking these CaChs on ACs would result in a reduction of the glycinergic inhibitory input. As a consequence, OFF-cone BCs and OFF-GCs no longer receive inhibitory rod input, normally mediated by glycinergic ACs. Whether the unexpected rise in $[Ca^{2+}]_i$ is confined to OFF-GCs is unknown. Under blockade of L- and N-types CaChs kainate induced higher calcium responses than under control conditions. This effect was absent in the presence of the A1R agonist, as 100% of the cells responded with RAs that were smaller than 50% of the initial RAs (Fig. 3.32). Activation of A1Rs had similar effects, though less marked, on NMDA-induced calcium responses, it shifted the responses to the left, meaning to further reduced changes in $[Ca^{2+}]_i$. These results led to the assumption that A1Rs may modulate the iGluRs, at least partially, in a direct way. However, it cannot be ruled out that under functional VGCCs, these latter may also be modulated by A1Rs as was seen in rat GCs (Hartwick *et al.* 2004). How A1Rs may act remains elusive. It should be noted that both A1Rs and D2Rs inhibit the cAMP/PKA pathway. Yet, the A1R agonist CPA and the D2R agonist quinpirole induce opposing effects on AMPA and kainate induced calcium responses. In the same vein, the classical downstream signaling pathways of A1 and A2 receptors should trigger opposite effects, still, in the retina they were found to act on PRs and GCs in a similar way by damping their excitability. While the suppression of Ca^{2+} influx in salamander PRs was linked to an A2R mechanism (Stella *et al.* 2002, Stella *et al.* 2003), inhibition in GCs was most likely associated with A1Rs (Hartwick *et al.* 2004).

Taken together, the present study has proposed the interaction between the ionotropic glutamate receptors and the neuromodulators dopamine, nitric oxide, melatonin and adenosine. In addition, there is a strong crosstalk between the different

retinal neuromodulators. Modulation of glutamatergic signaling may play an important role in adaptational processes of the retina.

4.4. DA and AD modulate the cAMP/PKA pathway in cultured retinal neurons

In order to monitor changes in $[cAMP]_i$ and PKA activity induced via activation of DRs and/or ARs, the cDNA encoding the FRET-based biosensor AKAR4 was transiently transfected into cultured retinal neurons by means of the Lipofectamine technique. Immunocytochemical analysis at DIV 5-7 of retinal neurons dissociated from P1-P4 mice revealed that all main types of retinal neurons were present in the culture system (see chapter 3.2.3.). In addition to ACs (Fig. 3.38), by using reliable cell markers, I also found PRs, BCs (different types) and HCs (very rarely) but no GCs, as they degenerate after dissecting the optic nerve (data not shown). The majority of the cultured retinal neurons express D1Rs; furthermore, almost all the D1R-positive cells express the regulatory subunit RIIβ of PKA. Thus, the culture system was well suited to monitor changes in PKA activity. Based on double-staining and the exclusion principle, it is fair to assume that the D1R-positive cells are ACs. The culture system was limited by the time of cultivation, as the survival rate decreased as a function of time (starting at DIV 9). In addition, the transfection process by the transfection reagent Lipofectamine 2000, can also initiate cell death.

Changes in the YFP/CFP ratio of the AKAR4 sensor were used to detect changes in PKA activity. The changes in the conformational state of the AKAR4 sensor, and consequently in the FRET ratio, result from phosphorylation of the sensor by active PKA. In all AKAR4-expressing cultured neurons, DA triggered an increase in PKA activity in a reversible and reproducible way. During blockade of PKA by the specific inhibitor H89, application of DA did not elicit any change in FRET ratio (Fig. 3.42, B). This indicates that DA activated the cAMP/PKA signaling pathway. In a similar way, AD activated the cAMP/PKA pathway, albeit only 20% of all AKAR4-expressing cultured neurons responded to AD. These findings indicate that at least a subpopulation of retinal neurons, most likely ACs, co-express DRs and ARs. In a small percentage of cells stimulated with DA twice and in between with AD, I found that the amplitude of the final DA-triggered response was strongly reduced compared to the first application (Fig. 3.44, C). This was not observed in ctrl experiments, in which retinal neurons were stimulated

with DA twice or three times but not with AD. My results suggest that this effect is due to crosstalk between the two receptor systems rather than to a rundown effect. However, this has to be interpreted with caution since the number of neurons that responded to AD was quite low.

The interaction between DA receptors and AD receptors was tested in the following way. Cells were stimulated with DA or the D1R specific agonist SKF 38393 to yield a sustained increase in PKA activity for several minutes. During this response, AD or the A1R specific agonist CPA was applied. When AD was applied onto DA, 36% of the cells responded to AD. An AD-induced increase in PKA activity was observed in 56% of these cells, a decrease in the remaining 44% of the cells. According to the classical understanding of ARs, the increase could be due to activation of A2Rs that stimulate the ACy, while the decrease might be elicited by activation of A1Rs that inhibit ACy (Stiles 1992, Jacobson *et al.* 1993). However, the situation seems to be more complicated. When the A1R agonist (CPA) was applied onto DA, only a decrease of PKA activity was expected; yet this was observed in only 25% or the responding cells, while an increase was observed in 75% of the responding cells (total percentage of responsive cells: 44%). When CPA was applied onto SKF 38393, all cells that responded to CPA displayed an increase in PKA activity, rather than the expected decrease. These findings are not in line with the classical understanding of A1R and D1R downstream signaling, which should induce opposite effects. The AD receptor specificity was tested by applying CPA in the presence of the specific A1R antagonist (DPCPX). Under these conditions, CPA had no effect on the PKA activity (Fig. 3.47, D). These findings underscore the complexity of interactions between AD and DA receptors, and more precisely between A1Rs and D1Rs. First, it cannot be ruled out that dopamine and adenosine receptors form heteromeric complexes with pharmacological profiles that differ from homomeric receptors. The evidence that adenosine receptors can form heteromers has accumulated in the last decades (Fredholm *et al.* 2011). The existence of the A1-D1 receptor heteromer was reported in fibroblast cells (Gines *et al.* 2000) and rat NAc (Toda *et al.* 2003). However, heteromers - including D1-D2 heteromers - have been shown to exhibit pharmacological and cell signaling properties distinct from dimers of the constituent receptors (Lee *et al.* 2004, So *et al.* 2007, Perreault *et al.* 2014). While D1Rs increase $[cAMP]_i$ and PKA activity by coupling to G_s-protein and D2Rs couple to G_i-protein, when they co-assemble as heteromers, they induce calcium signaling through activation of $G_{q/11}$ and PLC in NAc

(Perreault *et al.* 2014). What is the functional significance of multimeric receptors? Numerous functional studies reported that these complexes may be responsible for the antagonistic interactions between DRs and ARs, by uncoupling the DRs from their respective G-proteins and dampen receptor signaling (Franco *et al.* 2000, Franco *et al.* 2007, Fuxe *et al.* 2008). Activation of A1Rs alone in cultured retinal neurons did not induce any changes in PKA activity, the increase in PKA occurred only during co-activation of D1Rs. Second, simultaneous activation of different GPCRs may lead to "paradoxical" effects. It has been reported that the βγ complex of G_i-coupled receptors enhances the activity of the ACy isoforms ACy2, ACy4 and ACy7. This regulation depends on coincidental activation by G_s-coupled receptors (Sunahara & Taussig 2002). All these three ACy isoforms are highly expressed in the brain. Making the hypothesis that ACy2, ACy4 and/or ACy7 are expressed in the cultured retinal neurons, this could explain the A1R-triggered increase in PKA activity as it highly depends on co-activation of the D1Rs. This assumption is supported by the fact that the increase in PKA triggered by a G_i-coupled protein was not unique to A1Rs. Sieben found cells in the retinal culture that responded with a D2R-triggered increase in PKA activity during co-activation of D1Rs (Sieben 2016).

A possible source of AD in the retina could be the MCs and some GCs, as they were found to release AD via nucleoside transporters in rat retina (Uckermann *et al.* 2006). Moreover, ATP is released as a co-transmitter from synaptic terminals via vesicle-mediated exocytosis or by calcium-independent mechanisms (Abbracchio *et al.* 2009). Ecto-nucleotidases induce degradation of the extracellular ATP to ADP and finally to AD, which than can act on ARs (Perez *et al.* 1986, Santos *et al.* 1999, Abbracchio *et al.* 2009). Indeed, the availability of AD is tightly related to the presence of adenosine deaminases (ADA) that can exist as intracellular and extracellular variant and that transforms AD to inosine. Moreover, AD may also be removed from the extracellular environment by nucleoside transporters (Borea *et al.* 2016).

In summary, this study presents evidence for the modulation of iGluR-mediated signaling by DA, AD, NO and MT in the retina. A rise in $[Ca^{2+}]_i$ reflects increased activity of the GCs. Activation of distinct neurotransmitter receptors by specific agonists affected the iGluRs differentially. Reducing the sensitivity of the retina during light adaptation helps to prevent saturation by bright light stimuli and ensures the transition from rod-mediated to cone-mediated vision. The reduction in excitability of GCs by DA observed in

this study agrees well with the change in the excitability and the shift of the stimulus response curve of GCs to higher light intensities via D1Rs observed by Usai (Usai 2014). Similar, albeit weaker, modulation was also observed upon stimulation of A1Rs and very weakly of MT receptors. On the other hand, application of D2R agonist and NO increased the iGluR-induced signals, reflecting the ability of the retina to modulate activity in either direction. My results suggest that DA, AD, NO and probably MT affect the excitability of the GCs and may modulate signal transmission in the retina. However, there are still puzzles to be solved. For example, both DA and NO have been suggested to be released during light stimulation, yet they influence iGluR-induced signals in opposite ways. In a similar vein, DA acts on both D1Rs and D2Rs, yet they induce opposite effects. So, which of these effects predominate during light adaptation? These questions demonstrate that stimulation with exogenously applied ligands can only reveal parts of the complexe processes in retinal adaptation. For example, during stimulation with bath-applied agonists, ligand concentration is the same throughout the retina. When released in the retinal network, the concentration of the widely diffusing modulators can differ substantially between different retinal sites. Depending on the expression pattern of the receptor isoforms, their sensitivity, and their distance from the release site, the same modulator may activate different receptor types in different retinal cells. Moreover, simultaneous activation of A1Rs and D1Rs revealed “paradoxal effects”, an indication that in the retina, adaptation may arise from the concert of an enormously complex interplay of different modulators and their receptors.

The results performed in cultured retinal neurons - most likely ACs - indicate that changes in $[cAMP]_i$ and consequently PKA activity occur in response to DA and to AD. The changes could last up to 10 min. I could show that many cultured retinal neurons express both A1Rs and D1Rs. Moreover, the interaction between these receptors was found to be more complex than induced by distinct activation, suggesting that alternative signaling pathways are induced under particular conditions. Since AD and DA are synthesized at dark and light conditions, respectively, one may postulate that these interactions become relevant during change from scotopic to mesopic conditions.

4.5. Outlook

In this project, I made use of the genetically encoded FRET-based sensors TN-L15 and AKAR4 to monitor changes in two very important second messengers: Ca^{2+} and cAMP. By using calcium imaging combined with a pharmacological approach, I could demonstrate that DA, AD, NO and probably MT affect the vertical glutamatergic synaptic pathway and may also affect the lateral synaptic pathway by acting on ACs. Three ideas how this work can be extended in further studies are presented here.

1. It is generally accepted that $[Ca^{2+}]_i$ is a good indicator for the activity of neurons. Calcium imaging is relatively easy to perform; however, as the retina is a light sensitive tissue, optical imaging does not only monitor retinal activity, but may interfere with retinal signaling. One way to overcome this problem would be to use two-photon imaging that rests on excitation light in the infrared regime. Another problem in imaging arises, if pharmacological agents are coloured and, therefore, absorb excitation or emission light. It will, therefore, be an interesting approach to extend the findings of this study in several ways. First, the effects of the neurotransmitters employed in this study on retinal activity should be studied using electrophysiological recordings, e.g. with multi electrode arrays (MEA). As these recordings do not require light, they can be performed at any light level needed, to adjust the retina to the scotopic, mesopic, or photopic state.

2. The studies on cultured retinal cells using AKAR4 provided first and valuable insights into the regulation of the cAMP/PKA pathway by a variety of neuromodulators as well as their interaction. However, many neurotransmitters were reported to trigger additional signaling pathways, involving e.g. calcium. The studies on the regulation of internal messengers should be extended to dual imaging. For example, AKAR4 could be combined with a calcium indicator such as fura red, whose fluorescence emission does not overlap with that of AKAR4. This should provide valuable insight into the interaction of the two major second messenger pathways in retinal signaling. Finally, efficiency of the Lipofectamine transfection was very low. Usually, only few cells per coverslip were transfected. Other transfection techniques should be developed that may enable a higher transfection efficiency. The ultimate goal would be to express genetically encoded sensors not only in retinal cultures but also in the intact retina. This would allow the detection of crosstalk between different transmitter systems in the retinal network.

3. In cultured retina, the simultaneous application of A1R and D1R agonists revealed “paradoxical effects”, indicating that in addition to the classical pathways assumed to underlie AD and DA signaling, other signaling pathways were activated. In the intact retina, so far neuromodulators were investigated individually. It might be an interesting study to apply several neuromodulators at the same time.

References

Abbracchio, M. P., Burnstock, G., Verkhratsky, A. and Zimmermann, H. (2009) Purinergic signalling in the nervous system: an overview. *Trends in neurosciences,* **32,** 19-29.

Acuna Castroviejo, D., Rosenstein, R. E., Romeo, H. E. and Cardinali, D. P. (1986) Changes in gamma-aminobutyric acid high affinity binding to cerebral cortex membranes after pinealectomy or melatonin administration to rats. *Neuroendocrinology,* **43,** 24-31.

Ahmad, I., Leinders-Zufall, T., Kocsis, J. D., Shepherd, G. M., Zufall, F. and Barnstable, C. J. (1994) Retinal ganglion cells express a cGMP-gated cation conductance activatable by nitric oxide donors. *Neuron,* **12,** 155-165.

Andersen, P. H., Gingrich, J. A., Bates, M. D., Dearry, A., Falardeau, P., Senogles, S. E. and Caron, M. G. (1990) Dopamine receptor subtypes: beyond the D1/D2 classification. *Trends in pharmacological sciences,* **11,** 231-236.

Angulo, M. C., Lambolez, B., Audinat, E., Hestrin, S. and Rossier, J. (1997) Subunit composition, kinetic, and permeation properties of AMPA receptors in single neocortical nonpyramidal cells. *The Journal of neuroscience : the official journal of the Society for Neuroscience,* **17,** 6685-6696.

Arnold, W. P., Mittal, C. K., Katsuki, S. and Murad, F. (1977) Nitric oxide activates guanylate cyclase and increases guanosine 3':5'-cyclic monophosphate levels in various tissue preparations. *Proceedings of the National Academy of Sciences of the United States of America,* **74,** 3203-3207.

Baba, K., Benleulmi-Chaachoua, A., Journe, A. S. et al. (2013) Heteromeric MT1/MT2 melatonin receptors modulate photoreceptor function. *Science signaling,* **6,** ra89.

Baba, K., Pozdeyev, N., Mazzoni, F. et al. (2009) Melatonin modulates visual function and cell viability in the mouse retina via the MT1 melatonin receptor. *Proceedings of the National Academy of Sciences of the United States of America,* **106,** 15043-15048.

Baden, T., Berens, P., Franke, K., Roman Roson, M., Bethge, M. and Euler, T. (2016) The functional diversity of retinal ganglion cells in the mouse. *Nature,* **529,** 345-350.

Bai, N., Aida, T., Yanagisawa, M., Katou, S., Sakimura, K., Mishina, M. and Tanaka, K. (2013) NMDA receptor subunits have different roles in NMDA-induced neurotoxicity in the retina. *Molecular brain,* **6,** 34.

Barry, M. F. and Ziff, E. B. (2002) Receptor trafficking and the plasticity of excitatory synapses. *Current opinion in neurobiology,* **12,** 279-286.

Beaulieu, J. M. and Gainetdinov, R. R. (2011) The physiology, signaling, and pharmacology of dopamine receptors. *Pharmacological reviews,* **63,** 182-217.

Behar-Cohen, F. F., Goureau, O., D'Hermies, F. and Courtois, Y. (1996) Decreased intraocular pressure induced by nitric oxide donors is correlated to nitrite production in the rabbit eye. *Investigative ophthalmology & visual science,* **37,** 1711-1715.

Behrens, C., Schubert, T., Haverkamp, S., Euler, T. and Berens, P. (2016) Connectivity map of bipolar cells and photoreceptors in the mouse retina. *eLife,* **5**.

Bellocchio, E. E., Reimer, R. J., Fremeau, R. T., Jr. and Edwards, R. H. (2000) Uptake of glutamate into synaptic vesicles by an inorganic phosphate transporter. *Science,* **289,** 957-960.

Besharse, J. C. and Iuvone, P. M. (1983) Circadian clock in Xenopus eye controlling retinal serotonin N-acetyltransferase. *Nature,* **305,** 133-135.

Bettler, B., Egebjerg, J., Sharma, G., Pecht, G., Hermans-Borgmeyer, I., Moll, C., Stevens, C. F. and Heinemann, S. (1992) Cloning of a putative glutamate receptor: a low affinity kainate-binding subunit. *Neuron,* **8,** 257-265.

Bhangoo, S. K. and Swanson, G. T. (2013) Kainate receptor signaling in pain pathways. *Molecular pharmacology,* **83,** 307-315.

Bieda, M. C. and Copenhagen, D. R. (2004) N-type and L-type calcium channels mediate glycinergic synaptic inputs to retinal ganglion cells of tiger salamanders. *Visual neuroscience,* **21,** 545-550.

Blazynski, C. and Perez, M. T. (1991) Adenosine in vertebrate retina: localization, receptor characterization, and function. *Cellular and molecular neurobiology,* **11,** 463-484.

Blom, J., Giove, T., Deshpande, M. and Eldred, W. D. (2012) Characterization of nitric oxide signaling pathways in the mouse retina. *The Journal of comparative neurology,* **520,** 4204-4217.

Bloomfield, S. A. and Dacheux, R. F. (2001) Rod vision: pathways and processing in the mammalian retina. *Progress in retinal and eye research,* **20,** 351-384.

Bochet, P., Audinat, E., Lambolez, B., Crépel, F., Rossier, J., Iino, M., Tsuzuki, K. and Ozawa, S. (1994) Subunit composition at the single-cell level explains functional properties of a glutamate-gated channel. *Neuron,* **12,** 383-388.

Borea, P. A., Gessi, S., Merighi, S. and Varani, K. (2016) Adenosine as a Multi-Signalling Guardian Angel in Human Diseases: When, Where and How Does it Exert its Protective Effects? *Trends in pharmacological sciences,* **37,** 419-434.

Borghuis, B. G., Looger, L. L., Tomita, S. and Demb, J. B. (2014) Kainate receptors mediate signaling in both transient and sustained OFF bipolar cell pathways in mouse retina. *The Journal of neuroscience : the official journal of the Society for Neuroscience,* **34,** 6128-6139.

Boycott, B. B. and Wässle, H. (1974) The morphological types of ganglion cells of the domestic cat's retina. *The Journal of physiology,* **240,** 397-419.

Boycott, B. B. and Wässle, H. (1991) Morphological Classification of Bipolar Cells of the Primate Retina. *The European journal of neuroscience,* **3,** 1069-1088.

Braas, K. M., Zarbin, M. A. and Snyder, S. H. (1987) Endogenous adenosine and adenosine receptors localized to ganglion cells of the retina. *Proceedings of the National Academy of Sciences of the United States of America,* **84,** 3906-3910.

Brandstätter, J. H., Koulen, P. and Wässle, H. (1998) Diversity of glutamate receptors in the mammalian retina. *Vision research,* **38,** 1385-1397.

Broussard, J. A., Rappaz, B., Webb, D. J. and Brown, C. M. (2013) Fluorescence resonance energy transfer microscopy as demonstrated by measuring the activation of the serine/threonine kinase Akt. *Nature protocols,* **8,** 265-281.

Brydon, L., Roka, F., Petit, L. et al. (1999) Dual signaling of human Mel1a melatonin receptors via G(i2), G(i3), and G(q/11) proteins. *Molecular endocrinology,* **13,** 2025-2038.

Bu, F., Tian, H., Gong, S., Zhu, Q., Xu, G. Y., Tao, J. and Jiang, X. (2015) Phosphorylation of NR2B NMDA subunits by protein kinase C in arcuate nucleus contributes to inflammatory pain in rats. *Scientific reports,* **5,** 15945.

Bugnon, O., Schaad, N. C. and Schorderet, M. (1994) Nitric oxide modulates endogenous dopamine release in bovine retina. *Neuroreport,* **5,** 401-404.

Burns, M. E. and Baylor, D. A. (2001) Activation, deactivation, and adaptation in vertebrate photoreceptor cells. *Annual review of neuroscience,* **24,** 779-805.

C. Van Essen, D. (2004) *Organization of Visual Areas in Macaque and Human Cerebral Cortex*.

Cahill, G. M. and Besharse, J. C. (1993) Circadian clock functions localized in xenopus retinal photoreceptors. *Neuron,* **10,** 573-577.

Calvert, P. D., Govardovskii, V. I., Arshavsky, V. Y. and Makino, C. L. (2002) Two temporal phases of light adaptation in retinal rods. *The Journal of general physiology,* **119,** 129-145.

Cardinali, D. P. (1981) Melatonin.l A mammalian pineal hormone. *Endocrine reviews,* **2,** 327-346.

Cardinali, D. P., Lynch, H. J. and Wurtman, R. J. (1972) Binding of melatonin to human and rat plasma proteins. *Endocrinology,* **91,** 1213-1218.

Casson, R. J. (2006) Possible role of excitotoxicity in the pathogenesis of glaucoma. *Clinical & experimental ophthalmology,* **34,** 54-63.

Chen, Y., Saulnier, J. L., Yellen, G. and Sabatini, B. L. (2014) A PKA activity sensor for quantitative analysis of endogenous GPCR signaling via 2-photon FRET-FLIM imaging. *Frontiers in pharmacology,* **5,** 56.

Civelli, O., Bunzow, J. R. and Grandy, D. K. (1993) Molecular diversity of the dopamine receptors. *Annual review of pharmacology and toxicology,* **33,** 281-307.

Clegg, R. M., Murchie, A. I., Zechel, A. and Lilley, D. M. (1993) Observing the helical geometry of double-stranded DNA in solution by fluorescence resonance energy transfer. *Proceedings of the National Academy of Sciences of the United States of America,* **90,** 2994-2998.

Clements, J. D., Lester, R. A., Tong, G., Jahr, C. E. and Westbrook, G. L. (1992) The time course of glutamate in the synaptic cleft. *Science,* **258,** 1498-1501.

Cohen, A. I., Todd, R. D., Harmon, S. and O'Malley, K. L. (1992) Photoreceptors of mouse retinas possess D4 receptors coupled to adenylate cyclase. *Proceedings of the National Academy of Sciences of the United States of America,* **89,** 12093-12097.

Cohen, E. D. and Miller, R. F. (1994) The role of NMDA and non-NMDA excitatory amino acid receptors in the functional organization of primate retinal ganglion cells. *Visual neuroscience,* **11,** 317-332.

Coombs, J., van der List, D., Wang, G. Y. and Chalupa, L. M. (2006) Morphological properties of mouse retinal ganglion cells. *Neuroscience,* **140,** 123-136.

Curcio, C. A., Sloan, K. R., Kalina, R. E. and Hendrickson, A. E. (1990) Human photoreceptor topography. *The Journal of comparative neurology,* **292,** 497-523.

Davies, J., Evans, R. H., Francis, A. A. and Watkins, J. C. (1979) Excitatory amino acid receptors and synaptic excitation in the mammalian central nervous system. *Journal de physiologie,* **75,** 641-654.

Dawson, T. M., Bredt, D. S., Fotuhi, M., Hwang, P. M. and Snyder, S. H. (1991) Nitric oxide synthase and neuronal NADPH diaphorase are identical in brain and peripheral tissues. *Proceedings of the National Academy of Sciences of the United States of America,* **88,** 7797-7801.

Dearry, A. and Burnside, B. (1989) Light-induced dopamine release from teleost retinas acts as a light-adaptive signal to the retinal pigment epithelium. *Journal of neurochemistry,* **53,** 870-878.

Deisseroth, K., Feng, G., Majewska, A. K., Miesenbock, G., Ting, A. and Schnitzer, M. J. (2006) Next-generation optical technologies for illuminating genetically targeted brain circuits. *The Journal of neuroscience : the official journal of the Society for Neuroscience,* **26,** 10380-10386.

Depry, C., Allen, M. D. and Zhang, J. (2011) Visualization of PKA activity in plasma membrane microdomains. *Molecular bioSystems,* **7,** 52-58.

Deussen, A., Sonntag, M. and Vogel, R. (1993) L-arginine-derived nitric oxide: a major determinant of uveal blood flow. *Experimental eye research,* **57,** 129-134.

DeVries, S. H. (2000) Bipolar cells use kainate and AMPA receptors to filter visual information into separate channels. *Neuron,* **28,** 847-856.

DeVries, S. H. and Baylor, D. A. (1995) An alternative pathway for signal flow from rod photoreceptors to ganglion cells in mammalian retina. *Proceedings of the National Academy of Sciences of the United States of America,* **92,** 10658-10662.

DeVries, S. H. and Schwartz, E. A. (1989) Modulation of an electrical synapse between solitary pairs of catfish horizontal cells by dopamine and second messengers. *The Journal of physiology,* **414,** 351-375.

Diamond, J. S. and Copenhagen, D. R. (1993) The contribution of NMDA and non-NMDA receptors to the light-evoked input-output characteristics of retinal ganglion cells. *Neuron,* **11,** 725-738.

Ding, J. D. and Weinberg, R. J. (2007) Distribution of soluble guanylyl cyclase in rat retina. *The Journal of comparative neurology,* **502,** 734-745.

Dingledine, R., Borges, K., Bowie, D. and Traynelis, S. F. (1999) The glutamate receptor ion channels. *Pharmacological reviews,* **51,** 7-61.

Dixon, D. B. and Copenhagen, D. R. (1992) Two types of glutamate receptors differentially excite amacrine cells in the tiger salamander retina. *The Journal of physiology,* **449,** 589-606.

Djamgoz, M. B., Sekaran, S., Angotzi, A. R., Haamedi, S., Vallerga, S., Hirano, J. and Yamada, M. (2000) Light-adaptive role of nitric oxide in the outer retina of lower vertebrates: a brief review. *Philosophical transactions of the Royal Society of London. Series B, Biological sciences,* **355,** 1199-1203.

Dkhissi, O., Chanut, E., Versaux-Botteri, C., Minvielle, F., Trouvin, J. H. and Nguyen-Legros, J. (1996) Changes in retinal dopaminergic cells and dopamine rhythmic metabolism during the development of a glaucoma-like disorder in quails. *Investigative ophthalmology & visual science,* **37,** 2335-2344.

Dowling, J. E. (1987) *The retina : an approachable part of the brain*. Belknap Press of Harvard University Press, Cambridge, Mass.

Doyle, S. E., McIvor, W. E. and Menaker, M. (2002) Circadian rhythmicity in dopamine content of mammalian retina: role of the photoreceptors. *Journal of neurochemistry,* **83,** 211-219.

Dubocovich, M. L. (1988) Luzindole (N-0774): a novel melatonin receptor antagonist. *The Journal of pharmacology and experimental therapeutics,* **246,** 902-910.

Dubocovich, M. L. (1995) Melatonin receptors: are there multiple subtypes? *Trends in pharmacological sciences,* **16,** 50-56.

Dubocovich, M. L., Delagrange, P., Krause, D. N., Sugden, D., Cardinali, D. P. and Olcese, J. (2010) International Union of Basic and Clinical Pharmacology. LXXV. Nomenclature, classification, and pharmacology of G protein-coupled melatonin receptors. *Pharmacological reviews,* **62,** 343-380.

Dubocovich, M. L., Masana, M. I., Iacob, S. and Sauri, D. M. (1997) Melatonin receptor antagonists that differentiate between the human Mel1a and Mel1b recombinant subtypes are used to assess the pharmacological profile of the rabbit retina ML1 presynaptic heteroreceptor. *Naunyn Schmiedebergs Arch Pharmacol,* **355,** 365-375.

Dubocovich, M. L. and Weiner, N. (1985) Pharmacological differences between the D-2 autoreceptor and the D-1 dopamine receptor in rabbit retina. *The Journal of pharmacology and experimental therapeutics,* **233,** 747-754.

Dunn, F. A., Doan, T., Sampath, A. P. and Rieke, F. (2006) Controlling the gain of rod-mediated signals in the Mammalian retina. *The Journal of neuroscience : the official journal of the Society for Neuroscience,* **26,** 3959-3970.

Dunwiddie, T. V. and Masino, S. A. (2001) The role and regulation of adenosine in the central nervous system. *Annual review of neuroscience,* **24,** 31-55.

Euler, T., Haverkamp, S., Schubert, T. and Baden, T. (2014) Retinal bipolar cells: elementary building blocks of vision. *Nature reviews. Neuroscience,* **15,** 507-519.

Euler, T. and Wässle, H. (1995) Immunocytochemical identification of cone bipolar cells in the rat retina. *The Journal of comparative neurology,* **361,** 461-478.

Fain, G. L., Matthews, H. R., Cornwall, M. C. and Koutalos, Y. (2001) Adaptation in vertebrate photoreceptors. *Physiological reviews,* **81,** 117-151.

Farrow, K. and Masland, R. H. (2011) Physiological clustering of visual channels in the mouse retina. *Journal of neurophysiology,* **105,** 1516-1530.

Ferreira, I. L., Duarte, C. B. and Carvalho, A. P. (1996) Ca^{2+} influx through glutamate receptor-associated channels in retina cells correlates with neuronal cell death. *European journal of pharmacology,* **302,** 153-162.

Ferrendelli, J. A. and De Vries, G. W. (1983) Cyclic GMP systems in the retina. *Federation proceedings,* **42,** 3103-3106.

Ferrer-Montiel, A. V. and Montal, M. (1996) Pentameric subunit stoichiometry of a neuronal glutamate receptor. *Proceedings of the National Academy of Sciences of the United States of America,* **93,** 2741-2744.

Franco, R., Ferre, S., Agnati, L. et al. (2000) Evidence for adenosine/dopamine receptor interactions: indications for heteromerization. *Neuropsychopharmacology,* **23,** S50-59.

Franco, R., Lluis, C., Canela, E. I., Mallol, J., Agnati, L., Casado, V., Ciruela, F., Ferre, S. and Fuxe, K. (2007) Receptor-receptor interactions involving adenosine A1 or dopamine D1 receptors and accessory proteins. *J Neural Transm (Vienna),* **114,** 93-104.

Fredholm, B. B., AP, I. J., Jacobson, K. A., Linden, J. and Müller, C. E. (2011) International Union of Basic and Clinical Pharmacology. LXXXI. Nomenclature and classification of adenosine receptors--an update. *Pharmacological reviews,* **63,** 1-34.

Fredholm, B. B. and Dunwiddie, T. V. (1988) How does adenosine inhibit transmitter release? *Trends in pharmacological sciences,* **9,** 130-134.

Frerking, M., Schmitz, D., Zhou, Q., Johansen, J. and Nicoll, R. A. (2001) Kainate receptors depress excitatory synaptic transmission at CA3-->CA1 synapses in the hippocampus via a direct presynaptic action. *The Journal of neuroscience : the official journal of the Society for Neuroscience,* **21,** 2958-2966.

Frings S., M. F. (2014) *Biology der Sinne*. Springer Spektrum.

Fujieda, H., Hamadanizadeh, S. A., Wankiewicz, E., Pang, S. F. and Brown, G. M. (1999) Expression of mt1 melatonin receptor in rat retina: evidence for multiple cell targets for melatonin. *Neuroscience,* **93,** 793-799.

Fuxe, K., Marcellino, D., Rivera, A. et al. (2008) Receptor-receptor interactions within receptor mosaics. Impact on neuropsychopharmacology. *Brain research reviews,* **58,** 415-452.

Gamm, D. M., Barthel, L. K., Raymond, P. A. and Uhler, M. D. (2000) Localization of cGMP-dependent protein kinase isoforms in mouse eye. *Investigative ophthalmology & visual science,* **41,** 2766-2773.

Garthwaite, J. (2005) Dynamics of cellular NO-cGMP signaling. *Front Biosci,* **10,** 1868-1880.

Ghosh, K. K., Bujan, S., Haverkamp, S., Feigenspan, A. and Wässle, H. (2004) Types of bipolar cells in the mouse retina. *The Journal of comparative neurology,* **469,** 70-82.

Ghosh, K. K., Haverkamp, S. and Wässle, H. (2001) Glutamate receptors in the rod pathway of the mammalian retina. *The Journal of neuroscience : the official journal of the Society for Neuroscience,* **21,** 8636-8647.

Gines, S., Hillion, J., Torvinen, M. et al. (2000) Dopamine D1 and adenosine A1 receptors form functionally interacting heteromeric complexes. *Proceedings of the National Academy of Sciences of the United States of America,* **97,** 8606-8611.

Goldstein, I. M., Ostwald, P. and Roth, S. (1996) Nitric oxide: a review of its role in retinal function and disease. *Vision research,* **36,** 2979-2994.

Gorshkov, K. and Zhang, J. (2014) Visualization of cyclic nucleotide dynamics in neurons. *Front Cell Neurosci,* **8,** 395.

Gotzes, S., de Vente, J. and Müller, F. (1998) Nitric oxide modulates cGMP levels in neurons of the inner and outer retina in opposite ways. *Visual neuroscience,* **15,** 945-955.

Graham, F. L., Smiley, J., Russell, W. C. and Nairn, R. (1977) Characteristics of a human cell line transformed by DNA from human adenovirus type 5. *J Gen Virol,* **36,** 59-74.

Greferath, U., Grunert, U. and Wässle, H. (1990) Rod bipolar cells in the mammalian retina show protein kinase C-like immunoreactivity. *The Journal of comparative neurology,* **301,** 433-442.

Grunder, T., Kohler, K. and Guenther, E. (2000) Distribution and developmental regulation of AMPA receptor subunit proteins in rat retina. *Investigative ophthalmology & visual science,* **41,** 3600-3606.

Grunert, U., Haverkamp, S., Fletcher, E. L. and Wässle, H. (2002) Synaptic distribution of ionotropic glutamate receptors in the inner plexiform layer of the primate retina. *The Journal of comparative neurology,* **447,** 138-151.

Guimaraes, M. Z., Hokoc, J. N., Duvoisin, R., Reis, R. A. and De Mello, F. G. (2001) Dopaminergic retinal cell differentiation in culture: modulation by forskolin and dopamine. *The European journal of neuroscience,* **13,** 1931-1937.

Habermann, C. J., O'Brien, B. J., Wässle, H. and Protti, D. A. (2003) AII amacrine cells express L-type calcium channels at their output synapses. *The Journal of neuroscience : the official journal of the Society for Neuroscience,* **23,** 6904-6913.

Hamassaki-Britto, D. E., Hermans-Borgmeyer, I., Heinemann, S. and Hughes, T. E. (1993) Expression of glutamate receptor genes in the mammalian retina: the localization of GluR1 through GluR7 mRNAs. *The Journal of neuroscience : the official journal of the Society for Neuroscience,* **13,** 1888-1898.

Hampson, E. C., Vaney, D. I. and Weiler, R. (1992) Dopaminergic modulation of gap junction permeability between amacrine cells in mammalian retina. *The Journal of neuroscience : the official journal of the Society for Neuroscience,* **12,** 4911-4922.

Hartveit, E. (1997) Functional organization of cone bipolar cells in the rat retina. *Journal of neurophysiology,* **77,** 1716-1730.

Hartveit, E., Brandstätter, J. H., Sassoè-Pognetto, M., Laurie, D. J., Seeburg, P. H. and Wässle, H. (1994) Localization and developmental expression of the NMDA receptor subunit NR2A in the mammalian retina. *Journal of Comparative Neurology,* **348,** 570-582.

Hartwick, A. T., Lalonde, M. R., Barnes, S. and Baldridge, W. H. (2004) Adenosine A1-receptor modulation of glutamate-induced calcium influx in rat retinal ganglion cells. *Investigative ophthalmology & visual science,* **45,** 3740-3748.

Haverkamp, S. and Wässle, H. (2000) Immunocytochemical analysis of the mouse retina. *The Journal of comparative neurology,* **424,** 1-23.

Hayashida, Y., Rodriguez, C. V., Ogata, G., Partida, G. J., Oi, H., Stradleigh, T. W., Lee, S. C., Colado, A. F. and Ishida, A. T. (2009) Inhibition of adult rat retinal ganglion cells by D1-type dopamine receptor activation. *The Journal of neuroscience : the official journal of the Society for Neuroscience,* **29,** 15001-15016.

Heim, N., Garaschuk, O., Friedrich, M. W., Mank, M., Milos, R. I., Kovalchuk, Y., Konnerth, A. and Griesbeck, O. (2007) Improved calcium imaging in transgenic mice expressing a troponin C-based biosensor. *Nature methods,* **4,** 127-129.

Heim, N. and Griesbeck, O. (2004) Genetically encoded indicators of cellular calcium dynamics based on troponin C and green fluorescent protein. *The Journal of biological chemistry,* **279,** 14280-14286.

Herb, A., Burnashev, N., Werner, P., Sakmann, B., Wisden, W. and Seeburg, P. H. (1992) The KA-2 subunit of excitatory amino acid receptors shows widespread expression in brain and forms ion channels with distantly related subunits. *Neuron,* **8,** 775-785.

Hernandez, C. and Simo, R. (2012) Neuroprotection in diabetic retinopathy. *Current diabetes reports,* **12,** 329-337.

Hernandez-Lopez, S., Tkatch, T., Perez-Garci, E., Galarraga, E., Bargas, J., Hamm, H. and Surmeier, D. J. (2000) D2 dopamine receptors in striatal medium spiny neurons reduce L-type Ca^{2+} currents and excitability via a novel PLC[beta]1-IP3-calcineurin-signaling cascade. *The Journal of neuroscience : the official journal of the Society for Neuroscience,* **20,** 8987-8995.

Herrmann, R., Heflin, S. J., Hammond, T. et al. (2011) Rod vision is controlled by dopamine-dependent sensitization of rod bipolar cells by GABA. *Neuron,* **72,** 101-110.

Hofmann, F., Feil, R., Kleppisch, T. and Schlossmann, J. (2006) Function of cGMP-dependent protein kinases as revealed by gene deletion. *Physiological reviews,* **86,** 1-23.

Hollmann, M. and Heinemann, S. (1994) Cloned glutamate receptors. *Annual review of neuroscience,* **17,** 31-108.

Horn, T. F., Wolf, G., Duffy, S., Weiss, S., Keilhoff, G. and MacVicar, B. A. (2002) Nitric oxide promotes intracellular calcium release from mitochondria in striatal neurons. *FASEB J,* **16,** 1611-1622.

Huang, H., Lee, S. C. and Yang, X. L. (2005) Modulation by melatonin of glutamatergic synaptic transmission in the carp retina. *The Journal of physiology,* **569,** 857-871.

Huang, H., Wang, Z., Weng, S. J., Sun, X. H. and Yang, X. L. (2013) Neuromodulatory role of melatonin in retinal information processing. *Progress in retinal and eye research,* **32,** 64-87.

Huettner, J. E. (2003) Kainate receptors and synaptic transmission. *Progress in neurobiology,* **70,** 387-407.

Hunt, A. E., Al-Ghoul, W. M., Gillette, M. U. and Dubocovich, M. L. (2001) Activation of MT(2) melatonin receptors in rat suprachiasmatic nucleus phase advances the circadian clock. *Am J Physiol Cell Physiol,* **280,** C110-118.

Ikeda, K., Nagasawa, M., Mori, H., Araki, K., Sakimura, K., Watanabe, M., Inoue, Y. and Mishina, M. (1992) Cloning and expression of the epsilon 4 subunit of the NMDA receptor channel. *FEBS letters,* **313,** 34-38.

Ishii, T., Moriyoshi, K., Sugihara, H. et al. (1993) Molecular characterization of the family of the N-methyl-D-aspartate receptor subunits. *The Journal of biological chemistry,* **268,** 2836-2843.

Jacobson, K. A., van Galen, P. J., Ji, X. D., Ramkumar, V., Olah, M. E. and Stiles, G. L. (1993) Molecular Characterization of A(1) and A(2a) Adenosine Receptors. *Drug Dev Res,* **28,** 226-231.

Jones, R. S., Carroll, R. C. and Nawy, S. (2012) Light-induced plasticity of synaptic AMPA receptor composition in retinal ganglion cells. *Neuron,* **75,** 467-478.

Kamermans, M. and Fahrenfort, I. (2004) Ephaptic interactions within a chemical synapse: hemichannel-mediated ephaptic inhibition in the retina. *Current opinion in neurobiology,* **14,** 531-541.

Kaupp, U. B. and Seifert, R. (2002) Cyclic nucleotide-gated ion channels. *Physiological reviews,* **82,** 769-824.

Keeley, P. W. and Reese, B. E. (2010) Morphology of dopaminergic amacrine cells in the mouse retina: independence from homotypic interactions. *The Journal of comparative neurology,* **518,** 1220-1231.

Kim, I. B., Lee, E. J., Kim, K. Y., Ju, W. K., Oh, S. J., Joo, C. K. and Chun, M. H. (1999) Immunocytochemical localization of nitric oxide synthase in the mammalian retina. *Neuroscience letters,* **267,** 193-196.

Kiskin, N. I., Krishtal, O. A. and Tsyndrenko, A. (1986) Excitatory amino acid receptors in hippocampal neurons: kainate fails to desensitize them. *Neuroscience letters,* **63,** 225-230.

Klein, D. C. (2007) Arylalkylamine N-acetyltransferase: "the Timezyme". *The Journal of biological chemistry,* **282,** 4233-4237.

Koistinaho, J., Swanson, R. A., de Vente, J. and Sagar, S. M. (1993) NADPH-diaphorase (nitric oxide synthase)-reactive amacrine cells of rabbit retina: putative target cells and stimulation by light. *Neuroscience,* **57,** 587-597.

Kolb, H., Nelson, R. and Mariani, A. (1981) Amacrine cells, bipolar cells and ganglion cells of the cat retina: a Golgi study. *Vision research,* **21,** 1081-1114.

Kong, J. H., Fish, D. R., Rockhill, R. L. and Masland, R. H. (2005) Diversity of ganglion cells in the mouse retina: unsupervised morphological classification and its limits. *The Journal of comparative neurology,* **489,** 293-310.

Kothmann, W. W., Massey, S. C. and O'Brien, J. (2009) Dopamine-stimulated dephosphorylation of connexin 36 mediates AII amacrine cell uncoupling. *The Journal of neuroscience : the official journal of the Society for Neuroscience,* **29,** 14903-14911.

Kreutzberg, G. W., Barron, K. D. and Schubert, P. (1978) Cytochemical localization of 5'-nucleotidase in glial plasma membranes. *Brain research,* **158,** 247-257.

Kristensen, O., Kristensen, L. B., Mollerud, S., Frydenvang, K., Pickering, D. S. and Kastrup, J. S. (2016) The Structure of a High-Affinity Kainate Receptor: GluK4 Ligand-Binding Domain Crystallized with Kainate. *Structure,* **24,** 1582-1589.

Kurenny, D. E., Moroz, L. L., Turner, R. W., Sharkey, K. A. and Barnes, S. (1994) Modulation of ion channels in rod photoreceptors by nitric oxide. *Neuron,* **13,** 315-324.

Kuzhikandathil, E. V., Yu, W. and Oxford, G. S. (1998) Human dopamine D3 and D2L receptors couple to inward rectifier potassium channels in mammalian cell lines. *Molecular and cellular neurosciences,* **12,** 390-402.

Kvanta, A., Seregard, S., Sejersen, S., Kull, B. and Fredholm, B. B. (1997) Localization of adenosine receptor messenger RNAs in the rat eye. *Experimental eye research,* **65,** 595-602.

Kwon, H. B. and Castillo, P. E. (2008) Role of glutamate autoreceptors at hippocampal mossy fiber synapses. *Neuron,* **60,** 1082-1094.

Lamb, T. D. and Simon, E. J. (1976) The relation between intercellular coupling and electrical noise in turtle photoreceptors. *The Journal of physiology,* **263,** 257-286.

Lavine, N., Ethier, N., Oak, J. N. et al. (2002) G protein-coupled receptors form stable complexes with inwardly rectifying potassium channels and adenylyl cyclase. *The Journal of biological chemistry,* **277,** 46010-46019.

Lee, S. P., So, C. H., Rashid, A. J., Varghese, G., Cheng, R., Lanca, A. J., O'Dowd, B. F. and George, S. R. (2004) Dopamine D1 and D2 receptor Co-activation generates a novel phospholipase C-mediated calcium signal. *The Journal of biological chemistry,* **279,** 35671-35678.

Lerma, J. (1997) Kainate reveals its targets. *Neuron,* **19,** 1155-1158.

Li, H. and O'Brien, J. (2012) Regulation of gap junctional coupling in photoreceptors: *Bookchapter*: Photoreceptors: Physiology, Types and Abnormalities. *Chapter V*, 97-112. ISBN 978-1-61942-619-1

Li, H., Zhang, Z., Blackburn, M. R., Wang, S. W., Ribelayga, C. P. and O'Brien, J. (2013) Adenosine and dopamine receptors coregulate photoreceptor coupling via gap junction phosphorylation in mouse retina. *The Journal of neuroscience : the official journal of the Society for Neuroscience,* **33,** 3135-3150.

Liets, L. C. and Chalupa, L. M. (1996) The metabotropic glutamate agonist 2-amino-4-phosphonobutyric acid (APB) does not activate currents in postnatal retinal ganglion cells. *Neuroreport,* **7,** 2873-2877.

Lin, B. and Masland, R. H. (2006) Populations of wide-field amacrine cells in the mouse retina. *The Journal of comparative neurology,* **499,** 797-809.

Lin, M. Z. and Schnitzer, M. J. (2016) Genetically encoded indicators of neuronal activity. *Nature neuroscience,* **19,** 1142-1153.

Lindstrom, S. H., Ryan, D. G., Shi, J. and DeVries, S. H. (2014) Kainate receptor subunit diversity underlying response diversity in retinal off bipolar cells. *The Journal of physiology,* **592,** 1457-1477.

Linn, C. L. and Gafka, A. C. (2001) Modulation of a voltage-gated calcium channel linked to activation of glutamate receptors and calcium-induced calcium release in the catfish retina. *The Journal of physiology,* **535,** 47-63.

Liu, J., Clough, S. J., Hutchinson, A. J., Adamah-Biassi, E. B., Popovska-Gorevski, M. and Dubocovich, M. L. (2016) MT1 and MT2 Melatonin Receptors: A Therapeutic Perspective. *Annual review of pharmacology and toxicology,* **56,** 361-383.

Lukasiewicz, P. D., Wilson, J. A. and Lawrence, J. E. (1997) AMPA-preferring receptors mediate excitatory synaptic inputs to retinal ganglion cells. *Journal of neurophysiology,* **77,** 57-64.

MacNeil, M. A. and Masland, R. H. (1998) Extreme diversity among amacrine cells: implications for function. *Neuron,* **20,** 971-982.

Malinow, R. and Malenka, R. C. (2002) AMPA receptor trafficking and synaptic plasticity. *Annual review of neuroscience,* **25,** 103-126.

Marc, R. E. (1988) The role of glycine in the mammalian retina. *Progress in Retinal Research,* **8,** 67-107.

Marquez de Prado, B., Castaneda, T. R., Galindo, A., del Arco, A., Segovia, G., Reiter, R. J. and Mora, F. (2000) Melatonin disrupts circadian rhythms of glutamate and GABA in the neostriatum of the aware rat: a microdialysis study. *Journal of pineal research,* **29,** 209-216.

Masland, R. H. (2001) The fundamental plan of the retina. *Nature neuroscience,* **4,** 877-886.

Masland, R. H. (2012) The neuronal organization of the retina. *Neuron,* **76,** 266-280.

Massey, S. C. (1990) Chapter 11 Cell types using glutamate as a neurotransmitter in the vertebrate retina. *Progress in Retinal Research,* **9,** 399-425.

Massey, S. C. and Miller, R. F. (1990) N-methyl-D-aspartate receptors of ganglion cells in rabbit retina. *Journal of neurophysiology,* **63,** 16-30.

Mataruga, A., Kremmer, E. and Müller, F. (2007) Type 3a and type 3b OFF cone bipolar cells provide for the alternative rod pathway in the mouse retina. *The Journal of comparative neurology,* **502,** 1123-1137.

Matthews, G. and Watanabe, S. (1988) Activation of single ion channels from toad retinal rod inner segments by cyclic GMP: concentration dependence. *The Journal of physiology,* **403,** 389-405.

Mayer, M. L. and Westbrook, G. L. (1987) The physiology of excitatory amino acids in the vertebrate central nervous system. *Progress in neurobiology,* **28,** 197-276.

McArthur, A. J., Hunt, A. E. and Gillette, M. U. (1997) Melatonin action and signal transduction in the rat suprachiasmatic circadian clock: activation of protein kinase C at dusk and dawn. *Endocrinology,* **138,** 627-634.

McMahon, D. G. and Ponomareva, L. V. (1996) Nitric oxide and cGMP modulate retinal glutamate receptors. *Journal of neurophysiology,* **76,** 2307-2315.

Meguro, H., Mori, H., Araki, K. et al. (1992) Functional characterization of a heteromeric NMDA receptor channel expressed from cloned cDNAs. *Nature,* **357,** 70-74.

Missale, C., Nash, S. R., Robinson, S. W., Jaber, M. and Caron, M. G. (1998) Dopamine receptors: from structure to function. *Physiological reviews,* **78,** 189-225.

Mittman, S., Taylor, W. R. and Copenhagen, D. R. (1990) Concomitant activation of two types of glutamate receptor mediates excitation of salamander retinal ganglion cells. *The Journal of physiology,* **428,** 175-197.

Miyachi, E., Miyakawa, A. and Murakami, M. (1991) Modulation of electrical coupling between retinal horizontal cells by intracellular messengers. *Neuroscience research. Supplement : the official journal of the Japan Neuroscience Society,* **15,** S41-49.

Monyer, H., Sprengel, R., Schoepfer, R., Herb, A., Higuchi, M., Lomeli, H., Burnashev, N., Sakmann, B. and Seeburg, P. H. (1992) Heteromeric NMDA receptors: molecular and functional distinction of subtypes. *Science,* **256,** 1217-1221.

Morgans, C. W., Zhang, J., Jeffrey, B. G., Nelson, S. M., Burke, N. S., Duvoisin, R. M. and Brown, R. L. (2009) TRPM1 is required for the depolarizing light response in retinal ON-bipolar cells. *Proceedings of the National Academy of Sciences of the United States of America,* **106,** 19174-19178.

Morin, D., Simon, N., Depres-Brummer, P., Levi, F., Tillement, J. P. and Urien, S. (1997) Melatonin high-affinity binding to alpha-1-acid glycoprotein in human serum. *Pharmacology,* **54,** 271-275.

Moriyoshi, K., Masu, M., Ishii, T., Shigemoto, R., Mizuno, N. and Nakanishi, S. (1991) Molecular cloning and characterization of the rat NMDA receptor. *Nature,* **354,** 31-37.

Müller, F., Greferath, U., Wässle, H., Wisden, W. and Seeburg, P. (1992) Glutamate receptor expression in the rat retina. *Neuroscience letters,* **138,** 179-182.

Müller, F., Kaschuba, D., Gensch, T., Mank, M. and Griesbeck, O. (2007) Expression of the Genetically Encoded Calcium Sensor TN-L15 in Retinal Ganglion Cells of Transgenic Mice. *Investigative ophthalmology & visual science,* **48,** 2804-2804.

Müller, F. and Kaupp, U. B. (1998) Signaltransduktion in Sehzellen. *Naturwissenschaften,* **85,** 49-61.

Nakajima, Y., Iwakabe, H., Akazawa, C., Nawa, H., Shigemoto, R., Mizuno, N. and Nakanishi, S. (1993) Molecular characterization of a novel retinal metabotropic

glutamate receptor mGluR6 with a high agonist selectivity for L-2-amino-4-phosphonobutyrate. *The Journal of biological chemistry,* **268,** 11868-11873.

Nakanishi, S. (1992) Molecular diversity of glutamate receptors and implications for brain function. *Science,* **258,** 597-603.

Nakazawa, T., Endo, S., Shimura, M., Kondo, M., Ueno, S. and Tamai, M. (2005) Retinal G-substrate, potential downstream component of NO/cGMP/PKG pathway, is located in subtype of retinal ganglion cells and amacrine cells with protein phosphatases. *Brain Res Mol Brain Res,* **135,** 58-68.

Nathanson, J. A. and McKee, M. (1995) Identification of an extensive system of nitric oxide-producing cells in the ciliary muscle and outflow pathway of the human eye. *Investigative ophthalmology & visual science,* **36,** 1765-1773.

Nawy, S. and Jahr, C. E. (1990) Suppression by glutamate of cGMP-activated conductance in retinal bipolar cells. *Nature,* **346,** 269-271.

Negishi, K., Kato, S. and Teranishi, T. (1988) Dopamine cells and rod bipolar cells contain protein kinase C-like immunoreactivity in some vertebrate retinas. *Neuroscience letters,* **94,** 247-252.

Newman, E. A. (2003) Glial cell inhibition of neurons by release of ATP. *The Journal of neuroscience : the official journal of the Society for Neuroscience,* **23,** 1659-1666.

Nguyen-Legros, J. (1988) Chapter 5 morphology and distribution of catecholamine-neurons in mammalian retina. *Progress in Retinal Research,* **7,** 113-147.

Nguyen-Legros, J., Simon, A., Caille, I. and Bloch, B. (1997) Immunocytochemical localization of dopamine D1 receptors in the retina of mammals. *Visual neuroscience,* **14,** 545-551.

Nishi, A., Snyder, G. L. and Greengard, P. (1997) Bidirectional regulation of DARPP-32 phosphorylation by dopamine. *The Journal of neuroscience : the official journal of the Society for Neuroscience,* **17,** 8147-8155.

Niznik, H. B. and Van Tol, H. H. (1992) Dopamine receptor genes: new tools for molecular psychiatry. *J Psychiatry Neurosci,* **17,** 158-180.

Nomura, A., Shigemoto, R., Nakamura, Y., Okamoto, N., Mizuno, N. and Nakanishi, S. (1994) Developmentally regulated postsynaptic localization of a metabotropic glutamate receptor in rat rod bipolar cells. *Cell,* **77,** 361-369.

Osterberg, G. (1935) *Topography of the Layer of Rods and Cones in the Human Retina*. A. Busck.

Paes de Carvalho, R., Braas, K. M., Snyder, S. H. and Adler, R. (1990) Analysis of adenosine immunoreactivity, uptake, and release in purified cultures of developing chick embryo retinal neurons and photoreceptors. *Journal of neurochemistry,* **55,** 1603-1611.

Paes-De-Carvalho, R. (2002) Adenosine as a signaling molecule in the retina: biochemical and developmental aspects. *An Acad Bras Cienc,* **74,** 437-451.

Pang, J. J., Gao, F. and Wu, S. M. (2010) Light responses and morphology of bNOS-immunoreactive neurons in the mouse retina. *The Journal of comparative neurology,* **518,** 2456-2474.

Pankratov, Y. and Lalo, U. (2014) Calcium permeability of ligand-gated Ca^{2+} channels. *European journal of pharmacology,* **739,** 60-73.

Patneau, D. K. and Mayer, M. L. (1991) Kinetic analysis of interactions between kainate and AMPA: evidence for activation of a single receptor in mouse hippocampal neurons. *Neuron,* **6,** 785-798.

Peichl, L. (1989) Alpha and delta ganglion cells in the rat retina. *The Journal of comparative neurology,* **286,** 120-139.

Peichl, L. (1992) Prinzipien der Bildverarbeitung in der Retina der Säugetiere. *Biologie in unserer Zeit,* **22,** 45-53.

Peng, Y. W., Blackstone, C. D., Huganir, R. L. and Yau, K. W. (1995) Distribution of glutamate receptor subtypes in the vertebrate retina. *Neuroscience,* **66,** 483-497.

Perez, M. T., Arner, K. and Ehinger, B. (1988) Stimulation-evoked release of purines from the rabbit retina. *Neurochem Int,* **13,** 307-318.

Perez, M. T., Ehinger, B. E., Lindstrom, K. and Fredholm, B. B. (1986) Release of endogenous and radioactive purines from the rabbit retina. *Brain research,* **398,** 106-112.

Perreault, M. L., Hasbi, A., O'Dowd, B. F. and George, S. R. (2014) Heteromeric dopamine receptor signaling complexes: emerging neurobiology and disease relevance. *Neuropsychopharmacology,* **39,** 156-168.

Petit, L., Lacroix, I., de Coppet, P., Strosberg, A. D. and Jockers, R. (1999) Differential signaling of human Mel1a and Mel1b melatonin receptors through the cyclic guanosine 3'-5'-monophosphate pathway. *Biochem Pharmacol,* **58,** 633-639.

Pickard, G. E., Smeraski, C. A., Tomlinson, C. C., Banfield, B. W., Kaufman, J., Wilcox, C. L., Enquist, L. W. and Sollars, P. J. (2002) Intravitreal injection of the attenuated pseudorabies virus PRV Bartha results in infection of the hamster suprachiasmatic nucleus only by retrograde transsynaptic transport via autonomic circuits. *The Journal of neuroscience : the official journal of the Society for Neuroscience,* **22,** 2701-2710.

Pow, D. V. and Barnett, N. L. (2000) Developmental expression of excitatory amino acid transporter 5: a photoreceptor and bipolar cell glutamate transporter in rat retina. *Neuroscience letters,* **280,** 21-24.

Pow, D. V., Wright, L. L. and Vaney, D. I. (1995) The immunocytochemical detection of amino-acid neurotransmitters in paraformaldehyde-fixed tissues. *J Neurosci Methods,* **56,** 115-123.

Pugh, E. N., Jr., Nikonov, S. and Lamb, T. D. (1999) Molecular mechanisms of vertebrate photoreceptor light adaptation. *Current opinion in neurobiology,* **9,** 410-418.

Puller, C., Ivanova, E., Euler, T., Haverkamp, S. and Schubert, T. (2013) OFF bipolar cells express distinct types of dendritic glutamate receptors in the mouse retina. *Neuroscience,* **243,** 136-148.

Rauen, T. and Kanner, B. I. (1994) Localization of the glutamate transporter GLT-1 in rat and macaque monkey retinae. *Neuroscience letters,* **169,** 137-140.

Rauen, T., Taylor, W. R., Kuhlbrodt, K. and Wiessner, M. (1998) High-affinity glutamate transporters in the rat retina: a major role of the glial glutamate transporter GLAST-1 in transmitter clearance. *Cell Tissue Res,* **291,** 19-31.

Rein, M. L. and Deussing, J. M. (2012) The optogenetic (r)evolution. *Mol Genet Genomics,* **287,** 95-109.

Reppert, S. M., Godson, C., Mahle, C. D., Weaver, D. R., Slaugenhaupt, S. A. and Gusella, J. F. (1995) Molecular characterization of a second melatonin receptor expressed in human retina and brain: the Mel1b melatonin receptor. *Proceedings of the National Academy of Sciences of the United States of America,* **92,** 8734-8738.

Reppert, S. M., Weaver, D. R. and Ebisawa, T. (1994) Cloning and characterization of a mammalian melatonin receptor that mediates reproductive and circadian responses. *Neuron,* **13,** 1177-1185.

Ribelayga, C. and Mangel, S. C. (2005) A circadian clock and light/dark adaptation differentially regulate adenosine in the mammalian retina. *The Journal of neuroscience : the official journal of the Society for Neuroscience,* **25,** 215-222.

Rodieck, R. W. (1998) *The First Steps in Seeing*. Oxford University Press Inc.

Rodrigues, R. and Lerma, J. (2012) *Metabotropic signaling by kainate receptors*.

Rodriguez-Moreno, A. and Sihra, T. S. (2013) Presynaptic kainate receptor-mediated facilitation of glutamate release involves Ca^{2+}-calmodulin and PKA in cerebrocortical synaptosomes. *FEBS letters,* **587,** 788-792.

Rohrenbeck, J., Wässle, H. and Heizmann, C. W. (1987) Immunocytochemical labelling of horizontal cells in mammalian retina using antibodies against calcium-binding proteins. *Neuroscience letters,* **77,** 255-260.

Roka, F., Brydon, L., Waldhoer, M., Strosberg, A. D., Freissmuth, M., Jockers, R. and Nanoff, C. (1999) Tight association of the human Mel(1a)-melatonin receptor and G(i): precoupling and constitutive activity. *Molecular pharmacology,* **56,** 1014-1024.

Rosenmund, C., Stern-Bach, Y. and Stevens, C. F. (1998) The tetrameric structure of a glutamate receptor channel. *Science,* **280,** 1596-1599.

Roth, S. (2004) Endogenous neuroprotection in the retina. *Brain research bulletin,* **62,** 461-466.

Rozas, J. L., Paternain, A. V. and Lerma, J. (2003) Noncanonical signaling by ionotropic kainate receptors. *Neuron,* **39,** 543-553.

Sahu, A., Tyeryar, K. R., Vongtau, H. O., Sibley, D. R. and Undieh, A. S. (2009) D5 dopamine receptors are required for dopaminergic activation of phospholipase C. *Molecular pharmacology,* **75,** 447-453.

Sakimura, K., Morita, T., Kushiya, E. and Mishina, M. (1992) Primary structure and expression of the gamma 2 subunit of the glutamate receptor channel selective for kainate. *Neuron,* **8,** 267-274.

Sallert, M., Malkki, H., Segerstrale, M., Taira, T. and Lauri, S. E. (2007) Effects of the kainate receptor agonist ATPA on glutamatergic synaptic transmission and plasticity during early postnatal development. *Neuropharmacology,* **52,** 1354-1365.

Santos, P. F., Caramelo, O. L., Carvalho, A. P. and Duarte, C. B. (1999) Characterization of ATP release from cultures enriched in cholinergic amacrine-like neurons. *Journal of neurobiology,* **41,** 340-348.

Sapsford, K. E., Berti, L. and Medintz, I. L. (2006) Materials for fluorescence resonance energy transfer analysis: beyond traditional donor-acceptor combinations. *Angewandte Chemie,* **45,** 4562-4589.

Savaskan, E., Wirz-Justice, A., Olivieri, G., Pache, M., Krauchi, K., Brydon, L., Jockers, R., Müller-Spahn, F. and Meyer, P. (2002) Distribution of melatonin MT1 receptor immunoreactivity in human retina. *J Histochem Cytochem,* **50,** 519-526.

Scanziani, M. and Hausser, M. (2009) Electrophysiology in the age of light. *Nature,* **461,** 930-939.

Scher, J., Wankiewicz, E., Brown, G. M. and Fujieda, H. (2003) AII amacrine cells express the MT1 melatonin receptor in human and macaque retina. *Experimental eye research,* **77,** 375-382.

Schiller, P. H. (1982) Central connections of the retinal ON and OFF pathways. *Nature,* **297,** 580-583.

Schmetterer, L., Findl, O., Fasching, P., Ferber, W., Strenn, K., Breiteneder, H., Adam, H., Eichler, H. G. and Wolzt, M. (1997) Nitric oxide and ocular blood flow in patients with IDDM. *Diabetes,* **46,** 653-658.

Schmitz, Y. and Witkovsky, P. (1997) Dependence of photoreceptor glutamate release on a dihydropyridine-sensitive calcium channel. *Neuroscience,* **78,** 1209-1216.

Schubert, T. and Euler, T. (2010) Retinal processing: global players like it local. *Current biology : CB,* **20,** R486-488.

Sekar, R. B. and Periasamy, A. (2003) Fluorescence resonance energy transfer (FRET) microscopy imaging of live cell protein localizations. *J Cell Biol,* **160,** 629-633.

Senba, E., Daddona, P. E. and Nagy, J. I. (1986) Immunohistochemical localization of adenosine deaminase in the retina of the rat. *Brain research bulletin,* **17,** 209-217.

Shen, Y., Heimel, J. A., Kamermans, M., Peachey, N. S., Gregg, R. G. and Nawy, S. (2009) A transient receptor potential-like channel mediates synaptic transmission in rod bipolar cells. *The Journal of neuroscience : the official journal of the Society for Neuroscience,* **29,** 6088-6093.

Shen, Y., Liu, X. L. and Yang, X. L. (2006) N-methyl-D-aspartate receptors in the retina. *Molecular neurobiology,* **34,** 163-179.

Shiells, R. A. and Falk, G. (1992) The glutamate-receptor linked cGMP cascade of retinal on-bipolar cells is pertussis and cholera toxin-sensitive. *Proceedings. Biological sciences,* **247,** 17-20.

Shiells, R. A., Falk, G. and Naghshineh, S. (1981) Action of glutamate and aspartate analogues on rod horizontal and bipolar cells. *Nature,* **294,** 592-594.

Shimomura, O., Johnson, F. H. and Saiga, Y. (1962) Extraction, purification and properties of aequorin, a bioluminescent protein from the luminous hydromedusan, Aequorea. *Journal of cellular and comparative physiology,* **59,** 223-239.

Sibley, D. R. and Monsma, F. J., Jr. (1992) Molecular biology of dopamine receptors. *Trends in pharmacological sciences,* **13,** 61-69.

Sieben (2016) Visualization of dopaminergic signaling in the retina with optogenetic sensors. Doktorarbeit am ICS-4 (FZ-Jülich) in der AG-Müller.

Slaughter, M. M. and Miller, R. F. (1981) 2-amino-4-phosphonobutyric acid: a new pharmacological tool for retina research. *Science,* **211,** 182-185.

Slaughter, M. M. and Miller, R. F. (1983) Bipolar cells in the mudpuppy retina use an excitatory amino acid neurotransmitter. *Nature,* **303,** 537-538.

Snyder, G. L., Fienberg, A. A., Huganir, R. L. and Greengard, P. (1998) A dopamine/D1 receptor/protein kinase A/dopamine- and cAMP-regulated phosphoprotein (Mr 32 kDa)/protein phosphatase-1 pathway regulates dephosphorylation of the NMDA receptor. *The Journal of neuroscience : the official journal of the Society for Neuroscience,* **18,** 10297-10303.

So, C. H., Verma, V., O'Dowd, B. F. and George, S. R. (2007) Desensitization of the dopamine D1 and D2 receptor hetero-oligomer mediated calcium signal by agonist occupancy of either receptor. *Molecular pharmacology,* **72,** 450-462.

Sommer, B., Burnashev, N., Verdoorn, T. A., Keinanen, K., Sakmann, B. and Seeburg, P. H. (1992) A glutamate receptor channel with high affinity for domoate and kainate. *EMBO J,* **11,** 1651-1656.

Song, I. and Huganir, R. L. (2002) Regulation of AMPA receptors during synaptic plasticity. *Trends in neurosciences,* **25,** 578-588.

Sprenger, J. U. and Nikolaev, V. O. (2013) Biophysical techniques for detection of cAMP and cGMP in living cells. *Int J Mol Sci,* **14,** 8025-8046.

Stella, S. L., Jr., Bryson, E. J., Cadetti, L. and Thoreson, W. B. (2003) Endogenous adenosine reduces glutamatergic output from rods through activation of A2-like adenosine receptors. *Journal of neurophysiology,* **90,** 165-174.

Stella, S. L., Jr., Bryson, E. J. and Thoreson, W. B. (2002) A2 adenosine receptors inhibit calcium influx through L-type calcium channels in rod photoreceptors of the salamander retina. *Journal of neurophysiology,* **87,** 351-360.

Stella, S. L., Jr., Hu, W. D., Vila, A. and Brecha, N. C. (2007) Adenosine inhibits voltage-dependent Ca2+ influx in cone photoreceptor terminals of the tiger salamander retina. *Journal of neuroscience research,* **85,** 1126-1137.

Stiles, G. L. (1992) Adenosine receptors. *The Journal of biological chemistry,* **267,** 6451-6454.

Sullivan, J. M. and Lasater, E. M. (1992) Sustained and transient calcium currents in horizontal cells of the white bass retina. *The Journal of general physiology,* **99,** 85-107.

Sumbul, U., Song, S., McCulloch, K., Becker, M., Lin, B., Sanes, J. R., Masland, R. H. and Seung, H. S. (2014) A genetic and computational approach to structurally classify neuronal types. *Nature communications,* **5,** 3512.

Sun, D. and Kalloniatis, M. (2006) Mapping glutamate responses in immunocytochemically identified neurons of the mouse retina. *The Journal of comparative neurology,* **494,** 686-703.

Sun, W., Li, N. and He, S. (2002) Large-scale morphological survey of mouse retinal ganglion cells. *The Journal of comparative neurology,* **451,** 115-126.

Sunahara, R. K. and Taussig, R. (2002) Isoforms of mammalian adenylyl cyclase: multiplicities of signaling. *Mol Interv,* **2,** 168-184.

Tamura, T., Nakatani, K. and Yau, K. W. (1991) Calcium feedback and sensitivity regulation in primate rods. *The Journal of general physiology,* **98,** 95-130.

Toda, S., Alguacil, L. F. and Kalivas, P. W. (2003) Repeated cocaine administration changes the function and subcellular distribution of adenosine A1 receptor in the rat nucleus accumbens. *Journal of neurochemistry,* **87,** 1478-1484.

Tosini, G. and Dirden, J. C. (2000) Dopamine inhibits melatonin release in the mammalian retina: in vitro evidence. *Neuroscience letters,* **286,** 119-122.

Tosini, G. and Fukuhara, C. (2003) Photic and circadian regulation of retinal melatonin in mammals. *Journal of neuroendocrinology,* **15,** 364-369.

Tosini, G. and Menaker, M. (1998) The clock in the mouse retina: melatonin synthesis and photoreceptor degeneration. *Brain research,* **789,** 221-228.

Traynelis, S. F., Wollmuth, L. P., McBain, C. J. et al. (2010) Glutamate receptor ion channels: structure, regulation, and function. *Pharmacological reviews,* **62,** 405-496.

Tsien, R. W., Ellinor, P. T. and Horne, W. A. (1991) Molecular diversity of voltage-dependent Ca^{2+} channels. *Trends in pharmacological sciences,* **12,** 349-354.

Uckermann, O., Wolf, A., Kutzera, F., Kalisch, F., Beck-Sickinger, A. G., Wiedemann, P., Reichenbach, A. and Bringmann, A. (2006) Glutamate release by neurons evokes a purinergic inhibitory mechanism of osmotic glial cell swelling in the rat retina: activation by neuropeptide Y. *Journal of neuroscience research,* **83,** 538-550.

Usai (2014) Die potentielle Rolle des Neuromodulators Dopamin in der Helladaptation der Mausretina. Doktorarbeit am ICS-4 (FZ-Jülich) in der AG-Müller.

Vallone, D., Picetti, R. and Borrelli, E. (2000) Structure and function of dopamine receptors. *Neuroscience and biobehavioral reviews,* **24,** 125-132.

Vandenbranden, C. A., Kamphuis, W., Nunes Cardozo, B. and Kamermans, M. (2000) Expression and localization of ionotropic glutamate receptor subunits in the goldfish retina--an in situ hybridization and immunocytochemical study. *Journal of neurocytology,* **29,** 729-742.

Vandenbranden, C. A., Verweij, J., Kamermans, M., Müller, L. J., Ruijter, J. M., Vrensen, G. F. and Spekreijse, H. (1996) Clearance of neurotransmitter from the cone synaptic cleft in goldfish retina. *Vision research,* **36,** 3859-3874.

Vaney, D. I. (1990) Chapter 2 The mosaic of amacrine cells in the mammalian retina. *Progress in Retinal Research,* **9,** 49-100.

Vardi, N. (1998) Alpha subunit of Go localizes in the dendritic tips of ON bipolar cells. *The Journal of comparative neurology,* **395,** 43-52.

Vardi, N., Duvoisin, R., Wu, G. and Sterling, P. (2000) Localization of mGluR6 to dendrites of ON bipolar cells in primate retina. *The Journal of comparative neurology,* **423,** 402-412.

Vardi, N., Matesic, D. F., Manning, D. R., Liebman, P. A. and Sterling, P. (1993) Identification of a G-protein in depolarizing rod bipolar cells. *Visual neuroscience,* **10,** 473-478.

Varella, M. H., Correa, D. F., Campos, C. B., Chiarini, L. B. and Linden, R. (1997) Protein kinases selectively modulate apoptosis in the developing retina in vitro. *Neurochem Int,* **31,** 217-227.

Versaux-Botteri, C., Gibert, J. M., Nguyen-Legros, J. and Vernier, P. (1997) Molecular identification of a dopamine D1b receptor in bovine retinal pigment epithelium. *Neuroscience letters,* **237,** 9-12.

Versaux-Botteri, C., Nguyen-Legros, J., Vigny, A. and Raoux, N. (1984) Morphology, density and distribution of tyrosine hydroxylase-like immunoreactive cells in the retina of mice. *Brain research,* **301,** 192-197.

Veruki, M. L. and Wässle, H. (1996) Immunohistochemical localization of dopamine D1 receptors in rat retina. *The European journal of neuroscience,* **8,** 2286-2297.

Vielma, A. H., Agurto, A., Valdes, J., Palacios, A. G. and Schmachtenberg, O. (2014) Nitric oxide modulates the temporal properties of the glutamate response in type 4 OFF bipolar cells. *PloS one,* **9,** e114330.

Voglis, G. and Tavernarakis, N. (2006) The role of synaptic ion channels in synaptic plasticity. *EMBO Rep,* **7,** 1104-1110.

Volgyi, B., Chheda, S. and Bloomfield, S. A. (2009) Tracer coupling patterns of the ganglion cell subtypes in the mouse retina. *The Journal of comparative neurology,* **512,** 664-687.

Volgyi, B., Pan, F., Paul, D. L., Wang, J. T., Huberman, A. D. and Bloomfield, S. A. (2013) Gap junctions are essential for generating the correlated spike activity of neighboring retinal ganglion cells. *PloS one,* **8,** e69426.

Washburn, M. S., Numberger, M., Zhang, S. and Dingledine, R. (1997) Differential dependence on GluR2 expression of three characteristic features of AMPA receptors. *The Journal of neuroscience : the official journal of the Society for Neuroscience,* **17,** 9393-9406.

Wässle, H. (2004) Parallel processing in the mammalian retina. *Nature reviews. Neuroscience,* **5,** 747-757.

Wässle, H., Puller, C., Müller, F. and Haverkamp, S. (2009) Cone contacts, mosaics, and territories of bipolar cells in the mouse retina. *The Journal of neuroscience : the official journal of the Society for Neuroscience,* **29,** 106-117.

Watkins, J. C. and Evans, R. H. (1981) Excitatory amino acid transmitters. *Annual review of pharmacology and toxicology,* **21,** 165-204.

Weiler, R., Kohler, K., Kirsch, M. and Wagner, H. J. (1988) Glutamate and dopamine modulate synaptic plasticity in horizontal cell dendrites of fish retina. *Neuroscience letters,* **87,** 205-209.

Werner, P., Voigt, M., Keinanen, K., Wisden, W. and Seeburg, P. H. (1991) Cloning of a putative high-affinity kainate receptor expressed predominantly in hippocampal CA3 cells. *Nature,* **351,** 742-744.

West, A. E., Griffith, E. C. and Greenberg, M. E. (2002) Regulation of transcription factors by neuronal activity. *Nature reviews. Neuroscience,* **3,** 921-931.

Wexler, E. M., Stanton, P. K. and Nawy, S. (1998) Nitric oxide depresses GABAA receptor function via coactivation of cGMP-dependent kinase and phosphodiesterase. *The*

Journal of neuroscience : the official journal of the Society for Neuroscience, **18,** 2342-2349.

Wiencke, A. K., Nilsson, H., Nielsen, P. J. and Nyborg, N. C. (1994) Nonadrenergic noncholinergic vasodilation in bovine ciliary artery involves CGRP and neurogenic nitric oxide. *Investigative ophthalmology & visual science,* **35,** 3268-3277.

Willoughby, D., Wong, W., Schaack, J., Scott, J. D. and Cooper, D. M. (2006) An anchored PKA and PDE4 complex regulates subplasmalemmal cAMP dynamics. *EMBO J,* **25,** 2051-2061.

Winslow, R. L. (1989) Bifurcation analysis of nonlinear retinal horizontal cell models. I. Properties of isolated cells. *Journal of neurophysiology,* **62,** 738-749.

Witkovsky, P. (2004) Dopamine and retinal function. *Documenta ophthalmologica. Advances in ophthalmology,* **108,** 17-40.

Witkovsky, P., Nicholson, C., Rice, M. E., Bohmaker, K. and Meller, E. (1993) Extracellular dopamine concentration in the retina of the clawed frog, Xenopus laevis. *Proceedings of the National Academy of Sciences of the United States of America,* **90,** 5667-5671.

Wu, L. G. and Saggau, P. (1994) Adenosine inhibits evoked synaptic transmission primarily by reducing presynaptic calcium influx in area CA1 of hippocampus. *Neuron,* **12,** 1139-1148.

Wurtman, R. J. and Axelrod, J. (1968) The formation, metabolism and physiologic effects of melatonin. *Advances in pharmacology,* **6,** 141-151.

Xia, X. B. and Mills, S. L. (2004) Gap junctional regulatory mechanisms in the AII amacrine cell of the rabbit retina. *Visual neuroscience,* **21,** 791-805.

Xia, Y., Carroll, R. C. and Nawy, S. (2006) State-dependent AMPA receptor trafficking in the mammalian retina. *The Journal of neuroscience : the official journal of the Society for Neuroscience,* **26,** 5028-5036.

Xia, Y., Nawy, S. and Carroll, R. C. (2007) Activity-dependent synaptic plasticity in retinal ganglion cells. *The Journal of neuroscience : the official journal of the Society for Neuroscience,* **27,** 12221-12229.

Xin, D. and Bloomfield, S. A. (1999) Dark- and light-induced changes in coupling between horizontal cells in mammalian retina. *The Journal of comparative neurology,* **405,** 75-87.

Yan, Z., Song, W. J. and Surmeier, J. (1997) D2 dopamine receptors reduce N-type Ca2+ currents in rat neostriatal cholinergic interneurons through a membrane-delimited, protein-kinase-C-insensitive pathway. *Journal of neurophysiology,* **77,** 1003-1015.

Yang, X. L. (2004) Characterization of receptors for glutamate and GABA in retinal neurons. *Progress in neurobiology,* **73,** 127-150.

Yang, X. L. and Wu, S. M. (1991) Coexistence and function of glutamate receptor subtypes in the horizontal cells of the tiger salamander retina. *Visual neuroscience,* **7,** 377-382.

Yuste, R. and Konnerth, A. (2005) *Imaging in neuroscience and development : a laboratory manual*. Cold Spring Harbor Laboratory Press, Cold Spring Harbor, NY.

Zelphati, O., Wang, Y., Kitada, S., Reed, J. C., Felgner, P. L. and Corbeil, J. (2001) Intracellular delivery of proteins with a new lipid-mediated delivery system. *The Journal of biological chemistry,* **276,** 35103-35110.

Zhang, A. J., Jacoby, R. and Wu, S. M. (2011) Light- and dopamine-regulated receptive field plasticity in primate horizontal cells. *The Journal of comparative neurology,* **519,** 2125-2134.

Zhang, C., Hammassaki-Britto, D. E., Britto, L. R. and Duvoisin, R. M. (1996) Expression of glutamate receptor subunit genes during development of the mouse retina. *Neuroreport,* **8,** 335-340.

Zhang, C. and Schmidt, J. T. (1999) Adenosine A1 and class II metabotropic glutamate receptors mediate shared presynaptic inhibition of retinotectal transmission. *Journal of neurophysiology,* **82,** 2947-2955.

Zhang, D. Q., Stone, J. F., Zhou, T., Ohta, H. and McMahon, D. G. (2004) Characterization of genetically labeled catecholamine neurons in the mouse retina. *Neuroreport,* **15,** 1761-1765.

Zhang, J., Ma, Y., Taylor, S. S. and Tsien, R. Y. (2001) Genetically encoded reporters of protein kinase A activity reveal impact of substrate tethering. *Proceedings of the National Academy of Sciences of the United States of America,* **98,** 14997-15002.

Zhang, X., Zhang, M., Laties, A. M. and Mitchell, C. H. (2006) Balance of purines may determine life or death of retinal ganglion cells as A3 adenosine receptors prevent loss following P2X7 receptor stimulation. *Journal of neurochemistry,* **98,** 566-575.

Zhao (2015) Towards monitoring nitric oxide mediated cGMP metabolism in mouse retinal neurons using a FRET-based genetically encoded sensor. Doktorarbeit am ICS-4 (FZ-Jülich) in der AG-Müller. .

Zhao, Z. (2010) cGMP metabolism and its modulation by nitric oxide in the mouse inner retina. Masterarbeit am ICS-4 (FZ-Jülich) in der AG-Müller.

Zhong, Y. S., Wang, J., Liu, W. M. and Zhu, Y. H. (2013) Potassium ion channels in retinal ganglion cells (review). *Molecular medicine reports,* **8,** 311-319.

Danksagung

Ganz herzlich möchte ich mich bei Herrn Prof. Dr. Frank Müller für die Überlassung des spannenden Themas, die ausgezeichnete wissenschaftliche Betreuung, seine ständige Bereitschaft Ergebnisse, Probleme und weiterführende Ansätze zu diskutieren bedanken.

Ich danke Herrn Prof. Dr Marc Spehr für die Begutachtung dieser Arbeit. Ich danke Herrn Prof. Dr. Björn Kampa für die Übernahme der Drittprüfer-Funktion und Herrn Prof. Dr. Ralph Panstruga für die Übernahme des Prüfungsvorsitzes.

Darüber hinaus möchte ich mich bei Christoph Aretzweiler für die Unterstützung im Labor und die Hilfe bei allen Problemen, die die Imaging-Versuche mit sich brachten, bedanken. Für die freundschaftliche und entspannte Arbeitsatmosphäre möchte ich mich bei der gesamten Arbeitsgruppe bedanken. Vor allem danke ich Stefan Esser für die gute Zusammenarbeit, die Kaffeepausen, die abwechslungsreichen Diskussionen und das viel Lachen.

Ganz herzlich danke ich Frau Anita Eckert für ihre uneingeschränkte Hilfsbereitschaft und ihr Engagement, Herrn Prof. Dr. Arnd Baumann für die Ratschläge und die ständige Diskussionsbereitschaft und Nadine Jordan für ihre Hilfsbereitschaft und die intensiven Gespräche. Weiterhin möchte ich mich bei allen Kollegen des ICS-4-Instituts für die angenehme Arbeitsatmosphäre bedanken.

Je voudrais remercier ma chère famille pour son soutien, surtout mon chèr papa à qui je dédie ma thèse, merci pour ton amour et pour avoir toujours trouvè les bons mots pour me soutenir. Je remercie mes frères et soeurs pour avoir cru en moi et m'avoir soutenue durant toutes ces dernières années, surtout mon frère Abdou.

Aus tiefstem Herzen möchte ich mich bei einem ganz besonderen Menschen bedanken: Thomas Hoffmann. Danke für deine Unterstützung, für dein offenes Ohr und dafür, dass du für mich immer da bist. Danke, dass du mit mir geweint und gelacht hast. Danke.

Erklärung

Hiermit erkläre ich, dass ich die hier vorliegende Doktorarbeit selbstständig verfasst habe. Es wurden keine anderen als die in der Arbeit angegebenen Quellen und Hilfsmittel benutzt. Die wörtlichen oder sinngemäß übernommenen Zitate habe ich als solche kenntlich gemacht.

_____ _____

Ort, Datum Unterschrift